



Development and Semi-Automated Analysis of an *in vitro* Dissemination Model
for Myeloma Cells Interacting with Mesenchymal Stromal Cells

Entwicklung und semi-automatisierte Analyse eines *in vitro* Modells
für die Disseminierung von Myelomzellen in Interaktion mit mesenchymalen Stromazellen

Doctoral Thesis for a Doctoral Degree

at the

GRADUATE SCHOOL OF LIFE SCIENCES,
JULIUS-MAXIMILIANS-UNIVERSITÄT WÜRZBURG,
SECTION BIOMEDICINE

submitted by

Martin Kuric

from

Bad Neustadt a.d. Saale

Würzburg, 2024

Submitted on:

Office stamp

Members of the *Promotionskomitee*:

Chairperson: Prof. Dr. Uwe Gbureck

Primary Supervisor: Prof. Dr. rer. nat. Regina Ebert

Supervisor (Second): Prof. Dr. med. Franziska Jundt

Supervisor (Third): Prof. Dr. rer. nat. Torsten Blunk

Supervisor (Fourth): Prof. Dr. Thomas Dandekar

Date of Public Defense:

Date of Receipt of Certificates:

A digital version of this thesis will be made available at:

<https://github.com/markur4/Dissertation>

The L^AT_EX source code is found in this subfolder:

./THESIS

Videos are found in this subfolder:

./publications/Chapter1_Supplementary/

This work was conducted at the Department of Musculoskeletal Tissue Regeneration
(Bernhard-Heine-Centre for Locomotive Research), University of Würzburg from
08.10.2018 to 02.09.2024 under the supervision of Prof Dr. rer. nat. Regina Ebert.

Acknowledgements

I am deeply grateful to the following supporters who have contributed to the completion of this PhD thesis in myriad ways:

Doris Schneider, for her exceptional assistance in laboratory work. Her patience, focus, and dedication were invaluable to the experimental success of this research.

Regina Ebert, for her unwavering support and insightful guidance. Her patience and encouragement were instrumental in making plotastic a reality.

Franziska Jundt & Torsten Blunk, for their invaluable supervision of this project. Their professional feedback and honest critiques pushed me to strive for the highest quality in my work.

Marie-Nicole Kobsar, my beloved significant other, for her endless patience, kindness, and support throughout the entire doctoral journey. Her encouragement and understanding were a source of strength and motivation.

My Lab Colleagues & Collaborators, for their countless contributions, insights and constructive feedback throughout my doctorate.

My Family, for their unconditional support throughout my academic journey.

Additionally, I wish to extend my gratitude to all my friends who listened, discussed, and helped in various ways.

I would also like to acknowledge the funding bodies and institutions that supported this research, including the German Research Foundation (DFG), the Graduate School of Life Sciences (GSLS), and the University of Würzburg, whose contributions made this work possible.

Finally, a special thanks goes to the Elite Network Bavaria (ENB) and the University of Bayreuth for my education in molecular cell biology and biological physics. I felt well-prepared for my doctorate at the University of Würzburg, and am very grateful for the opportunities for interdisciplinary exchange with amazing physicists and other scientists.

Thank you all for your incredible support and encouragement.

Summary

This thesis integrates biomedical research and data science, focusing on an *in vitro* model for studying myeloma cell dissemination and a Python-based tool, `plotastic`, for semi-automated analysis of multidimensional datasets. Two major challenges are approached: (1) understanding the steps of myeloma dissemination and (2) improving data analysis efficiency to address the complexity- and reproducibility bottlenecks currently present in biomedical research.

In the experimental component, primary human mesenchymal stromal cells (hMSCs) are co-cultured with INA-6 myeloma cells to study their cell proliferation, attachment, and detachment. Time-lapse microscopy reveal that predominantly myeloma daughter cells detach from hMSCs after cell division. Novel separation techniques were developed to isolate myeloma subpopulations for further characterization by RNAseq, cell viability, and apoptosis assays. Adhesion and retention genes are upregulated by MSC adhering INA-6 cells, which correlates with patient survival. Overall, this work provides insights into myeloma dissemination mechanisms and identifies genes that potentially counteract dissemination through adhesion, which could be relevant for the design of new therapeutics.

To manage the complex data resulting from the *in vitro* model, a Python-based software named `plotastic` was developed that streamlines analysis and visualization of multidimensional datasets. `plotastic` is built on the idea that statistical analyses are performed based on how the data is visualized. This approach simplifies data analysis and semi-automates it in a standardized statistical protocol. The thesis becomes a case study as it reflects on the application of `plotastic` to the *in vitro* model, demonstrating how the software facilitates rapid adjustments and refinements in data analysis and presentation. Such efficiency could be crucial for handling semi-big datasets transparently, which—despite being manageable—are complex enough to complicate analysis and reproducibility.

Together, this thesis illustrates the synergy between experimental methodologies and new data analysis tools. The *in vitro* model provides a robust platform for studying myeloma dissemination, while `plotastic` addresses the need for efficient data analysis. Combined, they provide an approach for handling complex cell biological experiments and could advance both cancer biology and other research practices by supporting the exploratory investigation of challenging phenomena while communicating results transparently.

Zusammenfassung

Diese Doktorarbeit kombiniert biomedizinische Forschung und Datenwissenschaften und fokussiert sich auf ein *in vitro*-Modell zur Untersuchung der Dissemination von Myelomzellen sowie auf die Python-Software `plotastic` zur semi-automatisierten Analyse multidimensionaler Datensätze. Zwei Hauptfragen werden behandelt: (1) das Verständnis der Schritte der Myelomdissemination und (2) die Steigerung der Effizienz der Datenanalyse, um die in der biomedizinischen Forschung bestehenden Herausforderungen hinsichtlich Komplexität und Reproduzierbarkeit zu bewältigen.

Im experimentellen Teil werden primäre humane mesenchymale Stromazellen (hMSCs) mit INA-6-Myelomzellen kokultiviert, um ihre Proliferation, Anhaftung und Ablösung zu untersuchen. Zeitraffer-Mikroskopie zeigt, dass sich überwiegend Myelom-Tochterzellen nach Zellteilung von hMSCs ablösen. Neue Trennmethoden wurden entwickelt, um Myelom-Subpopulationen für weitere Charakterisierungen durch RNAseq, Zellviabilitäts- und Apoptose-Assays zu isolieren. Adhäsions- und Retentionsgene werden von MSC-adhärierenden INA-6 hochreguliert, was mit Patientenüberleben korreliert. Insgesamt bietet diese Arbeit Einblicke in die Mechanismen der Myelomdissemination und identifiziert Gene, die potenziell die Dissemination durch Adhäsion behindern könnten, was für die Entwicklung neuer Therapien von Bedeutung sein könnte.

Zur Handhabung der komplexen Daten, die bei dem *in vitro*-Modell entstanden sind, wurde eine Python-basierte Software namens `plotastic` entwickelt, welche die Analyse und Visualisierung der multidimensionaler Datensätze optimiert. `plotastic` basiert auf dem Prinzip, dass statistische Analysen abhängig davon durchgeführt werden, wie die Daten visualisiert werden. Dieser Ansatz vereinfacht die Datenanalyse nicht nur, sondern semi-automatisiert sie auch als standardisiertes statistisches Protokoll. Diese Arbeit fungiert als Fallstudie, da sie die Anwendung von `plotastic` auf das *in vitro*-Modell beleuchtet und zeigt, wie die Software schnelle Anpassungen und Verfeinerungen in der Datenanalyse und -präsentation ermöglicht. Eine solche Effizienz könnte entscheidend für den transparenten Umgang mit semi-großen Datenmengen sein, die trotz ihrer Handhabbarkeit komplex genug sind, um die Analyse und Reproduzierbarkeit zu erschweren.

Zusammenfassend zeigt diese Dissertation die Synergie zwischen experimentellen Methoden und neuen Werkzeugen der Datenanalyse. Das *in vitro*-Modell bietet eine robuste Plattform für die Untersuchung der Myelomdissemination, während `plotastic` den Bedarf an effizienter Datenanalyse unterstützt. Zusammen stellen sie einen Ansatz für die Bewältigung komplexer zellbiologischer Experimente dar, und könnten sowohl die Krebsbiologie als auch andere Forschungspraktiken fördern, indem sie die explorative Untersuchung anspruchsvoller Phänomene unterstützen und dabei Ergebnisse transparent kommunizieren.

Inhaltsverzeichnis

Summary / Zusammenfassung	viii
Abbreviations	xii
Glossary	xiv
Introduction	2
Multiple Myeloma and Other Monoclonal Gammopathies	3
Dissemination of Myeloma Cells	4
Retention of Myeloma Cells in the Bone Marrow	6
Release of Myeloma Cells from the Bone Marrow	7
MSCs: Mesenchymal Stromal (Stem) Cells	8
Molecular Interactions between MSCs Myeloma Cells	11
Multidimensional Data in Biomedical Research	14
Nontransparencies in Biomedical Data Analyses	15
Semi-Big Data: Big Enough to Cause Problems	16
The Shortcomings of Common Biomedical Analysis Tools	17
Modern Standards of Software Development	19
What makes Python an “Easy” Programming Language?	21
The Potential of Python Data Science Packages for Biomedicine	26
Aims	30
Additional Materials & Methods	32
Chapter 1: Modelling Myeloma Dissemination <i>in vitro</i>	36
Introduction	37
Materials and Methods	39
Results	43
Discussion	58
Chapter 2: Semi-Automating Data Analysis with <i>plotastic</i>	62
Introduction	63
Statement of Need	65
Example	66
Overview	66
Discussion	70
Summarizing Discussion	74
Semi-Automation was Critical for Establishing <i>in vitro</i> Methods	75
<i>plotastic</i> Exceeded in Re-Doing Statistical Analyses and Plots	77
Conclusion 1: Demonstrating the Advantages of Semi-Automation in Biomedical Data Analysis	79
How Exploratory Live-Cell Imaging Transformed the Research Focus	80
Potential and Challenges of Image Cytometry	82
Technical Considerations for Automated Microscopy	84
Conclusion 2: Automating Microscopy, an Emerging Trend for Exploring Unknown Phenomena?	86
Isolating & Quantifying Subpopulations within Cells in Direct Contact with MSCs	88
Integrating Evidence and Hypotheses for a Mechanistic Understanding of Dissemination	92
Hypothesis 1: Cells Change their Adhesion Dramatype during Dissemination	95
Hypothesis 2: Rapid Adhesional Plasticity Drives Aggression in Myeloma	98
Hypothesis 3: CAD is Highly Diverse Between Myeloma Patients	101
Hypothesis 4: Detachment is Caused by Multiple Cues of Varying Nature	102
Conclusion 3: The Dynamic Adhesion Hypothetical Framework for Myeloma Dissemination	105
Overall Conclusion	106

References	107
Appendices	134
A Supplementary Data & Methods	134
A.1 Figures	134
A.2 Tables	151
A.3 Materials & Methods	159
B Documentation of <i>plotastic</i>	173
B.1 Class Diagram	174
B.2 Readme	176
B.3 Example Analysis “qpcr”	189
C Submission Forms & Documents	196
C.1 Author Contributions	196
C.2 Affidavit	203
C.3 Curriculum Vitae	205

Abbreviations

APRIL A Proliferation-Inducing Ligand	6
aMM asymptomatic Multiple Myeloma	3
BAFF B-cell Activating Factor	6
BM Bone Marrow	3
BMME Bone Marrow Microenvironment	4
BMPC Bone Marrow Plasma Cell	6
BMSC Bone Marrow Stromal Cell	6
CAD Cell Adhesion Dynamics	93
CM hMSC-conditioned medium	39
CM-INA6 MSC-Conditioned-Medium-treated INA-6	50
CAM Cell Adhesion Molecule	6
CLI Command Line Interface	72
CXCL12 C-X-C Motif Chemokine Ligand 12	5
DKK1 Dickkopf-1	12
ECM Extracellular Matrix	6
EMT Epithelial-Mesenchymal Transition	5
FACS Fluorescence-Activated Cell Sorting	83
GFI1 Growth Factor Independence 1	13
GUI Graphical User Interface	72
HDAC1 Histone Deacetylase 1	13
hMSC human Mesenchymal Stromal Cell	9
HSC Hematopoietic Stem Cell	9
IL-6 Interleukin-6	6
IGF-1 Insulin-like Growth Factor 1	5
JNK c-Jun N-terminal Kinase	12
LLM Large Language Model	72
MA MSC-adhering	48
MACS Magnetic-Activated Cell Sorting	41
MIP-1α Macrophage Inflammatory Protein-1 α	12
MSC Mesenchymal Stromal Cell	8
MGUS Monoclonal Gammopathy of Undetermined Significance	3
MM Multiple Myeloma	3
MMR Multiple Myeloma Relapse	98
MBD Multiple Myeloma related Bone Disease	11
NDMM Newly Diagnosed Multiple Myeloma	4
NF-κB Nuclear Factor- κ B	12
nMA non-MSC-adhering	48
OS Overall Survival	54
PCL Plasma Cell Leukemia	4

PFS	Progression-Free Survival	54
PPAR-γ	Peroxisome Proliferator-Activated Receptor- γ	13
RUNX2	Runt-related Transcription Factor 2	12
RANKL	Receptor Activator of Nuclear Factor- κ B Ligand	12
SASP	Senescence-Associated Secretory Phenotype	12
SDF-1	Stromal Cell-Derived Factor-1	6
sMM	smouldering Multiple Myeloma	3
SOST	Sclerostin	12
SP	Solitary Plasmacytoma	3
TAD	Topologically Associated Domain	9
TGF-β	Transforming Growth Factor- β	8
TNF-α	Tumor Necrosis Factor- α	13
TNFSF13	Tumor Necrosis Factor Superfamily, Member 13	6
VCAM-1	Vascular Cell Adhesion Molecule-1	6
VEGF	Vascular Endothelial Growth Factor	6
VLA-4	Very Late Antigen-4—also known as CD49d or ITGA4 Subunit α —	6
Wnt	Wingless-related Integration Site	12
WPSC	Well Plate Sandwich Centrifugation	40

Glossary

¹*Image Features*: Discernable elements of an image, such as edges, corners, directions, colors. These features are mathematically extractable using *filters*—also referred to as *convolution kernels*—, which are functions or algorithms applied to the pixel values of an image. For instance, *gabor filters* can extract edges of one particular direction, resulting in an image of the same size as the input, but showing only edges of one direction. *Feature extraction* is the process of applying multiple filters, resulting in a stack of filtered images called a feature vector. (Szeliski, 2011; A. Gupta et al., 2019)

²*Convolutional Neural Networks (CNN)*: Machine learning algorithms that use the output of a feature extractor¹ to feed into a neural network. The network then learns to associate these feature vectors with a label, such as *cell* or *background*. This is called *supervised learning*.

³*Cell Interaction Scenario* (defined in this work): A combination of cellular interaction types describing direct contact or adhesion between cells. Cellular interaction types include those between similar cell types (homotypic interaction), different cell types (heterotypic interaction), or between cells and substrate. A cell interaction scenario usually implies that multiple cell interaction types occur simultaneously or in rapid succession, for instance, myeloma cells interacting with both other myeloma cells and MSCs. When interaction scenarios emerge from cell division, the term *growth conformation* is also used (see Chapter 1)

⁴*Adhesion Factor*: Any factor influencing cell adhesion, including—but not limited to—Cell Adhesion Molecules (CAMs), Extracellular Matrix (ECM) proteins, chemotactic factors associated with inducing adhesion factor expression—such as CXCR4 or CXCL12—, or factors listed in Gene ontology terms “*extracellular matrix organization*”, “*ECM proteoglycans*”, “*cell-substrate adhesion*”, and “*negative regulation of cell-substrate adhesion*”.

⁵*Cell Adhesion Dynamics (CAD)*: The observation and measurement of time-dependent changes in cell adhesion and detachment events. CAD expands traditional *cell adhesion* by a time component and implies an intention to predict the timepoint of detachment events. Such focus on dynamics is especially relevant for suspension cells that exhibit intricate adhesion behaviors. Chapter 1 also refers to CAD as attachment/detachment dynamics.

⁶*CAD Dramatype* (defined in this work): Specific adhesion behavior caused by proximate environmental factors. The term *dramatype* was inspired from laboratory animal science (van Zutphen et al., 2001). A CAD dramatype is characterized by the duration cells spend in distinct adhesive states or interaction scenarios³, and the cause of transitions between these states and scenarios. Adhesive states include attached, migrating, or detached; interaction scenarios include homotypic, heterotypic or substrate interactions. CAD dramatypes are associated with molecular signatures, such as CAM expression patterns or signal transduction mediated by proximate environmental factors. The term dramatype distinguishes itself from *phenotype* by focusing on dynamic and transient states available within transcriptional plasticity, while *phenotypes* focus on relatively persistent states such as genetic and epigenetic backgrounds.

⁷*Adhesion Dramatype* (defined in this work): Short version for CAD dramatype⁶. Since the term *dramatype* implies dynamic changes, *CAD dramatypes* and *adhesion dramatypes* are interchangeable.

⁸*Retentive Adhesion Factors*: The subset of adhesion factors that promotes anchorage of myeloma cell in the BMME, and promote better patient survival at high expression as shown in Chapter 1.

⁹*Adhesional Plasticity*: The overall repertoire of adhesion dramatypes⁷ that individual myeloma cells can deploy.

Introduction

Multiple Myeloma and Other Monoclonal Gammopathies

Multiple Myeloma (MM) is a hematological malignancy characterized by the clonal expansion of malignant plasma cells primarily within multiple sites of the Bone Marrow (BM) (P. Yang et al., 2022). This cancer arises from the antibody-producing cells of the immune system—plasma cells—which undergo malignant transformation. This results in uncontrolled growth and antibody secretion, but also disruption of normal bone marrow function—both of which will be covered across this thesis. The prevalence of multiple myeloma has tripled across both Europe and USA from 1980 to 2014 due to an aging population (Ocias et al., 2016; Turesson et al., 2018). For 2024, 35780 new MM cases and 12540 deaths are estimated for the USA alone (Siegel et al., 2024).

To understand the progression of a healthy plasma cell to MM, one can review other *monoclonal gammopathies*. These are defined by the presence of monoclonal immunoglobulin in the blood serum which is indicative of abnormal plasma cell clones overexpressing the same type of dysfunctional antibody. (Kyle, 1997; Fermand et al., 2018). When no further disease manifestations are present, the condition is termed *Monoclonal Gammopathy of Undetermined Significance* (MGUS), which is the most commonly diagnosed monoclonal gammopathy (Kyle, 1997). MGUS has a 1-5 % annual risk of progression to MM (Rajkumar et al., 2014).

To distinguish MM from other monoclonal gammopathies, diagnosis of MM requires not only identification of a minimum of clonal plasma cells, but also a *myeloma defining event* which is evidence of malignancy or end-organ damage, for instance hypercalcemia, renal insufficiency, anemia, or bone lesions (Rajkumar et al., 2014). A localized smaller[†] mass of clonal plasma cells together with a singular primary bone lesion is diagnosed as Solitary Plasmacytoma (SP). SP can progress to MM in 32 % of cases with a median follow-up of 9.7 years (Thumallapally et al., 2017; S. Gao et al., 2024). Studies from Kyle (1997) show that SP cases are rare, constituting only 2.5 % of monoclonal gammopathy diagnoses, whereas MM represent 18 %. Another rare precursor of MM is *asymptomatic Multiple Myeloma* (aMM)—also termed *smouldering Multiple Myeloma* (sMM)—, representing 3 % of monoclonal gammopathies (Kyle, 1997). aMM is diagnosed when no myeloma defining event is detected, although the quantities of clonal plasma cells or monoclonal protein align with respective criteria for MM diagnosis (Rajkumar et al., 2014). Recent reports show that if left untreated, 72 % of aMM patients progress to MM, whereas early treatment can

[†] Rajkumar et al. (2014):

“Solitary plasmacytoma with 10 % or more clonal plasma cells is regarded as multiple myeloma. [...] If bone marrow has less than 10 % clonal plasma cells, more than one bone lesion is required to distinguish [MM] from solitary plasmacytoma with minimal marrow involvement.”

lower the progression rate to 11 % within up to 7.6 years until last follow-up[†] (Abdallah et al., 2024; Mateos María-Victoria et al., 2013). MM itself can progress to advanced stages, such as *extramedullary involvement/disease* which describes colonization of soft tissues outside the bone marrow (Bladé et al., 2022), but also Plasma Cell Leukemia (PCL) which is characterized by high levels of circulating plasma cells (Jung & Lee, 2022). However, the most common cause of death is renal failure during the MM stage, caused by excess immunoglobulins or hypercalcemia due to bone degradation (Kundu et al., 2022).

With a 5-year survival rate of 50 % (Turesson et al., 2018), MM can be considered incurable and deadly. MM relapses (MMR) within the first year in 16 % of patients, others face relapse at a later time or only continued response to treatment (Majithia et al., 2016). Although treatments have improved, the age-adjusted mortality rate of MM has decreased from 1999 to 2020 by only –1.6 % (Doddi & Rashid, 2024). Engelhardt et al. (2024) describes the current standard care for transplant-eligible Newly Diagnosed Multiple Myeloma (NDMM) patients as follows: Induction with a CD38 antibody, proteasome inhibitor, immunomodulatory drug, dexamethasone, and potentially followed by bone marrow transplantation and lenalidomide maintenance (Rajkumar & Kumar, 2020). A major challenge to these treatments is the continued cycle of remission and relapse, with each relapse generally being harder to treat (Podar & Leleu, 2021). Development of such resistance is well described in the literature, often arising from the intraclonal genetic heterogeneity within the myeloma cell population and the protective niche provided by the Bone Marrow Microenvironment (BMME) (Solimando et al., 2022).

Dissemination of Myeloma Cells

As the name suggests, *multiple* myeloma involves spreading of clonal plasma cells in multiple sites within the body, a process that's described with the term *dissemination*. A single large plasmacytoma is still classified as MM (Rajkumar et al., 2014); however, the presence of multiple tumor lesions within the BM is very common. More than one or 25 such lesions predict poor prognosis for asymptomatic and symptomatic MM patients, respectively (Kastritis et al., 2014; Mai et al., 2015). Additionally, MM cells can disseminate to extramedullary sites of virtually any tissue, highlighting MM as a systemic disease with potential multi-organ impact (Rajkumar & Kumar, 2020; Bladé et al., 2022). Hence, dissemination is a major contributor to MM progression and poor prognosis, enabling MM cells to colonize

[†] From Abdallah et al. (2024): For non-high risk aMM patients, treatment lowered MM progression rate to 9 %, compared to 31 % for untreated patients (within up to 6.7 and 7.6 years of follow-up, respectively). For high-risk aMM patients, treatment lowered aMM progression rate to 11 %, compared to 72 % for untreated patients (within up to 5.2 years of follow-up and median time to progression of 2.2 years, respectively).

new niches that favor survival, quiescent states or are less accessible for therapy, especially with high subclonal heterogeneity (Forster & Radpour, 2022; Keats et al., 2012).

Dissemination of MM is reminiscent of *metastasis*, a term typically associated with solid tumors describing the spread of cancer cells to distant sites. However, it substantially differs from metastasis due to the hematological or “liquid” nature of MM. Long-lived plasma cells originate from migratory B-cells, negating the need for extensive transformative processes such as Epithelial-Mesenchymal Transition (EMT), which is required for escaping tightly connected solid tissues to enter the bloodstream (Ribatti et al., 2020). Although referred to as “liquid tumor”, MM cells still accumulate as distinct foci within the bone marrow, somewhat mirroring the localized growth of solid tumors. This characteristic has led to MM being proposed as a model for studying solid “micrometastases” (Ghobrial, 2012), highlighting its unique blend of liquid and solid tumor properties and providing insights into the mechanisms of cancer dissemination and colonization of new niches.

The exact mechanism of MM dissemination is not entirely understood. Nevertheless, attempts to dissect this process have been made by Zeissig et al. (2020), describing MM dissemination in five steps:

1. Retention in the BM
2. Release from the BM
3. Intravasation
4. Extravasation
5. Colonization

According to this multi-step model, MM dissemination begins with MM cells overcoming retention and adhesion within the BMME. Following release, MM cells undergo *intravasation* into the bloodstream, where they can circulate before extravasating into new BM sites. Plasma cell migration is directed by chemokines and growth factors produced by cells in the BM. For instance, C-X-C Motif Chemokine Ligand 12 (CXCL12) and Insulin-like Growth Factor 1 (IGF-1) are critical in guiding MM cells back to the BM, a process called *homing* (Vande Broek et al., 2008). Once returned to the BM, they can *colonize* and form new tumor foci.

The review by Zeissig et al. (2020) implies a sequential order of such steps, yet direct proof of this is lacking. Still, the review provides a framework that integrates multiple complex research topics into one coherent context. For instance, it is stated that two adhesive processes are critical for successful dissemination: Lowered adhesion to the BM, but increased adhesion to the endothelium to initiate extravasation (Asosingh et al., 2001; Mrozik et al., 2015). This alone implies stringent separation of different adhesive processes

during the dissemination process. Given that Cell Adhesion Molecules (CAMs) have become attractive targets for treating MM (Bou Zerdan et al., 2022; Katz, 2010), such detailed understanding of cell adhesion is crucial for developing successful therapies.

Retention of Myeloma Cells in the Bone Marrow

According to Zeissig et al. (2020), overcoming retention and adhesion to the BME is critical to MM dissemination. Retention of plasma cells to the BME is mediated by multiple mechanisms, which are categorized here into *direct adhesion*, *soluble survival factors* and *chemotaxis*. A fourth notable mechanism is the physical boundary that is bone tissue and Extracellular Matrix (ECM), which could become important for MM dissemination once degradation of bone tissue has progressed.

Direct adhesion of MM cells to the BM is mediated through ECM components and cell adhesion to other BM resident cells like osteoblasts, osteoclasts and Bone Marrow Stromal Cells (BMSCs) (Teoh & Anderson, 1997; Bou Zerdan et al., 2022). ECM components include fibronectin, collagens, and proteoglycans such as decorin (X. Hu et al., 2021; Huang et al., 2015; Katz, 2010; Kibler et al., 1998). BMSCs are vital in this niche, supporting cell adhesion through CAMs but also by secretion of (ECM) components (Katz, 2010). Such adhesion acts both as physical anchorage but also provides signaling cues for growth, survival, and drug resistance (W.-C. Chen et al., 2020). A classic example is the binding of MM cell integrins to Vascular Cell Adhesion Molecule-1 (VCAM-1) on BMSCs, such as $\alpha 4\beta 1$ [commonly termed Very Late Antigen-4—also known as CD49d or ITGA4 Subunit α — (VLA-4)] (Bou Zerdan et al., 2022). Since direct adhesion promotes both retention and tumour growth, it could play an ambiguous role during MM dissemination.

Soluble survival factors contribute to BM retention, since plasma cells can not survive outside the bone marrow without them. For example, deleting BCMA—a receptor for survival factors—leads to loss of Bone Marrow Plasma Cells (BMPCs) due to unsustained maintenance of cell survival (O'Connor et al., 2004). Soluble survival factors include Interleukin-6 (IL-6), IGF-1, B-cell Activating Factor (BAFF), Vascular Endothelial Growth Factor (VEGF), and A Proliferation-Inducing Ligand (APRIL)—also known as Tumor Necrosis Factor Superfamily, Member 13 (TNFSF13). Among these factors, IGF-1 has proven to be the primary survival factor (Sprynski et al., 2009). These signals are secreted by BMSCs and adipocytes (Kibler et al., 1998; García-Ortiz et al., 2021). *Chemotaxis* is also crucial for BM retention (T. R. Ullah, 2019). CXCL12—also known as Stromal Cell-Derived Factor-1 (SDF-1)—and CXCL8 are soluble chemotactic signals produced by BMSCs and attract MM cells, but also primes their cytoskeleton and integrins for adhesion (Aggarwal et al., 2006; Alsayed et al., 2007). Roccaro et al. (2015) demonstrated that

inhibiting CXCR4—the receptor of CXCL12/SDF-1—with the monoclonal antibody Ulocuplumab decreased MM cell homing to the BM and reduced dissemination via factors associated with EMT. Consequently, CXCL12:CXCR4 signaling has emerged as a promising target of several treatments aiming at preventing myeloma cell migration, as reviewed by Ito et al. (2021) who conclude a need for further studies to develop combined therapies explicitly against tumor cell dissemination.

Together, BMSCs play a critical role in MM retention, providing direct adhesion, soluble survival factors, and chemotactic signals.

Release of Myeloma Cells from the Bone Marrow

Zeissig et al. (2020) describes the release of myeloma cells from the BMME as all steps required for overcoming bone marrow retention, but also putative triggers leading to migration out of the BME. To the author's knowledge, release of MM cells is the least understood among disseminative processes. Still, in order to gain understanding of how MM dissemination is initiated, one can summarize reports that could be involved.

Studies suggest that CAMs expression indeed plays a role in MM dissemination. For instance, studies demonstrate that circulating MM cells exhibit reduced levels of integrin $\alpha 4\beta 1/VLA-4$, in contrast to those located in the BM (Paiva et al., 2013, 2011). Given that dissemination can be induced in mice by overexpressing the CAM shedding protease heparanase (Y. Yang et al., 2005), it seems reasonable that dynamic loss of adhesive strength is causing release of MM cells from the BM. Another useful comparison is that of CAMs expression at different disease stages, indicative of their role in disease progression, which in turn could serve as a proxy for disseminative potential. For example, Terpos et al. (2016) reported an increase in adhesion molecule expression of ICAM-1 and VCAM-1 in patients with MM compared to those with MGUS and aMM. However, Pérez-Andrés et al. (2005) reported that CD40 is downregulated in PCL patients, hence, different CAMs could serve ambiguous roles in MM progression. Together, the regulation of CAMs can depend on both momentary microenvironmental factors, but also on the stage of the disease, while the specific stimuli regulating their expression are not fully defined. A study from Akhmetzyanova et al. (2020) presents CD138 (*aka* Syndecan-1) as a potential *switch* between adhesion and release, as mice treated with CD138 blocking antibodies exhibited rapid mobilization of MM cells from the BM to peripheral blood, confirming that alterations in adhesion molecule expression are sufficient to cause MM cell release. A. Brandl et al. (2022) builds on that finding, showing that JAM-C inversely correlates with CD138 expression while promoting MM progression in a mouse model.

Another often overlooked requirement for MM cell release is the need for independence from essential growth and survival signals provided by BMSC. Autocrine signaling has been proposed as a key mechanism through which myeloma cells gain independence from essential survival factors such as IL-6 (Frassanito et al., 2001; Urashima et al., 1995). Autocrine signaling could also disrupt responsiveness to Mesenchymal Stromal Cell (MSC)-derived chemotactic signals, since MM cells from BM biopsies were shown to express CXCL12 under hypoxic conditions induced by HIF-2 α (Martin et al., 2010). Since MM niches turn increasingly hypoxic and circulating myeloma cells upregulate hypoxia associated genes, hypoxia is a promising factor for understanding the release of MM (Garcés et al., 2020).

The degradation of bone tissue could also play a critical role in myeloma cell release by eliminating adhesive anchorage within the ECM, considering that ECM is remodeled even at the MGUS stage Glavey et al. (2017). This degradation is part of a ‘vicious cycle’ that is well described in osteotropic cancer types and is the key pathway of bone destruction, dissolving bone-resident growth factors like Transforming Growth Factor- β (TGF- β) that further drive tumor growth (Harada et al., 2021; Siclari et al., 2007; Wang et al., 2019). Notably, it is reasonable to assume that bone destruction drives dissemination by removing physical barriers, yet such concept was not proven yet.

In summary, the release of MM cells from the BM is a complex process that involves dynamic regulation of CAMs, autocrine signaling, and hypoxia, but also the degradation of bone tissue. These processes are not fully understood and require further investigation to formulate strategies that prevent uncontrolled spread of MM cells and support modern therapies.

MSCs: Mesenchymal Stromal (Stem) Cells

The previous sections mentioned MSCs several times as BMSCs, being a crucial component of the BMME in the context of multiple myeloma (Mangolini & Ringshausen, 2020). Before discussing their role in MM specifically, it is important to understand what an MSC is and what impact this cell type has on biomedical research.

Explaining what an MSC is, can be challenging. MSCs are derived from multiple different sources, serve a wide array of functions and are always isolated as a heterogenous group of cells. This makes it particularly challenging to find a consensus on their exact definition, nomenclature, exact function and *in vivo* differentiation potential. Therefore, the following paragraphs provide a brief overview of the biology of MSCs set within a historical context.

MSCs first gained popularity as a stem cell. Because of their significance in biology and

regenerative medicine, stem cells have become a prominent subject in modern research. human Mesenchymal Stromal Cells (hMSCs) have been presented as promising candidate in the context of regeneration, given that they feature intriguing immunomodulatory capabilities, easy isolation and *in vitro* expansion, and safety for both autologous and allogeneic transplantation (I. Ullah et al., 2015).

Stem cells lay the foundation of multicellular organisms. A traditional definition of a stem cell is that of an undifferentiated cell that divides asymmetrically, generating one daughter cell with maintained stemness and one differentiated daughter cell (Cooper, 2000; Shenghui et al., 2009). However, asymmetric cell division is no absolute requirement for maintaining stemness[†], or for generating differentiated cells (Morrison & Spradling, 2008; Yamashita et al., 2010; Shahriyari & Komarova, 2013; Nakamura et al., 2018). Recent findings explain differentiation with epigenetic mechanisms, where chromosomes are reorganized on a macroscopic scale (Dixon et al., 2015): Chromosomal regions of mega-base size called Topologically Associated Domains (TADs)—each containing approximately 3 genes (Long et al., 2022)—are condensed to heterochromatin (Ciabrelli & Cavalli, 2015). Heterochromatin renders genes inaccessible and hence decreases the overall transcriptional plasticity of a cell (Stancheva, 2011; Xie et al., 2013; C. Chen et al., 2019). Differentiation can be initiated by one transcription factor per lineage, which in turn activates an array of genes to facilitate epigenetic, morphological, and functional changes in the cell (Almalki & Agrawal, 2016; Walewska et al., 2023).

Embryonic stem cells orchestrate growth and patterning during embryonic development. They are pluripotent, meaning they can differentiate into any cell type of the adult body. *Adult stem cells*—also known as *somatic stem cells*—maintain tissue homeostasis and repair during adulthood. They are multipotent, meaning they can differentiate into a limited number of cell types. The concept of adult stem cell was coined through research on Hematopoietic Stem Cells (HSCs), the primary progenitors of all types of blood cells (Lee & Hong, 2019; Nunes & Loeffler, 2024). The decade-long lack of proof for asymmetric cell division in human adult stem cells has led to a debate on whether the term *adult stem cell* is a misnomer, with some proposing their classification as *progenitor cells* instead (Bhartiya, 2015). However, this claim seems to be refuted: For once, Nunes & Loeffler (2024) summarize recent evidence of asymmetric distribution of cell fate determinants in HSCs. But as previously noted, asymmetric cell division is not a strict requirement for stemness (Shahriyari & Komarova, 2013).

[†] Morrison & Spradling (2008):

“Overall, the evidence suggests that mammalian stem cells employ both symmetric and asymmetric divisions to regulate their numbers and tissue homeostasis, and that neither mechanism is likely to be constitutively used as a way of sustaining the niche”

Despite proven multipotency, the term *Stem* in MSC is deprecated, with *Stroma* being preferred. This improves precision by avoiding confusion with *mesenchymal tissue*, which is found only in embryos, whereas *stroma* implies an adult identity (Robey, 2017). Robey (2017) argues to abandon the term MSC completely, but rather use tissue specific names such as BMSC, given the profound differences between MSCs from different sources (Jansen et al., 2010; Sacchetti et al., 2016).

Mesenchyme is a term used by histologists that describes a transitory connective tissue first appearing during embryonic development (Robey, 2017). It emerges from mesoderm, which in turn emerges from epithelial cells committed to a mesodermal fate, followed by a loss of cell junctions and free migration away from the epithelial layer. This process is called Epithelial-Mesenchymal Transition (EMT), a process often exploited by cancer cells to metastasize (Tam & Beddington, 1987; Nowotschin & Hadjantonakis, 2010). Hence, the term mesenchyme describes non-epithelial embryonic tissue differentiating into mesodermal lineages such as bone, muscles and blood.

MSCs were first isolated from adult bone marrow, but weren't immediately associated with mesenchyme. They were described as osteogenic precursors since they were shown to differentiate into bone tissue (A. J. Friedenstein et al., 1966; A. Friedenstein & Kuralesova, 1971; Bianco, 2014). Decades later, A. Caplan (1991) coined the term *mesenchymal stem cell* and proposed the “*mesengenic process*”-hypothesis: This concept states that mesenchymal stem cells serve as progenitors for multiple mesodermal tissues (bone, cartilage, muscle, marrow stroma, tendon, fat, dermis and connective tissue) during both adulthood and embryonic development (A. I. Caplan, 1994). Such mesenchymal property was confirmed partially when BMSCs were shown to differentiate into adipocytic (fat) and chondrocytic (cartilage) lineages (Pittenger et al., 1999). Since then, the term “*mesenchymal stem cell*” (MSC) has grown popular as an adult multipotent precursor to a couple of mesodermal tissues. BMSCs were successfully differentiated into osteocytes, chondrocytes, adipocytes and cardiomyocytes (Gronthos et al., 1994; Muruganandan et al., 2009; Xu et al., 2004). Most impressively, these cells also exhibited ectodermal and endodermal differentiation potential, as they produced cells with neuronal, pancreatic and hepatocytic properties (Barzilay et al., 2009; Wilkins et al., 2009; Gabr et al., 2013; Stock et al., 2014).

It was later established that cultures with MSC-like properties can be isolated from ‘*virtually every post-natal organs and tissues*’, and not just bone marrow (da Silva Meirelles et al., 2006). However, depending on which tissue they originated from, MSCs can differ greatly in their transcription profile and *in vivo* differentiation potential (Jansen et al., 2010; Sacchetti et al., 2016), leading to great debate on MSC terminology (Robey, 2017).

Since MSCs are a heterogenous group of cells, they were defined by their *in vitro*

characteristics. A minimal set of criteria are the following (Dominici et al., 2006): First, MSCs must be plastic adherent. Second, they must express or lack a set of specific surface antigens (positive for CD73, CD90, CD105; negative for CD45, CD34, CD11b, CD19). Third, MSCs must differentiate to osteoblasts, adipocytes and chondroblasts *in vitro*. Together, MSCs exhibit diverse differentiation potentials and can be isolated from multiple sources of the body.

Today, the potential in MSCs lies not their stemness, but rather in their immunomodulatory capabilities. Although, MSCs are not yet established in routine clinical practice—despite thousands of clinical trials covering most of the human body's organs—, they still are among the most studied cell types and are topic of vast research (Abdelrazik, 2023). MSCs are valued for their very high treatment tolerance, but also as an adaptive platform for modifications to improve their therapeutic effects (D'souza et al., 2015). For example, H. Chen & Zhou (2022) boldly announced the translation of modified MSCs into the clinical practice of treating ischemic strokes, whereas Moñivas Gallego & Zurita Castillo (2024) conclude that *further studies are needed*, a statement that's ubiquitous in publications on MSCs based therapies[†]. Still, many fields of research benefit from this vast general understanding of MSCs biology, including this work and the study of the BMME in the context of cancer pathologies such as MM.

Molecular Interactions between MSCs Myeloma Cells

As mentioned in previous sections, MSCs are key drivers of MM progression through mediating retention and survival of MM cells in the bone marrow through e.g. cell adhesion and chemoattractant (Zeissig et al., 2020). However, the impact of MM cells on BMSCs is a lot more far-reaching, influencing cell cycle progression, immune response and bone metabolism (Dotterweich et al., 2016; Fernando et al., 2019). Hence, BMSCs play a complex role in the overall pathology of MM (Mangolini & Ringshausen, 2020). Since bone tissue represents a sturdy physical barrier that MM cells might have to overcome to disseminate, it is crucial to revisit the impact that myeloma cells leave on the BMME.

In healthy bone tissue, there's an equilibrium between bone formation and degradation to maintain turnover, repair and remodelling. (Väänänen, 1993): Mesenchymal stromal cells (BMSCs) differentiate into bone forming osteoblasts, while bone degrading osteoclasts are derived from hematopoietic stem cells. Myeloma cells shift the equilibrium of bone turnover towards degradation, leading to Multiple Myeloma related Bone Disease (MBD)

[†] Abdelrazik (2023):

“Altogether, the articles published in this Special Issue raise more questions than they answer, given that most of the conclusions carry the statement ‘further studies are needed’.”

(Hideshima et al., 2007). MBD is present in 80% of patients at diagnosis and is characterized by osteolytic lesions, osteopenia and pathological fractures (Terpos et al., 2018).

MM cells establish this shift in bone turnover on multiple levels: They directly stimulate osteoclast activity by secreting Macrophage Inflammatory Protein-1 α (MIP-1 α) (Oba et al., 2005), but also indirectly through reprogramming BMSCs by having them produce osteoclast stimulating factor Receptor Activator of Nuclear Factor- κ B Ligand (RANKL) (Tsubaki et al., 2020). This is mediated by Nuclear Factor- κ B (NF- κ B) signaling, a pathway that's crucial for MM pathology which is activated through direct cell-cell contact between myeloma cells and BMSCs via e.g. VCAM-1 (Cippitelli et al., 2023; Roy et al., 2018). NF- κ B is activated in both myeloma cells and BMSCs, but with different outcomes: In myeloma cells, NF- κ B transduces survival signaling and is also a key driver of cell adhesion mediated drug resistance (Roy et al., 2017; Landowski et al., 2003). BMSCs however react with stress-induced senescence and secretion of multiple factors that drive MM pathology, such as RANKL and components of the Senescence-Associated Secretory Phenotype (SASP) (Chauhan et al., 1996; Fairfield et al., 2020).

Another fundamental factor contributing to bone destruction is the suppression of osteogenic differentiation of BMSCs by myeloma cells: MM cells secrete Dickkopf-1 (DKK1) and Sclerostin (SOST) (Qiang et al., 2008; F. Zhou et al., 2013; Colucci et al., 2011). Both inhibit Wingless-related Integration Site (Wnt) signaling that otherwise induces the key osteogenic transcription factor Runt-related Transcription Factor 2 (RUNX2) (Gaur et al., 2005). Myeloma cells also inhibit osteogenic TGF- β signaling by secretion of Activin A, which is induced by adhesion-mediated c-Jun N-terminal Kinase (JNK) activation (Vallet et al., 2010).

Studying MBD shifted the focus onto *antiresorptive therapies* (Hiasa et al., 2021; Johansen et al., 2023). For example, bisphosphonates such as zoledronic acid reduces osteoclast numbers, while antibodies sequester soluble mediators of bone destruction (Johansen et al., 2023). The anti-RANKL antibody *Denosumab* can be used as a replacement of bisphosphonates, especially for patients with renal impairment (Raje et al., 2018). Antibodies against SOST such as *Romosozumab*—initially developed to treat bone fragility during osteoporosis (Iolascon et al., 2023)—showed potential in treating MBD in a mouse model, increasing osteoblastic activity and bone trabecular volume, while decreasing bone destruction (McDonald et al., 2017; Ngomdir et al., 2023). SOST is also overexpressed by osteocytes after direct contact with myeloma cells (Delgado Calle et al., 2013). Another antibody called BHQ880 developed against DKK1 passed a phase IB trial (Iyer et al., 2014). For targeting Activin A, the antibody *Sotatercept* passed two phase 2 clinical trials for treating chemotherapy-induced anemia and MBD (Raftopoulos et al., 2016; Abdulkadyrov

et al., 2014).

Instead of the osteogenic lineage, myeloma cells drive BMSCs towards the adipogenic lineage MM by VCAM-1 signaling, with MM cells stabilizing the adipogenic transcription factor Peroxisome Proliferator-Activated Receptor- γ (PPAR- γ) (Dotterweich et al., 2016; Liu et al., 2020). Furthermore, MM inhibit osteogenic differentiation of BMSCs on an epigenetic level (Allegra et al., 2022). A key mediator of osteogenic differentiation inhibition is Growth Factor Independence 1 (GFI1), a zinc finger protein activated by Tumor Necrosis Factor- α (TNF- α) which recruits Histone Deacetylase 1 (HDAC1) to the promoter of *RUNX2* (D’Souza et al., 2011; Adamik et al., 2017). Intriguingly, the same group was able to prevent activation of GFI1 and rescue osteogenic differentiation by inhibition of p62, an adapter protein involved in autophagy that bridges several signaling pathways, including NF- κ B (Adamik et al., 2018). Teramachi et al. (2016) previously treated mice with the same inhibitor XRK3F2, which resulted in bone formation restricted to MM containing bones. This approach is intriguing, since NF- κ B has remained an untreatable target given its ubiquitous role in cell survival. However, a review by Verzella et al. (2022) clearly disagrees with this notion[†], shifting the focus onto upstream activators and downstream effectors of NF- κ B signaling, a principle that was exemplified by the work of Adamik et al. (2018) on the GFI1/p62 interface. This highlights the need for a thorough characterization of the transcriptional programs elicited by NF- κ B signaling in MM cells and BMSCs, especially during direct cell adhesion.

Overall, MSCs are pivotal within the BMME, serving both structural and responsive roles in MM. NF- κ B signaling, essential in MSC-myeloma interactions, plays a crucial role in myeloma survival and MSC function modification (Cippitelli et al., 2023; Roy et al., 2018). Direct contact is necessary to activate these pathways, aggravating MM pathology. Targeting components of NF- κ B signaling offers therapeutic potential, aiming to disrupt key interactions and inhibit myeloma progression. Deeper molecular understanding of the MSC–Myeloma interactions could lead to therapies that effectively target a cancer microenvironment that’s driving MM progression.

[†] Verzella et al. (2022):

“Collectively, this bulk of evidence demonstrates that the safe and cancer-selective inhibition of the NF- κ B pathway is clinically achievable and promises profound benefit to patients with NF- κ B-driven cancers”

Multidimensional Data in Biomedical Research

As modern biosciences advance, researchers increasingly encounter datasets that are influenced by a variety of independent variables, such as time, dosage, and environmental conditions. These variables introduce multidimensional complexity into datasets, challenging traditional analysis methods. For instance, cell adhesion studies, which are crucial for understanding cellular interactions and cancer metastasis, often require analyses across multiple time points and varying adhesion molecule concentrations, demonstrating a time-dependent variability that significantly impacts biological interpretations (Rebl et al., 2010; McKay et al., 1997; Bolado-Carrancio et al., 2020).

Multidimensional data encompass datasets where multiple *independent variables* (here referred to as *factors*) can influence one *dependent variables* (*outcomes*) (Krzywinski & Savig, 2013). In biomedicine, dependent variables are often continuous (intervals or ratios), whereas independent variables are often categorical (ordinal or nominal), respectively. Categorical variables comprise discrete values called categories or *levels*, which are assigned to experimental conditions or measurement modalities, for example the factor '*time*' could comprise three levels: '*0 h*', '*24 h*', and '*48 h*'. Such setups are attractive, because they are compatible with common hypothesis tests, such as ANOVA (Motulsky, 2017): If the levels of one factor are associated with a different outcome, that factor is considered to have an influence on the dependent variable. Multiple factors address multiple hypotheses, including the influence from each individual factor, but also potential interactions between factors. This makes it crucial to design analysis strategies that can reveal the true structure and value of the data (Krzywinski & Savig, 2013).

A primary example of multidimensional data is multiplex RT-qPCR, where the expression levels of various genes are measured across different samples under varying conditions (Bustin, 2014). Here, the dependent variable is typically the fold change expression values derived from $\Delta\Delta Ct$ calculations (Brankatschk et al., 2012). The independent variables include the genes being measured and the experimental conditions under which the samples are processed.

Microscopy data further illustrate the complexity of multidimensional datasets (Rueden et al., 2017). In this context, the dependent variable might be a quantifiable feature, such as cell count or morphological metrics extracted from image analyses. The independent variables can expand immensely to include factors such as well-plate coordinates in a 96-well plate, Z-positions in confocal microscopy, and time points in time-lapse studies.

Lastly, big-data aggregation tools like Metascape provide a rich source of multidimensional data by integrating various dependent variables, such as gene expression fold

changes and associated *p*-values, with independent variables spanning gene identifiers, gene ontology terms, and ontology classes derived from multiple databases (Y. Zhou et al., 2019). Despite the provision of summarized graphical outputs, the raw data often remain in complex, nested formats within Excel sheets, posing significant challenges for hypothesis-driven research.

This extensive integration of multiple dimensions requires sophisticated visualization and analysis techniques. While basic statistical visualizations suffice for one- or two-dimensional data, more complex data sets necessitate advanced techniques, which allow researchers to visualize and interact with data in ways that elucidate the underlying patterns and relationships (Dunn et al., 2017). However, the gap between available visualization tools and the needs of clinicians or biologists without extensive bioinformatics training remains wide, emphasizing the need for intuitive, user-friendly tools that bridge this knowledge gap and enhance the accessibility of complex data analyses (Dunn et al., 2017).

Nontransparencies in Biomedical Data Analyses

The advent of advanced technologies in biosciences has ushered in an era of *big data*, characterized by unprecedented volumes and complexities of data (Bubendorf, 2001; A. Yang et al., 2017; Ekmekci et al., 2016). This rise has been paralleled by significant challenges in data analysis, particularly impacting the reproducibility of scientific research. 70 % of researchers confirm to have attempted and failed to reproduce published experiments (Baker, 2016), highlighting a reproducibility crisis that questions the reliability of scientific findings (Begley & Ioannidis, 2015; Ioannidis, 2005).

Reproducibility is considered foundational to scientific research, ensuring that findings are reliable and verifiable. Still, its meaning requires precise definition (Goodman et al., 2016). The common understanding of scientific reproduction implies not only that detailed information is provided to enable independent repetition (*transparency*), but also that time and effort is invested into repeating the experiments (*corroboration*). However, since modern biomedical journals are demanding novelty research, and since experiments have become highly specialized and time-intensive, repeating someone else's work is considered neither interesting[†] nor possible for most publications (Flier, 2022; Peng, 2011). Hence, the meaning of reproducibility is confined to *transparency*, a concept that has been applied to many fields, including clinical trials (Goodman et al., 2016; Committee on Strategies for Responsible Sharing of Clinical Trial Data et al., 2015).

[†] Flier (2022):

“There are no scientists with the interest, resources, or incentives to “repeat” or confirm this vast sea of published work, so whether the findings they report are reproducible will simply never be assessed.”

Nevertheless, there is a surprising amount of evidence for nontransparencies in biomedical data analyses: For Microarray-based miRNA profiling, raw data was not reported in more than 40 % of 127 articles, making independent verification impossible (Witwer, 2013). The same study also found that re-analysis of data often times did not support the original conclusions. Furthermore, 44 % of 233 preclinical articles describe statistical tests insufficiently, while few don't describe them at all (Gosselin, 2021). Another study reviewed 147 papers in the field of optometrics and found that 91 % did not discuss their rationale of correcting *p*-values for multiple comparisons (e.g. Bonferroni correction) (Armstrong, 2014). However, given that the exact use of multiple comparisons corrections has been under debate for decades, it is reasonable to assume that researchers lack the confidence to report their technique in detail (Perneger, 1998; Moran, 2003; Sullivan & Feinn, 2021). In general, *p*-values are target of extreme scrutiny and also the cause of many arguments, which themselves are of questionable statistical reasoning[†] (Leek & Peng, 2015). Additionally, statistical illiteracy is a well-known problem among clinicians (Lakhlifi et al., 2023). Among biomedical researchers, 77 % state that they have not received formal training in data literacy, including visualization and public deposition of data, although they understand its high relevance (Federer et al., 2016). Correspondingly, it has been communicated that there is a lack of intuitive tools to embed computational work into publications, but also a lack of bioinformaticians to translate computation into clinics (Mesirov, 2010; Smith et al., 2018; Gómez-López et al., 2019). Therefore, nontransparencies in biomedical analyses are not only caused by a habit[‡] of insufficient reporting, but could be exacerbated by the confusions caused by currently available methodologies and the lack of proper training.

Semi-Big Data: Big Enough to Cause Problems

Recent advances in big data analysis have significantly improved the standardization of both raw data availability and processing pipelines (Gomez-Cabrero et al., 2014). Particularly in RNAseq analysis, automation and the use of sophisticated software have established standards that enhance reproducibility across studies. For example, tools such as STAR and HISAT for sequence alignment, and Cufflinks and DESeq for differential expression analysis, rely on scripts that standardize processing steps to produce repeatable and verifiable results (Dobin et al., 2013; Kim et al., 2015; Trapnell et al., 2012; Love et al., 2014). These frameworks not only automate data handling but also ensure that data analysis protocols

[†] Leek & Peng (2015):

“Arguing about the P value is like focusing on a single misspelling, rather than on the faulty logic of a sentence”

[‡] Peng (2011):

“[...] old habits die hard, and many will be unwilling to discard the hours spent learning existing systems.”

are followed consistently, reducing human error and variability between different users or laboratories.

However, this level of standardization and automation has not been mirrored in the analysis of *semi-big data*. Semi-big data, as introduced in this thesis, describes datasets that are on the cusp of manageability: substantial enough to overwhelm manual analysis methods yet not sufficiently large or uniform to justify the heavy computational frameworks developed for big data. Such data are frequently generated in experiments like automated microscopy or multiplex qPCR, where the scale and complexity of the data can vary significantly depending on the experimental design and objectives (Krzywinski & Savig, 2013).

Researchers often revert to basic tools such as *Microsoft Excel* for analyzing these semi-big datasets (Incerti et al., 2019). While Excel provides familiarity and immediate accessibility, it lacks the sophisticated data handling capabilities necessary for efficient and error-free processing of complex (multidimensional) datasets. This reliance on manual methods not only makes the analysis laborious and prone to mistakes but also significantly impedes the reproducibility of research findings. The time and effort required to replicate analyses done manually mean that validating findings from semi-big data can be prohibitively challenging for peer reviewers and other researchers in the field.

Given these challenges, there is a critical need for developing new tools and frameworks specifically tailored for semi-big data. These tools should bridge the gap between the simplicity of user-friendly software like Excel and the robust, script-based automation seen in big data frameworks. By providing standardized, repeatable, and easy-to-use methods for handling complex datasets, such tools could significantly enhance the reliability and efficiency of research involving semi-big data, ultimately supporting broader scientific inquiry and verification.

The Shortcomings of Common Biomedical Analysis Tools

Interactive software systems commonly used for exploratory data analysis in biomedical research often lack mechanisms to track and reproduce the researcher's actions systematically. Even when analysis is performed using scripting languages, the integration of results from multiple packages without a coherent record of the commands and code used undermines reproducibility. This practice can obscure analysis, making it difficult, if not impossible, for other researchers to replicate the results (Leek & Peng, 2015; Peng, 2011; Mesirov, 2010; Localio et al., 2018).

A particularly illustrative example is *GraphPad Prism*, a tool ubiquitously employed

across biomedical disciplines for statistical analysis. Despite its widespread use, it does contribute to data analysis nontransparencies due to *Prism*'s closed-source nature and the common journal practice of not requiring detailed methodological transparency in its usage, a practice that is common in biostatistics literature (Gosselin, 2021; Localio et al., 2018). Furthermore, *GraphPad Prism* still requires manual data entry and lacks the robustness and automation necessary for handling multidimensional or semi-big data. Although, *GraphPad Prism* is compatible “*multiple variable tables*”—similar to long-form tables known from Wickham (2014)—, but does not automatically graph these kinds of tables, but only user specified subsets (*GraphPad Prism 10 User Guide*, 2024).

Moreover, *Microsoft Excel*, another staple in data processing in biomedicine, is notoriously inadequate for handling multidimensional data and complex statistical analyses. Its limitations include poor error tracking, absence of change documentation (audit trails), and a propensity for introducing errors that often go unnoticed, such as converting gene names to dates (Ziemann et al., 2016). To compensate for these shortcomings, *Microsoft* has recently integrated a Python interpreter into *Excel*, allowing researchers to automate tasks and analyze data efficiently and correctly (Excel, 2023).

Indeed, many common tools in biomedicine allow for scripting or automation to handle semi-big data more effectively. For example, *Fiji/ImageJ*, a popular image processing platform, supports extensive macro and scripting capabilities (Rueden et al., 2017). These features enable researchers to automate batch processing of image data, streamlining tasks that would otherwise require laborious manual input. Similarly, *PyMOL*, a leading tool in protein structural biology, utilizes Python scripting to automate complex tasks, allowing for detailed molecular modeling and visualization that are reproducible and scalable across datasets (Schrödinger, LLC, 2015; Rigsby & Parker, 2016).

Although automation scripts used in tools like *Fiji/ImageJ* and *PyMOL* improve transparency for publishing singular data analysis pipelines, they still face challenges that can impede their reproducibility (Peng, 2011; Sandve et al., 2013): These scripts sometimes require specialized software environments, where setting up dependencies and configurations can be complex enough to discourage replication efforts. Additionally, these scripts do not always provide comprehensive outputs of intermediate steps, which is crucial for verifying and understanding the progression of data analysis (Sandve et al., 2013).

On the other hand, when scripts are designed to be more generalized and distributed—for instance, as a *Fiji/ImageJ* plugin or a standalone application—they can make substantial contributions to scientific research by enabling other researchers to apply these tools to their own data sets (Pichler et al., 1998; Wilkinson et al., 2016). However, this approach also comes with its own set of challenges (Sandve et al., 2013). These generalized

tools often lack comprehensive user-manuals (*documentation*) and are not thoroughly tested across different platforms or data sets, which can lead to unexpected errors that can not be fixed by the user. Moreover, even when these tools are available, they frequently suffer from low adoption rates, meaning that few people are familiar with the details of such tools, further decreasing the confidence and reproducibility in the final results.

Given these complexities, there is a pressing need for new analytical tools specifically designed for semi-big data. These tools must strike a balance between the ease of use found in basic software and the robust, analytical capabilities of more sophisticated systems. By providing standardized workflows, comprehensive documentation, and ensuring cross-platform compatibility, these tools can significantly enhance reproducibility. They not only allow researchers to perform analyses more efficiently but also ensure that these analyses are robust, transparent, and easily verifiable by the broader scientific community.

This thesis presents a software environment developed in Python, designed to bridge this gap. It demonstrates that even minimal coding skills can be leveraged to create powerful tools that standardize and accelerate the analysis of semi-big data, ultimately fostering more reproducible and trustworthy scientific research.

Modern Standards of Software Development

A main reason to write software is to define reusable instructions for task automation (Pichler et al., 1998). The complexity of software code makes it prone to errors, which can prevent its usage by persons other than the author himself. This is a problem for the general scientific community, as the software is often essential for reproduction (Sandve et al., 2013). Hence, modern journals aim to enforce standards to software development, including software written and used by biological researchers (Smith et al., 2018). Here, we provide a brief overview of the standards utilized by `plotastic` that ensure its reliability and reproducibility by the scientific community (Peng, 2011).

Modern software development is a long-term commitment of maintaining and improving code after initial release (Boswell & Foucher, 2011). Hence, it is good practice to write the software such that it is *scalable*, *maintainable* and *usable*. *Scalability* or, to be precise, *structural scalability* means that the software can easily be expanded with new features without major modifications to its architecture (Bondi, 2000). This is achieved by writing the software in a modular fashion, where each module is responsible for a single function. *Maintainability* means that the software can easily be fixed from bugs and adapted to new requirements (Kazman et al., 2020). This is achieved by writing the code in a clear and readable manner, and by writing tests that ensure that the code works as expected

(Boswell & Foucher, 2011). *Usability* is hard to define (Brooke, 1996), yet one can consider a software as usable if the commands have intuitive names and if the software's manual, termed *documentation*, is up-to-date and easy to understand for new users with minimal coding experience. A software package that has not received an update for a long time (approx. one year) could be considered abandoned. Abandoned software is unlikely to be fully functional, since it relies on other software (dependencies) that has changed in functionality or introduce bugs that were not expected by the developers of all dependencies. Together, software that's scalable, maintainable and usable requires continuous changes to its codebase. There are best practices that standardize the continuous change of the codebase, including version control, continuous integration (often referred to as CI), and software testing.

Version control is a system that records changes to the codebase line by line, documenting of the detailed history of the codebase, including the person and timepoint of every change. This is required to isolate new and experimental features into newer versions and away from the stable version that's known to work. The most popular version control system is Git, which is considered the industry standard for software development (Chacon & Straub, 2014). Git can use GitHub.com as a platform to store and host codebases in the form of software repositories. GitHub's most famous feature is called "pull request". A pull request is a request from anyone registered on GitHub to include changes to the codebase (as in "*please pull this into your main code*"). One could see pull requests as the identifying feature of the open source community, since it exposes the codebase to potentially thousands of independent developers, reaching a workforce that is impossible to achieve with closed source models used by paid software companies.

Continuous integration (CI) is a practice of software development where code changes are integrated several times a day into a shared repository (Duvall et al., 2007). Each integration triggers the test suite, aiming to detect errors as soon as possible. The test suite includes building the software, setting up an environment for the software to run, and then executing the programmed tests, ensuring that the software runs as a whole. Continuous integration is often used together with software branches. Branches are independent copies of the codebase that are meant to be merged back into the original code once the changes are finished. Since branches accumulate multiple changes over time, this can lead to minor incompatibilities between the branches of all developers (integration conflicts), which is something that CI helps to prevent.

Continuous integration especially relies on a thorough software testing suite. Software testing is the practice of writing code that checks if the codebase works as expected (Myers et al., 2011). The main type of software testing is unit testing, which tests the smallest

units of the codebase (functions and classes) in isolation (Listing 1). Software testing is automated by specialized frameworks that execute the tests and report the results, a popular example being `pytest`, which is utilized by `plotastic` (Krekel et al., 2004).

Listing 1: Example of an arbitrary Python function and its respective unit test function. The first function simply returns the number 5. The second function tests if the first function indeed returns the number 5. The test function is named with the prefix “`test_`” and is placed in a file that ends with the suffix “`_test.py`”. Testing frameworks such as `pytest` scan the repository for files that end with “`_test.py`” and execute the functions that start with “`test_`”. Note that code after “`#`” is considered a comment and won’t be executed.

```
1 # Define a function called "give_me_five" that returns the number 5
2 def give_me_five():
3     return 5
4 # Define a test function asserting that "give_me_five" returns 5
5 def test_give_me_five():
6     assert give_me_five() == 5
```

The quality of the software testing suite is measured by the code coverage, the precision of the tests, and the number of test-cases that are checked. The code coverage is the percentage of the codebase that is called by the testing functions, which should be as close to 100% as possible, although it does not measure how well the code is tested. The precision of the test is not a measurable quantity, but it represents if the tests truly checks if the code works as expected. The number of test-cases is the number of different scenarios that are checked by the testing functions, for example testing every possible option or combinations of options for functions that offer multiple options.

Together, the standards of software development, including version control, continuous integration, and software testing, ensure that the software is scalable, maintainable, and usable. This is especially important for software that is used by the scientific community, as it ensures that the software is working as expected at defined versions years after publishing scientific results.

What makes Python an “Easy” Programming Language?

Here, we provide a general overview of the Python programming language, explaining terms like “`type`”, “`method`”, etc., in order to prepare readers without prior programming experience for the following chapters. We also describe the design principles of Python to lay out the key concepts that differentiate Python compared to other programming languages. A more detailed tutorial on Python that’s specialized for bioscientists is found in Ekmekci et al. 2016.

Languages such as Python are considered “*high-level*”, meaning that it is designed to be easy to read and write, but also independent of hardware by hiding (“*abstracting*”)

underlying details (*The Python Language Reference*, 2024). A key principle of Python is the emphasis on implementing a syntax that is concise and close to human language (Listing 2, Listing 3).

Listing 2: Example of readable Python code. This one-line code returns the words (string) "Hello, World!" when executed. The command is straightforward and easy to understand.

```
1 print("Hello, World!")
2 # Expected output: Hello, World!
```

Listing 3: Example of less readable code written in the low-level programming language C. This code is doing exactly the same as the Python code in Listing 2, but is harder to understand because more steps are needed, including the import of a library stdio.h and the definition of a function called main. Note that C uses // to begin comment sections.

```
1 #include <stdio.h>           // Import functions for standard input & output
2 int main() {                  // Define a function called 'main'
3     printf("Hello, World!");
4     return 0;
5 }
6 // Expected output: Hello, World!
```

Furthermore, Python is an *interpreted* language, which means that the code is executed line by line. This makes coding easier because the programmer can see the results of the code immediately after writing it, and error messages point to the exact line where the error occurred (Listing 4). This is in contrast to *compiled* languages, where the code has to be compiled into machine code before it can be executed. The advantage of compiled languages is that the code runs faster, because the machine code is optimized for the hardware.

Listing 4: Example of an error message. Since Python is case-sensitive, the error is caused by miss-spelling the variable name hi as Hi. The error message begins with the type of error (NameError), followed by a traceback that shows the sequence of function calls that led to the error. The traceback located the source of the error in the file errormessage.py and points to the line that caused the error. Finally, the error message explains the error, stating that 'Hi' is undefined.

```
1 hi = "Hello World" # Define a variable 'hi' with the value "Hello World"
2 print(Hi)          # Print the value of the undefined variable 'Hi'
3
4 # Expected Output:
5 # -----
6 # NameError                                 Traceback (most recent call last)
7 # File /Users/martinkuric/Documents/errormessage.py:2
8 #     1 hi = "Hello World"
9 # ----> 2 print(Hi)
10
11 # NameError: name 'Hi' is not defined
```

Python automates tasks that would otherwise require an advanced understanding of computer hardware, like the need for manual allocation of memory space. This is achieved by using a technique called “*garbage collection*”, which automatically frees memory space

that is no longer needed by the program. This is a feature that is not present in low-level programming languages like C or C++, that were designed to maximize control over hardware.

Another hallmark of Python is its *dynamic typing system*. In Python the type is inferred automatically during code execution (Listing 5). This is in contrast to *statically typed* languages like C, where the type of a variable has to be declared explicitly and cannot be changed during code execution (Listing 6) (*The Python Language Reference*, 2024).

Listing 5: Example of dynamic typing in Python. The variable “a” is assigned the value 5, which is of type integer. The variable “a” is then overwritten with the value “Hello, World!”, which is of type string. Python allows dynamic re-assignment of variables with different types. Note that code after “#” is considered a comment and won’t be executed.

```
1 a = 5 # Type integer
2 a = 5.0 # Type float
3 a = 'Hello, World!' # Type string
4 a = True # Type boolean
5 a = False # Type boolean
6 a = [1, 2, 3] # Type list of integers
7 a = {'name': 'Regina'} # Type dictionary
```

Listing 6: Example of static typing in C. The variable “a” is declared as an integer (int), and can only store integers. The variable “a” is then assigned the value 5, which is an integer. The variable “a” is then assigned the value ‘Hello, World!’, which is a string. This results in a compilation error, because the variable “a” can only store integers. Note that code after “//” is considered a comment and won’t be executed.

```
1 int a; // Declare type as integer
2 a = 5;
3 a = 'Hello, World!'; // Compilation error!
```

Dynamic typing makes Python a very beginner-friendly language, since one does not have to keep track of the type of each variable. However, this also makes Python a slower language, because the interpreter has to check the type of each variable during code execution. Also, developing code with dynamic typing systems is prone to introducing bugs (TypeError), because it allows unexperienced developers to convert variables from one type to another without noticing, leading to unexpected behavior. Hence, larger Python projects require disciplined adherence to programming conventions. One such convention is *type hinting*, which is a way to explicitly note the type of a variable. Type hinting does not have an effect on the code, but it makes the code more readable and understandable for other developers, and allows for development environments to detect type errors before execution (Listing 7) (van Rossum et al., 2014).

To make Python as easy as possible, python packages aim to reduce the amount of code that has to be written by the user. For example, the package `matplotlib` is a plotting

Listing 7: Example of type hints used in Python. Explicitly stating the type of the variable is optional and does not change the behavior of the code, but behaves exactly as shown in Listing 5.

```
1 a: int = 5
2 a: str = 'Hello, World!'
```

library where every command is written such that the user immediately understands its purpose, like plotting a line or labeling an axis (Listing 8). Hence matplotlib code is a sequence of simple function calls, where the state of the plot is modified and saved in the background line by line.

Listing 8: Example of using pre-written functions of a Python package. The functions of the package `matplotlib.pyplot` become accessible by importing the package as `plt`, where `plt` serves as an alias (or rather shortcut) to access the functions of the package. Then, two arbitrary lists are defined, `x` and `y`. These datapoints are plotted (scatterplot) using the function `plot`. The plots x- and y-axes are then labeled and saved as an image. The code is written in a sequence of function calls, where the state of the plot is saved in the background. The plot is then displayed using the function `show`.

```
1 import matplotlib.pyplot as plt # Make functions accessible via plt
2 x = [1, 2, 3, 4, 5]           # Define arbitrary x values
3 y = [1, 4, 9, 16, 25]         # Define arbitrary y values
4 plt.plot(x, y)               # Plot x against y
5 plt.xlabel('Timepoint')       # Add a label to the x axis
6 plt.ylabel('Foldchange')      # Add a label to the y axis
7 plt.title('Gene Expression') # Add a title above the plot
8 plt.savefig('plot.png')       # Save plot as image onto harddrive
9 plt.show()                   # Show the plot preview
```

However, when no pre-written functions or packages are available, Python offers the tools of a general purpose programming language to write and deploy custom code easily. Programming styles can be classified into two main paradigms: *functional* and *object-oriented* programming, which can be understood as different ways to structure code. Python supports both paradigms. In *functional* programming, the code is written in a way that the program is a sequence of function calls, where each function call returns a value that is used in the next function call (Listing 9). This approach is useful when multiple actions have to be performed on the same data and the structure of the data is relatively simple, for example a string of a DNA sequence.

When the data itself gains in complexity, for example when storing not just the gene sequence, but also the promoter sequence, an *object-oriented* approach is more suitable (Listing 10). Object-oriented programming is a paradigm that uses objects and classes. An object is a collection of both data and functions, and a class is a blueprint for creating objects. The data of an object is stored as *attributes*. Functions that are associated with an object are called *methods*. A major benefit of using an object oriented versus a functional approach is that the data itself is programmable, enabling the programmer to define the behavior of the data through methods. This is achieved by using ‘self’ to reference the

Listing 9: Example of functional programming in Python. The code defines a function called “find_restriction_site” that finds the position of a restriction site in a DNA sequence. The function “cut” uses the function “find_restriction_site” to cut the sequence at the restriction site. To execute both functions, we first define an arbitrary DNA sequence and then call the function cut passing the sequence as an argument.

```

1 def find_restriction_site(sequence: str): # Define a function
2     return sequence.find('GCGC')           # Find the position of 'GCGC'
3
4 def cut(sequence: str):                  # Define another function
5     position = find_restriction_site(sequence) # Use the function above
6     return sequence[position:]             # Cut sequence at the position
7
8 seq1 = 'TGAGCTGAGCTGATGCGCTATTTAGGCG' # Define an arbitrary sequence
9 seq1_cut = cut(seq1)                   # Cut the sequence
10 print(seq1_cut)                      # Show the result
11 # Expected output: GCGCTATTTAGGCG

```

objects themselves inside the class. `self` can be understood as “*this object*”, and is a placeholder for objects that are to be created from the blueprint. `self` is required to access attributes and methods before specific objects are created in order to program how the objects are to be changed when calling methods.

Listing 10: Example of object oriented programming in Python. The class is called “Gene” and acts as a blueprint to create Gene objects. Gene has four methods, “`__init__`”, “`find_promoter`”, “`find_restriction_site`” and “`cut`”. The method “`__init__`” is called when creating (“initializing”) an object, which fills the object with user-defined data. The parameter “`self`” is a placeholder for the objects that are to be created. “`find_promoter`” is a method that finds the position of the promoter in the gene and is called during object initialization.

```

1 class Gene:                         # Define a Gene class
2     def __init__(self, sequence: str): # Define how a Gene object is created
3         self.sequence: str = sequence # Save sequence as attribute
4         self.promoter: str = self.find_promoter() # Automatically find promoter
5         # Add further Gene attributes here
6     def find_promoter(self):        # Define how to find the promoter
7         return self.sequence.find('TATA')
8     def find_restriction_site(self): # Define how to find restriction site
9         return self.sequence.find('GCGC') # Find the position of 'GCGC'
10    def cut(self):                 # Define how to cut the DNA sequence
11        position = self.find_restriction_site() # Call the method above
12        return self.sequence[position:] # Cut the gene at the position
13
14 gene1 = Gene(sequence='TGAGCTGAGCTGATGCGCTATTTAGGCG') # Create Gene object
15 print(gene1.cut())                           # Cut gene and show result
16 # Expected output: GCGCTATTTAGGCG

```

When designing software, both functional and object oriented programming can be used together, where object oriented programming is often used to design the program’s overall architecture, and functional programming is used to implement the algorithms of the program’s features. This allows for scalability of the software, as every single class is extended through the addition of new methods.

Furthermore, classes can be expanded in their functionalities through *inheritance* (Listing 11). Inheritance is a feature of object-oriented programming that allows a class to access every attribute and method of a parent class. For example, one could extend the class “Gene” with a class “mRNA”, by writing a class “mRNA” that inherits from the class “Gene”.

Listing 11: Example of inheritance in Python. The class “mRNA” inherits from the class “Gene”, and has two methods, “`__init__`” and “`find_stopcodon`”. “`find_stopcodon`” loops through a list of stop codons (for `x` in `list`): For each stop codon, the position is found. If a codon wasn’t found, the `.find()` method returns -1, which leads to a different print message. Note that `f` formats strings to include variables.

```

1 class mRNA(Gene):          # Define the mRNA class, inheriting from Gene class
2     def __init__(self, sequence: str):    # Define how an mRNA object is created
3         super().__init__(sequence)        # Get attributes from parent class
4         self.sequence = self.sequence.replace('T', 'U') # Replace T with Uracil
5     def find_stopcodons(self):           # Define how to find stop codons
6         for stopcodon in ['UGA', 'UAA', 'UAG']:   # Loop over stop codons
7             position: int = self.sequence.find(stopcodon) # Find the position
8             if position == -1:                 # If position is -1, codon wasn't found
9                 print(f"{stopcodon} not found") # Message if not found
10            else:                      # If position isn't -1, codon was found
11                print(f"{stopcodon} found at {position}")
12
13 mrna1 = mRNA(sequence='TGAGCTGAGCTGATGCGCTATATTAGGCG') # Create an mRNA object
14 mrna1.find_stopcodons()                                # Show the position of stop codons
15 # Expected outputs:
16 # UGA found at 0
17 # UAA not found
18 # UAG found at 24

```

Together, Python is not just beginner-friendly, but also well respected for its ease in development, which is why it is widely used in professional settings for web development, data analysis, machine learning, biosciences and more (Ekmeekci et al., 2016; Rayhan & Gross, 2023).

The Potential of Python Data Science Packages for Biomedicine

Python includes a vast number of built-in packages used for basic data-types, software development, simple math operations, etc., (*The Python Language Reference*, 2024). Still, Python relies on packages developed by its users to provide specialized tools for data analysis. A Python package consists of multiple Python *modules*, where each module is a text-file with a `.py` ending containing Python code. Famous examples of such packages are pytorch and tensorflow, that are used to build models of artificial intelligence, including *ChatGPT* (Paszke et al., 2019; Abadi et al., 2016; Openai/Gpt-2, 2024). Here, we outlay the most important packages used for plotastic in Chapter 2 and present examples how these

packages are utilized in modern biomedical research.

Interactive Python: The standard Python interface is insufficient for data science, because it lacks the tools to quickly and conveniently visualize and explore data. IPython can be understood as an enhanced version of the standard Python interpreter, designed to improve the interactivity of Python code execution (Perez & Granger, 2007). IPython introduces features like rich media support to display graphics, but also helps users to use correct python data types through dynamic type introspection, detecting errors in the code. This functionality is akin to what *MATLAB* and *RStudio* provide through their advanced graphical user interfaces and extensive debugging tools. IPython is most often utilized in the form of *Jupyter Notebooks*.

Jupyter: Jupyter is an evolution of IPython, introducing the *Jupyter notebook* format, which has the file-ending .ipynb (Kluyver et al., 2016). Jupyter Notebooks are documents that combine both code and text structured as *code cells* and *markdown cells*, respectively. Markdown cells allow the author to provide additional information with text formatting, for example structuring the document with headings and subheadings, adding hyperlinks, images and mathematical formulas. Code cells can be executed individually, displaying the output directly below the cell. This allows for an interactive exploration of data, but also makes Jupyter Notebooks a very human-readable format that outlays data analysis in a clear manner with precise and reproducible documentation of all data processing steps. Another major benefit of Jupyter Notebooks are interchangeable *Kernels*, allowing the execution of code in different programming languages, such as R, Julia, and C++ (Giorgi et al., 2022). Today, Jupyter Notebooks have become a standard format compatible with collaborative platforms like *Google Colab* and *JupyterLab*, but also professional software development tools like *VS Code*, and *PyCharm*. For biomedical research, Jupyter Notebooks are a powerful solution for improving reproducibility: They elegantly combine both documentation and code execution into a concise presentation of the data analysis process, hence being an intuitive tool that directly captures and embeds computational work into papers, a requirement postulated by Mesirov (2010). Jupyter notebooks are increasingly found in the supplemental of modern publications of both bioinformatics and wet-lab research (Taskiran et al., 2024; Bosch-Queralt et al., 2022; Howe & Chain, 2015).

NumPy: Central processing units (CPU) usually execute one instruction on one data point at a time. For manipulating tabular data, this is inefficient as the same instruction must be repeatedly loaded for every data point. NumPy accelerates the mathematical capabilities of Python by enabling large-scale operations on multi-dimensional arrays and matrices with high efficiency (Harris et al., 2020). One key feature of NumPy is the implementation of “vectorization” or SIMD (Single Instruction, Multiple Data) instructions.

SIMD allows multiple data points to be processed simultaneously, significantly speeding up operations that are inherently parallelizable, such as matrix addition or multiplication. NumPy's syntax and functional approach to array manipulation have set a standard for matrix computation, influencing the design of advanced AI frameworks such as PyTorch and mxl, which mirrors several of NumPy's functionalities to facilitate ease of use for those familiar with NumPy (Paszke et al., 2019; Hannun et al., 2023). This standardization has made NumPy an attractive tool not only in genomics (Ding et al., 2023), but also for modern clinical applications like imaging technologies and augmented-reality in surgery (Thompson et al., 2020).

Pandas: Tables are the most common way to store experimental results. Pandas extends Python with a tabular datatype, called DataFrame, which allows for easy data manipulation with integrated indexing (McKinney, 2011). The intuitive interface of Pandas can be likened to *Microsoft Excel*; however, it is vastly more powerful due to its speed, functionality, and ability to handle larger datasets, e.g. by running efficient numpy vectorization in the background. Unlike *Excel*, Pandas enables automation by summarizing processing commands into scripts, documenting each step, and ensuring reproducibility. Pandas is used in biomedicine for data wrangling, data cleaning, and data analysis, as it allows for the integration of multiple data sources into a single table (Santos et al., 2020).

matplotlib: matplotlib is a plotting library that provides a wide range of static, animated, and interactive plots and graphs (Listing 8) (Hunter, 2007). It serves as the foundation for many visualization tools and is particularly valued for its flexibility and customization options. For example, Pandas uses matplotlib to plot column datapoints directly from a DataFrame object, creating histograms or scatter plots, which is useful for preliminary data analysis and checking data distributions. However, matplotlib uses a low-level syntax, hence plots generated by matplotlib can be cumbersome to format and customize.

seaborn: While the low-level syntax of matplotlib is valued for its flexibility, formatting publication grade plots can be laborious, and its inconsistent syntax can make it difficult to remember the correct commands for different plot types. seaborn is a high-level interface on top of matplotlib that offers a more intuitive and highly standardized syntax across a wide array of plot types (Waskom, 2021). seaborn also integrates closely with Pandas data structures: It automatically groups datapoints, calculates measures of both central tendency (e.g. mean, median) and variance (e.g. standard deviation), and displays them into the plot (e.g. error bars). This completely replaces manual calculation of descriptive statistics. seaborn also offers intuitive grouping (*facetting*) of data points, which simplifies the creation of complex visualizations involving multidimensional data,

making it easier to reveal patterns and relationships via color encoding, faceting, and automated statistical fits. This is particularly useful in biomedical research for visualizing and understanding complex datasets, such as large quantities of protein data (Krzywinski & Savig, 2013; Weiss, 2022). `seaborn` could indirectly contribute to improving reproducibility in biomedical research by making visualizations of complex data very accessible through an easy and standardized syntax.

Pingouin: Integrating both data visualization and statistical analysis is beneficial for researchers who wish to conduct advanced statistical analysis without switching between different software environments. `Pingouin` is designed to be a user-friendly statistical tool that offers a straightforward syntax for performing statistical tests, which are commonly implemented in R (Vallat, 2018). Unlike R, `Pingouin` integrates seamlessly within the Python ecosystem, which allows combining data manipulation, analysis, and visualization all in one platform. This improves reproducibility by reducing the number of software tools required to analyze data. Despite its potential to streamline the data analysis process, `Pingouin` has not been widely adopted by biomedical research, yet. One example of a study that utilized `Pingouin` is the work of Kelly et al. (2023) in the field of Patient Public Involvement (PPI), producing an ethical matrix to organize stakeholder opinion in medical research design. This lack of `Pingouin`'s adoption in biomedicine could be due to recent development and the dominance of R in the field. However, since Python offers multiple benefits over R in syntax, software development, runtime performance and integration with other tools (like including performant C++ code), `Pingouin` is an attractive standard for future statistical analyses in biomedicine (Gorelick & Ozsváld, 2020).

statannotations: While `seaborn` and `matplotlib` offer a wide range of statistical plots, they lack the ability to automatically annotate plots with *p*-values often abbreviated by stars. `statannotations` is a package that extends `seaborn` by providing an interface to add statistical annotations to plots, but also perform simple statistical tests (Charlier et al., 2022). It is limited to only pairwise comparisons such as t-tests and can not perform omnibus tests like ANOVA.

Together, these python packages form the backbone of modern data analysis in Python, often times combining software from different languages to accelerate certain features, while retaining the ease of use and readability that Python is known for. This is particularly advantageous in the field of biomedicine, where the requirements of modern data analysis are often complex and require a high degree of flexibility and customization.

Aims

This PhD thesis is designed to bridge significant gaps in the understanding and analysis of myeloma cell behavior and the handling of complex biomedical datasets. The specific aims are as follows:

- Develop an *in vitro* model to elucidate the mechanisms of myeloma cell dissemination in interaction with mesenchymal stromal cells (hMSCs), focusing particularly on:
 - Observing and quantifying cell proliferation, attachment, and detachment dynamics using time-lapse microscopy.
 - Isolating and characterizing distinct myeloma subpopulations interacting with hMSCs to understand differential gene expression related to cell adhesion and patient survival.
- Design and implement a Python-based software tool, `plotastic`, to facilitate the analysis of multidimensional datasets generated in biomedical research. This tool will aim to:
 - Streamline the data analysis process, making it more efficient and reproducible.
 - Integrate visualization and statistical analysis capabilities to ensure that data analysis protocols are aligned with the ways in which data is visualized.
 - Provide a case study demonstrating the application of `plotastic` in the analysis of *in vitro* dissemination experiments, emphasizing the tool's ability to handle semi-big data and enhance reproducibility.
- Synthesize the findings from the experimental and software development components to advance the understanding of myeloma dissemination and improve research practices in biomedical data analysis.

These aims are crafted to address both the biological and technical challenges in current cancer research methodologies and data science applications in biomedicine, fostering advancements that could lead to novel therapeutic strategies and more robust scientific inquiries.

Additional Materials & Methods

Erklärung zur Nutzung von *ChatGPT*, *GitHub Copilot* und sonstiger Software

Als Grundlage dieses Schreibens nennt der Autor die Eidesstattliche Erklärung (Affidavit), welche zur Angabe von Hilfsmitteln auffordert, aber nicht explizit die Nutzung von Hilfsmitteln als Einschränkung der Eigenständigkeit des Autors betrachtet. Ebenso wird auf die Stellungnahme des Präsidiums der Deutschen Forschungsgemeinschaft (DFG) zum Einfluss generativer Modelle für die Text- und Bilderstellung auf die Wissenschaften und das Förderhandeln der DFG (September 2023) verwiesen: Der Einsatz generativer Modelle wie *ChatGPT* soll nicht ausgeschlossen werden, sondern erfordert transparente und nachvollziehbare Dokumentation, um wissenschaftliche Integrität zu gewährleisten. Wissenschaftler müssen offenlegen, ob und wie sie generative Modelle verwendet haben, und sicherstellen, dass keine Verletzung geistigen Eigentums oder wissenschaftliches Fehlverhalten vorliegt.

KI-Chatverläufe sind in der digitalen Version dieser Arbeit einsehbar (<https://github.com/markur4/Dissertation>) und dienen als Beweis zur Einhaltung der hier genannten Prinzipien. Dem ist hinzuzufügen, dass die in den Chat-Verläufen generierten Texte einen weiteren manuellen Bearbeitungsverlauf nicht dokumentieren, weswegen auch ignorierte oder auch vollständig vom Autor umgeschriebene Abschnitte in den Chat-Verläufen enthalten sind.

Der Autor bemerkte selbstständig folgende Mängel generativer KI-Modelle:

- Fehlerhafte Logik
- Tendenz, die Meinung des Nutzers zu bestätigen
- Mangel an Präzision und Nutzung abstrakter Formulierungen
- Halluzinieren von nicht existierenden wissenschaftlichen Quellen

Der Autor entschied sich, auch zur Wahrung wissenschaftlicher Integrität, dass KI keinen entscheidenden Einfluss auf die Kernaussagen der bearbeiteten Abschnitte ausüben sollte. Um dies sicherzustellen, wurden generative KI-Modelle für folgende Zwecke nicht genutzt:

1. Übernahme wissenschaftlicher Fakten, die über etabliertes Lehrbuchwissen hinausgeht.

2. Erweiterung des Ideengehalts der Arbeit, die über eine Verfeinerung von selbstständig erdachten oder recherchierten Konzepten hinausgeht.
3. Übernahme KI-generierter Texte ohne nachfolgender Überarbeitung durch den Autor.
4. Analyse und Interpretation von Daten.

ChatGPT (Versionen 3.5, 4 und 4.0) wurde für folgende Zwecke benutzt:

1. Ausformulierung kohärenter Textabschnitte basierend auf manuell erstellten rohen Textabschnitten und Stichpunkten.
2. Iterative Verbesserung der Formulierungen: Erstellen einer Erstfassung ausgehend von einer Rohfassung, Ausgabe einer durch *ChatGPT* verbesserten Version, Abänderung durch den Autor, etc.
3. Erstellung von zusammenfassenden Abschnitten (z.B.: Summary, Aims, Conclusion) mit nachfolgender Überarbeitung.
4. Prüfung auf akademische Sorgfalt bei fest etablierter Terminologie, z.B. um Neudeinitionen bereits bestehender Konzepte zu verhindern.
5. Übersetzen der Summary von Englisch auf Deutsch
6. Programmierhilfe zur Formatierung in LaTeX.
7. Suche nach weiteren Quellen zu bereits erarbeiteten Inhalten, falls nicht halluziniert.

GitHub Copilot (Version 1.198.0) ist als Programmierhilfe spezialisiert und wurde genutzt, um begonnene Sätze oder Code zu vervollständigen und Bugs zu beheben.

Aus diesen Grundsätzen ist ersichtlich, dass generative KI-Modelle ausschließlich als Programmier-, Phrasierungs- und Zusammenfassungshilfe genutzt wurden, vergleichbar mit als unbedenklich geltenden Tools wie Grammarly. Dem entsprechend hätte diese Arbeit problemlos ohne *ChatGPT* oder *GitHub Copilot* angefertigt werden können, was die Eigenständigkeit des Autors sicherstellt.

Ebenso wurde folgende sonstige Software verwendet:

- *Visual Studio Code (VS Code)* als Code und LaTeX Editor, einschließlich Plugins (z.B. zur Korrektur von Grammatik)
- LaTeX (MacTeX Distribution)
- *Zotero* zur Zitation von Quellen und automatisierten Erstellung des Quellenverzeichnisses, einschließlich Plugins (ZotFile, Better BibTex, etc.)
- *Affinity Publisher* zur Montage von Abbildungen

Declaration of *ChatGPT*, *GitHub Copilot*, and Other Software Usage

The basis of this declaration is the Affidavit, which requires the disclosure of aids but does not explicitly consider the use of aids as a limitation on the author's independence. Additionally, the statement by the Presidium of the German Research Foundation (DFG) on the influence of generative models for text and image creation on the sciences and DFG funding (September 2023) is referenced: The use of generative models like *ChatGPT* should not be excluded but requires transparent and comprehensible documentation to ensure scientific integrity. Scientists must disclose whether and how they used generative models and ensure that no intellectual property is violated or scientific misconduct occurs.

AI-chat logs are accessible in the digital version of this work (<https://github.com/markur4/Dissertation>) and serve as proof of compliance with the principles outlined here. It should be noted that the texts generated in the chat logs do not document subsequent manual revision, which is why ignored or also completely rewritten sections by the author are included in the chat logs.

The author independently noticed the following deficiencies of generative AI models:

- Logical flaws
- Tendency to confirm the user's opinion
- Lack of precision and use of abstract formulations
- Hallucination of non-existent scientific sources

The author decided to maintain scientific integrity by preventing AI from having a decisive influence on the core statements of the processed sections. To ensure this, generative AI models were not used for the following purposes:

1. Adopting scientific facts that transcends established textbook knowledge
2. Expansion of the idea content of the work that transcends the refinement of independently conceived or researched concepts
3. Adoption of AI-generated texts without subsequent revision by the author.
4. Analysis and interpretation of data.

ChatGPT (versions 3.5, 4, and 4.0) was used for the following purposes:

1. Formulation of coherent text sections based on manually created raw text sections and notes
2. Iterative improvement of formulations: Creating a first draft based on a raw draft, generating a version improved by *ChatGPT*, revising by the author, etc.

3. Creation of summarizing sections (e.g., Summary, Aims, Conclusion) with subsequent revision
4. Checking for academic rigor with well-established terminology, e.g. to prevent redefinitions of already existing concepts.
5. Translating the Summary from English to German
6. Programming assistance for formatting in LaTeX
7. Searching for additional sources for already developed content, if not hallucinated

GitHub Copilot (version 1.198.0) is specialized as a programming aid and was used to complete started sentences or code and to fix bugs.

From these principles, it is evident that generative AI models were used exclusively as programming, phrasing, and summarizing aids, comparable to tools such as Grammarly, which are considered unobjectionable. Accordingly, this work could have been completed without *ChatGPT* or *GitHub Copilot*, ensuring the author's independence.

The following other software was also used:

- *Visual Studio Code (VS Code)* as code and LaTeX editor, including plugins (e.g., for grammar correction)
- LaTeX (MacTex distribution)
- *Zotero* for citation of sources and automated creation of the bibliography, including plugins (*ZotFile*, *Better BibTex*, etc.)
- *Affinity Publisher* for image montage

Chapter 1: Modelling Myeloma Dissemination *in vitro*

The following chapter—including referenced appendices—has been taken with slight adjustments from Kuric et al. (2024), published in *Cancer Research Communications* under the CC BY 4.0 license.

Abstract

Multiple myeloma involves early dissemination of malignant plasma cells across the bone marrow; however, the initial steps of dissemination remain unclear. Human bone marrow- derived mesenchymal stromal cells (hMSCs) stimulate myeloma cell expansion (e.g., IL-6) and simultaneously retain myeloma cells via chemokines (e.g., CXCL12) and adhesion factors. Hence, we hypothesized that the imbalance between cell division and retention drives dissemination. We present an *in vitro* model using primary hMSCs co-cultured with INA-6 myeloma cells. Time-lapse microscopy revealed proliferation and attachment/detachment dynamics. Separation techniques (V-well adhesion assay and well plate sandwich centrifugation) were established to isolate MSC-interacting myeloma subpopulations that were characterized by RNA-seq, cell viability and apoptosis. Results were correlated with gene expression data ($n = 837$) and survival of myeloma patients ($n = 536$). On dispersed hMSCs, INA-6 saturate hMSC-surface before proliferating into large homotypic aggregates, from which single cells detached completely. On confluent hMSCs, aggregates were replaced by strong heterotypic hMSC-INA-6 interactions, which modulated apoptosis time-dependently. Only INA-6 daughter cells (nMA-INA6) detached from hMSCs by cell division but sustained adherence to hMSC-adhering mother cells (MA-INA6). Isolated nMA-INA6 indicated hMSC-autonomy through superior viability after IL-6 withdrawal and upregulation of proliferation-related genes. MA-INA6 upregulated adhesion and retention factors (CXCL12), that, intriguingly, were highly expressed in myeloma samples from patients with longer overall and progression-free survival, but their expression decreased in relapsed myeloma samples. Altogether, *in vitro* dissemination of INA-6 is driven by detaching daughter cells after a cycle of hMSC-(re)attachment and proliferation, involving adhesion factors that represent a bone marrow-retentive phenotype with potential clinical relevance.

Statement of Significance

Novel methods describe *in vitro* dissemination of myeloma cells as detachment of daughter cells after cell division. Myeloma adhesion genes were identified that counteract *in vitro* detachment with potential clinical relevance.

Introduction

Multiple myeloma arises from clonal expansion of malignant plasma cells in the bone marrow (BM). At diagnosis, myeloma cells have disseminated to multiple sites in the skeleton and, in some cases, to “virtually any tissue” (Bladé et al., 2022; Rajkumar et al., 2014). However, the mechanism through which myeloma cells initially disseminate remains unclear. Dissemination is a multistep process involving invasion, intravasation, intravascular arrest, extravasation, and colonization (Zeissig et al., 2020). To initiate dissemination, myeloma cells overcome adhesion, retention, and dependency on the BM microenvironment, which could involve the loss of adhesion factors such as CD138 (Akhmetzyanova et al., 2020; García-Ortiz et al., 2021). BM retention is mediated by multiple factors: First, chemokines (CXCL12 and CXCL8) produced by mesenchymal stromal cells (MSCs), which attract plasma cells and prime their cytoskeleton and integrins for adhesion (Aggarwal et al., 2006; Alsayed et al., 2007). Second, myeloma cells must overcome the anchorage and physical boundaries of the extracellular matrix (ECM), consisting of e.g. fibronectin, collagens, and proteoglycans such as decorin (X. Hu et al., 2021; Huang et al., 2015; Katz, 2010; Kibler et al., 1998). Simultaneously, ECM provides signals inducing myeloma cell cycle arrest or progression the cell cycle (X. Hu et al., 2021; Katz, 2010). ECM is also prone to degradation, which is common in several osteotropic cancers, and is the cause of osteolytic bone disease. This is driven by a ‘vicious cycle’ that maximizes bone destruction by extracting growth factors (EGF and TGF- β) that are stored in calcified tissues (Glavey et al., 2017). Third, direct contact with MSCs physically anchors myeloma cells to the BM (Zeissig et al., 2020; Sanz-Rodríguez et al., 1999). Fourth, to disseminate to distant sites, myeloma cells require, at least partially, independence from essential growth and survival signals provided by MSCs in the form of soluble factors or cell adhesion signaling (García-Ortiz et al., 2021; Chatterjee et al., 2002; Hideshima et al., 2007). For example, the VLA-4 (Myeloma)–VCAM-1 (MSC)-interface activates NF- κ B in both myeloma and MSCs, inducing IL-6 expression in MSCs. The independence from MSCs is then acquired through autocrine survival signaling (Frassanito et al., 2001; Urashima et al., 1995). In short, anchorage of myeloma cells to MSCs or ECM is a ‘double-edged sword’: adhesion counteracts dissemination, but also presents signaling cues for growth, survival, and drug resistance (Solimando et al., 2022).

To address this ambiguity, we developed an *in vitro* co-culture system modeling diverse adhesion modalities to study dissemination, growth, and survival of myeloma cells and hMSCs. Co-cultures of hMSCs and the myeloma cell line INA-6 replicated tight interactions and aggregate growth, akin to “microtumors” in Ghobrial’s metastasis concept (Ghobrial, 2012). We characterized the growth conformations of hMSCs and INA-6 as homotypic aggregation *vs.* heterotypic hMSC adherence and their effects on myeloma cell

survival. We tracked INA-6 detachments from aggregates and hMSCs, thereby identifying a potential “disseminated” subpopulation lacking strong adhesion. Furthermore, we developed innovative techniques (V-well adhesion assay and well plate sandwich centrifugation) to separate weakly and strongly adherent subpopulations for the subsequent analysis of differential gene expression and cell survival. Notably, our strategy resolves the differences in gene expression and growth behavior between cells of one cell population in “direct” contact with MSCs. In contrast, previous methods differentiated between “direct” and “indirect” cell-cell contact using transwell inserts (Dziadowicz et al., 2022). To evaluate whether genes mediating adhesion and growth characteristics of INA-6 were associated with patient survival, we analyzed publicly available datasets (Seckinger et al., 2017, 2018).

Materials and Methods

See Appendix A.3 for a complete method list and description.

Ethics Statement

Primary human MSCs were collected with the written informed consent of all patients. The procedure was conducted in accordance with recognized ethical guidelines (Helsinki Declaration) and approved by the local Ethics Committee of the University of Würzburg (186/18).

Cultivation and Co-Culturing of primary hMSCs and INA-6

Primary human MSCs were obtained from the femoral head of 34 non-myeloma patients (Appendix A: Tabelle 1: 21 male and 13 female, mean age 68.9 ± 10.6) undergoing elective hip arthroplasty. The INA-6 cell line (*DSMZ Cat# ACC-862, RRID:CVCL_5209*, link) was initially isolated from a pleural effusion sample obtained from an 80-year-old male with multiple myeloma (Burger et al., 2001; Gramatzki et al., 1994). hMSCs were not tested for mycoplasma, whereas stocks of INA-6 were tested in this study (Appendix A: Tabelle 1) using the *Venor GeM OneStep* kit (Minerva Biolabs, Berlin, Germany). For each co-culture, hMSCs were seeded 24 h before INA-6 addition to generate the hMSC-conditioned medium (CM). INA-6 cells were washed with PBS, resuspended in MSC medium, and added to hMSCs so that the co-culture comprised 33 % (v/v) of CM gathered directly from the respective hMSC donor. The co-cultures were not substituted for IL-6 (Chatterjee et al., 2002).

Cell Viability and Apoptosis Assay

Cell viability and apoptosis rates were measured using *CellTiter-Glo Luminescent Cell Viability Assay* and *Caspase-Glo 3/7 Assay*, respectively (Promega GmbH, Mannheim, Germany).

Automated Fluorescence Microscopy

Microscopic images were acquired using an Axio Observer 7 (Zeiss) with a COLIBRI LED light source and motorized stage top using 5x and 10x magnification. The tiled images had an automatic 8–10 % overlap and were not stitched.

Live Cell Imaging

hMSCs (stained with PKH26) were placed into an ibidi Stage Top Incubation System and equilibrated to 80 % humidity and 5 % CO₂. INA-6 (2×10^3 cells/cm²) were added directly before the start of acquisition. Brightfield and fluorescence images of up to 13 mm² of the co-culture area were acquired every 15 min for 63 h. Each event of interest was manually analyzed and categorized into defined event parameters.

V-well Adhesion Assay

INA-6 cells were arrested during mitosis by two treatments with thymidine, followed by nocodazole. Arrested INA-6 were released and added to 96 V-well plates (10⁴ cells/cm²) on top of confluent hMSCs and adhered for 1–3 h. The co-culture was stained with calcein-AM (Thermo Fisher Scientific, Darmstadt, Germany) before non-adherent INA-6 were pelleted into the tip of the V-well (555 g, 5–10 min). MSC-adhering INA-6 cells were manually detached by rapid pipetting. The pellet brightness was measured microscopically and the pellet was isolated by pipetting.

Cell Cycle Profiling by Image Cytometry

Isolated INA-6 cells were fixed in 70 % ice-cold ethanol, washed, resuspended in PBS, distributed in 96-well plates, and stained with Hoechst 33342. The plates were scanned at 5x magnification. A pre-trained convolutional neural network (Intellesis, Zeiss) was fine-tuned to segment the scans into single nuclei and exclude fragmented nuclei. Nuclei were filtered to exclude extremes of size and roundness. The G0/G1 frequency was determined by Gaussian curve fitting.

Well Plate Sandwich Centrifugation (WPSC)

hMSCs were grown to confluence in 96-well plates coated with collagen I (rat tail; Corning, NY, USA). INA-6 cells were added and the cells were allowed to adhere for 24 h. A second plate (“catching plate”) was attached upside down to the top of the co-culture plate. That “well plate sandwich” was turned around and the content of the co-culture plate was centrifuged into the catching plate three times (40 s at 110 g) while gently adding 30 µL of medium in between centrifugation steps. Non-MSC-adhering INA-6 cells were collected from the catching plate, whereas MSC-adhering INA-6 cells were isolated by digesting the co-culture with accutase. For RNA sequencing (RNAseq), all samples were purified using

anti-CD45 Magnetic-Activated Cell Sorting (MACS) (Miltenyi Biotec B.V. & Co. KG, Bergisch Gladbach).

RNA Isolation

RNA was isolated using the *NucleoSpin RNA II Purification Kit* (Macherey-Nagel) according to the manufacturer's instructions. RNA was isolated from INA-6 cells co-cultured with a unique hMSC donor ($n = 5$ for RNA sequencing, $n = 11$ for qPCR).

RNA sequencing, Differential Expression, and Functional Enrichment Analysis

RNA sequencing (RNAseq) was performed at the Core Unit Systems Medicine, University of Würzburg. mRNA was enriched with polyA beads. Fastq files were aligned to the GRCh38 reference genome using STAR (*RRID:SCR_004463*, link) and raw read counts were generated using HTseq (*RRID:SCR_005514*, link) (Anders et al., 2015; Dobin et al., 2013; Zerbino et al., 2018). Differential gene expression was analyzed using edgeR in R (version 3.6.3) (*RRID:SCR_012802*, link). Functional enrichment analysis was performed using Metascape (*RRID:SCR_016620*, link) (Y. Zhou et al., 2019).

RT-qPCR

RNA (1 µg) was reverse transcribed using *SuperScript IV reverse transcriptase* (Thermo Fisher Scientific). qPCR was performed using 10 µL *GoTaq qPCR Master Mix* (Promega), 1 : 10 diluted cDNA, and 5 pmol of primers obtained from Biomers.net or Qiagen (Appendix A: Tabelle 3).

Statistical Analysis

Inferential statistics were performed using Python (IPython, *RRID:SCR_001658*, link) (3.10) packages *pingouin* (0.5.1) and *statsmodels* (0.14.0) (Vallat, 2018; Seabold & Perktold, 2010). The figures were plotted using *plotastic* (0.0.1) (Kuric & Ebert, 2024). Normality (for $n \geq 4$) and sphericity were ensured using Mauchly's and Shapiro-Wilk tests, respectively. Data points were Log_{10} transformed to convert the scale from multiplicative to additive or to fulfill sphericity requirements. $p = 0.05 > * > 0.01 > ** > 10^{-3} > *** > 10^{-4} > ****$. p -values were either adjusted (*p*-adj) or not adjusted (*p*-unc) for family wise error rate. Power calculations were not performed to determine the sample size.

Patient Cohort, Analysis of Survival and Expression

Survival and gene expression data were obtained as previously described (Seckinger et al., 2017, 2018) and are available at the European Nucleotide Archive (ENA) under accession numbers PRJEB36223 and PRJEB37100. The expression level was categorized into “high” and “low” using `maxstat` (Maximally selected Rank Statistics) thresholds (Hothorn & Lausen, 2017).

Data Availability Statement

A detailed description of the methods is provided in the Supplementary Material section. Raw tabular data and examples of analyses and videos are available in the github repository, [link](#). Raw RNAseq data are available from the NCBI Gene Expression Omnibus (GEO) (*RRID:SCR_005012*, [link](#)) (GSE261423). Microscopy data are available at BioStudies (EMBL-EBI) (*RRID:SCR_004727*, [link](#)) (S-BIAD1092).

Results

INA-6 Cells Saturate hMSC-Interaction to Proliferate into Aggregates

hMSCs are isolated as a heterogeneous cell population. To analyze whether INA-6 cells could adhere to every hMSC, we saturated hMSCs with INA-6. A seeding ratio of 1:4 (hMSC:INA-6) resulted in the occupation of $93 \pm 6\%$ of single hMSCs by one or more INA-6 cells within 24 hours after INA-6 addition, escalating to 6% after 48 hours (Abbildung 1A, B). Therefore, most hMSCs provide an interaction surface for INA-6 cells.

INA-6 exhibits homotypic aggregation when cultured alone, a phenomenon observed in some freshly isolated myeloma samples (up to 100 cells after 6 hours) (Kawano et al., 1991; Okuno et al., 1991). Adding hMSCs at a 1:1 ratio led to smaller aggregates after 24 hours (size 1–5 cells), all of which were distributed over $52 \pm 2\%$ of all hMSCs (Abbildung 1A, B). Intriguingly, INA-6 aggregation was notably absent when grown on confluent hMSCs, and occurred only when heterotypic interactions were limited to 0.2 hMSCs per INA-6 cell (Abbildung 1C). We concluded that INA-6 cells prioritize heterotypic over homotypic interactions.

To monitor the formation of such aggregates, we conducted live-cell imaging of hMSC/INA-6 co-cultures for 63 hours. We observed that INA-6 cells adhered long after cytokinesis, constituting $55 \pm 12\%$ of all homotypic interactions between 13 hours and 26 hours, increasing to more than 75% for the remainder of the co-culture (Abbildung 1D). Therefore, homotypic INA-6 aggregates were mostly formed by cell division.

Apoptosis of INA-6 Depends on Ratio Between Heterotypic and Homotypic Interaction

Although direct interaction with hMSCs has been shown to enhance myeloma cell survival through NF- κ B signaling (Hideshima et al., 2007), the impact of aggregation on myeloma cell viability during hMSC interaction remains unclear. To address this, we measured the cell viability (ATP) and apoptosis rates of INA-6 cells growing as homotypic aggregates compared to those in heterotypic interactions with hMSCs by modulating hMSC density (Abbildung 1E). To equalize the background signaling caused by soluble MSC-derived factors, all cultures were incubated in hMSC-conditioned medium and the results were normalized to INA-6 cells cultured without direct hMSC contact (Abbildung 1E, left).

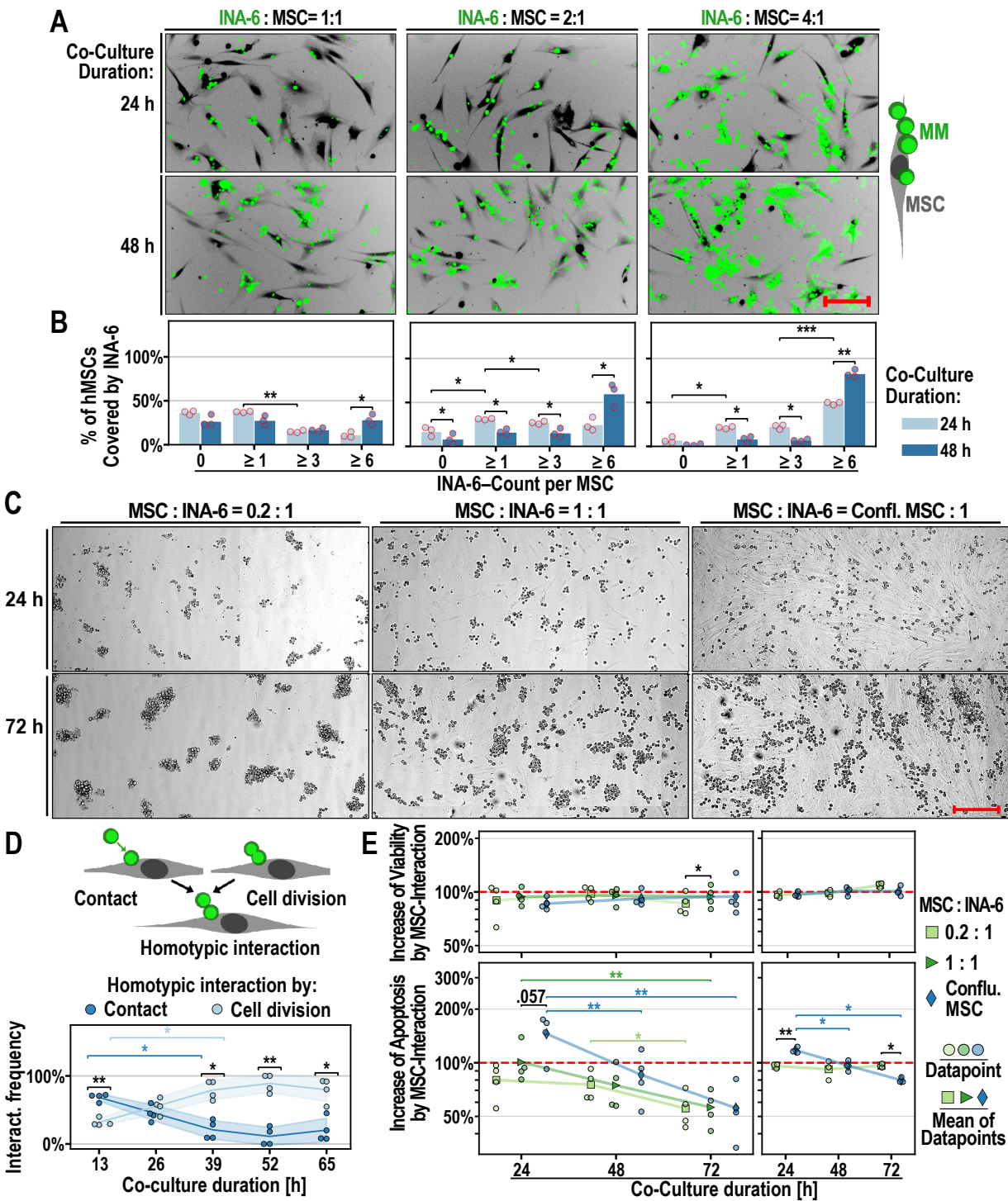


Figure 1: INA-6 growth conformations and survival on hMSCs. **A:** Interaction of INA-6 (green) with hMSCs (black, negative staining) at different INA-6 densities (constant hMSC densities). Scale bar = 200 µm. **B:** Frequency of single hMSCs (same as A) that are covered by INA-6 of varying group sizes. Technical replicates = three per datapoint; 100 single hMSCs were evaluated per technical replicate. **C:** Interaction of INA-6 with hMSCs at different hMSC densities (constant INA-6 densities). Scale bar = 300 µm. **D:** Two types of homotypic interaction: Attachment after cell contact and sustained attachment of daughter cells after cell division. Datapoints represent one of four independent time-lapse recordings, each evaluating 116 interaction events. – *continued on next page*

Figure 1: continued from previous page – **E:** Effects of hMSC-density on the viability (ATP, top) and apoptosis (Caspase3/7 activity, bottom). INA-6:MSC ratio = 4:1; Technical replicates = four per datapoint; **E left:** Signals were measured in INA-6 washed off from hMSCs and normalized by INA-6 cultured in MSC-conditioned medium (= red line) ($n = 4$). **E right:** Signals were measured in co-cultures and normalized by the sum of the signals measured in hMSC and INA-6 cultured separately (= red line) ($n = 3$). **Statistics:** Paired t-test, two-factor RM-ANOVA. Datapoints represent independent co-cultures with hMSCs from three (A, B, D, E right), four (E left) unique donors. Confl. = Confluent. This content has been taken as is from Kuric et al. (2024), published in *Cancer Research Communications* under the CC BY 4.0 license.

INA-6 viability (ATP) was not affected by the direct adhesion of hMSCs at any density. However, apoptosis rates decreased over time [$F(2, 6) = 23.29, p\text{-unc} = 1.49 \times 10^{-3}$] (Two-factor RM-ANOVA), interacting significantly with MSC density [$F(4, 12) = 6.98, p\text{-unc} = 3.83 \times 10^{-3}$] For example, 24 hours of adhesion to confluent MSCs increased apoptosis rates by 1.46 ± 0.37 fold, while culturing INA-6 cells on dispersed hMSCs (ratio 1:1) did not change the apoptosis rate (1.01 ± 0.26 fold).

We presumed that sensitive apoptotic cells might have been lost when harvesting INA-6 cells from hMSCs. Hence, we measured survival parameters in the co-culture and in hMSC and INA-6 cells cultured separately (Abbildung 1E, right). We defined MSC interaction effects when the survival measured in the co-culture differed from the sum of the signals measured from INA-6 and hMSCs alone. RM-ANOVA confirmed that adherence to confluent MSCs increased apoptosis rates of INA-6 cells 24 hours after adhesion and decreased after 72 hours [$F(2, 4) = 26.86, p\text{-unc} = 4.80 \times 10^{-3}$] (interaction between MSC density and time, Two-factor RM-ANOVA), whereas INA-6 cells were unaffected when grown on dispersed hMSCs. In summary, the growth conformation of INA-6 cells, measured as the ratio between homotypic aggregation and heterotypic MSC interactions, affected apoptosis rates of INA-6 cells.

Single INA-6 Cells Detach Spontaneously from Aggregates of Critical Size

Using time-lapse microscopy, we observed that $26 \pm 8\%$ of INA-6 aggregates growing on single hMSCs spontaneously shed INA-6 cells (Abbildung 2A, B; Supplementary Video 1). Notably, all detached cells exhibited similar directional movements, suggesting entrainment in convective streams generated by temperature gradients within the incubation chamber. INA-6 predominantly detached from other INA-6 cells or aggregates (Abbildung 2C), indicating weaker adhesive forces in homotypic interactions than in heterotypic interactions. The detachment frequency increased after 52 hours, when most aggregates that shed INA-6 cells were categorized as large (greater than 30 cells) (Abbildung 2D). Since approximately 10-20 INA-6 cells already fully covered a single hMSC, we suggest that myeloma cell detachment depended not only on hMSC saturation but also required

a minimum aggregate size. Interestingly, INA-6 detached mostly as single cells, independent of aggregate size categories [$F(2, 6) = 4.68, p\text{-unc} = 0.059$] (Two-factor RM-ANOVA) (Abbildung 2E), showing that aggregates remained mostly stable despite losing cells.

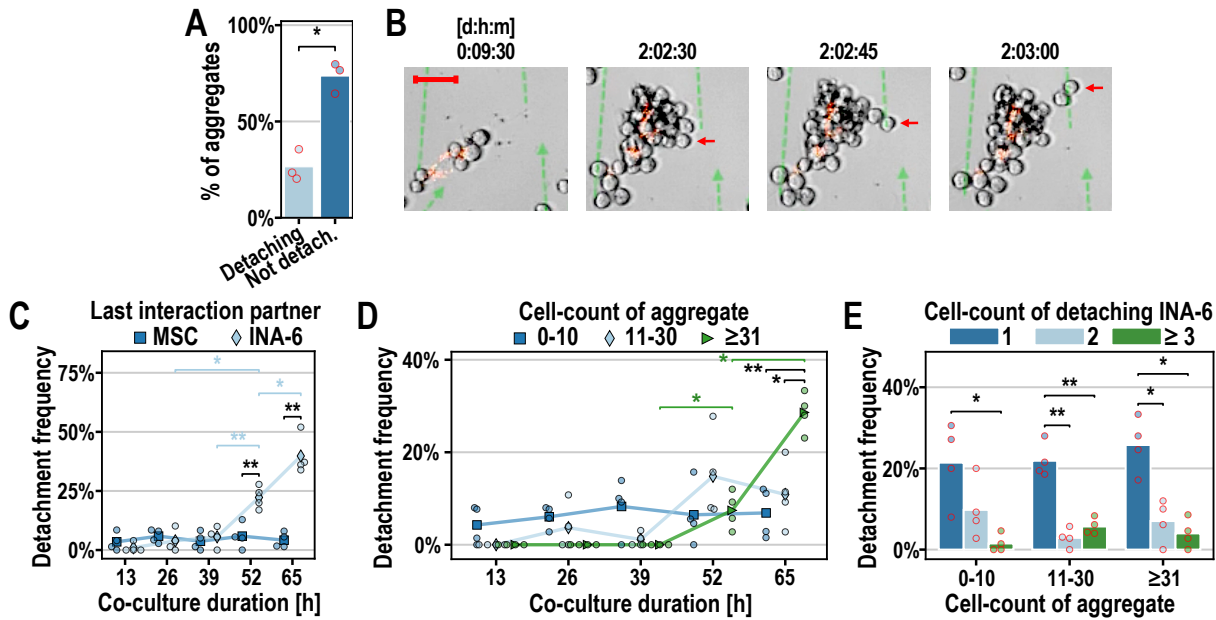


Figure 2: Time-lapse analysis of INA-6 detachment from INA-6 aggregates and hMSCs. **A:** Frequency of observed INA-6 aggregates that did or did not lose INA-6 cell(s). 87 aggregates were evaluated per datapoint. **B:** Example of a “disseminating” INA-6 aggregate growing on fluorescently (PKH26) stained hMSC (from A-D). Dashed green lines are trajectories of detached INA-6 cells. Scale bar = 50 µm. **C-E:** Quantitative assessment of INA-6 detachments. 45 detachment events were evaluated per datapoint. Seeding ratio INA-6:MSC = 4:1. **C:** Most INA-6 cells dissociated from another INA-6 cell and not from an hMSC [$F(1, 3) = 298, p\text{-unc} = 4.2 \times 10^{-4}$]. **D:** Detachment frequency of aggregate size categories. **E:** Detachment frequency of INA-6 cells detaching as single, pairs or more than three cells. **Statistics:** (A): Paired-t-test; (C-E): Paired-t-test, Two-factor RM-ANOVA; Datapoints represent three (A) or four (C-E) independent time-lapse recordings of co-cultures with hMSCs from two (A) or three (C-E) unique donors. This content has been taken as is from Kuric et al. (2024), published in *Cancer Research Communications* under the CC BY 4.0 license.

Cell Division Generates a Daughter Cell Detached from hMSC

We suspected that cell division drives detachment because we observed that MSC-adhering INA-6 cells could generate daughter cells that “roll over” the mother cell (Abbildung 3A; Supplementary Video 2). We recorded and categorized the movement of INA-6 daughter cells in confluent hMSCs after cell division. Half of all INA-6 divisions yielded two daughter cells that remained stationary, indicating hMSC adherence (Abbildung 3B, C; Supplementary Video 3). The other half of division events generated one hMSC-adhering cell and one non-hMSC-adhering cell, which rolled around the MA-INA6 cell for a median time of 2.5 hours post division (Q1=1.00 hour, Q3=6.25 hours) until it stopped and re-adhered

to the hMSC monolayer (Abbildung 3D; Supplementary Video 2, Supplementary Video 4). Thus, cell division establishes a time window in which one daughter cell can detach.

To validate that cell division reduced adhesion, we measured both the size and cell cycle profile of the nMA-INA6 and MA-INA6 populations using an enhanced V-well assay (method described in Abbildung 3E, Appendix A: Abbildung 1, 2). For comparison, we fully synchronized and arrested INA-6 cells at mitosis and released their cell cycle immediately before addition to the hMSC monolayer, rendering them more likely to divide while adhering. Mitotic arrest significantly increased the number of nMA-INA6 cells and decreased the number of MA-INA6 cells (Abbildung 3F). Furthermore, the nMA-INA6 population contained significantly more cells cycling in the G0/G1 phase than the MA-INA6 population, both in synchronously and asynchronously cycling INA-6 (Abbildung 3G, Appendix A: Abbildung 3, 4). The number of nMA-INA6 INA-6 cells increased due to a higher cell division frequency. Taken together, we showed that INA-6 detach from aggregates by generating one temporarily detached daughter cell after cell division, a process that potentially contributes to the initiation of dissemination.

RNAseq of Non-MSC-Adhering and MSC-Adhering Subpopulations

To characterize the subpopulations separated by WPSC, we conducted RNAseq, revealing 1291 differentially expressed genes between nMA-INA6 *vs.* CM-INA6, 484 between MA-INA6 *vs.* CM-INA6, and 195 between MA-INA6 *vs.* nMA-INA6. We validated RNAseq and found that the differential expression of 18 genes correlated with those measured with qPCR for each pairwise comparison (Abbildung 4C–E, Appendix A: Abbildung 5): nMA-INA6 *vs.* CM-INA6 [$\rho(16) = .803, p = 6.09 \times 10^{-5}$], MA-INA6 *vs.* CM-INA6 [$\rho(16) = .827, p = 2.30 \times 10^{-5}$], and MA-INA6 *vs.* nMA-INA6 [$\rho(16) = .746, p = 3.74 \times 10^{-4}$] (Spearman’s rank correlation). One of the 18 genes (*MUC1*) measured by qPCR showed a mean expression opposite to that obtained by RNAseq (nMA-INA6 *vs.* CM-INA6), although the difference was insignificant (Abbildung 4C). For nMA-INA6 *vs.* CM-INA6, the difference in expression measured by qPCR was significant for only two of the 11 genes (*DKK1, OPG*), whereas the other genes (*DKK1, OPG, BCL6, BMP4, BTG2, IL10RB, IL24, NOTCH2, TNFRSF1A, TRAF5*) only confirmed the tendency measured by RNAseq (Abbildung 4C–E). For MA-INA6 *vs.* CM-INA6 qPCR validated the significant upregulation of seven genes (*DKK1, OPG, BCL6, BMP4, BTG2, IL10RB, IL24, NOTCH2, TNFRSF1A, TRAF5, TGM2, DCN, LOX, MMP14, MMP2, CXCL12, CXCL8*), whereas the downregulation of *BMP4* was insignificant.

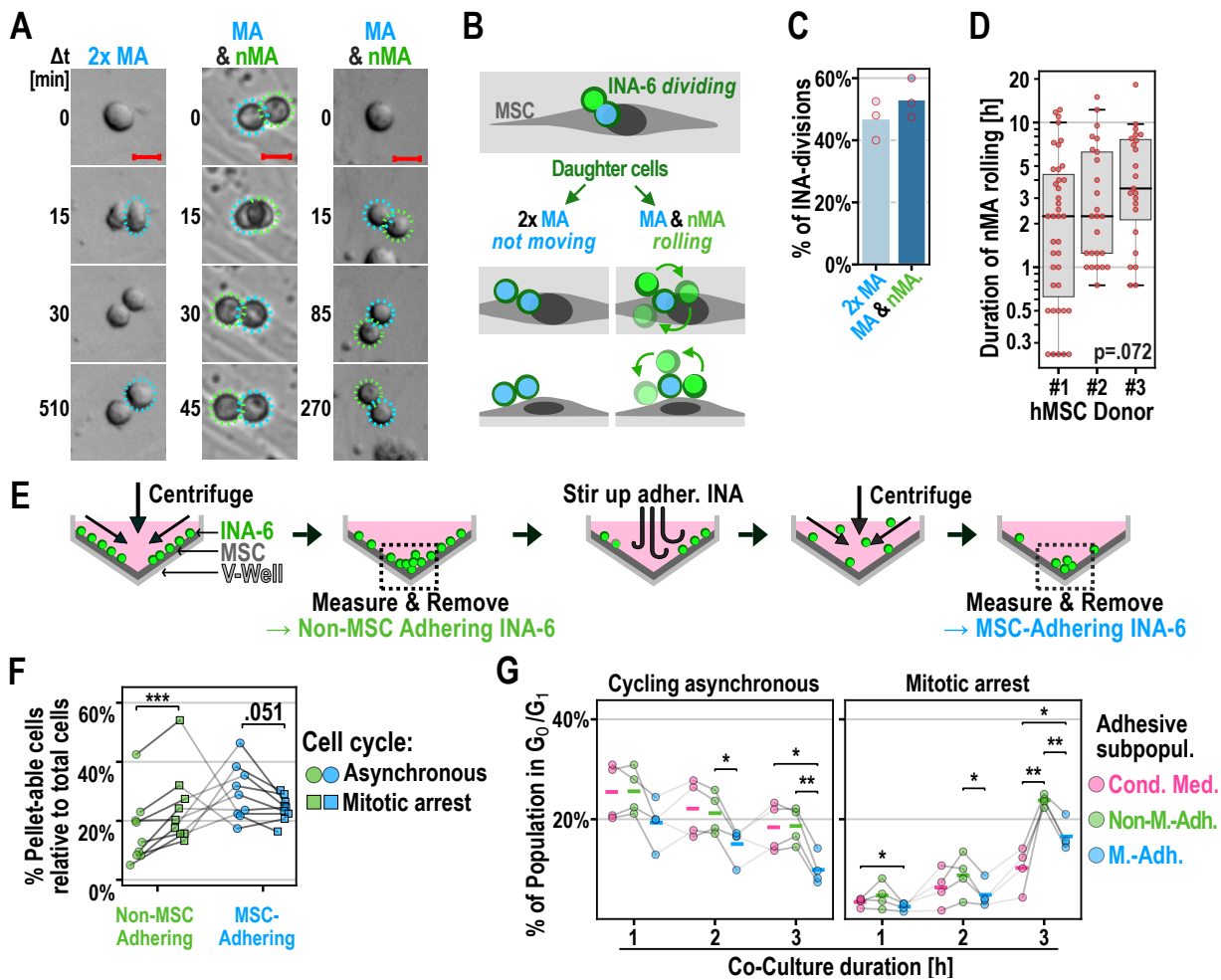


Figure 3: Detachment of INA-6 daughter cells after Cell Division. **A-D:** INA-6 divisions in interaction with confluent hMSCs. Seeding ratio INA-6:MSC = 4:20. **A:** Three examples of dividing INA-6 cells generating either two MA, or one MA and one nMA daughter cells as described in (G). Dashed circles mark mother cells (white), MA cell (blue), and first position of nMA cell (green). Scale bar: 20 μ m. **B:** Cell division of MSC-adhering (MA) mother cell can yield one mobile non-MSC-adhering (nMA) daughter cell. **C:** Frequencies of INA-6 pairs defined in (A, B) per observed cell division. 65 divisions were evaluated for each of three independent time-lapse recordings. **D:** Rolling duration of nMA cells after division did not depend on hMSC donor [$H(2) = 5.250$, $p_{\text{unc}} = .072$]. Datapoints represent single nMA-cells after division. **E-G:** Adhesive and cell cycle assessment of MSC-interacting INA-6 subpopulations using the V-Well assay. **E:** Schematic of V-Well Assay (see Appendix A: Abbildung 1 for detailed analysis). MSC-interacting subpopulations were separated by subsequent centrifugation and removal of the pellet. The pellet size was quantified by its total fluorescence brightness. Adhering subpopulations were resuspended by rough pipetting. **F:** Relative cell pellet sizes of adhesive INA-6 subpopulations that cycle either asynchronously or were synchronized at mitosis. Gray lines in-between points connect dependent measurements of co-cultures ($n = 9$) that shared the same hMSC-donor and INA-6 culture. Co-cultures were incubated for three different durations (1 h, 2 h und 3 h after INA-6 addition). Time points were pooled, since time did not show an effect on cell adhesion [$F(2, 4) = 1.414$, $p_{\text{unc}} = 0.343$] Factorial RM-ANOVA shows an interaction between cell cycle and the kind of adhesive subpopulation [$F(1, 8) = 42.67$, $p_{\text{unc}} = 1.82 \times 10^{-4}$]. Technical replicates = 4 per datapoint. **G:** Cell cycles were profiled in cells gathered from the pellets of four independent co-cultures ($n = 4$) and the frequency of G_0/G_1 cells are displayed depending on co-culture duration (see Appendix A: Abbildung 3 for cell cycle profiles). Four technical replicates were pooled after pelleting. **Statistics:** (D): Kruskal-Wallis H-test. (F): Paired t-test, (G): Paired t-test, two-factor RM-ANOVA. Datapoints represent INA-6 from independent co-cultures with hMSCs from three unique donors. This content has been taken as is from Kuric et al. (2024), published in *Cancer Research Communications* under the CC BY 4.0 license.

Non-MSC-Adhering INA-6 and MSC-Adhering INA-6 Have Distinct Expression Patterns of Proliferation or Adhesion, Respectively

To functionally characterize the unique transcriptional patterns in nMA-INA6 and MA-INA6, we generated lists of genes that were differentially expressed *vs.* the other two subpopulations [termed nMA *vs.* (MA & CM) and MA *vs.* (nMA & CM)]. Functional enrichment analysis was performed, and the enriched terms were displayed as ontology clusters (Abbildung 5A). nMA-INA6 upregulated genes enriched with loosely connected term clusters associated with proliferation (e.g., “positive regulation of cell cycle”).

MA-INA6 upregulated genes enriched with tightly connected term clusters related to cell adhesion and the production of ECM factors (e.g., “cell-substrate adhesion”). Similar ontology terms were enriched in the gene lists obtained from pairwise comparisons nMA *vs.* CM, MA *vs.* CM, and MA *vs.* nMA (Abbildung 5B). In particular, nMA *vs.* CM (but not MA *vs.* CM) upregulated genes that were enriched with “G1/S transition”, showing that WPSC isolated nMA-INA6 daughter cells after cell division.

To check for similarities between lists of differentially expressed genes from hMSC-interacting subpopulations, we performed enrichment analysis on gene lists from the overlaps (“ \cap ”) between all pairwise comparisons (Abbildung 5B, Appendix A: Abbildung 6), and showed the extent of these overlaps in circos plots (Abbildung 5C). The overlap between MA *vs.* CM and nMA *vs.* CM showed neither enrichment with proliferation- nor adhesion-related terms but with apoptosis-related terms. A direct comparison of MSC-interacting subpopulations (MA *vs.* nMA) showed a major overlap with MA *vs.* CM (Abbildung 5C, middle). This overlap was enriched with terms related to adhesion but not proliferation. Hence, MA-INA6 and nMA-INA6 mostly differed in their expression of adhesion genes.

To assess whether nMA-INA6 and MA-INA6 were regulated by separate transcription factors, we examined the enrichment of curated regulatory networks from the TRRUST database (Abbildung 5B, bottom). All the lists were enriched for p53 regulation. E2F1 regulation was observed only in genes upregulated in nMA *vs.* CM and downregulated in MA *vs.* nMA. Genelists involving MA-INA6 were enriched in regulation by subunits of NF- κ B (NFKB1/p105 and RELA/p65) and factors of immediate early response (SRF, JUN). Correspondingly, NF- κ B and JUN are known to regulate the expression of adhesion factors in multiple myeloma and B-cell lymphoma, respectively (Blonska et al., 2015; Tai et al., 2006).

Taken together, MSC-interacting subpopulations showed unique regulatory patterns, focusing on either proliferation or adhesion.

nMA-INA6 and MA-INA6 Show Increased Apoptosis Signaling Mediated by ER-Stress, p53 and Death Domain Receptors

As previously stated, apoptosis rates increased in INA-6 cells grown on confluent hMSCs compared with MSC-Conditioned-Medium-treated INA-6 (CM-INA6) cells after 24 hours of co-culture (Abbildung 1D). Since this setup was similar to that used to separate hMSC-interacting subpopulations using WPSC, we looked for enrichment of apoptosis-related terms (Abbildung 5B). “Regulation of cellular response to stress” and “intrinsic apoptotic signaling pathway (in response to ER-stress)” are terms that were enriched in nMA *vs.* CM, MA *vs.* CM and their overlap.

We also found specific stressors for either nMA-INA6 (“intrinsic apoptotic signaling pathway by p53 class mediator”) or MA-INA6 (“extrinsic apoptotic signaling pathway via death domain receptor”). Therefore, apoptosis may be driven by ER stress in both nMA-INA6 and MA-INA6, but also by individual pathways such as p53 and death domain receptors, respectively.

nMA-INA6 and MA-INA6 Regulate Genes Associated with Bone Loss

Myeloma cells cause bone loss by degradation and dysregulation of bone turnover via *DKK1* and *OPG* (Standal et al., 2002; Van Valckenborgh et al., 2004; F. Zhou et al., 2013). RNAseq of hMSC-interacting subpopulations showed enrichment with functional terms “skeletal system development” and “ossification” (Abbildung 5A, Appendix A: Abbildung 6), as well as the regulation of *MMP2*, *MMP14*, *DKK1*, and *OPG*. Validation by qPCR (Abbildung 4C, D) showed that MA-INA6 significantly upregulated both *MMP14* and *MMP2* compared with either nMA-INA6 or CM-INA6. The expression of *DKK1*, however, was upregulated significantly in nMA-INA6 (and not significantly upregulated in MA-INA6), while *OPG* was significantly downregulated only in nMA-INA6.

Together, hMSC-interacting subpopulations might contribute to bone loss through different mechanisms: MA-INA6 expression of matrix metalloproteinases and nMA-INA6 cells via paracrine signaling.

MA-INA6 Upregulate Collagen and Chemokines Associated with Bone Marrow Retention

Retention of myeloma cells within the bone marrow is mediated by adhesion to the ECM (e.g., collagen VI) and the secretion of chemokines (*CXCL8* and *CXCL12*), potentially counteracting dissemination (Alsayed et al., 2007; Katz, 2010).

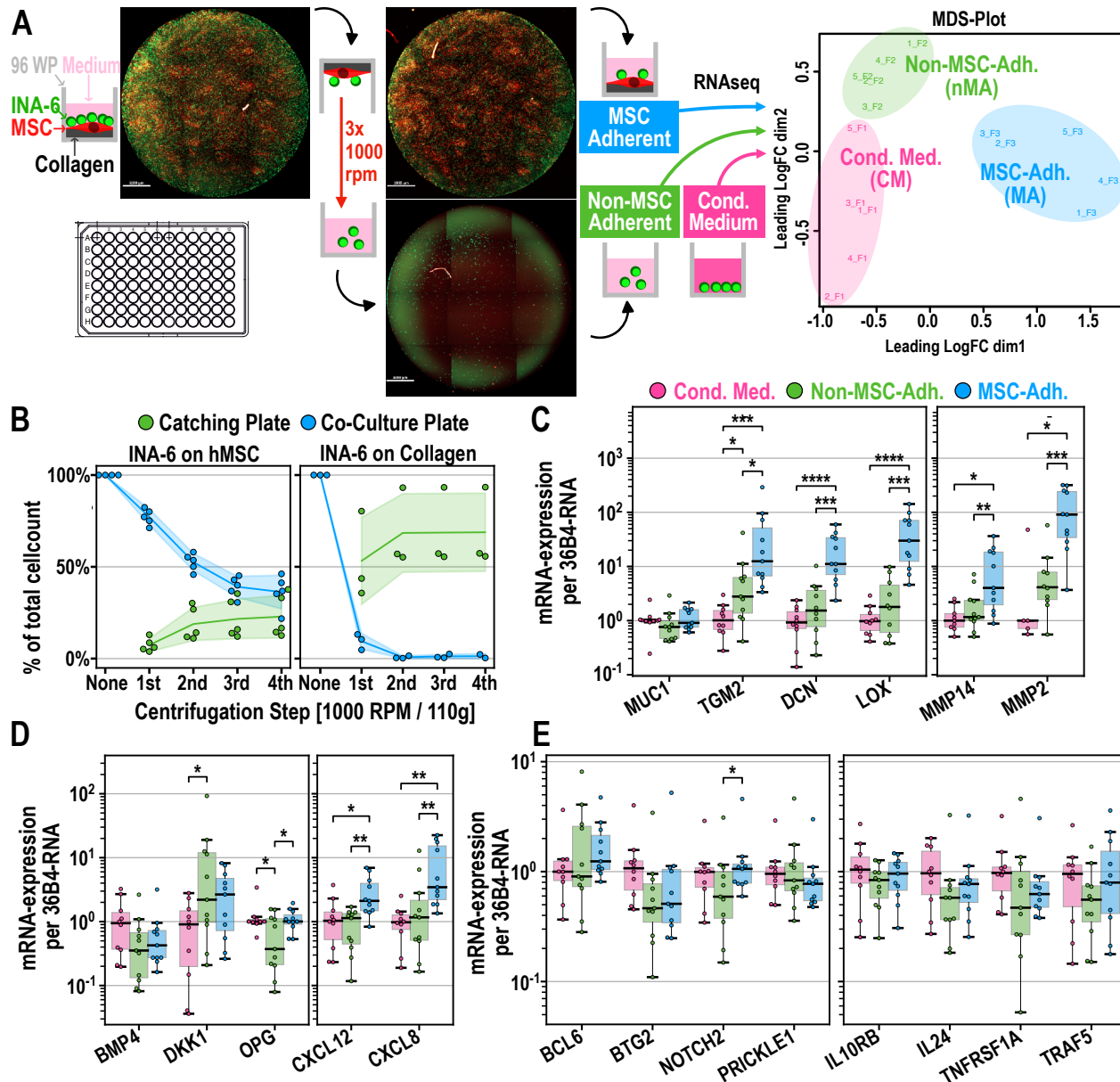


Figure 4: Separation and gene expression of INA-6 subpopulations. **A:** Schematic of “Well-Plate Sandwich Centrifugation” (WPSC) separating nMA- from MA-INA6. A co-culture 96-well plate is turned upside down and attached on top of a “catching plate”, forming a “well-plate sandwich”. nMA-INA6 cells are collected in the catching plate by subsequent rounds of centrifugation and gentle washing. MA-INA6 are enzymatically dissociated from hMSCs or by rough pipetting. Subsequent RNAseq of MSC-interacting subpopulations reveals distinct expression clusters [right, multidimensional scaling plot (MDS) ($n = 5$)]. **B:** Separation was microscopically tracked after each centrifugation step. **C-E:** RT-qPCR of genes derived from RNAseq results. Expression was normalized to the median of CM-INA6. Samples include those used for RNAseq and six further co-cultures ($n = 11$; non-detects were discarded). **C:** Adhesion factors, ECM proteins, and matrix metalloproteinases. **D:** Factors involved in bone remodeling and bone homing chemokines. **E:** Factors involved in (immune) signaling. **Statistics:** (C-E): Paired t-test. Datapoints represent the mean of three (B-E) technical replicates. INA-6 were isolated from independent co-cultures with hMSCs from five (A, B), nine (C-E) unique donors. This content has been taken as is from Kuric et al. (2024), published in *Cancer Research Communications* under the CC BY 4.0 license.

RNAseq of hMSC-interacting subpopulations showed that genes upregulated in MA-INA6 were enriched with collagen biosynthesis and modifying enzymes, as well as chemotaxis and chemotaxis-related terms (Abbildung 5B). Using qPCR, we validated the upregulation of collagen crosslinkers (*LOX* and *TGM2*), collagen-binding *DCN*, and chemokines (*CXCL8* and *CXCL12*) in MA-INA6 compared with both nMA-INA6 and CM-INA6 (Abbildung 4D). Therefore, MA-INA6 can provide both an adhesive surface and soluble signals for the retention of malignant plasma cells in the bone marrow.

nMA-INA6 Show Highest Viability During IL-6 Withdrawal

Although RNAseq did not reveal IL-6 induction in any WPSC-isolated subpopulation, nMA-INA6 upregulated *IGF-1* 1.35-fold [RNAseq, nMA vs. (MA & CM)], which was shown to stimulate growth in CD45+ and IL-6 dependent myeloma cell lines such as INA-6, implying increased autonomy for nMA-INA6 (40). To test the autonomy of hMSC-interacting INA-6 subpopulations, we isolated them using WPSC after 24 hours and 48 hours of co-culture, sub-cultured them for 48 hours under IL-6 withdrawal, and measured both viability and apoptosis (Abbildung 5D). Among the subpopulations, nMA-INA6 was the most viable. Compared to MA-INA6, nMA-INA6 increased cell viability by 8 or 4 fold when co-cultured for 24 hours or 48 hours, respectively [Hedges *g* of $\text{Log}_{10}(\text{Fold Change}) = 2.31$ or 0.82]. However, the difference was no longer significant after 48 hours of co-culture, probably because nMA-INA6 adhered to the hMSC layer (turning into MA-INA6) during prolonged co-culture, which could also explain why the viability of MA-INA6 cell subcultures increased with prolonged co-culture. Nevertheless, nMA-INA6 did not achieve the same viability as that of INA-6 cells cultured with IL-6. Despite the differences in viability, subcultures of hMSC-interacting subpopulations did not show any differences in caspase 3/7 activity when co-cultured for 48 hours (Abbildung 5D, right).

Overall, among the hMSC-interacting subpopulations, nMA-INA6 had the highest chance of surviving IL-6 withdrawal.

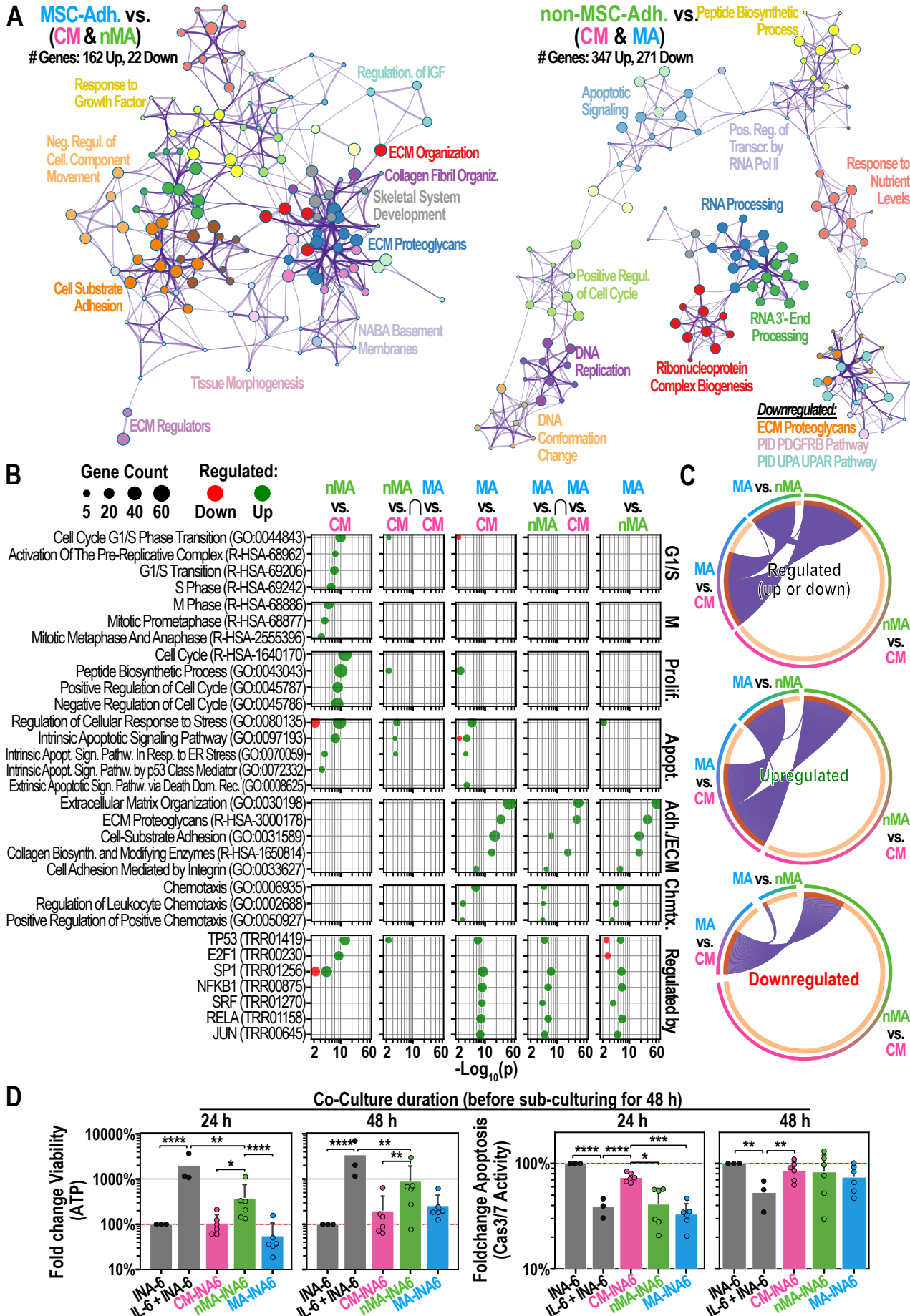


Figure 5: Functional analysis of MSC-interacting subpopulations (**A-C**): Functional enrichment analysis of differentially expressed genes (from RNAseq) using Metascape. **A:** Gene ontology (GO) cluster analysis of gene lists that are unique for MA (left) or nMA (right) INA-6. Circle nodes represent subsets of input genes falling into similar GO-term. Node size grows with the number of input genes. Node color defines a shared parent GO-term. Two nodes with a similarity score > 0.3 are linked. **B:** Enrichment analysis of pairwise comparisons between MA subpopulations and their overlaps (arranged in columns). GO terms were manually picked and categorized (arranged in rows). Raw Metascape results are shown in Appendix A: Abbildung 6. For each GO-term, the p-values (x-axis) and the counts of matching input genes (circle size) were plotted. The lowest row shows enrichment of gene lists from the TRRUST-database. **C:** Circos plots by Metascape. Sections of a circle represent lists of differentially expressed genes. Purple lines connect same genes appearing in two gene lists. \cap : Overlapping groups, MA: MSC-adhering, nMA: non-MSC-adhering, CM: MSC-Conditioned Medium. **D:** INA-6 were co-cultured on confluent hMSC for 24 h or 48 h, separated by WPSC and sub-cultured for 48 h under IL-6 withdrawal ($n = 6$), except the control (IL-6 + INA-6) ($n = 3$). Signals were normalized (red line) to INA-6 cells grown without hMSCs and IL-6 ($n = 3$). **Statistics:** (D): Paired t-test, two-factor RM-ANOVA. Datapoints represent the mean of four technical replicates. INA-6 were isolated from independent co-cultures with hMSCs from six unique donors. This content has been taken as is from Kuric et al. (2024), published in *Cancer Research Communications* under the CC BY 4.0 license.

Genes Upregulated by MA-INA6 are Associated with an Improved Disease Prognosis

To relate the adhesion of MA-INA6 observed *in vitro* to the progression of multiple myeloma, we assessed patient survival [$n = 535$, Seckinger et al. (2017, 2018)] depending on the expression level of 101 genes, which were upregulated in MA *vs.* (nMA & CM) and are part of the ontology terms “Extracellular matrix organization,” “ECM proteoglycans,” “cell-substrate adhesion,” and “negative regulation of cell-substrate adhesion” (Abbildung 6A, Appendix A: Tabelle 2). As a reference, we generated a list of 173 cell cycle-related genes that were upregulated by nMA *vs.* (MA & CM).

As expected, longer patient survival was associated with low expression of the majority of cell cycle genes [71 or 68 genes for Progression-Free Survival (PFS) or Overall Survival (OS)]. Only a few cell cycle genes (two for PFS and seven for OS) were associated with survival when highly expressed. Intriguingly, adhesion genes showed an inverse pattern: a large group of adhesion genes (24 for PFS and 26 for OS) was significantly associated with improved survival when highly expressed, whereas only a few genes (two for PFS and four for OS) improved survival when expressed at low levels (Tabelle 1). We concluded that the myeloma-dependent expression of adhesion factors determined in our *in vitro* study correlates with improved patient survival.

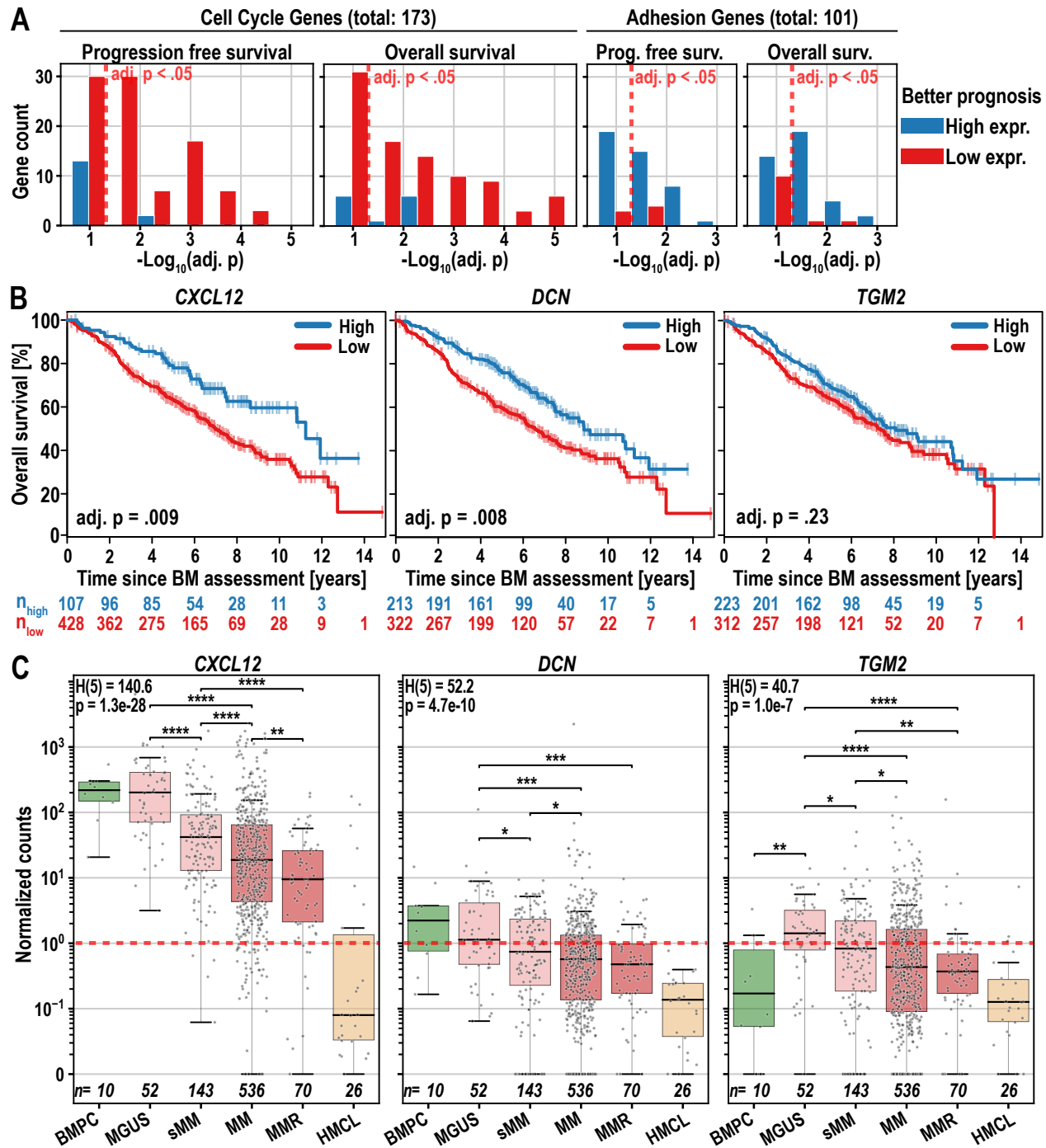


Figure 6: Survival of patients with multiple myeloma regarding the expression levels of adhesion and bone retention genes. **A:** p-value distribution of genes associated with patient survival ($n = 535$) depending on high or low expression levels. Red dashed line marks the significance threshold of $p\text{-adj} = 0.05$. Histogram of p -values was plotted using a bin width of $-\log_{10}(0.05)/2$. Patients with high and low gene expression were delineated using maximally selected rank statistics (maxstat). **B:** Survival curves for three genes taken from the list of adhesion genes shown in (A), maxstat thresholds defining high and low expression were: *CXCL12*: 81.08; *DCN*: 0.75; *TGM2*: 0.66 normalized counts. – *continued on next page*

Figure 6: continued from previous page – **C:** Gene expression (RNAseq, $n = 873$) measured in normalized counts (edgeR) of *CXCL12*, *DCN* in Bone Marrow Plasma Cell (BMPC), Monoclonal Gammopathy of Undetermined Significance (MGUS), smoldering Multiple Myeloma (sMM), Multiple Myeloma (MM), Multiple Myeloma Relapse (MMR), Human Myeloma Cell Lines (HMCL). The red dashed line marks one normalized read count. **Statistics:** (A, B): Log-rank test; (C): Kruskal-Wallis, Mann–Whitney U Test. All p -values were corrected using the Benjamini-Hochberg procedure. This content has been taken as is from Kuric et al. (2024), published in *Cancer Research Communications* under the CC BY 4.0 license.

Expression of Adhesion- or Retention-related Genes (*CXCL12*, *DCN* and *TGM2*) is Decreased During Progression of Multiple Myeloma

To examine how the disease stage affects the adhesion and bone marrow retention of myeloma cells *in vitro*, we analyzed the expression of *CXCL12* in healthy plasma cell (BMPC) cohorts of patients at different disease stages and in myeloma cell lines (HMCL) [described in Seckinger et al. (2018)] (Abbildung 6C). We also included *DCN* and *TGM2* since both are suggested to inhibit metastasis in different cancers by promoting cell-matrix interactions (X. Hu et al., 2021; Tabolacci et al., 2019). In accordance with independent reports (Huang et al., 2015; Bao et al., 2013), high expression of *CXCL12* and *DCN* by myeloma cells was associated with improved overall survival (adj. $p = .009$ and $.008$, respectively) (Abbildung 6B).

CXCL12 is expressed by BMPCs (median = 219 normalized counts), but its expression levels are significantly lower from MGUS to relapsed multiple myeloma (MMR) (median = 9 normalized counts in MMR and absent expression in most HMCL). *DCN* (but not *TGM2*) was weakly expressed in BMPCs ($Q_1 = 0.7$, $Q_3 = 3.7$, normalized counts), whereas *TGM2* was weakly expressed only in patients with monoclonal gammopathy of undetermined significance (MGUS) ($Q_1 = 0.4$, $Q_3 = 4.1$ normalized counts). The median and upper quartiles of both *DCN*- and *TGM2* decreased continuously after each stage, ending at $Q_3 = 0.9$ and $Q_3 = 0.6$, respectively, in MMR. 49 of the 101 adhesion genes (Abbildung 6A) followed a similar pattern of continuous downregulation in the advanced stages of multiple myeloma (Appendix A: Abbildung 7 and 8), of which 19 genes were associated with longer PFS when they were highly expressed. The other 52 (out of 101) adhesion genes that were not downregulated across disease progression (or were expressed at a level too low to make that categorization) contained only five genes that were associated with longer PFS at high expression (Tabelle 1, Appendix A: Tabelle 2).

Together, the expression of adhesion or bone marrow retention-related markers (*CXCL12*, *DCN*, and *TGM2*) is reduced or lost at advanced stages of multiple myeloma, which could enhance dissemination and reduce retention in the BM microenvironment.

Table 1: Adhesion and ECM genes (shown in Abbildung 6A) were filtered by their association with patient survival ($p\text{-adj.} < 0.01$) and were categorized as continuously downregulated during disease progression. The complete list is presented in Appendix A: Tabelle 2. Bone Marrow Plasma Cells (BMPC), Monoclonal Gammopathy of Undetermined Significance (MGUS), smoldering Multiple Myeloma (sMM), Multiple Myeloma (MM), and Multiple Myeloma Relapse (MMR). $p\text{-unc}$: unadjusted p-values; $p\text{-adj}$: p-values adjusted using the Benjamini-Hochberg method with 101 genes. This content has been taken as is from Kuric et al. (2024), published in *Cancer Research Communications* under the CC BY 4.0 license.

Regulation during disease progression	Gene	Ensemble ID	Progression Free / Overall Survival	Better Prognosis with high/low expression	Association of expression with survival	
					[p-unc]	[p-adj]
Not Downregulated (or overall low expression)	CCNE2	ENSG00000175305	Overall	low	5.34E-04	8.64E-03
	MMP2	ENSG00000087245	Prog. Free	high	2.29E-05	2.32E-03
	OSMR	ENSG00000145623	Prog. Free	high	5.67E-04	7.15E-03
Continuously Downregulated (BMPC > MGUS > sMM > MM > MMR)	AXL	ENSG00000167601	Overall	high	3.64E-05	1.84E-03
	COL1A1	ENSG00000108821	Prog. Free	high	3.03E-04	4.37E-03
			Overall	high	5.93E-04	8.64E-03
	CXCL12	ENSG00000107562	Prog. Free	high	1.16E-04	2.93E-03
			Overall	high	6.48E-04	8.64E-03
	CYP1B1	ENSG00000138061	Overall	high	6.84E-04	8.64E-03
	DCN	ENSG00000011465	Overall	high	2.47E-04	8.33E-03
	LRP1	ENSG00000123384	Overall	high	4.34E-04	8.64E-03
	LTBP2	ENSG00000119681	Prog. Free	high	9.03E-05	2.93E-03
	CYP1B1	ENSG00000138061	Overall	high	6.84E-04	8.64E-03
	DCN	ENSG00000011465	Overall	high	2.47E-04	8.33E-03
	LRP1	ENSG00000123384	Overall	high	4.34E-04	8.64E-03
	LTBP2	ENSG00000119681	Prog. Free	high	9.03E-05	2.93E-03
	MFAP5	ENSG00000197614	Prog. Free	high	2.43E-04	4.09E-03
	MMP14	ENSG00000157227	Prog. Free	high	6.93E-05	2.93E-03
	MYL9	ENSG00000101335	Prog. Free	high	1.46E-04	2.95E-03
			Overall	high	1.56E-05	1.57E-03

Discussion

In this study, we developed an *in vitro* model to investigate the attachment/detachment dynamics of INA-6 cells to/from hMSCs and established methods to isolate the attached and detached intermediates nMA-INA6 and MA-INA6. Secondly, we characterized a cycle of (re)attachment, division, and detachment, linking cell division to the switch that causes myeloma cells to detach from hMSC adhesion (Abbildung 7). Thirdly, we identified clinically relevant genes associated with patient survival, where better or worse survival was based on the adherence status of INA-6 to hMSCs.

INA-6 cells emerged as a robust choice for studying myeloma dissemination *in vitro*, showing rapid and strong adherence, as well as aggregation exceeding MSC saturation. The IL-6 dependency of INA-6 enhanced the resemblance of myeloma cell lines to patient samples, with INA-6 ranking 13th among 66 cell lines (Sarin et al., 2020). Despite variations in bone marrow MSCs between multiple myeloma and healthy states, we anticipated the robustness of our results, given the persistent strong adherence and growth signaling from MSCs to INA-6 during co-cultures (Dotterweich et al., 2016).

We acknowledge that INA-6 cells alone cannot fully represent the complexity of myeloma aggregation and detachment dynamics. However, the diverse adhesive properties of myeloma cell lines pose a challenge. We reasoned that attempting to capture this complexity within a single publication would not be possible. Our focus on INA-6 interactions with hMSCs allowed for a detailed exploration of the observed phenomena, such as the unique aggregation capabilities that facilitate the easy detection of detaching cells *in vitro*. The validity of our data was demonstrated by matching the *in vitro* findings with the gene expression and survival data of the patients (e.g., *CXCL12*, *DCN*, and *TGM2* expression, $n = 873$), ensuring biological consistency and generalizability regardless of the cell line used. The protocols presented in this study offer a cost-efficient and convenient solution, making them potentially valuable for a broader study of cell interactions. We encourage optimizations to meet the varied adhesive properties of the samples, such as decreasing the number of washing steps if the adhesive strength is low. We caution against strategies that average over multiple cell lines without prior understanding their diverse attachment/detachment dynamics, such as homotypic aggregation. Such detailed insights may prove instrumental when considering the diversity of myeloma patient samples across different disease stages (Kawano et al., 1991; Okuno et al., 1991).

The intermediates, nMA-INA6 and MA-INA6, were distinct but shared similarities in response to cell stress, intrinsic apoptosis, and regulation by p53. Unique regulatory patterns were related to central transcription factors: E2F1 for nMA-INA6; and NF- κ B,

SRF, and JUN for MA-INA6. This distinction may have been established through antagonism between p53 and the NF- κ B subunit RELA/p65 (Wadgaonkar et al., 1999; Webster & Perkins, 1999). Similar regulatory patterns were found in transwell experiments with RPMI1-8226 myeloma cells, where direct contact with the MSC cell line HS5 led to NF- κ B signaling and soluble factors to E2F signaling (Dziadowicz et al., 2022).

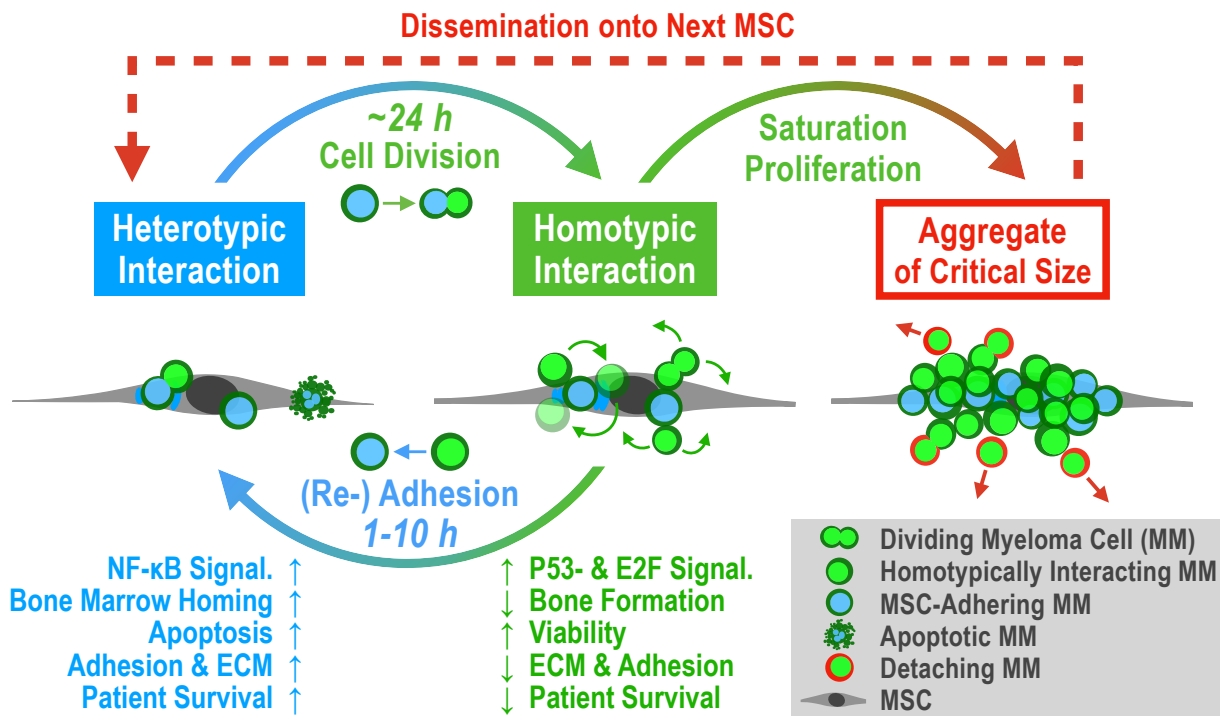


Figure 7: Proposed model of “Detached Daughter Driven Dissemination” (DDDD) in aggregating multiple myeloma. **Heterotypic Interaction:** Malignant plasma cells colonize the bone marrow microenvironment by adhering to an MSC (or osteoblast, ECM, etc.) to maximize growth and survival through paracrine and adhesion mediated signaling, even if contact may trigger initial apoptosis. Gene expression will focus on establishing a strong anchor within the bone marrow, but also on attracting other myeloma cells (via secretion of ECM factors and CXCL12/CXCL8, respectively). **Cell Division:** Cell fission can generate one daughter cell that no longer adheres to the MSC (nMA). **Homotypic Interaction:** If myeloma cells have the capacity to grow as aggregates, the daughter cell stays attached to their MSC-adhering mother cell (MA). **Re-Adhesion:** The daughter cell “rolls around” the mother cell until it re-adheres to the MSC. Our model estimates the rolling duration to be 1–10 h long. **Proliferation & Saturation:** We estimate that a single myeloma cell covers one MSC completely after roughly four population doublings. When heterotypic adhesion is saturated, subsequent daughter cells benefit from a homotypic interaction, since they stay close to growth-factor secreting MSCs and focus gene expression on proliferation (e.g. driven by E2F) and not adhesion (driven by NF- κ B). **Critical Size:** Homotypic interaction is weaker than heterotypic interaction, and each cell fission destabilizes the aggregate. Hence, detachment of myeloma cells may depend mostly on aggregate size. **Dissemination:** After myeloma cells have detached, they gained a viability advantage through IL-6-independence (with unknown duration), which enhances their survival outside of the bone marrow and allows them to spread throughout the body. This content has been taken as is from Kuric et al. (2024), published in *Cancer Research Communications* under the CC BY 4.0 license.

The first subpopulation, nMA-INA6, represented proliferative and disseminative cells; They drove detachment through cell division, which was regulated by E2F, p53, and likely their crosstalk (Polager & Ginsberg, 2009). nMA-INA6 upregulate cell cycle progression genes associated with worse prognosis, because proliferation is a general risk factor for an aggressive disease course (Hose et al., 2011). Additionally, nMA-INA6 survived IL-6 withdrawal better than CM-INA6 and MA-INA6, implying their ability to proliferate independently of the bone marrow (Bladé et al., 2022). Indeed, xenografted INA-6 cells developed autocrine IL-6 signaling but remained IL-6-dependent after explantation (Burger et al., 2001). The increased autonomy of nMA-INA6 cells can be explained by the upregulation of *IGF-1*, being the major growth factor for myeloma cell lines (Sprynski et al., 2009). Other reports characterized disseminating cells differently: Unlike nMA-INA6, circulating myeloma tumor cells were reported to be non-proliferative and bone marrow retentive (Garcés et al., 2020). In contrast to circulating myeloma tumor cells, nMA-INA6 were isolated shortly after detachment and therefore these cells are not representative of further steps of dissemination, such as intravasation, circulation or intravascular arrest (Zeissig et al., 2020). Furthermore, Brandl et al. described proliferative and disseminative myeloma cells as separate entities, depending on the surface expression of CD138 or JAM-C (Akhmetzyanova et al., 2020; A. Brandl et al., 2022). Although CD138 was not differentially regulated in nMA-INA6 or MA-INA6, both subpopulations upregulated JAM-C, indicating disease progression (A. Brandl et al., 2022).

Furthermore, nMA-INA6 showed that cell division directly contributed to dissemination. This was because INA-6 daughter cells emerged from the mother cell with distance to the hMSC plane in the 2D setup. A similar mechanism was described in an intravasation model in which tumor cells disrupt the vessel endothelium through cell division and detach into blood circulation (Wong & Searson, 2017). Overall, cell division offers key mechanistic insights into dissemination and metastasis.

The other subpopulation, MA-INA6, represented cells retained in the bone marrow; MA-INA6 strongly adhered to MSCs, showed NF- κ B signaling, and upregulated several retention, adhesion, and ECM factors. The production of ECM-associated factors has recently been described in MM.1S and RPMI-8226 myeloma cells (Maichl et al., 2023). Another report did not identify the upregulation of such factors after direct contact with the MSC cell line HS5; hence, primary hMSCs may be crucial for studying myeloma-MSC interactions (Dziadowicz et al., 2022). Moreover, MA-INA6 upregulated adhesion genes associated with prolonged patient survival and showed decreased expression in relapsed myeloma. As myeloma progression implies the independence of myeloma cells from the bone marrow (Bladé et al., 2022; Sarin et al., 2020), we interpreted these adhesion genes as mediators of bone marrow retention, decreasing the risk for dissemination and thereby

potentially prolonging patient survival. However, the overall impact of cell adhesion and ECM on patient survival remains unclear. Several adhesion factors have been proposed as potential therapeutic targets (A. Brandl et al., 2022; Bou Zerdan et al., 2022). Recent studies have described the prognostic value of multiple ECM genes, such as those driven by NOTCH (Maichl et al., 2023). Another study focused on ECM gene families, of which only six of the 26 genes overlapped with our gene set (Appendix A: Tabelle 2) (Evers et al., 2023). The expression of only one gene (*COL4A1*) showed a different association with overall survival than that in our cohort. The lack of overlap and differences can be explained by dissimilar definitions of gene sets (homology *vs.* gene ontology), methodological discrepancies, and cohort composition.

In summary, our *in vitro* model provides a starting point for understanding the initiation of dissemination and its implications for patient survival, providing innovative methods, mechanistic insights into attachment/detachment, and a set of clinically relevant genes that play a role in bone marrow retention. These results and methods might prove useful when facing the heterogeneity of disseminative behaviors among myeloma cell lines and primary materials.

Chapter 2: Semi-Automating Data Analysis with `plotastic`

The following chapter has been taken with slight adjustments from Kuric & Ebert (2024), published in *Journal of Open Source Software* under the CC BY 4.0 license, and was expanded with introduction and discussion sections.

Abstract

`plotastic` addresses the challenges of transitioning from exploratory data analysis to hypothesis testing in Python’s data science ecosystem. Bridging the gap between `seaborn` and `pingouin`, this library offers a unified environment for plotting and statistical analysis. It simplifies the workflow with user-friendly syntax and seamless integration with familiar `seaborn` parameters (`y`, `x`, `hue`, `row`, `col`). Inspired by `seaborn`’s consistency, `plotastic` utilizes a `DataAnalysis` object to intelligently pass parameters to `pingouin` statistical functions. Hence, statistics and plotting are performed on the same set of parameters, so that the strength of `seaborn` in visualizing multidimensional data is extended onto statistical analysis. In essence, `plotastic` translates `seaborn` parameters into statistical terms, configures statistical protocols based on intuitive plotting syntax and returns a `matplotlib` figure with known customization options and more. This approach streamlines data analysis, allowing researchers to focus on correct statistical testing and less about specific syntax and implementations.

Introduction

The reproducibility crisis in research highlights a significant challenge in contemporary biosciences, where a substantial portion of studies faces reproducibility issues (Baker, 2016; Begley & Ioannidis, 2015; Gosselin, 2021). One critical yet often overlooked aspect contributing to this crisis is data management. The literature most often refers to *big data* as the main challenge (Gomez-Cabrero et al., 2014). However, these challenges are also present in smaller datasets, which the author refers to as *semi-big data*. This term describes datasets that – while not extensive enough to necessitate advanced computational tools typically reserved for *big data* – are sufficiently large to render manual analysis very time-intensive. Semi-big data is often generated by methods like automated microscopy or multiplex qPCR, which produce volumes of data that are manageable on a surface level, but pose substantial barriers for in-depth, manual reproducibility (Bustin, 2014; Incerti et al., 2019). This is further complicated by the complexity inherent in multidimensional datasets (Krzywinski & Savig, 2013): Modern biosciences describe processes (e.g. cell-adhesion) that are highly dependent on multiple experimental parameters (factors), like ‘*time*’ or ‘*kinds of treatments*’ (Rebl et al., 2010; McKay et al., 1997). Manually grouping the data by multiple factors (facetting) is challenging and error-prone, especially when the data is not structured in a way that is immediately compatible with statistical tests. Without a clearly documented data analysis protocol and standardized data formats, analysis of multidimensional data becomes nontransparent and too overwhelming for reproduction (Bustin, 2014).

The evolving standards in data analysis advocate for the standardization of analytical pipelines, rationalization of sample sizes, and enhanced infrastructure for data storage, addressing some of these challenges (Goodman et al., 2016; Wilkinson et al., 2016). However, these advancements can place undue pressure on researchers, particularly those with limited training in statistics, underscoring the need for intuitive, user-friendly analytical tools (Federer et al., 2016; Lakhlifi et al., 2023; Armstrong, 2014; Gómez-López et al., 2019; Leek & Peng, 2015).

In this context, `plotastic` emerges as a tool designed to democratize access to sophisticated statistical analysis, offering a user-centric interface that caters to researchers across varying levels of statistical proficiency. `plotastic` simplifies inferential statistics building on a simple idea: Statistical analyses are often performed based on how the data is visualized. For example, the results of a qPCR are categorized by gene; hence, both ANOVA and plot can be accomplished in parallel for every gene independently and automatically. This principle is not only intuitive but also statistically sound, because the parameters that structure the figure (e.g. facetting) are often times re-used for statistical testing (e.g. independent variables or factors). By integrating robust statistical methodologies within an accessible framework, `plotastic` could contribute to enhancing the reproducibility of research in the biosciences (Gomez-Cabrero et al., 2014).

`plotastic` key design feature is centralizing the facetting parameters utilized by `seaborn` into a `DataAnalysis` object. `seaborn` uses the parameters `x`, `hue`, `col`, `row` as arguments for many plotting functions. These parameters lay out the structure of the plot, such as which data points are shown on the x-axis, what categories are highlighted by color (`hue`), and how data is grouped into separate plots (by columns and/or rows). By centralizing these parameters, `plotastic` ensures that all subsequent analysis steps do not require the user to re-specify these parameters, automating not only statistical analysis, but also all edits applied to the plot, such as *p*-value annotations.

The user-centric approach of `plotastic` distinguishes itself from the fully automated pipelines used

for big data, which are designed to handle extensive computational tasks. Instead, plotastic focuses on ease-of-use and structures its commands to enable an interactive review of intermediate outputs, a concept the author refers to as *semi-automation* (Tabelle 1).

Table 1: Key Principles of Semi-Automation and their Implementation in plotastic

No.	Principle	Implementation in plotastic
1	Standardized input: The data to-be-analyzed follows a strict standardized format. The user should be able to convert their data into that format.	Long-format pandas DataFrames are used as input
2	Automation over flexibility: If there is an obvious way to do things, automate it and minimize user input. User options should be added with good reason. Avoid situations where the user is asked to pass the same parameter twice. This reduces the risk of human error, confusion and time spent on configuration.	E.g. passing the parameter “subject” once makes the rest of the pipeline switch automatically to the paired versions of statistical tests.
3	Out of the box functionality: The software’s default configuration should provide acceptable (but potentially sub-optimal) results. Beginners should be invited to experiment without the need to learn custom configurations. Options are still available to allow feature-rich adaptions according to the needs of both data and user.	Default tests are standard unpaired t-tests and ANOVA
4	Focus on intermediate outputs: The user composes the analysis pipeline using smaller commands that are each designed to provide human-readable output of an intermediate result. Each step is a stage to control quality, allowing quick error detection and troubleshooting.	Processing steps are separated into main steps: assumption tests, factor analysis, post-hoc analysis and plotting
5	Highly useful error messages: Never leave the user hanging. Tell him what went wrong <i>and</i> what the software was expecting.	E.g.: ValueError: User passed 'subect' as subject, please choose one of ['subject', 'event', 'region']

The need for plotastic in this specific project is described in detail in the summarizing discussion (p. 75), since this chapter focuses on the software itself. In short, two main challenges arose that led to the development of plotastic: The first is the author’s need for a tool that could handle the complex, multidimensional data generated by e.g. qPCR experiments. These experiments involved the analysis of multiple outcomes across multiple genes, timepoints, method variations, cell-types, biological replicates, technical replicates etc., resulting in datasets with about 2970 datapoints spread over four dimensions: three subpopulations, one timepoint, eleven biological replicates, and three technical replicates. Such complexity was necessary, since establishing new methods required extensive controls and creative variation of the experimental setup. Data analysis had to be automated somehow, since the lab-work itself was already time-intensive.

The second challenge was to accept the potential of plot-configured statistical analyses. The author believes that the way data is visualized is often the way it should be analyzed, e.g. accomplishing both plot and ANOVA in parallel for every gene when showing qPCR results. This vision is not limited to biomedical application, but a general principle that could benefit the scientific community overall. Making plotastic a generalized tool was a conscious decision to maximize its adoption rate and ensure its long-term relevance and quality, of which biomedical research will also benefit.

Statement of Need

Python's data science ecosystem provides powerful tools for both visualization and statistical testing. However, the transition from exploratory data analysis to hypothesis testing can be cumbersome, requiring users to switch between libraries and adapt to different syntaxes. `seaborn` has become a popular choice for plotting in Python, offering an intuitive interface. Its statistical functionality focuses on descriptive plots and bootstrapped confidence intervals (Waskom, 2021). The library `pingouin` offers an extensive set of statistical tests, but it lacks integration with common plotting capabilities (Vallat, 2018). `statannotations` integrates statistical testing with plot annotations, but uses a complex interface and is limited to pairwise comparisons (Charlier et al., 2022).

`plotastic` addresses this gap by offering a unified environment for plotting and statistical analysis. With an emphasis on user-friendly syntax and integration of familiar `seaborn` parameters, it simplifies the process for users already comfortable with `seaborn`. The library ensures a smooth workflow, from data import to hypothesis testing and visualization.

Example

The following code demonstrates how plotastic analyzes the example dataset “fmri”, similar to Waskom (2021) (Abbildung 1).

```
1  ### IMPORT PLOTASTIC
2  import plotastic as plst
3
4  # IMPORT EXAMPLE DATA
5  DF, _dims = plst.load_dataset("fmri", verbose = False)
6
7  # EXPLICITLY DEFINE DIMENSIONS TO FACET BY
8  dims = dict(
9      y = "signal",    # y-axis, dependent variable
10     x = "timepoint", # x-axis, independent variable (within-subject factor)
11     hue = "event",   # color, independent variable (within-subject factor)
12     col = "region"   # axes, grouping variable
13 )
14 # INITIALIZE DATAANALYSIS OBJECT
15 DA = plst.DataAnalysis(
16     data=DF,           # Dataframe, long format
17     dims=dims,         # Dictionary with y, x, hue, col, row
18     subject="subject", # Datapoints are paired by subject (optional)
19     verbose=False,     # Print out info about the Data (optional)
20 )
21 # STATISTICAL TESTS
22 DA.check_normality() # Check Normality
23 DA.check_sphericity() # Check Sphericity
24 DA.omnibus_rm_anova() # Perform RM-ANOVA
25 DA.test_pairwise()   # Perform Posthoc Analysis
26
27 # PLOTTING
28 (DA
29 .plot_box_strip()    # Pre-built plotting function initializes plot
30 .annotate_pairwise(  # Annotate results from DA.test_pairwise()
31     include="__HUE" # Use only significant pairs across each hue
32 )
33 )
```

Overview

The functionality of plotastic revolves around a seamless integration of statistical analysis and plotting, leveraging the capabilities of pingouin, seaborn, matplotlib and statannotations (Vallat, 2018; Waskom, 2021; Hunter, 2007; Charlier et al., 2022). It utilizes long-format pandas DataFrames as its primary input, aligning with the conventions of seaborn and ensuring compatibility with existing data structures (Wickham, 2014; Team, 2020; McKinney, 2010).

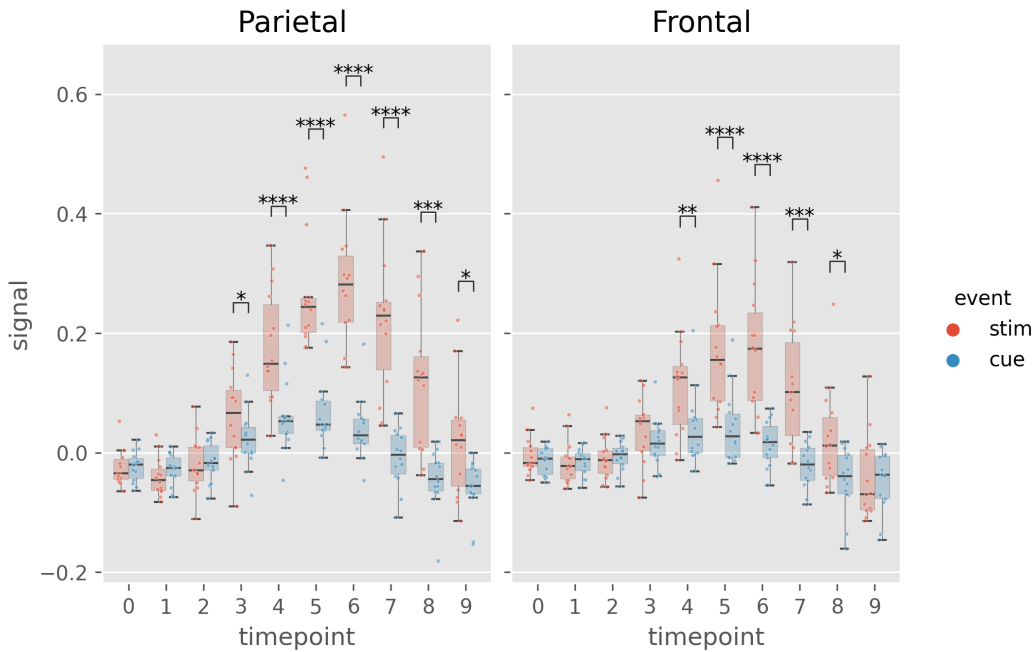


Figure 1: Example figure of plotastic (version 0.1). Image style was set by `plt.style.use('ggplot')`. This content has been taken as is from Kuric & Ebert (2024), published in *Journal of Open Source Software* under the CC BY 4.0 license.

plotastic was inspired by seaborn using the same set of intuitive and consistent parameters (`y`, `x`, `hue`, `row`, `col`) found in each of its plotting functions (Waskom, 2021). These parameters intuitively delineate the data dimensions plotted, yielding ‘faceted’ subplots, each presenting `y` against `x`. This allows for rapid and insightful exploration of multidimensional relationships. plotastic extends this principle to statistical analysis by storing these seaborn parameters (referred to as dimensions) in a `DataAnalysis` object and intelligently passing them to statistical functions of the pingouin library. This approach is based on the impression that most decisions during statistical analysis can be derived from how the user decides to arrange the data in a plot. This approach also prevents code repetition and streamlines statistical analysis. For example, the `subject` keyword is specified only once during `DataAnalysis` initialisation, and plotastic selects the appropriate paired or unpaired version of the test. Using pingouin alone requires the user to manually pick the correct test and to repeatedly specify the `subject` keyword in each testing function.

In essence, plotastic translates plotting parameters into their statistical counterparts. This translation minimizes user input and also ensures a coherent and logical connection between plotting and statistical analysis. The goal is to allow the user to focus on choosing the correct statistical test (e.g. parametric vs. non-parametric) and worry less about specific implementations.

At its core, plotastic employs iterators to systematically group data based on various dimensions, aligning the analysis with the distinct requirements of tests and plots. Normality testing is performed on each individual sample, which is achieved by splitting the data by all grouping dimensions and also the `x`-axis (`hue`, `row`, `col`, `x`). Sphericity and homoscedasticity testing is performed on a complete sampleset listed on the `x`-axis, which is achieved by splitting the data by all grouping dimensions (`hue`, `row`, `col`) (Tabelle 2). For omnibus and posthoc analyses, data is grouped by the `row` and `col` dimensions in parallel to the matplotlib axes, before performing one two-factor analysis per axis using `x` and `hue` as the within/between-factors. (Tabelle 3).

Table 2: Results from DA.check_sphericity(). plotastic assesses sphericity after grouping the data by all grouping dimensions (hue, row, col). For example, DA.check_sphericity() grouped the ‘fmri’ dataset by “region” (col) and “event” (hue), performing four subsequent sphericity tests for four datasets. This content has been taken as is from Kuric & Ebert (2024), published in *Journal of Open Source Software* under the CC BY 4.0 license.

‘region’, ‘event’	spher	W	chi2	dof	pval	group count	n per group
‘frontal’, ‘cue’	True	3.26e+20	-462.7	44	1	10	[14]
‘frontal’, ‘stim’	True	2.45e+17	-392.2	44	1	10	[14]
‘parietal’, ‘cue’	True	1.20e+20	-452.9	44	1	10	[14]
‘parietal’, ‘stim’	True	2.44e+13	-301.9	44	1	10	[14]

Table 3: Results of DA.omnibus_rm_anova(). plotastic performs one two-factor RM-ANOVA per axis (grouping the data by row and col dimensions) using x and hue as the within-factors. For this example, DA.omnibus_rm_anova() grouped the ‘fmri’ dataset by “region” (col), performing two subsequent two-factor RM-ANOVAs. Within-factors are “timepoint” (x) and “event” (hue). For conciseness, GG-Correction and effect sizes are not shown. This content has been taken as is from Kuric & Ebert (2024), published in *Journal of Open Source Software* under the CC BY 4.0 license.

‘region’	Source	SS	ddof1	ddof2	MS	F	p-unc	stars
‘parietal’	timepoint	1.583	9	117	0.175	26.20	3.40e-24	****
‘parietal’	event	0.770	1	13	0.770	85.31	4.48e-07	****
‘parietal’	timepoint * event	0.623	9	117	0.069	29.54	3.26e-26	****
‘frontal’	timepoint	0.686	9	117	0.076	15.98	8.28e-17	****
‘frontal’	event	0.240	1	13	0.240	23.44	3.21e-4	***
‘frontal’	timepoint * event	0.242	9	117	0.026	13.031	3.23e-14	****

DataAnalysis visualizes data through predefined plotting functions designed for drawing multi-layered plots. A notable emphasis within plotastic is placed on showcasing individual datapoints alongside aggregated means or medians. In detail, each plotting function initializes a matplotlib figure and axes using plt.subplots() while returning a DataAnalysis object for method chaining. Axes are populated by seaborn plotting functions (e.g., sns.boxplot()), leveraging automated aggregation and error bar displays. Keyword arguments are passed to these seaborn functions, ensuring the same degree of customization. Users can further customize plots by chaining DataAnalysis methods or by applying common matplotlib code to override plotastic settings. Figures are exported using plt.savefig().

plotastic also focuses on annotating statistical information within plots, seamlessly incorporating p-values from pairwise comparisons using statannotations (Charlier et al., 2022). This integration simplifies the interface and enables options for pair selection in multidimensional plots, enhancing both user experience and interpretability.

For statistics, plotastic integrates with the pingouin library to support classical assumption and hypothesis testing, covering parametric/non-parametric and paired/non-paired variants. Assumptions such as normality, homoscedasticity, and sphericity are tested. Omnibus tests include two-factor RM-ANOVA, ANOVA, Friedman, and Kruskal-Wallis. Posthoc tests are implemented through pingouin.pairwise_tests(), offering (paired) t-tests, Wilcoxon, and Mann-Whitney-U.

To sum up, plotastic stands as a unified and user-friendly solution catering to the needs of researchers

and data scientists, seamlessly integrating statistical analysis with the power of plotting in Python. It streamlines the workflow, translates `seaborn` parameters into statistical terms, and supports extensive customization options for both analysis and visualization.

Discussion

As awareness of the complexities associated with multidimensional data in biomedical research increases, there is a growing demand for tools that not only simplify analysis but also enhance its intuitiveness and effectiveness (Dunn et al., 2017). `plotastic` is designed to meet this demand by seamlessly integrating data visualization with inferential statistics, making sophisticated statistical methods accessible to researchers of all expertise levels. This integration could be pivotal as it allows the visualization of data —how it is grouped and presented— to directly guide the statistical analysis, reducing the need for in-depth statistical knowledge and ensuring that the analyses are intuitively aligned with the visual aspects of the data. This approach could not only simplify the analytical process but also enhance the transparency and reproducibility of research findings.

Statistical Features: A detailed list of implemented and planned features is provided on the GitHub page of the project (Kuric, 2024). `plotastic` is comprehensive in its current scope, incorporating a robust suite of statistical tests that cater to a wide range of research needs. It includes assumption tests for normality, homoscedasticity, and sphericity, alongside classical statistical tests such as ANOVA and t-tests, available in both parametric and non-parametric forms, as well as paired and unpaired variants. However, its reliance on the `pingouin` library means that `plotastic` is subject to the same limitations as `pingouin` itself. For instance, it does not yet support survival analysis tools like log-rank tests and Kaplan-Meier plots, which are critical for certain biomedical applications. While there are external packages that offer these capabilities, integrating them into `plotastic` could significantly expand its utility and provide a more unified user experience (Davidson-Pilon, 2019).

One known issue in `plotastic` is its handling of multiple testing corrections. Currently, `plotastic` might not correctly apply these corrections when the data is split across different facets with their own y-axes (facetted by `row` and `col` keywords), which can lead to potentially incorrect statistical inferences. This is a fixable issue, and plans are in place to address it in upcoming versions to ensure that corrections for multiple testing are appropriately applied across the complete dataset. Additionally, bivariate analysis tools like correlation and regression are not yet implemented, since `plotastic` focused on data with a categorical x-axis, which is more common in biomedical research.

Plotting Features: The plotting capabilities of `plotastic` employ all of `seaborn`'s non-facetgrid plotting functions (e.g. `sns.boxplot()`), which include a wide range of plot types but may not cover all possible visualizations (Waskom, 2021). Future versions could expand the range of specialized plots, for example QQ-plots. `plotastic` focuses on offering both high- and low-level plotting configuration: Multiplots automate overlaying multiple plot types, which is extremely useful for displaying raw data points alongside aggregated statistics (barplots, boxplots, etc.), a feature that can be cumbersome to implement manually. Low-level plotting configuration is supported just like in `seaborn`, since `plotastic` uses `matplotlib` as its backend. This level of flexibility is unique to `plotastic`, serving both beginners and advanced users.

Plot Annotation: Annotating statistical results into plots (e.g. *** above barplots) is a key requirement in modern biomedical journals and could be key feature why researchers choose proprietary software like *GraphPad Prism* over other solutions. `plotastic` automates this process as well, making it a strong competitor to other statistical software. This is especially useful for re-arranging plots, since the statistical annotations are automatically updated when the plot is re-drawn. This feature is unique to `plotastic` and could be a key selling point for the software.

Software Testing: The development of `plotastic` adheres to modern software engineering principles to ensure reliability and maintainability. The project utilizes continuous integration practices, which means that with every change to the codebase, a comprehensive test suite is automatically run to identify potential bugs and ensure that new contributions do not disrupt existing functionalities. This test suite covers approximately 79 % of the testable lines of code, a statistic tracked automatically by an independent service called codecov, highlighting a strong commitment to software quality (*Codecov, o. J.*).

No Official Support for Interactive Plots: Interactive plots are a popular feature in modern data visualization tools, allowing users to explore data dynamically, e.g. hovering over data points to display additional information, or zooming in on specific regions of a plot. Python has several libraries that support interactive plotting, such as `plotly` and `bokeh` (Inc., 2015; Bokeh Development Team, 2018). The ability to include interactive 3D figures into .pdf articles without commercial software have been around for over a decade (Barnes et al., 2013). `plotastic` could also support interactive plotting through its `matplotlib` backend, but there are no plans to officially support this feature.

Documentation: Documentation serves as a critical resource for enhancing user experience and adoption, especially for software aimed at users with varying levels of expertise. Currently, `plotastic`'s documentation is focused on basic functionalities. These include detailed installation instructions, example analyses using five test datasets from `seaborn` that are commonly used in teaching statistics, guidelines on dimension switching with commands like `DataAnalysis.switch()`, and tutorials on constructing and configuring plots, annotating statistical data, and utilizing multiplot capabilities.

However, the documentation of `plotastic` could be significantly enhanced. Currently, it lacks a dedicated website, relying instead on GitHub-hosted Jupyter notebooks. While useful, these notebooks are not the most user-friendly or maintainable format for documentation as they can be challenging to navigate and don't update synchronously with software changes. A more robust approach would involve leveraging services like Read the Docs or Sphinx to generate and host documentation directly from the codebase (*Read the Docs*, 2024; G. Brandl, 2021). This would not only ensure that the documentation remains up-to-date with the latest software developments but also provide a more accessible and navigable user experience, meeting the expectations of users who prefer a dedicated website for software documentation.

Usability for Non-Statisticians: `plotastic` aims to make statistical analysis more accessible to researchers without extensive statistical training by intuitively mapping plotting concepts to statistical operations. To the author's knowledge, this approach is unique to `plotastic` and has great potential to make statistics easier and educational for non-statisticians. Still, the software requires responsible and self-critical usage, as emphasized by the thorough disclaimer on its GitHub page regarding the software's statistical robustness, (Kuric, 2024). The disclaimer highlights that while `plotastic` can facilitate gaining practical experience with statistics and provide a preliminary analysis, it is not a substitute for professional statistical consultation. It is designed to aid users in generating publication-grade figures and performing statistical tests, provided they have a basic understanding of the procedures involved or have their results verified by a statistician. To enhance usability for non-statisticians, `plotastic` could incorporate a system to suggest appropriate statistical tests based on data characteristics, like parametric tests for normally distributed data. This feature would guide users in selecting the correct tests, thereby augmenting the tool's functionality and broadening its appeal. Additionally, the GitHub page provides critical guidelines for responsible statistical practice, urging users to document their work in detail, understand the limitations of the tests applied, and consult professionals to validate their findings, ensuring that `plotastic` supports but does not replace thorough statistical analysis (Sandve et al., 2013; Kuric, 2024).

Usability for Non-Programmers: Despite the advantages of `plotastic`, its adoption among non-programmers in biomedicine may be challenging due to its reliance on a Command Line Interface (CLI), which is less intuitive for those accustomed to Graphical User Interface (GUI). However, the integration of Large Language Models (LLMs), such as *ChatGPT*, presents a compelling case for embracing CLI. Indeed, *ChatGPT* is believed to potentially revolutionize medical research (Ruksakulpiwat et al., 2023).

Unlike GUIs, CLIs are highly compatible with text-based AI technologies, which can significantly lower the barrier to entry. In fact, both *ChatGPT*-3.5 and 4 demonstrate impressive performance in python (Arefin et al., 2024). This is a game changer, since researchers can now use similar tools as programmers and are only limited by their methodological expertise to formulate a correct prompt (Qureshi et al., 2023)[†]. For instance, when a software is not working as intended, users of a GUI are likely to be stuck without help or further research. Users of a CLI however, could utilize *ChatGPT* to ask for code-corrections or explanations of the code line-by-line, but also for advice on how to proceed with a statistical analysis and how to implement new features (e.g. editing a plot). Attempts to integrate AI into GUIs however have proven challenging (D. Gao et al., 2024).

Still, *ChatGPT* requires responsible use, as it is not sufficient as a standalone tool for statistical analysis (Ordak, 2023). It should also be noted that `plotastic` is not yet known to *ChatGPT*, but could be included in future versions, depending on the popularity of `plotastic`.

Overall, the transition to a new data analysis software, especially one that incorporates coding, presents a learning curve. However, the advantages of `plotastic` in terms of analytical clarity, speed, and depth are anticipated to outweigh these initial challenges.

Adoption and Open-Source Contributions: The adoption rate of `plotastic` is a critical factor for its sustainability, particularly in the open-source environment where community contributions can significantly support the author in improving and maintaining the software. Between its publication in the Journal of Open Source Software on the 09.03.2024 and the print of this thesis on the 02.09.2024, `plotastic` has garnered 10 *stars*—similar to a ‘like’ on social media platforms—on its GitHub page. This level of engagement, while modest, shows initial interest and potential for growth. Active involvement from the community is essential for ongoing improvements; hence, efforts are being made to enhance the software’s documentation and structure to attract more contributors: `plotastic`’s GitHub page shows a detailed outline of the software’s architecture as a class diagram in unified modeling language (UML) format, helping potential contributors orient themselves within `plotastic`’s several modules and classes (shown in Appendix B.1). But further efforts are required, e.g. only few functions are documented with docstrings, which help understanding the purpose and usage of each function. Still, `plotastic` is a general-purpose data analysis software designed not only for biologists but for a broad range of scientific disciplines, making it a versatile tool with promising potential for wider adoption.

Contributions to Methodological Transparency and Biomedicine: `plotastic` standardizes statistical analysis by ensuring that it is performed alongside visual representations. This integrated approach simplifies both analysis and interpretation, facilitating smooth replication of analyses. Although it streamlines the data analysis process, it is not a complete solution to the reproducibility crisis in scientific research. Researchers must still possess a basic understanding of data analysis principles and be

[†] Kelleher (2024):

“*You can now recognize and learn the language of almost anything with structure, and you can translate it to anything with structure — so text-protein, protein-text. [...] Everybody is a programmer, and the programming language of the future is called ‘human.’*”

cautious about their reliance on scripting solutions like Python, which is less familiar to some biomedical researchers.

Statistical literacy and lack of training is a well-documented challenge among clinicians and biomedical researchers, decreasing the confidence in presenting their analyses in detail (Lakhli et al., 2023; Federer et al., 2016). Since `plotastic` alleviates some need for statistical knowledge by automating the configuration of statistical tests, the room for error is reduced, and the user can lay off some responsibility to the software, gaining confidence in presenting their analysis transparently.

Furthermore, `plotastic`'s compatibility with the Jupyter ecosystem leverages “*simple, intuitive ways to both capture and embed computational work directly into our papers*” as advocated by Mesirov (2010). This integration makes `plotastic` not just a tool for analysis but also a means of enhancing the accessibility and reproducibility of scientific work. As Peng (2011) suggests, data exploration and analysis code could sufficiently verify the quality of scientific claims. This seems plausible, given that statistical tests themselves pose rigorous requirements on the data, while data explorations provide the context necessary for independent interpretation. Thus, combining `plotastic` with Jupyter Notebooks provides a compelling solution to transparently integrate and document both intermediate results and analytical processes, thus furthering scientific rigor and replicability.

Overall, `plotastic` is useful statistical tool with the potential to improve methodological transparency and reproducibility of research in biomedicine.

Summarizing Discussion

The subsequent sections will discuss the chapters presented earlier, focusing on how they fit within current scientific fields and the technical and academic challenges encountered during this project. Given the extensive scope of the topics covered, this discussion is divided into three main sections: Data analysis, microscopy and cancer cell biology. Each section will detail key experiments that led to shifts in understanding and present intermediary conclusions to ensure clarity on broad topics.

Semi-Automation was Critical for Establishing *in vitro* Methods

In vitro research is valued for their speed at creating precise data (Moleiro et al., 2017). In this work, the development and publication of innovative *in vitro* methodologies necessitated the adoption of semi-automated data analysis tools. These novel methods introduced complexities that span multiple experimental parameters, making the results multidimensional. This demanded precise, efficient and standardized data handling capabilities which were facilitated by Python tools like seaborn and plotastic (Waskom, 2021; Kuric & Ebert, 2024).

Inherent Multidimensionality of Adhesion Studies: Cell adhesion studies often involve multiple independent parameters, posing significant analytical challenges. Two critical dimensions are particularly notable: ‘*Subpopulation*’ and ‘*Time*’. Analyzing cell adhesion often involves isolation of adherent and non-adherent subpopulations, effectively introducing ‘*Subpopulation*’ as a vital dimension in the dataset (Dziadowicz et al., 2022). This study specifically categorized cells into three levels of MSC-interaction: CM-INA6, nMA-INA6, and MA-INA6, representing INA-6 cells incubating in MSC-conditioned medium, INA-6 cells not adhering to MSCs, and INA-6 cells adhering to MSCs, respectively. Furthermore, the dynamic nature of cell adhesion processes is profoundly influenced by the factor ‘*Time*’, making it a crucial experimental parameter for investigation (Rebl et al., 2010; McKay et al., 1997; Bolado-Carrancio et al., 2020). In fact, the lack of time-series measurements was brought forward as a central roadblock[†] for understanding cancer as a dynamic system. (Uthamacumaran & Zenil, 2022). This work includes extensive time-lapse microscopy experiments utilizing a high time resolution (1 frame every 15 min), similar to those time resolutions used by Purschke et al. (2010). This precision was required for key mechanistic insights on hMSC-INA-6 interaction dynamics. These included identifying rolling movements of nMA-INA6 daughter cells around MA-INA6 mother cells, measuring the minimum time for INA-6 detachments to begin, and measuring the time required for daughter cells to re-attach to the hMSC monolayer, etc. Next to mechanistic insights, adhesion time played a crucial methodological role in this study as well: During the V-Well adhesion experiments, we did not know initially how long INA-6 cells required to form strong adhesion with hMSCs before pelleting nMA-INA6, but required a timepoint with hour precision to capture detachments after cell division that was accelerated through prior cell cycle synchronization at M-Phase.

The extensive facetting features of seaborn and plotastic were essential for visualizing these multi-dimensional datasets, allowing for quick exploration of the data (Waskom, 2021).

Further Contributions and Remedies to Multidimensional Complexity: In addition to ‘*Subpopulation*’ and ‘*Time*’, this study faced additional layers of complexity that were managed through semi-automated analysis.

Experiments typically involved at least three biological replicates and corresponding technical replicates. Although replicates were not treated as independent variables—instead serving for displaying variance—they can add substantially to the data management workload. In this work, semi-automation nullified the manual burdens of handling technical replicates: pandas was used to automate aggregation of technical replicates into means after removing technical outliers thorough z-score thresholding, while the

[†] Uthamacumaran & Zenil (2022):

“The lack of time-series measurements in single-cell multi-omics (e.g., gene expression dynamics, protein oscillations, histone marks spreading, etc.) and cell population fluctuations (i.e., ecological dynamics), in patient-derived tumor and liquid biopsies, remains a central roadblock in reconstructing cancer networks as complex dynamical systems.”

jupyter notebook format allowed for reviewing filtered data for specific data losses. The removal of technical noise was especially relevant for qPCR data, where low gene expression can lead to sudden increase in Ct value (non-detects). In fact, the decision to remove or impute non-detects is under active discussion, however, available algorithms are hard to understand for non bioinformaticians, but also do not separate biological from technical variance, which is considered bad practice by Motulsky (2017) (McCall et al., 2014; Sherina et al., 2020). Semi-automation also nullified the burden of handling biological replicates: The automatic aggregation of datapoints during plotting is a key feature of seaborn, on which plotastic was built. Without such automation, calculating means and standard deviations for simple barplots would have required extensive manual computation in *Microsoft Excel*, or tedious plot configurations in *GraphPad Prism* due to limited facetting functionality of multiple variable tables (*GraphPad Prism 10 User Guide*, 2024).

Replicates can expand datasets as this factor comprises a lot of levels. Similarly, the factor ‘*Gene*’ multiplied the dataset by a total of 30 genes when validating RNAseq data with RT-qPCR. With three subpopulations, one timepoint, eleven biological replicates, and three technical replicates, the qPCR dataset used in this study grew to 2970 datapoints to be statistically analyzed and visualized. This is a manageable size for manual analysis, but the effort involved illustrates the definition of semi-big data.

Methodological variability also introduced additional dimensions: The Well Plate Sandwich Centrifugation (WPSC) used two different techniques to dissociate MA-INA6 cells from the hMSC monolayer: Strong pipetting (‘*Wash*’) and repeated Accutase treatment followed by magnetic activated cell sorting (‘*MACS*’). These variations, recorded as the factor ‘*method*’, further complicated the dataset. Although this distinction is not discussed in this work—rather pooled into one group—, this showcases how protocol changes can add dimensions to the dataset that are not necessarily relevant for the biological question but essential for method optimizations and validation.

Agility During Establishment of V-Well Assay: The concept of agility in laboratory research, inspired by the Agile Manifesto’s principle of “*Responding to change over following a plan*” (Beck et al., 2001), is increasingly relevant in biomedical research (West, 2018; Quanbeck et al., 2022). This adaptive approach was particularly crucial during the development of the V-Well adhesion assay in this study. This experiment was planned such that the author performed fluorescent readout using microscopy and preliminary analysis, while a technical assistant prepared the samples for the next timepoint. Semi-automation accelerated the preliminary data analysis and visualization to a point that results were reviewable before the next sample timepoint was prepared and ready for fluorescent readout. This enabled immediate adjustments to the experimental protocol inbetween sample measurements, allowing for quick troubleshooting of small and avoidable problems that are often unforeseeable when establishing new methodologies. Without such agility, these problems would have been identified after the experiment, requiring a complete re-run of a very work-intensive experiment that included cell cycle synchronization. Such an agile and adaptive work environment, facilitated by python tools and seaborn, proved invaluable for refining the *in vitro* methods being developed.

Additionally, the simplicity offered by seaborn for complex data plotting, such as the cell cycle profiling shown in Appendix A.1: Abbildung 3, which required minimal code to produce a detailed series of 24 histograms, underscores the utility of semi-automation in enhancing laboratory efficiency. While this work does not quantify the full benefits of semi-automation, the author’s experiences suggest potential impacts on the speed and adaptability of method development in biomedical research.

plotastic Exceled in Re-Doing Statistical Analyses and Plots

Establishing new methods of *in vitro* dissemination required not just innovative experimental protocols, but also adaptive ways to visually present complex data. This need for adaptability is crucial during the publication process, where researchers must often experiment with different ways to visually represent their findings to best convey their significance. This process typically involves frequent adjustments to how data is displayed in plots. Such adjustments become especially cumbersome when subsequent adjustments are involved. Traditional tools (*Microsoft Excel* or *Graphpad Prism*) fail at handling semi-big data, while Python packages like *seaborn* reach their limits in terms of adaptability, making the development of *plotastic* a critical step in this work.

plotastic addresses these challenges by not only automating statistics, but also by enhancing the adaptability of data visualization as well, making it easier to modify how data is presented without repetitive manual adjustments. The author saw four key steps that required streamlining through *plotastic*:

1. Re-arranging facets
2. Plotting multiple layers of different plot types
3. Statistical Re-Analysis and Re-Annotation
4. Fine-Tuning for publication grade quality

These adjustment steps made re-plotting tedious, since a change in prior steps required a complete re-work of following steps, something which *plotastic* prevented. Its key design feature is the centralized storage of facetting parameters (*x*, hue, col, row). These parameters define which data points are shown on the x-axis, what categories are highlighted by color (hue), and how data is grouped into separate plots (by columns and/or rows) into separate plots. This centralization means that once these parameters are set, they not only automate statistical analysis, but also can be automatically applied across all subsequent adjustments made to the plot. This contrasts with *seaborn*, where changing these parameters required adjusting multiple lines of subsequent code.

Re-arranging Facets: *plotastic*'s `.switch()` method allowed for easily shifting the arrangement of plots—for example, switching the data represented on the x-axis with that represented by color—to explore different perspectives of the data quickly. This proved particularly useful when trying to find the most effective way to illustrate complex interactions or trends that might not be immediately apparent. In *seaborn*, changing facets is easy and proved useful during intermediate data analysis, but unfeasable when plots involved multiple layers, sophisticated style edits or statistical annotations, as this can require re-writing subsequent adjustments.

Plotting Multiple Layers of Different Plot Types: Modern journal standards increasingly demand the representation of individual datapoints alongside aggregated data, for example plotting datapoints above a bar- or boxplots. *seaborn* does not automate this, but can require calling two plotting functions in sequence, e.g. `sns.boxplot()` followed by `sns.swarmplot()`. This can get repetitive, as adjusting the style of these plots to match each other, e.g. defining the point size or transparency of individual data points to fit into a barplot. *plotastic* was designed for multi-layered plotting, offering single-line functions for plot combinations with pre-configured style-parameters.

Statistical Re-Analysis and Re-Annotation To the author's knowledge, *plotastic*'s capability of streamlining statistical re-analysis is unique and unmatched. *seaborn* alone can not perform this without multiple lines of `statannotations` (Charlier et al., 2022). *plotastic* automates the inclusion of statistical

annotations directly into plots. This is a significant enhancement because it ensures that any statistical significance noted in the data is immediately visible and correctly updated whenever the data presentation is changed. This feature proved particularly useful during the peer review process of Kuric et al. (2024), where a reviewer asked for a complete statistical analysis of Chapter 1 Fig. 5 D, which at that time included only paired t-tests between selected groups.

Fine-Tuning for Publication Grade Quality: `plotastic` simplified the creation of publication-quality figures by automating style adjustments that are typically manually coded with `matplotlib` when using `seaborn`. These include adjustments like angled x-axis labels or consistent visual styles across multiple figures, which are important for maintaining the professional appearance of published data.

Key Insight: Could `plotastic` Address a Re-Analysis Bottleneck? Re-doing analyses and plots is often overlooked bottlenecks in the reproducibility of scientific research, although it does overlap with two principles of the FAIR-guidelines for scientific data management and stewardship: Interoperability[†] and Re-Usability (Wilkinson et al., 2016). This challenge was exemplified during this work's experiments using RT-qPCR. The field of qPCR, where reproducibility issues have been notoriously prevalent. As Bustin (2014) noted, many publications using PCR-based methods have been seriously flawed, underscoring the need for updated approaches (Bustin et al., 2013; Ruiz-Villalba et al., 2021). Furthermore, the evolution of the $\Delta\Delta Ct$ formula over recent years highlights the dynamic nature of data analysis standards in biomedicine (Pfaffl, 2001; Ramakers et al., 2003; Ruijter et al., 2021). Despite these challenges, current data analysis infrastructures seldom facilitate a smooth revision or complete redoing of figures, which could hamper efforts to re-analyse and apply the latest techniques to existing datasets, which could be requested e.g. during peer-review (Wilkinson et al., 2016). In response, `plotastic` was specifically designed to streamline the reconfiguration and reanalysis of data visualizations. This work serves as a case study showing that—according to the author's experiences—the manual effort involved was effectively reduced, making the task of re-analysis seem a lot more inviting, especially for handling semi-big data.

[†] Wilkinson et al. (2016):

“Interoperability—the ability of data or tools from non-cooperating resources to integrate or work together with minimal effort.”

Conclusion 1: Demonstrating the Advantages of Semi-Automation in Biomedical Data Analysis

This thesis illustrates the challenges and solutions associated with managing the inherent complexity of adhesion studies and related methodologies, such as Cell Cycle profiling. These methodologies necessitate sophisticated data handling tools to address two primary challenges: (1) the multidimensionality of semi-big data and (2) the rapid iterative loop of results evaluation and protocol adjustments, a process for which *in vitro* methods are valued.

`seaborn` and `plotastic` have been instrumental in addressing these challenges. `seaborn` facilitated the rapid processing of intermediate results during method development, while `plotastic` was crucial for crafting publication-grade analyses and figures, filling in the capabilities that `seaborn` lacks. This includes facilitating the easy (re-)design of visualizations and statistical analyses, which are critical for late-stage data processing.

Though this work does not provide empirical evidence quantifying the benefits of semi-automation, it serves as a practical case study demonstrating the transformative potential of such technologies in biomedical research. The integration of semi-automation tools streamlined complex *in vitro* methodologies, significantly enhancing operational agility. This case study bridges biomedical research with bioinformatics, highlighting how semi-automation can reduce data analysis workloads and enable researchers to focus more on exploratory research within the laboratory setting.

To the author's experience, the gained efficiencies not only saved valuable time but also enhanced the clarity and communicative power of the research findings. This is particularly crucial in fields like myeloma dissemination, where precise and transparent data presentation is essential for advancing understanding and treatment strategies. This conclusion suggests a need for further empirical research to validate these benefits more broadly and encourage wider adoption of semi-automation tools in biomedical research.

However, adopting `plotastic` poses its own set of challenges, particularly in the realm of biomedicine where researchers may prefer graphical user interfaces (GUIs) over command-line interfaces (CLIs). While `plotastic` offers a powerful CLI that is efficient and capable of handling complex data manipulation and visualization tasks, the transition from GUIs to CLIs can be intimidating for those accustomed to more visual interaction with software. This barrier can be mitigated by the integration of tools like ChatGPT, which can facilitate the use of CLIs by offering context understanding, code assistance, and error identification.

How Exploratory Live-Cell Imaging Transformed the Research Focus

Exploratory experimentation emphasizes discovering and characterizing novel phenomena (Mättig, 2022). Exploratory cell biology often leverages emerging technologies to visualize and analyze the mechanisms of cell behavior dynamically. Such approaches allow real-time observations that can lead to unexpected insights and breakthroughs. In this project, the application of live-cell imaging proved pivotal.

Direct Observation of Complexity and Novelty: Initially, the project did not focus on *in vitro* myeloma cell dissemination. The project's research focus shifted when making the unexpected—or arguably insignificant—observation of cancer cells detaching from aggregates. This shows the transformative power of time-lapse microscopy or live cell imaging (Cole, 2014). For the author, live-cell imaging provides an observation method that's unmatched in intuition and directness. Unlike RNA sequencing, which can obscure biological processes behind cryptic data, live-cell imaging offers a clear view into the dynamic cellular events as they unfold.

Such clarity was particularly effective in revealing the detachment of cells following division, a phenomenon that might be overlooked in static analyses. Multiple parameters can be read out in parallel, such as both time and aggregate size for detachments to begin. Also, complex cellular behavior can be deduced from movement, or rather lack thereof, which was interpreted as re-attachment of INA-6 daughter cells to the hMSC monolayer. This allowed for measuring the duration of nMA-INA6 existing until re-attaching and turning into MA-INA6. This information was helpful when designing experiments to prove that dissemination is initiated by cell division, requiring precise timing to capture the detached daughter cells right after cell division. Together, live cell imaging enabled key mechanistic insights in understanding the dynamics involved in multicellular interactions by integrating the study of multiple phenomena at once.

Difficulties Connecting Observation with Academic Terminology Exploring video data begins with the search of scientific novelties. In order to correctly identify cellular phenomena relevant to the research question, a deep understanding of cell biology is required, e.g. in field of cell dynamics to read migratory behavior (Nalbant & Dehmelt, 2018). This is a challenge for both students and experienced researchers, since finding the academically correct terms to describe observations is difficult, especially for novel phenomena or a sequence of events that can overlap. After all, cell biology is taught using textbooks, not videos. For this project in particular, the used terminology was revised frequently, being caused by the constant struggle of finding the middle-ground between the precise description of observations, the compatibility with results from other experiments, comprehensability, and memorability. Ultimately, comprehensability and memorability were prioritized to maximize adoption of the new terminology by other researchers. For instance, *non MSC adherence* was chosen over *mobile interaction*, *aggregation* over *homotypic interaction*, and *detachment event* over *in vitro metastasis*. In general, the gap between observations and their description remains a challenge in exploratory cell biology that might be overlooked. This gap could be bridged by currently available multimodal LLMs like *ChatGPT-4o*: These models could match recorded phenomena with descriptions and images that were amassed in the literature over decades. By doing so, researchers not only use established terminology instead of inventing new terms, but also minimize the risk of missing potential discoveries.

Why Hide Videos Behind a Download Link? A major challenge remains in how to effectively present these dynamic observations in a publishable format, as traditional scientific publications and websites are not equipped to display video data. Instead, it is common practice to assemble video frames

into static figures, presumably to support both online and printed reading habits (Peras et al., 2023). Representative example videos are then relegated to supplementary data, similar to the publication from Chapter 1 (Kuric et al., 2024). Although supplementary data is downloaded often, most biomedical researchers favor a presentation of additional figures and tables directly on the journal's website (Price et al., 2018). Given the increasing availability of video data[†]. Embedding video content next to figures and tables on the article's website does make a compelling case. In fact, the journal *Nature* does offer this feature already, but rarely used (*Nature Video Content*, o. J.). In the end, there is no reason to not present videos alongside figures and tables, as they can be as informative, and potentially more so. Such new standards can benefit other fields of medicine, as videos provide the best medium for first aid, medical emergency and education (D. Gupta et al., 2023).

Key Points: Overall, Live-cell imaging has proven indispensable in exploratory cell biology, uncovering dynamic cellular phenomena that static analyses often miss, probably. This is exemplified in this work, where live-cell imaging shifted the research focus by revealing unexpected cell behaviors, like detachment during division, emphasizing the need for integrating real-time observations with molecular data. By making such dynamic processes visible, live-cell imaging not only enriches our understanding but also challenges us to enhance how scientific findings are presented, advocating for greater accessibility of video data in scientific publications.

[†] The total number of PubMed articles with “*live cell imaging*” has doubled from 1012 in the year 2011 to 1967 in 2023

Potential and Challenges of Image Cytometry

Quantifying microscopy data is critical for both analytic and exploratory approaches to microscopy: For instance, microscopic assessment of live/dead cells should produce bar charts presenting cell viabilities (Spaepen et al., 2011), whereas describing novel phenomena should be supported by charts proving the reproducibility of claimed observations. Microscopy data is source of vast amount and types of information: cell morphology; organelle count, shape, and distribution; membrane and lipid distribution; protein localization, DNA content, et cetera. However, leveraging this information has always been limited by the ability to extract quantitative data from microscopy images (Galbraith, 2023). This extraction process is the essence of *image cytometry*, a field that has seen significant advances by integrating machine learning for automating image analysis tasks. (A. Gupta et al., 2019). The following sections discuss the experiences gained from this project in quantifying microscopy data and outlines potentials and challenges of image cytometry.

Considering Automated Analysis for Future Live-Cell Imaging: This work would have benefited from computational automation for the analysis of live-cell imaging, for example, the task of associating INA-6 cell detachment with INA-6 aggregate size and time: Manual analysis consisted of zooming in closely and watching the time-lapse over and over again until a detachment event was found. A very tedious and error-prone task that had to be repeated approx. 50 times for every one of four independent videos. Instead of manually counting the number of single INA-6 cells across time, a pixel segmentation algorithm could have been trained to detect cells and background. Single cells would be discernable from aggregates by filtering cells by size. The count of single cells would then be representative of detached cells, given that the vast majority of INA6 cells were part of aggregates.

The workload of manual video analysis motivated the purchase of Intellesis, a software package by Zeiss for the Zen microscopy software ecosystem. Intellesis is a machine learning-based pixel segmentation software (*Zeiss OAD Feature Extractors*, o. J.). As a feature extractor¹, it uses the first convolution layers of VGG19, which is convolutional neural network² (Simonyan & Zisserman, 2015). Intellesis does not contain a deep neural network for segmentation, but instead classifies pixel features using a *random forest classifier*. Random forest is a machine learning algorithm that—for small sets of training images—performs almost as well as deep neural networks, but are computationally far less demanding (Breiman, 2001; Richardson et al., 2023). A comparable hybrid approach was also used by Qamar et al. (2023) to segment images of bacterial spores into eight distinct pixel classes using only 50 training images. Also, free alternatives to Intellesis exist, such as Ilastik (Berg et al., 2019).

Intellesis proved useful for segmenting single multi-channel images. However, live cell imaging adds another layer of complexity to image analysis: The addition of a time axis encodes the motion of objects and other image features. This concept can be described with the term *optical flow* (Niekhorster, 2021). Mathematically speaking, optical flow is a vector field that describes the motion of image features¹

¹*Image Features*: Discernable elements of an image, such as edges, corners, directions, colors. These features are mathematically extractable using *filters*—also referred to as *convolution kernels*—, which are functions or algorithms applied to the pixel values of an image. For instance, *gabor filters* can extract edges of one particular direction, resulting in an image of the same size as the input, but showing only edges of one direction. *Feature extraction* is the process of applying multiple filters, resulting in a stack of filtered images called a feature vector. (Szeliski, 2011; A. Gupta et al., 2019)

²*Convolutional Neural Networks (CNN)*: Machine learning algorithms that use the output of a feature extractor¹ to feed into a neural network. The network then learns to associate these feature vectors with a label, such as *cell* or *background*. This is called *supervised learning*.

between consecutive frames of a video. It can be used to train machine learning models on video data efficiently (Robitaille et al., 2022). Without tricks like optical flow, machine learning algorithms like Intellesis segment the video frame by frame, ignoring the feature similarities between frames. This makes segmentation computationally inefficient, but not impossible (Pylvänäinen et al., 2023).

Together, future analyses of live-cell imaging data could benefit from the use of modern machine learning based tools that have been released recently, as summarised in Pylvänäinen et al. (2023).

Image Cytometry is Precise, Fast, Flexible and Accessible: In this study, image cytometry was indispensable for validating prior cell divisions within the nMA-INA6 cell population by profiling their DNA content. The complexity of this experiment required a method capable of managing a high throughput across three subpopulations, four timepoints, and two conditions, involving up to 24 samples per trial (Appendix A.1: Abbildung 3). Despite having access to automated Fluorescence-Activated Cell Sorting (FACS) equipment offered by the Core Unit FACS at the University of Würzburg, the author saw a more time- and cost-effective solution in the laboratory microscope equipped with motorized stage top and Intellesis. This setup scanned 96 different samples in 1.5 h, and resulting large scans were processed by Intellesis overnight, quantifying thousands of DNA-stained nuclei. This demonstrated that image cytometry could match the throughput and precision of FACS with modern standard microscopy equipment (Appendix A.1: Abbildung 2).

The advantages of image cytometry could have of great impact for the future of cell biology: It is applicable to adherent cell cultures (Roukos et al., 2015) and provides diverse readouts like structure, brightness, size, and shape. Moreover, image cytometry's capacity to evaluate cell viability without the need for staining or expensive analytical chemicals makes it an exceptionally cost-efficient approach for drug screening, reducing operational costs to cell culturing and electricity for microscopy (Pattarone et al., 2021). However, challenges such as the need for sophisticated automation in microscopic scans, including autofocus and shading adjustments, and the computational demands of AI processing remain.

Interestingly, the author's initial unfamiliarity with image cytometry and limited experience in image processing did not prevent the effective use of this technology. This underscores the accessibility of current imaging tools to biologists without specialized training in image analysis. As confirmed by recent advancements (Nitta et al., 2023), image cytometry is becoming increasingly competitive with established techniques like FACS. Despite its limitations, the simplicity and efficiency of image cytometry could be pivotal for its broader acceptance and integration into biological research. The exclusivity of Intellesis to Zeiss microscopes could be a major hurdle, however there are free alternatives offering potentially comparable accessibility, such as ilastik (Berg et al., 2019).

Manual Analysis Remains Robust for Complex and Unique Phenomena: Many biologists lack the access to tools like Intellesis, or the computational expertise to automate analysis of microscopy data, often reverting to manual analysis. This project also utilized manual strategies for the detailed characterization of dynamic intercellular interactions such as attachment, aggregation, detachment, and division. This was very time-consuming and required a thoughtful categorization strategy and a disciplined, bias-free execution. However, some analysis tasks are simply unfeasable for automation. For example, this work manually counted if two INA-6 cells interacted homotypically due to coming into contact with each other, or by staying connected as two daughter cells after cell division. Automating such a task would require a very sophisticated algorithm and developing such would be unfeasable for a task that unique. Hence, manual analysis is unmatched in terms of flexibility and complexity of categorizations, when compared to computational techniques of image processing.

Key Points: In summary, image cytometry significantly enhanced this project by merging the precision of FACS with the cost-efficiency of modern microscopy. Utilizing *Intellessis* simplified complex image analyses, making advanced cytometric techniques more accessible. Manual analysis of image data remains essential for unique and complex phenomena. While challenges like automation and software availability persist, the potential of image cytometry to advance biomedical research and discovery remains substantial.

Technical Considerations for Automated Microscopy

Live-cell imaging and image cytometry leverage hardware and software automation to capture large amounts of potentially unknown complexity. Careful consideration of technical aspects is crucial to ensure successful data acquisition and analysis. This section discusses additional challenges and considerations encountered in this project.

Acquiring Accurate Image Data: In order to capture rare cellular events with a frequency sufficient for statistical analysis, this study chose high temporal resolution and spatial depth: We utilized 1 frame every 15 min, suitable for tracking cell migration (Huth et al., 2010), but too slow for intricate movements or intracellular processes. Spatial resolution is a compromise between detail and the total observed surface area. We favored the latter to allow the exploration of potentially rare events, and acquired a—somewhat arbitrarily—large surface area of up to 13 mm². Ultimately, we assessed only approx. a quarter of the acquired surface area, as that was sufficient to gather enough events for each time bin. Such extensive automated video acquisition poses high demands on microscopy equipment, including an incubation setup and motorized stage top. The total size of video files can also complicate storage, transfer and analysis. The raw video data from chapter 1 comprises 80 GB (BioStudies, o.J.); however, far more data was acquired due to protocol optimizations and treatments not shown in this work. File size could have been reduced by acquiring in an 8-bit image format, although a larger bit-depth could be necessary for precise and/or sensitive fluorescence microscopy. Minimizing the acquired surface area could have reduced file size as well, however the meniskus of the medium led to significant shading effects that complicated the choice of the surface area for phase contrasting. Also, archiving large surface scans allows for the search of very rare events in the course of future projects. After all, HDD space is cheap, while re-acquiring data is not. Hence, exploratory live cell imaging benefits from settings that are higher-than-required, if raw data is properly documented and remain accessible.

Generating Training Datasets: In this project, considerable effort was dedicated to training the machine learning software *Intellessis* for image segmentation, particularly for fluorescent images. It was also utilized for phase contrast, yet training required far more effort in generating annotated training images. Phase contrast or brightfield images often display low contrast between cell edges and the background, complicating the task of differentiating individual cells from their surroundings. Such complexity necessitates extensive annotation of training images – a process that can be both time-consuming and demanding.

To address these challenges and enhance the efficacy of *Intellessis*, pre-processing steps could be incorporated to emphasize essential image features and reduce irrelevant ones. For instance, edge-enhancing filters can clarify cell boundaries, or a median filter to suppress noise and unnecessary details while preserving edges. Especially noise reducing filters can normalize different sets of images, since machine learning models are very sensitive to variations in image quality. These filters, available within the Zen software

suite, help simplify the machine learning task by focusing the algorithm's learning on pertinent features, thereby potentially reducing the volume of data needed for effective training.

This approach streamlines the training process for *Intellesis*, enabling more efficient and accurate segmentation of complex microscopy images. By refining the feature extraction phase, the project could have improved the performance of the segmentation algorithm but also significantly cut down on the labor and frustration typically associated with preparing large sets of annotated training data.

Conclusion 2: Automating Microscopy, an Emerging Trend for Exploring Unknown Phenomena?

This study employed two methods that rely heavily on both hard- and software automation: live-cell imaging and image cytometry. These methods were instrumental in investigating the complex interactions between INA-6 cells and hMSCs, offering significant insights into myeloma cell behavior. The findings underscored the critical role of MSC-interactions in shaping cell behavior, for instance the observed preference of INA-6 cells for heterotypic interactions with hMSCs. Live-cell imaging and image cytometry revealed dynamic processes, such as INA-6 cell growing into clonal aggregates and subsequent cell detachments. These processes were pivotal for understanding cryptic RNAseq data, exemplifying how such techniques complement molecular approaches to understand disease mechanisms like dissemination.

Live-cell imaging proved instrumental in capturing real-time cellular behaviors that static methods cannot, such as the detachment of INA-6 cells during division. This ability to directly observe dynamic processes provided a deeper understanding of the cellular mechanisms that may contribute to myeloma dissemination. However, it also presented challenges, such as the extensive manual analysis required, difficulties in identifying observed phenomena, and the complexities of extracting quantitative data and presenting dynamic observations in traditional scientific formats. These limitations highlight the potential benefits of incorporating automation and machine learning in future research to streamline data analysis (A. Gupta et al., 2019; Cheng et al., 2023).

Image cytometry facilitated high-throughput and precise analysis of cellular interactions, despite challenges related to automation and computational requirements. The integration of manual and automated techniques in this study facilitated complex analyses, combining the precision of automation with the flexibility of manual approaches. The accessibility and availability of live-cell imaging equipment and machine learning software suggest a promising potential for broader adoption in biomedical research. This could lead to new discoveries of complex cellular dynamics and multicellular interactions.

These findings underscore a potentially emerging trend of innovative imaging and analyses techniques which could be driven by recent breakthroughs in machine learning. This trend could mark a significant advancement over molecular and static approaches of cell biological research questions.

Isolating & Quantifying Subpopulations within Cells in Direct Contact with MSCs

This project aimed to develop methodologies for isolating cells after direct contact with hMSCs. The primary challenge was the scarcity of *in vitro* methods that could effectively separate and isolate adhering cell subpopulations for subsequent molecular analysis. Most available techniques predominantly focus on the quantification of cell adhesion (Khalili & Ahmad, 2015; Kashef & Franz, 2015), and often employ indirect contact setups, complex micromanipulation—such as Atomic Force Microscopy (AFM)—or are unsuitable for using live plastic-adherent cells as the immobilizing surface. To address the limitations of current adhesion assays, we developed and enhanced innovative methodologies, specifically the Well Plate Sandwich Centrifugation (WPSC) and V-Well adhesion assays.

Variability of Washing Steps: Given the complexity of the requirements, this project first attempts relied on simple and traditional adhesion assays that rely on manual washing steps (Humphries, 2009). Washing involves aspirating the medium, dispensing washing buffer, and potentially repeating these steps multiple times. This introduces variability due to differences in pipetting techniques, which affect the accuracy of volume transfer (Guan et al., 2023; Pushparaj, 2020). However, adhesion assays don't rely on precise volume transfer, but accurate detachment of cells adhering at the well bottom. This introduces a new set of considerations for the pipetting technique, especially since cells are highly sensitive to shear forces applied by fluid flow. From the author's experience with washing experiments and subsequent microscopic evaluations (data not shown), several factors could contribute to the variability of washing steps:

1. The distance of the pipette tip from the well bottom, which decreases during aspiration.
2. The position of the pipette tip relative to the well bottom (center or edge).
3. The angle of the pipette tip.
4. The speed of aspiration.
5. Accidental or intended contact between the pipette tip and the cell layer.
6. The residual volume left after aspiration.
7. *The same considerations apply when dispensing the washing buffer.*

In addition to user-dependent factors, other variables such as the cells' position on the well bottom can significantly impact the outcome. To the author's experience, cells located at the edge of the well don't detach as easily as those in the center, while cells touching the edge are almost impossible to remove. This phenomenon is likely related to the *boundary layer effect*, where fluids slow down near the edges of the well (Weyburne, 2014).

Together, since both user-dependent and independent factors can affect the outcome of washing steps, adhesive assays that replace washing are highly desirable. Still, since washing is straightforward and some variability is alleviated by the disciplined execution of washing protocols, it remains a common method for adhesion assays.

Directly Interacting Cells Contain Unexplored Interaction Scenarios: It is evident that direct and indirect contact to MSCs have varying effects on myeloma cells. That difference is crucial for understanding changes in the BMME during MM progression (Fairfield et al., 2020; Dziadowicz et al., 2022). These studies utilize well-inserts to co-culture myeloma cells in close—indirect—contact with MSCs. However, such comparison of indirect *vs.* direct co-culturing methods might not fully represent the

complexity of intercellular interactions scenarios³ found in the BMME. This is exemplified by this project, as it relied on the complex growth behavior: INA-6 cells aggregated homotypically in direct proximity to those adhering heterotypically to hMSCs, and detached through cell division. Furthermore, such methods fail to capture the subtle variations in paracrine signaling concentrations, where even a few micrometers of distance could significantly alter cellular responses.

Such knowledge shifted this project's point of view as well: Initially, our hypothesis focused on direct heterotypic interactions, not expecting a nMA-INA6 population, but rather subpopulations within MA-INA6 cells that are separable by varying adhesion strengths. Hence, our assay employed strict conditions favoring one growth scenario—heterotypic interactions—, with co-cultures providing unlimited hMSC-surface availability causing predominantly heterotypic adhesion, while the short incubation time prevented the formation of aggregates. Despite these measures, our assay still captured cells emerging from recent cell divisions rather than from weak heterotypic adherence as initially hypothesized. This demonstrates the robustness of our method in separating subpopulations that arise from unexpected interaction scenarios³. This can be a major advantage over methods that summarize direct interactions as one population. Analysing the non-adhering subpopulation within directly interacting cells could provide valuable insights not just in multiple myeloma, but also metastasis of other cancer types.

Minimizing Variability: There are innovative adhesion assays that both support the isolation of nonadherent subpopulations from directly interacting cells, and avoid variability introduced by washing steps.

One simple method involves flipping over a 96-well plate, with surface tension preventing medium spills as non-adhering cells fall to the surface for collection (Zepeda-Moreno et al., 2011). However, we found that the medium in fact did spill occasionally (not shown). Other approaches involve sealing the plate, such as with PCR plate seals, and using centrifugation to separate cells (Reyes & García, 2003; Y. Chen et al., 2021). Despite our efforts, we could not consistently avoid air bubbles, which, after flipping, would contact the cell layer and create dry regions during centrifugation.

The V-Well adhesion assay does not flip, but collects non-adhering cells into the nadir of V-shaped wells during centrifugation (Weetall et al., 2001). This work profited greatly from this method, while—to our knowledge—being the first to use cell monolayers as the immobilizing surface. We value this method for its precision, as centrifugation applies a uniform and configurable force, while the readout remains straightforward, relying on the total fluorescent brightness rather than individual cell counting.

Specializing in Quantifying Adhesion or Isolating Subpopulations: Most adhesion assays primarily focus on quantification rather than isolation. The author attempted to combine both quantification and isolation, but found that the two goals can be mutually exclusive. The author summarizes the key differences between quantification and isolation approaches as such:

- Cell Manipulation for Harvest *vs.* Readout:
 - Isolation methods are designed to manipulate cells for easy harvest. For instance, the WPSC method uses a catching plate to collect non-adherent cells for subsequent analysis.

³ *Cell Interaction Scenario* (defined in this work): A combination of cellular interaction types describing direct contact or adhesion between cells. Cellular interaction types include those between similar cell types (homotypic interaction), different cell types (heterotypic interaction), or between cells and substrate. A cell interaction scenario usually implies that multiple cell interaction types occur simultaneously or in rapid succession, for instance, myeloma cells interacting with both other myeloma cells and MSCs. When interaction scenarios emerge from cell division, the term *growth conformation* is also used (see Chapter 1)

- Quantification methods, on the other hand, manipulate cells to simplify the readout process. For example, the V-Well assay, which pellets cells into a single location, allowing for a pooled fluorescence measurement without the need for extensive cell handling.
- Optimization for Subsequent Analysis *vs.* Sample Throughput:
 - Isolation methods are optimized for detailed subsequent analyses, such as RNA or protein analysis. For example, WPSC minimizes the introduction of biases such as those from fluorescent staining, making it suitable for downstream molecular assays.
 - Quantification methods are optimized for high sample throughput. The V-Well assay, as an end-point assay, is designed to efficiently handle multiple treatments simultaneously, providing quick and comparative results with lower cell numbers.
- Handling of Cell Numbers:
 - Isolation methods, such as WPSC, require multiple wells (e.g., 96 wells) to gather a sufficient amount of cells per subpopulation, which is crucial for robust downstream analyses.
 - Quantification methods, exemplified by the V-Well assay, are highly efficient even with low cell numbers.

Thus, this adopted two distinct techniques for isolating and quantifying directly interacting subpopulations, each optimizing for different outcomes, but also supporting the separation of subpopulations within direct intercellular interactions. Still, it is theoretically possible to insert microscopy steps into the WPSC method to scan the well bottom for later cell counting. Also, this work effectively isolated cell pellets from the V-well plate for subsequent fixation and cell cycle profiling. The process was tedious and required multiple technical replicates to achieve sufficient cell numbers for analysis. It also required removing hMSC from the V-well nadir to prevent contamination during pellet aspiration.

Together, while both methods can combine quantification and isolation, they are optimized towards either of them. Knowing these strengths and weaknesses could help to advance these methods in future studies.

Rationales of the Well Plate Sandwich Centrifugation: Inspired by the principles of both flipping and V-Well adhesion assays, we developed the Well Plate Sandwich Centrifugation (Well Plate Sandwich Centrifugation (WPSC)) method to address the challenges of isolating cell populations. This method innovatively combines elements from both techniques to provide a more reliable approach to cell isolation. One of the key advantages of WPSC is its ability to reduce the variability commonly introduced by manual pipetting. Instead of relying on aspiration, which introduce variability in cell collection and requires touching the well bottom for complete removal of medium, WPSC employs centrifugation to remove non-adhering cells. Medium is then returned by pipetting to repeat the process and maximize non-adhering cell collection, as the number of detachable cells plateau after few rounds of centrifugation. Hence, this approach compromises between minimizing washing variability and isolating larger quantities of cells.

The 96 well plate format has advantages, reducing spilling when flipping the sandwich, as surface tension kept fluids in place. The 96 well plate format also reduces per-well variability by performing the same washing procedure up to 96 times.

The slow centrifugation speeds used during WPSC are also decided after thorough consideration. For this, one has to discuss how exactly non-adhering cells detach during centrifugation. While centrifugal force is an obvious factor, the properties of cell adhesion are unclear under dry conditions during centrifugation.

The author assumed that the cells are being pulled along by the medium as it is centrifuged into the catching plate. Hence, the centrifugation speed was chosen as fast enough to transfer the medium, without completely drying the co-culture plate and minimizing overall cell stress.

A challenge in WPSC is the dissociation of MA-INA6 from the hMSC monolayer. WPSC employs two distinct techniques to achieve this dissociation. The first technique involves repeated treatment with the gentle digestive enzyme Accutase followed by MACSs. MACS, despite being effective, is costly, time-consuming, reduces overall cell yield, and potentially introduces biases due to CD45 antibody selection and the requirement for cold-treatment. The second technique utilizes strong pipetting to physically detach non-adhering cells (termed '*Wash*'). It is important to note that these techniques did not affect the protocol on detaching nMA-INA6 from the co-culture, hence providing for a consistent ratio of isolated MA-INA6 to nMA-INA6 across all experiments. Ultimately, we preferred *Wash*, as MACS had to be performed on all samples to ensure comparability, reducing overall cell yield which became limiting for downstream applications, especially for nMA-INA6 cells. Both methods achieved comparable purity of MA-INA6 cells, with few hMSCs per 10^4 MA-INA6 cells (purity assessment not shown). *Wash* probably profited from the highly durable nature of primary hMSC monolayers, whereas *MACS* required dissociation of the co-culture.

Together, WPSC offers a versatile solution for isolating hMSC-interacting myeloma cells. It successfully balances the need for precision with the ability to handle larger cell quantities. WPSC could be adapted to other cell types that combines monolayer forming and suspension cells.

Key Points on Adhesion Assays: Ultimately, this work established two methodologies that could represent a significant advancement in the field of adhesion assays, providing cost-effective, precise, reliable, and reproducible techniques for both isolating and quantifying subpopulations within co-cultures of directly interacting cell types. They offered valuable insights into the mechanisms of MM detachment and are potentially applicable to other research questions that focus on growth and interaction scenarios involving multiple cell types.

Integrating Evidence and Hypotheses for a Mechanistic Understanding of Dissemination

The results outlined in Chapter 1 encompass various aspects of multiple myeloma research, including colonization of the BMME, myeloma-MSC interactions, and the association of adhesion factor⁴ expression with patient survival and disease stages. Such a broad scope invites the formulation of generalized conclusions, potentially compromising scientific rigor. The following sections aim to clearly separate hypotheses from evidence to guide further research on myeloma dissemination.

Integrating Observations of INA-6 in the Multistep Dissemination Model: The results gained in this work fit well into the multistep model proposed by Zeissig et al. (2020). For most steps, observations were made that could inspire further hypotheses and research:

1. Retention:

- *This work's Observation:* INA-6 cells attach quickly and strongly to hMSCs, forming stable aggregates.
- *Hypothesis:* Myeloma cells are retained in the bone marrow microenvironment (BMME) through strong adhesion to hMSCs and stable homotypic aggregation.
- *Suggested Experiment:* Inject INA-6 cells into mice and examine bone lesions. Compare the growth patterns in mice co-injected with an ICAM-1 or LFA-1 α antibody, which dissolve homotypic aggregates *in vitro* and prevent INA-6 growth *in vivo* (Kawano et al., 1991; Klausz et al., 2017). If disrupting aggregation leads to diffuse bone colonization rather than focal lesions, it supports the hypothesis that strong adhesion and aggregation are crucial for retention in the BMME.

2. Release:

- *This work's Observation:* INA-6 cells detach from hMSCs through cell division, and external forces can detach single cells from INA-6 aggregates.
- *Hypothesis:* Myeloma cells detach from the BMME through cell division and external forces after reaching a minimal aggregate size.
- *Suggested Experiment:* Inject Bromodeoxyuridine (BrdU) stained INA-6 cells into mice and compare the cell cycle profiles and BrdU signals of circulating cells versus those in the bone marrow. Enrichment of G1/G0 cells among circulating cells would support the hypothesis that detachment is more likely shortly after cell division.

3. Intra-/Extravasation:

- This study did not make experiments to study for intra-/extravasation, but these phenomena could be explored with similar methods, if MSCs were replaced by endothelial cells, similar to Solimando et al. (2018).

4. Colonization:

- *This work's Observation:* INA-6 cells exhibit quick attachment to hMSCs within one hour and rapidly upregulate numerous adhesion factors, including ECM factors.

⁴*Adhesion Factor:* Any factor influencing cell adhesion, including—but not limited to—Cell Adhesion Molecules (CAMs), Extracellular Matrix (ECM) proteins, chemotactic factors associated with inducing adhesion factor expression—such as CXCR4 or CXCL12—, or factors listed in Gene ontology terms “*extracellular matrix organization*”, “*ECM proteoglycans*”, “*cell-substrate adhesion*”, and “*negative regulation of cell-substrate adhesion*”.

- *Hypothesis:* Quick attachment and fast expression of adhesion factors enhance the potential to colonize new niches. This is particularly relevant as INA-6 cells were isolated from the pleura, indicating an ability to colonize extramedullary sites (Burger et al., 2001).
- *Suggested Experiment:* Inject INA-6 cells into mice and observe if they colonize extramedullary sites. Compare this to INA-6 cells with reduced adaptability to test the hypothesis. Research is required to find techniques to reduce such putative adaptability: One potential option is using XRK3F2 to inhibit p62, an upstream activator of NF- κ B (Adamik et al., 2018). In fact, NF- κ B signaling seems a robust target, given that it plays a role both in MM patients (Sarin et al., 2020), and inducing adhesion factor expression in INA-6 (this work). Other targetable genes are those proposed by Shen et al. (2021) to be master regulators of myeloma progression.

These hypotheses—based on observations from INA-6 cells—provide a starting point for understanding myeloma dissemination. While these insights are specialized for the INA-6 cell line, they inspire the development of a more generalized framework applicable to a broader range of myeloma cases.

Constructing a Generalizable Hypothetical Framework of Dissemination: A mechanistic understanding of myeloma dissemination remains elusive. Although Zeissig et al. (2020) described dissemination as a multistep process, evidence is largely collected for individual steps, leaving the connections between these steps unproven. As a result, the process of dissemination is a patchwork of evidence fragments. The following sections aim to integrate such fragments, especially those derived from the INA-6 cell line in this work, to construct a more coherent understanding of myeloma dissemination. To do so, this work specifies new terminology, including *Cell Adhesion Dynamics (CAD)*⁵ and *CAD dramatype*⁶ or short *adhesion dramatype*⁷.

Distinguishing Phenotype and Dramatype: INA-6 cells exhibited great reactivity to hMSCs. Describing this new state as a *phenotype* would correctly imply the influence of both genetic and environmental factors. However, this usage overloads the term *environmental factors*, as it includes the donor's history, *in vitro* culturing conditions, the experimental model simulating the BMME, and experimental conditions—such as the ratio of MSCs to INA-6 cells. Animal studies faced a similar issue and thus introduced the term *dramatype* (van Zutphen et al., 2001). A dramatype describes the state resulting from proximate environmental factors, while a phenotype summarizes the overall environmental background prior to encountering that environment. In cancer research, the term dramatype is rarely used (Hino,

⁵ *Cell Adhesion Dynamics (CAD):* The observation and measurement of time-dependent changes in cell adhesion and detachment events. CAD expands traditional *cell adhesion* by a time component and implies an intention to predict the timepoint of detachment events. Such focus on dynamics is especially relevant for suspension cells that exhibit intricate adhesion behaviors. Chapter 1 also refers to CAD as attachment/detachment dynamics.

⁶ *CAD Dramatype* (defined in this work): Specific adhesion behavior caused by proximate environmental factors. The term *dramatype* was inspired from laboratory animal science (van Zutphen et al., 2001). A CAD dramatype is characterized by the duration cells spend in distinct adhesive states or interaction scenarios³, and the cause of transitions between these states and scenarios. Adhesive states include attached, migrating, or detached; interaction scenarios include homotypic, heterotypic or substrate interactions. CAD dramatypes are associated with molecular signatures, such as CAM expression patterns or signal transduction mediated by proximate environmental factors. The term dramatype distinguishes itself from *phenotype* by focusing on dynamic and transient states available within transcriptional plasticity, while *phenotypes* focus on relatively persistent states such as genetic and epigenetic backgrounds.

⁷ *Adhesion Dramatype* (defined in this work): Short version for CAD dramatype⁶. Since the term *dramatype* implies dynamic changes, *CAD dramatypes* and *adhesion dramatypes* are interchangeable.

2004), with some researchers preferring terms like *phenotype switching* (Wouters et al., 2020). However, this blurs the distinction between clonal heterogeneity and transient cell signaling. The author proposes using *dramatypes* in cell biology to focus on transient states within the bounds of transcriptional plasticity, while *phenotypes* describe relatively persistent genetic and epigenetic backgrounds. These *dramatypes* could then define distinct adhesive behaviors of myeloma cells observed at each step of dissemination, considering the microenvironmental and adhesional changes encountered.

Introducing Adhesion Dramatypes: The concept of CAD⁵ describes the time-dependent changes in cell adhesion and detachment, linking these phases to molecular signatures such as CAM expression or microenvironment-mediated cell signaling. Emphasizing the time component is particularly useful for predicting the behavior of suspension cells with complex attachment and detachment dynamics, such as INA-6. In this context, MA-INA6 and nMA-INA6 represent two distinct *in vitro* adhesion dramatypes. The MA-INA6 dramatype is characterized by the expression of adhesion factors and stable heterotypic adhesion to hMSCs, addressing the retention and colonization steps in the multistep model of dissemination. MA-INA6 cells then transition to the nMA-INA6 dramatype through cell division and the loss of MSC adhesion, characterized by unstable homotypic aggregation from which single cells detach. This may represent the release step in the dissemination process.

Key Hypotheses: The author introduces the *Dynamic Adhesion Hypothetical Framework for Myeloma Dissemination*, which leverages direct observations of CAD⁵, and is structured around four key hypotheses. Each address fundamental aspects of myeloma cell dissemination based on both literature and the results of this work:

1. **Myeloma cells change their adhesion dramatype during dissemination.** In response to different environmental cues faced during dissemination, myeloma cells switch, change or adapt their CAD. These states are characterized by adhesion dramatypes⁷. Different steps in dissemination involve distinct adhesion dramatypes, or instance, one for specialized colonizing new sites and one specialized for vascular interactions.
2. **Rapid changes of adhesional dramatypes drives aggressive dissemination in myeloma.** Adhesional plasticity describes the overall repertoire of adhesion dramatypes⁷ that individual myeloma cells can deploy. However, such plasticity is limited by the rapidness of deploying a specialized adhesion dramatype during steps of dissemination.
3. **CAD is highly diverse between myeloma patients.** Transcriptional plasticity and clonal heterogeneity introduce variability into myeloma cell populations. These variations are primarily determined by other patient-specific factors such as disease stage and genomic background. Consequently, the interactions between these factors, along with other influences like the tumor microenvironment and therapeutic interventions, suggest a myriad of manifestations of CAD and differing dissemination mechanisms among patients.
4. **Detachment is caused by multiple cues of varying nature.** Given the diversity of myeloma CAD, detachment could be both a consequence of ongoing processes, but also triggered by timely defined events. Both could combine external mechanical forces, cell division, loss of CAM expression, or even pure chance.

This framework sets the stage for a detailed exploration of each hypothesis, linking empirical data with hypothetical constructs to provide a comprehensive framework that can help to identify commonalities in myeloma dissemination, but also inform the development of targeted therapies.

Hypothesis 1: Cells Change their Adhesion Dramatype during Dissemination

As presented in Chapter 1, MA-INA6 cells exhibited upregulation of both adhesion factors and chemoattractants (p. 54), switching their CAD dramatype from homotypic aggregation to MSCs adhesion. Given that INA-6 cells were isolated from an extramedullary site—the pleura—(Burger et al., 2001), such changes likely facilitate colonization of new microenvironments. This section explores the hypothesis that MM cells adapt or change their adhesion dramatype not only during colonization, but at each step of dissemination.

Adhesion Dramatypes Assume Distinguishable Niches: The multistep model proposed by Zeissig et al. (2020) posits that myeloma cells acquire regulatory mechanisms specialized for each step of dissemination. The author hypothesizes that the different niches involved in these steps are unique enough to induce distinct adhesion dramatypes. This requires thorough knowledge of separate niches. Granata et al. (2022) categorizes the BM into sinusoidal, arteriolar, and endosteal niches, each spatially and molecularly distinguishable. The endosteal niche is home to MSC and a majority of plasma cells[†], and the vascular niches—sinusoidal and arteriolar—include endothelial cells (Zehentmeier et al., 2014; Wilmore & Allman, 2017). Other niches encountered during dissemination include peripheral blood, lymph nodes, and extramedullary sites. Comprehensive mapping and characterization of these niches, including their adhesion molecules and soluble factors, is necessary to understand the adhesion requirements for each niche. This is a highly complex task, yet summarizing available information per niche could provide a powerful basis.

Distinct Adhesion Dramatypes Transitioning between Niches: Adhesion processes are well-documented in MM progression, particularly within the BMME (Bou Zerdan et al., 2022). However, the dynamism of these processes remains unclear. Overall, Frede et al. (2021) have shown that individual myeloma cells can switch between alternate transcriptional states through differential epigenetic regulation. Such states were associated with distinct transcriptional signatures like those of endothelial progenitors or enhancers linked to CXCR4. This is indicative of myeloma cells having different CAD dramatypes. In other cancers, different adhesive phenotypes and transitions, such as those seen in EMT, are common (Geng et al., 2014). For myeloma, EMT-like phenotypes have been described, but a clear association with distinct adhesion behaviors is hindered by the cells maintaining their suspension state (Roccaro et al., 2015; Qian et al., 2023). This work might be the first to identify adhesion dramatypes through functional separation of detachable myeloma cells. As presented earlier, exploring these findings further could reveal transitions between adhesion dramatypes during MM dissemination, such as attaching for colonization, or initiating release.

Extramedullary Niche: Changing adhesion dramatypes predicts a specialized set of adhesion factors for extramedullary niches. A distinct phenotype has been proposed for extramedullary myeloma[‡], characterized by changes in expression of CD44, CD56, VLA-4, and CXCR4 (S. Gupta et al., 2022). In support of this, (Hathi et al., 2022) demonstrated that VLA-4 seems to direct myeloma cells to the

[†] Wilmore & Allman (2017):

“We suggest that it is reasonable to approach the notion of physical plasma cell survival niches with some skepticism. It is clear that most BM plasma cells rely heavily on access to APRIL or BLyS (66, 70), and it appears that mature plasma cells are relatively stationary (59). However to us, that plasma cells must remain indefinitely in physical survival niches to survive is less obvious.”

[‡] S. Gupta et al. (2022):

BM, since ablating VLA-4 reduced medullary disease, but increased extramedullary involvement. Furthermore, the role of CXCR4 in mediating adhesion factor expression is well established, particularly in extramedullary MM cells (Roccaro et al., 2015; S. Gupta et al., 2022): Extramedullary myeloma cells overexpress CXCR4, making them more responsive to cues that induce adhesion factor expression, such as CD44/H-CAM.

Vascular Niche: Changing adhesion dramatypes predicts a specialized set of adhesion factors for endothelial interaction, supporting intravasation and extravasation. Although not assessed in this thesis, the vascular niche is a popular therapeutic target for preventing dissemination (Neri & Bahlis, 2012). Key adhesion factors like JAM-A, JAM-C and N-Cadherin have been highlighted as potential targets (Solimando et al., 2020; Mrozik et al., 2015; A. Brandl et al., 2022). Such factors were not differentially expressed between subpopulations isolated in Chapter 1. A. Brandl et al. (2022) has described JAM-C co-localizing with blood vessels in the BM and dynamic expression by MM cells in both patients and mice. These results suggest distinct adhesive mechanisms for vascular *versus* MSC interactions.

Circulating MM: Changing adhesion dramatypes would predict that circulating MM cells lose adhesion factors. Studies confirm that—compared to BM-resident cells—circulating MM cells exhibit reduced expression[†] of multiple adhesion factors, including $\alpha 4\beta 1$ and CD138/Syndecan-1 (Paiva et al., 2013, 2011; Akhmetzyanova et al., 2020). Evidence suggests that a dynamic loss of CD138/Syndecan-1 and gain of JAM-C causes intravasation, circulation, and dissemination of MM cells (Akhmetzyanova et al., 2020; A. Brandl et al., 2022). This thesis also shows that nMA-INA6 cells, after emerging as daughter cells from MA-INA6, not only lose adhesion factor expression but also exhibit increased survival during IL-6 deprivation, potentially aiding survival in circulation.

Intermediary Conclusion: Available Evidence of Adhesion Phenotypes Lacks Functional Characterization and Proof of Dramatypic Transitions: The concept of changing adhesion dramatypes is supported by the existence of distinct BM niches and the identification of separable adhesion phenotypes. However, the author identifies two major gaps in the current literature: First, most phenotypic characterizations of adhesion phenotypes are limited to surface CAM expression, ignoring potential secretion of ECM proteins. Second, the transitions between these phenotypes during dissemination are unexplored.

Functional characterization of adhesive phenotypes—including ECM factors—and their transitions could provide a robust framework for understanding dissemination as a multistep process, reinforcing the dynamic adhesion hypothetical framework. Mapping adhesive properties for each involved niche could aid this endeavor.

Considerations for Research on Myeloma Cell Adhesion: The evidence presented here sets the stage for a more detailed exploration of adhesion factors in MM. Characterizations of bulk myeloma will not capture the dynamic changes in adhesion factor expression that occur during dissemination. Studying adhesion factors in MM *in vitro* requires considering the specific microenvironmental context.

“Our analysis concluded that the gain of CD44, loss of CD56, loss of very late antigen-4 (VLA-4), imbalance of the chemokine receptor-4-chemokine ligand-12 (CXCR4-CXCL12) axis, [...] show an increased propensity [...] to leave the bone marrow and hone in extramedullary sites giving rise to more aggressive extramedullary diseases.”

[†] Paiva et al. (2013):

“Our results show that CTCs typically represent a unique subpopulation of all BM clonal PCs, characterized by downregulation ($P < .05$) of integrins (CD11a, CD11c, CD29, CD49d, CD49e), adhesion (CD33, CD56, CD117, CD138), and activation molecules (CD28/CD38/CD81).”

Some adhesion factors are not present in MM cells but can be rapidly expressed with appropriate signals.

Also, further studies should differentiate between initial adhesion and upregulated adhesion factors. For example, performing a WPSC assay after 30 minutes of adhesion could separate INA-6 cells based on initial adhesion capability, with RNAseq of nMA-INA6 *vs* MA-INA6 identifying initial adhesion factors. Distinguishing between initial and upregulated adhesion factors could be crucial for predicting colonization potential across niches. Such initial adhesion is likely to be essential for subsequent growth in BM or extramedullary environments.

Most importantly, it is imperative that characterizations of adhesional properties should not only include surface CAMs, but also ECM proteins secreted by myeloma cells. The role of ECM proteins in myeloma dissemination is well-established (Ibraheem et al., 2019), and this thesis identified a potential role for ECM proteins in myeloma adhesion and colonization. Further research on ECM-expression of pheno- and dramatypes could prove pivotal in understanding myeloma dissemination.

Implications for Therapy: Adhesion molecules have been targeted for therapy for over a decade (Nair et al., 2012; Neri & Bahlis, 2012). Especially inhibiting adhesion molecules involved in interaction with the endothelium effectively reduces tumor burden in mouse models (Asosingh et al., 2001; Mrozik et al., 2015). A deeper understanding of how myeloma cells regulate CAD could be key to predicting and preventing dissemination.

Changing adhesion dramatypes suggests that different adhesion factors should be either antagonized or agonized depending on their role. For instance, adhesion factors involved in intravasation and extravasation should be antagonized, while those facilitating BM retention⁸ should be agonized. However, care should be taken to not agonize adhesion factors that also provide survival signals. For instance, the short polypeptide SP16 can activate the receptor LRP1—its high expression being associated with improved survival of MM patients in this work—passed phase I clinical trial for treating inflammatory diseases (Wohlford et al., 2021), but could potentially increase survival of MM through PI3K/Akt signaling (Potere et al., 2019; Heinemann et al., 2022). However, the risk of promoting cell survival when agonizing adhesion factors can be mitigated by using targets identified in Chapter 1, since Tabelle 2 (p. 154) provides a list of retention targets⁸ that were associated with improved patient survival when highly expressed. This could also mitigate the risk of promoting colonization of new sites through increased adhesion, but since colonization is limited by initial release, this risk is probably low.

Most intriguingly, CAR-T cell therapy could benefit from the concept of adhesion dramatypes: Arming CAR-T cells against targets listed in Tabelle 2 (p. 154) could specialize in targeting colonizing cells, while those factors upregulated in nMA-INA6 cells could specialize in targeting detached cells. Specifically targeting circulating MM cells could effectively reduce dissemination, as demonstrated in a proof-of-concept study aimed at preventing metastasis using Granzyme B-based CAR-T cells (Sun et al., 2024).

Concluding Remarks and Future Directions: Evidence of changing adhesion phenotypes across various niches reveals a complex interplay between myeloma cells and their environments, characterized by dynamic regulation of adhesion factors. Introducing the concept of dramatypes to distinguish between phenotypic and dynamic adhesion behaviors provides a more detailed framework for understanding the intricacies of myeloma dissemination. Available evidence supports the hypothesis that myeloma cells adapt their adhesion dramatype in response to different microenvironments encountered during dissemination. This suggests potential therapeutic strategies targeting these specific adhesion mechanisms. Since the ma-

⁸ *Retentive Adhesion Factors:* The subset of adhesion factors that promotes anchorage of myeloma cell in the BMME, and promote better patient survival at high expression as shown in Chapter 1.

jority of currently available phenotypic characterizations have ignored ECM factor secretion, an important axis of potential adhesive interactions has been overlooked.

Distinguishing adhesion dramatypes among vascular, bone marrow, and extramedullary niches highlights the need for targeted therapy to either promote retention or prevent dissemination. Identifying bone marrow retentive factors that do not induce survival signaling is crucial—such as CXCR4 or CXCL12—, with the gene-list from this work providing a strong starting point (Appendix A.2: Tabelle 1).

Future research should include characterization of ECM factor expression to fully clarify the functional roles and transitions of these adhesion dramatypes. This would validate the changing adhesion dramatype hypothesis and identify therapeutic targets to disrupt dissemination at various stages. Controlled *in vitro* studies simulating specific microenvironments, integrating RNA sequencing and live-cell imaging, will enhance understanding of adhesion factor regulation and inform the development of precise interventions for multiple myeloma management.

Hypothesis 2: Rapid Adhesional Plasticity Drives Aggression in Myeloma

Chapter 1 presented diverse observations of rapid transitions between adhesion dramatypes: Within three days, INA-6 cells transitioned from homotypic aggregation to MSC adhesion, then back to aggregation followed by detachment of single cells. This not only shows diverse adhesional plasticity⁹ but also an intriguing capacity for speed. Since INA-6 were isolated from highly advanced PCL (Burger et al., 2001), such rapid adhesional plasticity could be driving an aggressive phenotype of myeloma.

Associating Adhesion Factors with Disease Progression & Aggressiveness: The hypothesis of rapid adhesional plasticity is predicated on the association between adhesion factors and cancer aggressiveness. The transformative processes in MM pathogenesis have been recognized for decades, typically observed over months or years (Hallek et al., 1998). Much of this research has focused on transformations in resistance mechanisms acquired during chemotherapy, with cell adhesion factors being well-established drivers of survival signaling via NF- κ B, contributing to the selection of drug-resistant myeloma clones (Landowski et al., 2003; Solimando et al., 2022).

Recent research has provided detailed characterizations of adhesion factors driving myeloma aggressiveness. For instance, specific adhesion and migration factors have been proposed as master regulators of myeloma progression (Shen et al., 2021). Additionally, a recent study identified 18 adhesion factors as the basis for a prognostic model to identify high-risk variants in newly diagnosed MM patients (Q. Hu et al., 2024). Another recent study demonstrated the prognostic value of mutated ECM proteins expressed by myeloma (Evers et al., 2023).

This thesis contributes to this field by showing that bone-retentive adhesion factors and ECM proteins are continuously downregulated during MGUS, aMM, MM, and Multiple Myeloma Relapse (MMR). Other studies of bulk myeloma biopsies confirm changes in adhesion factor expression at some point

⁹ *Adhesional Plasticity:* The overall repertoire of adhesion dramatypes⁷ that individual myeloma cells can deploy.

between MGUS and PCL^{†‡}, reporting increased levels of VCAM-1, ICAM-1, L-selectin, CD56, CD86, CD126, & CD95, decreased levels of CD38, HLA-I, β 2-microglobulin, & CD40, and no changes in CD130 (Terpos et al., 2016; Pérez-Andrés et al., 2005).

Intriguingly, not only the surface expression of adhesion factors plays a role during progression, but also the surrounding ECM. ECM from myeloma patients exhibits tumor-promoting properties, in stark contrast to the tumor-abrogating ECM from healthy donors (Ibraheem et al., 2019).

Together, recent advances have effectively associated changes in cell adhesion expression phenotypes with aggressive myeloma. Further insights can be drawn from the databases used in Chapter 1 (p. 55) (Seckinger et al., 2018), identifying adhesion genes differentially expressed between cohorts of different disease stages, followed by functional categorization into GO-terms associated with dissemination steps. However, these studies do not focus on a mechanistic understanding of how cell adhesion drives aggressive dissemination, nor do they discuss the speed of adaptations in adhesion phenotypes.

Adhesional Plasticity and Speed: Clonal dynamics have established that rapid mutations can drive aggressive progression on a genomic scale (Keats et al., 2012; Evers et al., 2023). The hypothesis of rapid adhesional plasticity extends this idea to the activity of adhesion factors, encompassing dynamic (post-)transcriptional regulation and adhesion kinetics regulated at the protein level. In solid cancers, sufficient information on regulatory dynamics of EMT exists to train a deep learning model (Tong et al., 2023). This model infers transcriptional changes over time from static single-cell RNAseq data, demonstrating that dynamic phenotypic changes can be projected along selected transcriptional trajectories—in this case EMT—, and aiding in the prediction of future detachment dynamics.

However, for hematological cancers such as MM, high time resolutions of up to minutes or even seconds might be required. As previously discussed, the speed of dynamic changes is inherent to adhesional processes (p. 75), but time remains an often overlooked dimension in molecular cancer research^{††} (Uthamacumaran & Zenil, 2022). The author hypothesizes that this rapidness is crucial for colonizing new sites. Adhesional plasticity alone might not be sufficient for successful attachment or survival: INA-6 cells failed to adhere to MSC during live-cell imaging if the motorized stage top was moving too fast, necessitating decelerated microscopy configuration (data not shown). This indicates that colonization attempts are thwarted by fast-moving environments, despite strong MSC adhesion potential.

[†] Terpos et al. (2016):

“Patients with NDMM had increased VCAM-1 and ICAM-1 compared with MGUS and sMM patients. [...] MM patients at first relapse had increased levels of ICAM-1 and L-selectin, even compared with NDMM patients and had increased levels of VCAM-1 compared with MGUS and sMM.”

[‡] Pérez-Andrés et al. (2005):

“Clonal PC from all MG [Monoclonal Gammopathies] displayed significantly increased levels of CD56, CD86 and CD126, and decreased amounts of CD38 ($P < 0.001$). Additionally, HLA-I and β 2-microglobulin were abnormally highly expressed in MGUS, while CD40 expression was decreased in MM and PCL ($P < 0.05$). Interestingly, a progressive increase in the soluble levels of β 2-microglobulin was found from MGUS to MM and PCL patients ($P < 0.03$). In contrast, all groups showed similar surface and soluble amounts of CD126, CD130 and CD95, except for increased soluble levels of CD95 observed in PCL.”

^{††} Uthamacumaran & Zenil (2022):

“These predominant snapshot approaches are fundamental limiting factors in the advancement of precision oncology since they are causal agnostic, i.e., they remove the notion of time (dynamics) from cancer datasets. [...] The lack of time-series measurements in single-cell multi-omics [...] and cell population fluctuations (i.e., ecological dynamics), in patient-derived tumor and liquid biopsies, remains a central roadblock in reconstructing cancer networks as complex dynamical systems.”

Similar to Hypothesis 1, the evidence for this hypothesis is limited by the current understanding of transitions between adhesion dramatypes. Hypothesizing the rapidity of such transitions adds further complexity, requiring a time-dimension for every experiment. Nonetheless, there is evidence of rapid transitions towards detaching and invasive dramatypes, implying swiftness in these processes: A sudden loss of the adhesion factor CD138 can occur either through antibody treatment or shedding by heparanase (Y. Yang et al., 2005; Akhmetzyanova et al., 2020). Exploring such rapid dynamisms is a major challenge for future research but also presents a significant opportunity to establish a new field of research in myeloma dissemination focused on CAD.

Potential Mechanisms Facilitating the Fast Switch of Adhesion Dramatypes: The hypothesis of rapid adhesional plasticity suggests that aggressive myeloma cells can swiftly alter their adhesion dramatype, as observed in INA-6-MSC co-cultures. To facilitate such rapid changes, several molecular mechanisms might be utilized: Integrins can undergo rapid conformational changes from active to inactive forms, a process used to detach B-cell leukemia cells through small molecule treatment (Ruan et al., 2022). Additionally, myeloma cells can express proteases like heparanase to shed adhesion factors from their cell surface (Y. Yang et al., 2005). For INA-6 cells, the author proposes three mechanisms that could explain this swiftness:

Rapid NF- κ B Signaling: First, NF- κ B signaling is enriched in MA-INA6 cells. NF- κ B is known as one of the fastest signaling pathways, capable of regulating the transcription of target genes within seconds (Gallego-Selles et al., 2022; Zarnegar et al., 2008). This signaling pathway is relevant for both *in vitro* experiments and MM patients (Sarin et al., 2020), making its downstream effectors robust targets for treatment.

(Asymmetric) Cell Divisions? This work provides proof of concept that cell division directly causes detachments, a mechanism also reported for gastric cancer and intravasation (Monster et al., 2024; Wong & Searson, 2017). Since a cell with a new adhesive state is generated instantly, this mechanism also contributes to rapid adhesional plasticity.

Furthermore, asymmetric cell division could explain the rapid loss of adhesion gene mRNA transcripts observed in nMA-INA6 cells that emerged from MA-INA6 cells through cell division. This process—popularized by stem cell research for facilitating self-renewal (Shenghui et al., 2009)—, has underlying molecular mechanisms conserved in asymmetrically dividing cells and cellular polarization processes as well (Inaba & Yamashita, 2012; St Johnston & Ahringer, 2010). Asymmetry can be established *intrinsically*, where factors are segregated between daughter cells, or *extrinsically*, by placing two daughters into distinct microenvironments (Inaba & Yamashita, 2012). It is debatable whether the definition of extrinsic asymmetric cell division is fulfilled by this work's observation: nMA-INA6 daughter cells emerging out of range of MSCs, thereby delaying direct adhesion until the nMA-INA6 re-attaches to an MSC.

Intrinsic mechanisms could be explored by live-cell imaging of cell division events in INA-6-MSC co-cultures, followed by *in situ* hybridization using fluorescently labeled antisense RNA probes. If successful, this could represent the first evidence for asymmetric cell division in MM, which could be useful for the popular *cancer stem cell hypothesis*. However, MA-INA6 cells do not currently fulfill the multipotency criterion required by stem cell terminology (Johnsen et al., 2016; Z. Li et al., 2022).

Speed and Flexibility of ECM Interactions: Third, the role of ECM in facilitating rapid adhesional plasticity must be considered. The ECM regulates cell adhesion and migration rapidly, and its composition is altered by myeloma cells, which include various mutated ECM proteins (Ibraheem et al., 2019; Evers et al., 2023). For the case of myofibroblasts, contractile cell-matrix interactions can involve

calcium signalling, where transduction takes less than 1 s (Yamada et al., 2022). Additionally, myeloma cells can remodel the ECM on site, reducing the need for adaptations in cell surface factor expression, providing an additional axis for potential adhesive interactions and improved flexibility in changing adherent sites. Although MA-INA6 cells never detached from MSC themselves, ECM is a viable candidate for facilitating rapid adhesional plasticity in myeloma cells.

Implications for Research on Myeloma Cell Adhesion: Rapid adhesional plasticity could explain the high variance in adhesion factor expression that's independent of donor-to-donor variability: Even within the same disease stage and niche, subsets of myeloma cells could exhibit rapidly interchanging adhesion dramatypes. This underscores the relevance of *in vitro* studies involving direct contact with stromal or endothelial cells, as they can capture subpopulations with different adhesion dramatypes, akin to MA-INA6 and nMA-INA6.

Rapid adhesional plasticity also explains the arguably paradoxical trend of decreasing expression of bone retentive adhesion factors⁸ during disease progression, as described in Chapter 1: Hypothetically speaking, partial loss of adhesion factors improves overcoming BM retention, while quick re-upregulation of these factors allows for rapid reattachment—if required. Quick re-upregulation could then facilitate exploration of new niches or an acute need of CAM mediated survival signaling. This dynamic switching could give myeloma cells a competitive advantage in various microenvironments. Adhesional plasticity further gains flexibility, if cells not only regulate surface CAM expression, but also utilize secretion of ECM as an additional axis for adhesive interactions.

Implications for Therapy: Rapid adhesional plasticity could significantly impact the development of targeted therapies: Different myeloma dramatypes might lack traditional prognostic markers but still possess the ability to rapidly express these markers, potentially leading to the misidentification of high-risk patients. Therefore, targeted therapies should incorporate multiple markers obtained from various tissue sources to enhance the accuracy of prognostic predictions. This could ensure that high-risk patients receive the most appropriate therapeutic interventions.

Concluding Remarks: The hypothesis of rapid CAD plasticity is supported by the association between adhesion factors and myeloma aggressiveness, although direct evidence for the speed of these adaptations remains limited. Advanced stages of myeloma and aggressive phenotypes are linked to distinct adhesion dramatypes. The scarce evidence of dramatype transitions only imply rapidness, lacking precise dynamics require. If proven true, this hypothesis underscores the need for future research to focus on the mechanisms and speed of these adhesion changes to develop robust personalised therapies.

Hypothesis 3: CAD is Highly Diverse Between Myeloma Patients

Adhesion factor expression in myeloma cells exhibits large variability: The interquartile range of CXCL12 fold-change expression spans more than one order of magnitude (Chapter 1, Abbildung 6, p. 55). Such between-patient variance further adds to the previously discussed adhesional plasticity⁹. High variance poses both a challenge and an opportunity for cancer research, as dissecting the sources of this variability can reveal how specific forms of CAD contribute to myeloma progression in various ways.

Prognostic Power of Genomic Variants: Genetic diversity is a major source of between-patient variability. Ongoing genomic research continues to identify recurrent patterns of chromosomal aberrations and mutational signatures, defining both structural and single nucleotide variants (Kumar & Rajkumar,

2018; Hoang et al., 2019). The prognostic value of these genetic variants in MM is well established (Sharma et al., 2021), and their identification is becoming increasingly cost-effective, paving the way for targeted therapies (Zou et al., 2024; Budurlean et al., 2024). Recent advances associating high-risk myeloma with ECM mutations or adhesion factor expression, as discussed in Hypothesis 2 (p. 98), could potentially explain the diversity of adhesion dramatypes between patients (Evers et al., 2023; Q. Hu et al., 2024).

However, while these prognostic associations are valuable, they do not fully explain the mechanisms by which these genetic variants drive myeloma progression.

Integrating *in vitro* CAD Characteristics into a Mechanistic Understanding: INA-6 cells form aggregates, a behavior that was fundamental in Chapter 1 for understanding how these cells might disseminate *in vivo* (Abbildung 7, p. 59). Not just INA-6 cells, but also primary myeloma cell cultures are known to exhibit aggregation behavior (Kawano et al., 1991; Okuno et al., 1991). The *in vitro* adhesion phenotype of various myeloma cell lines also varies widely, differing in plastic/MSC adherence and aggregation behavior (Tabelle 4). This diversity suggests that the CAD of myeloma cells is complex and variable *in vivo*.

Cell Line	Plastic Adhering	MSC Adhering	H. Aggregating
MM1.S	Yes	Moderate	No
INA-6	No	Strong	Yes
U266	Moderate	Weak	No
AMO1	No	Moderate	No
OPM2	No	Moderate	No

Table 4: *In vitro* adhesion phenotypes of myeloma cell lines. MSC adhesion for MM1.S, INA-6 and U266 was measured in Appendix A.1: Abbildung 1 (p. 136); other data is based on laboratory experience. H. Aggregating: Homotypically Aggregating.

Given these insights, it would be informative to examine if other myeloma cell lines exhibit behavior similar to INA-6 cells, especially with aggregating cell lines. By characterizing their CAD in terms of plastic/MSC adherence, aggregation behavior, detachments under live-cell imaging, and gene expression profiles, followed by comparative *in vivo* studies on dissemination behavior, researchers could associate these *in vitro* CAD parameters with dissemination patterns observed after injecting these cells into mice. This approach could provide a deeper understanding of how different *in vitro* CAD patterns contribute to myeloma dissemination.

Hypothesis 4: Detachment is Caused by Multiple Cues of Varying Nature

Detachment mechanisms observed in Chapter 1 primarily involved mechanical forces. Myeloma cells,—growing as homotypic aggregates—remained stable, yet it seemed that they progressively lost adhesion force with each cell division. Eventually, convective streams were sufficient to detach single INA-6 cells from homotypic aggregates. While this process was visibly mechanical, it was predisposed by cellular interactions that destabilized adhesive strength through the saturation of hMSC surfaces and changes in aggregate shape due to cell division. This complexity suggests a multifaceted mechanism behind cell

detachment, warranting exploration of various triggers. The following paragraphs discuss potential mechanisms that could trigger myeloma cell detachment.

Other Potential Detachment Mechanisms:

- **Intercellular interaction scenarios:** INA-6 cells demonstrated that saturation of MSC adhesion and unstable aggregates ultimately contribute to detachment *in vitro*. It is reasonable to question if similar scenarios apply *in vivo*, where MSCs are less abundant and ECM provides more substrates for adhesion. However, INA-6 cells adhere to MSC-derived osteoblasts as well, potentially providing ample surface for intercellular interactions (Dotterweich et al., 2016). The principle that adhesion surfaces are limited and can become saturated has not been thoroughly explored in the literature, yet it could be a critical piece of understanding detachment events.
- **Rapid loss of surface CAMs:** The loss of CD138, either through antibody treatment or intrinsic expression of heparanase, highlights rapid changes in adhesion molecules (Y. Yang et al., 2005; Akhmetzyanova et al., 2020). This suggests that detachment might not always be a gradual process but can occur swiftly due to biochemical changes.
- **Slow loss of surface CAMs:** Since bone marrow-retentive adhesion molecules gradually decrease (Abbildung 6, p. 55), it is plausible that the final detachment of MM cells is a slow culmination of diminishing adhesion, with the actual separation triggered by other events, such as external forces.
- **Sudden gain of endothelial CAMs:** Conversely, A. Brandl et al. (2022) has shown that JAM-C is dynamically expressed in MM cells co-localizing with blood vessels. One can assume that release could be triggered when endothelial cells are in close vicinity and competes with BM stroma for MM cell adhesion.
- **Loss of substrate adhesion:** Myeloma cells actively contribute to the degradation of the bone matrix (Terpos et al., 2018), which could directly facilitate detachment. This mechanism is straightforward but might be insufficient to explain early-stage dissemination where extensive bone degradation hasn't occurred yet. However, in cases of myeloma with severe bone disease, this aspect could be critical, as weakened or destroyed physical barriers may be an overlooked contributor to dissemination.
- **Soluble signals:** Cytokines and chemokines—such as MIP-1 α , MCP-1, IL-8, and CXCL12/SDF-1—play a well-established role in influencing MM adhesion within the bone marrow (BM) (Aggarwal et al., 2006; Alsayed et al., 2007). For instance, myeloma cells overexpress MIP-1 α constitutively, which reduces adhesion and triggers migration in an autocrine manner (Lentzsch et al., 2003; Abe et al., 2002). Constitutive expression of these signals may prime MM cells for detachment. Additionally, if the accumulation of such signals surpasses a certain threshold, it is reasonable to assume they could act as an isolated trigger for detachment.
- **Purely mechanical forces:** It is conceivable that physical changes in the bone matrix, such as bending or breaking, could mechanically dislodge myeloma cells from their niche. This process could become more pronounced with advancing bone destruction, but its direct impact on cell detachment remains speculative at this point. It is of particular note, that mechanical loading of bone has been shown to enhance bone health in a myeloma mouse model, as the beneficial mechanoresponse positively modulates bone turnover (Rummel et al., 2021).
- **Pure chance:** Detachment might occasionally occur randomly, without a specific trigger, although this notion is purely speculative and included for completeness.

Implications for Future Research: Detachment events are critical not only as isolated key events

in dissemination but also for their implications on subsequent steps in the process. Cells that detach due to soluble signals are likely to assume different adhesion dramatypes influenced by downstream signalling compared to cells detached by mechanical forces. Understanding these nuances can inform targeted interventions.

A rational categorization of disease stages could be instrumental in understanding detachment mechanisms. However, there is currently no solid mechanistic basis for such categorizations. Possible approaches could involve weighing mechanical versus molecular contributions to detachment, or distinguishing between direct detachment signals, or indirect detachment due to substrate destruction. This would be particularly useful if the severity of bone disease indeed influences the detachment mechanism, as advanced bone disease implies indirect detachment after substrate destruction.

While *in vivo* studies offer valuable snapshots, a mechanistic understanding of detachment probably requires a high time-resolution, such as that provided by *in vitro* live-cell imaging. In this work, *in vitro* studies were limited by the absence of surrounding 3D substrate. However, this setup provided sufficient insights into detachment mechanisms that seem at least reasonably inferable to an *in vivo* context. Most importantly, the identified targets and their association with clinical outcomes remained consistent regardless of the experimental setup. Therefore, this approach could bridge the gap between *in vivo* and *in vitro* studies, offering a more controlled environment to study specific detachment mechanisms with specialized setups only possible in *in vitro* studies.

Implications for Therapy: Understanding the specific reasons behind myeloma cell detachment could be crucial for predicting subsequent steps of dissemination. For instance, as myeloma progresses, the degradation of bone and loss of physical barriers could alter detachment mechanisms. Therefore, advanced disease states may require specialized treatment strategies that address these unique detachment processes.

Concluding Remarks: These paragraphs elucidated the complex interplay of mechanical and molecular factors in myeloma cell detachment, highlighting the multifaceted nature of this process. Mechanical forces, such as those mediated by cell division and convective streams, alongside molecular dynamics like the modulation of cell adhesion molecules and bone matrix integrity, could play crucial roles in cell detachment. The process is probably not governed by a singular molecular mechanism but results from the dynamic expression of adhesion factors, changes within the bone marrow microenvironment, and external mechanical forces. These insights underscore the need to categorize detachment mechanisms based on their triggers, for instance distinguishing between either directed cell signals or substrate-dependent mechanical contributions.

The variability introduced by patient-specific factors, such as the onset or severity of bone destruction, suggests that categorizing detachment mechanisms could significantly impact therapeutic strategies. Our findings advocate for an integrated approach that combines *in vitro* temporal precision with *in vivo* relevance, aiming to precisely counteract the early stages of myeloma dissemination. Future research should continue to explore these mechanisms, potentially using advanced imaging and 3D culture systems, to further refine our understanding of detachment processes and their implications for treatment.

Conclusion 3: The Dynamic Adhesion Hypothetical Framework for Myeloma Dissemination

This thesis demonstrates the plasticity of myeloma Cell Adhesion Dynamics (CAD)⁵, with findings indicating rapid adaptability of myeloma cells to diverse microenvironments. This adaptability is encapsulated in the concept of “*adhesion dramatype*”⁶, introduced to describe dynamic states of adhesion due to proximate environmental factors, distinguishing it from more persistent *phenotypic* characteristics. Observations from INA-6 cells support the idea that cell detachment can result from mechanical forces, cell division, and the instability of homotypic aggregates. This work has also advanced methodologies for adhesion assays, providing new tools to isolate and quantify subpopulations within co-cultures, crucial for understanding the nuances of MM detachment.

While the evidence from this work provides a comprehensive foundation for understanding CAD in multiple myeloma, many aspects remain speculative, particularly concerning the speed and precise mechanisms of CAD changes. Literature supports these findings, but evidence remains fragmented across many fields, including genetic diversity in adhesion and ECM factors, signaling pathways modulating adhesion, and differential expression of CAMs between microenvironmental niches or disease stages. The integration of such fragments highlight a complex interplay yet to be fully deciphered. For instance, although the prognostic value of CAM and ECM proteins is well-established, the detailed pathways through which these variants contribute to myeloma dissemination remain less clear, necessitating more functional validation. Recurring concepts, such as the plasticity of CAD, unexplored mechanical contributions, and the influence of microenvironmental cues emphasize the need for a mechanistic understanding of dissemination.

Future research should prioritize the development of precise *in vitro* models that mimic specific microenvironments like the BMME, integrating advanced live-cell imaging and adhesion assays. The novel assays developed in this work, particularly for myeloma-MSC interactions, could be adapted to study other niches such as vascular environments. This approach will enhance our understanding of how different adhesional patterns or dramatypes influence myeloma progression and dissemination, providing deeper insights that could lead to targeted therapeutic interventions.

The dynamic nature of CAD underscores the need for personalised therapeutic strategies that consider specific adhesion dramatypes and niche-specific interactions. Targeting CAD could prevent dissemination, especially in advanced disease stages where bone degradation modifies detachment mechanisms. Therapies could also benefit from a multifactorial approach that includes strengthening ECM or cell adhesion to enhance bone marrow retention. However, it is critical to ensure that these strategies do not inadvertently promote survival signaling, colonization of extramedullary sites or aggravate myeloma bone disease. Understanding the triggers and mechanisms of cell detachment informs the design of effective interventions that could adapt to the progression of the disease and the specific needs of the patient.

Overall Conclusion

Insights into Myeloma Dissemination and Analytical Innovations: This thesis successfully developed an in vitro model that provided new insights into the interaction dynamics between multiple myeloma (MM) cells and mesenchymal stromal cells (MSCs), alongside the creation of `plotastic`, a Python-based tool designed to enhance data analysis and reproducibility in biomedical research. The study's findings revealed the dynamic adhesion behaviors of myeloma cells, highlighting their adaptability to changes in the microenvironment, which is crucial for understanding cancer progression and developing therapeutic interventions.

Challenges and Achievements: One major challenge was capturing and analyzing the rapid adhesion changes of myeloma cells, addressed by the development of `plotastic`. This tool facilitated the management and interpretation of complex datasets, potentially improving research reproducibility. Despite these advancements, integrating high-throughput data with real-time observations remains a challenge, pointing to a gap between static data collection and dynamic biological processes. The initial aims to enhance mechanistic understanding of myeloma dissemination and improve data analysis in biological studies were largely achieved through these efforts.

Future Research and Therapeutic Directions: Future research could refine the adhesion model by incorporating additional cellular components or environmental factors, enhancing our understanding of the interactions that promote metastasis and resistance. The adaptability of myeloma cells observed suggests potential therapeutic strategies that could disrupt these interactions. Specifically, targeting adhesion molecules that facilitate bone marrow retention could limit disease progression. This hypothesis, while promising, requires rigorous testing in clinical settings to validate potential therapies.

Conclusion: While the evidence presented in this thesis offers valuable contributions to the field of cancer biology, it also opens several speculative avenues. The hypothesis that altered adhesion dynamics could serve as a therapeutic target needs to be rigorously tested in pre-clinical settings. Moreover, the potential for `plotastic` to facilitate similar research in other types of cancer or complex diseases presents an exciting prospect for broader applications.

This thesis has advanced our understanding of the dynamic adhesion behavior of myeloma cells and their interactions with the bone marrow microenvironment. By integrating experimental and computational approaches, new methodologies for studying cell adhesion and detachment were developed. The findings emphasize the need for personalized therapeutic strategies that address specific adhesion dramatypes, offering potential for improving the management and treatment of multiple myeloma. While significant progress has been made, ongoing research is essential to fully elucidate the mechanisms behind myeloma cell dissemination and to translate these insights into clinical practice.

References

- Abadi, M., Agarwal, A., Barham, P., Brevdo, E., Chen, Z., Citro, C., ... Zheng, X. (2016, März). *TensorFlow: Large-Scale Machine Learning on Heterogeneous Distributed Systems* (Nr. arXiv:1603.04467). arXiv. Zugriff auf <https://www.tensorflow.org/> doi: 10.48550/arXiv.1603.04467
- Abdallah, N. H., Lakshman, A., Kumar, S. K., Cook, J., Binder, M., Kapoor, P., ... Rajkumar, S. V. (2024, Januar). Mode of progression in smoldering multiple myeloma: A study of 406 patients. *Blood Cancer Journal*, 14 (1), 1–7. Zugriff auf <https://www.nature.com/articles/s41408-024-00980-5> doi: 10.1038/s41408-024-00980-5
- Abdelrazik, H. (2023, August). Mesenchymal Stem Cells: A Hope or a Hype? *International Journal of Molecular Sciences*, 24 (17), 13218. Zugriff auf <https://www.ncbi.nlm.nih.gov/pmc/articles/PMC10487858/> doi: 10.3390/ijms241713218
- Abdulkadyrov, K. M., Salogub, G. N., Khuazheva, N. K., Sherman, M. L., Laadem, A., Barger, R., ... Terpos, E. (2014). Sotatercept in patients with osteolytic lesions of multiple myeloma. *British Journal of Haematology*, 165 (6), 814–823. Zugriff auf <https://onlinelibrary.wiley.com/doi/abs/10.1111/bjh.12835> doi: 10.1111/bjh.12835
- Abe, M., Hiura, K., Wilde, J., Moriyama, K., Hashimoto, T., Ozaki, S., ... Matsumoto, T. (2002, September). Role for macrophage inflammatory protein (MIP)-1 α and MIP-1 β in the development of osteolytic lesions in multiple myeloma. *Blood*, 100 (6), 2195–2202. Zugriff auf <https://doi.org/10.1182/blood.V100.6.2195> doi: 10.1182/blood.V100.6.2195
- Adamik, J., Jin, S., Sun, Q., Zhang, P., Weiss, K. R., Anderson, J. L., ... Galson, D. L. (2017, April). EZH2 or HDAC1 Inhibition Reverses Multiple Myeloma-Induced Epigenetic Suppression of Osteoblast Differentiation. *Molecular cancer research: MCR*, 15 (4), 405–417. doi: 10.1158/1541-7786.MCR-16-0242-T
- Adamik, J., Silbermann, R., Marino, S., Sun, Q., Anderson, J. L., Zhou, D., ... Galson, D. L. (2018). XRK3F2 Inhibition of p62-ZZ Domain Signaling Rescues Myeloma-Induced GFI1-Driven Epigenetic Repression of the Runx2 Gene in Pre-osteoblasts to Overcome Differentiation Suppression. *Frontiers in Endocrinology*, 9, 344. doi: 10.3389/fendo.2018.00344
- Aggarwal, R., Ghobrial, I. M. & Roodman, G. D. (2006, Oktober). Chemokines in multiple myeloma. *Experimental hematology*, 34 (10), 1289–1295. Zugriff auf <https://www.ncbi.nlm.nih.gov/pmc/articles/PMC3134145/> doi: 10.1016/j.exphem.2006.06.017
- Akhmetzyanova, I., McCarron, M. J., Parekh, S., Chesi, M., Bergsagel, P. L. & Fooksman, D. R. (2020). Dynamic CD138 surface expression regulates switch between myeloma growth and dissemination. *Leukemia*, 34 (1), 245–256. Zugriff auf <https://www.ncbi.nlm.nih.gov/pmc/articles/PMC6923614/> doi: 10.1038/s41375-019-0519-4
- Allegra, A., Casciaro, M., Barone, P., Musolino, C. & Gangemi, S. (2022, Mai). Epigenetic Crosstalk between Malignant Plasma Cells and the Tumour Microenvironment in Multiple Myeloma. *Cancers*, 14 (11), 2597. Zugriff auf <https://www.ncbi.nlm.nih.gov/pmc/articles/PMC9179362/> doi: 10.3390/cancers14112597
- Almalki, S. G. & Agrawal, D. K. (2016). Key Transcription Factors in the Differentiation of Mesenchymal Stem Cells. *Differentiation; research in biological diversity*, 92 (1-2), 41–51. Zugriff auf <https://www.ncbi.nlm.nih.gov/pmc/articles/PMC5010472/> doi: 10.1016/j.diff.2016.02.005
- Alsayed, Y., Ngo, H., Runnels, J., Leleu, X., Singha, U. K., Pitsillides, C. M., ... Ghobrial, I. M. (2007, April). Mechanisms of regulation of CXCR4/SDF-1 (CXCL12)-dependent migration and homing in

- multiple myeloma. *Blood*, 109 (7), 2708–2717. doi: 10.1182/blood-2006-07-035857
- Anders, S., Pyl, P. T. & Huber, W. (2015, Januar). HTSeq—a Python framework to work with high-throughput sequencing data. *Bioinformatics (Oxford, England)*, 31 (2), 166–169. doi: 10.1093/bioinformatics/btu638
- Andrews, S. (2010). *FastQC - A quality control tool for high throughput sequence data*. Zugriff auf <https://www.bioinformatics.babraham.ac.uk/projects/fastqc/>
- Arefin, S., Heya, T., Al-Qudah, H., Ineza, Y. & Serwadda, A. (2024). Unmasking the Giant: A Comprehensive Evaluation of ChatGPT's Proficiency in Coding Algorithms and Data Structures:. In *Proceedings of the 16th International Conference on Agents and Artificial Intelligence* (S. 412–419). Rome, Italy: SCITEPRESS - Science and Technology Publications. Zugriff auf <https://www.scitepress.org/DigitalLibrary/Link.aspx?doi=10.5220/0012467100003636> doi: 10.5220/0012467100003636
- Armstrong, R. A. (2014, September). When to use the Bonferroni correction. *Ophthalmic & Physiological Optics: The Journal of the British College of Ophthalmic Opticians (Optometrists)*, 34 (5), 502–508. doi: 10.1111/opo.12131
- Asosingh, K., Günthert, U., De Raeve, H., Van Riet, I., Van Camp, B. & Vanderkerken, K. (2001). A unique pathway in the homing of murine multiple myeloma cells: CD44v10 mediates binding to bone marrow endothelium. *Cancer Research*, 61 (7), 2862–2865.
- Baker, M. (2016, Mai). 1,500 scientists lift the lid on reproducibility. *Nature*, 533 (7604), 452–454. Zugriff auf <https://www.nature.com/articles/533452a> doi: 10.1038/533452a
- Bao, L., Lai, Y., Liu, Y., Qin, Y., Zhao, X., Lu, X., ... Huang, X. (2013, September). CXCR4 is a good survival prognostic indicator in multiple myeloma patients. *Leukemia Research*, 37 (9), 1083–1088. doi: 10.1016/j.leukres.2013.06.002
- Barnes, D. G., Vidiassov, M., Ruthensteiner, B., Fluke, C. J., Quayle, M. R. & McHenry, C. R. (2013, September). Embedding and Publishing Interactive, 3-Dimensional, Scientific Figures in Portable Document Format (PDF) Files. *PLOS ONE*, 8 (9), e69446. Zugriff auf <https://journals.plos.org/plosone/article?id=10.1371/journal.pone.0069446> doi: 10.1371/journal.pone.0069446
- Barzilay, R., Ben-Zur, T., Bulvik, S., Melamed, E. & Offen, D. (2009, Mai). Lentiviral delivery of LMX1a enhances dopaminergic phenotype in differentiated human bone marrow mesenchymal stem cells. *Stem cells and development*, 18 (4), 591–601. doi: 10.1089/scd.2008.0138
- Beck, K., Beedle, M., van Bennekum, A., Cockburn, A., Cunningham, W., Fowler, M., ... Thomas, D. (2001). *Manifesto for agile software development*. Zugriff auf <http://www.agilemanifesto.org/>
- Begley, C. G. & Ioannidis, J. P. A. (2015, Januar). Reproducibility in science: Improving the standard for basic and preclinical research. *Circulation Research*, 116 (1), 116–126. doi: 10.1161/CIRCRESAHA.114.303819
- Berg, S., Kutra, D., Kroeger, T., Straehle, C. N., Kausler, B. X., Haubold, C., ... Kreshuk, A. (2019, Dezember). Ilastik: Interactive machine learning for (bio)image analysis. *Nature Methods*, 16 (12), 1226–1232. Zugriff auf <https://www.nature.com/articles/s41592-019-0582-9> doi: 10.1038/s41592-019-0582-9
- Bhartiya, D. (2015, Februar). Stem cells, progenitors & regenerative medicine: A retrospection. *The Indian Journal of Medical Research*, 141 (2), 154–161. Zugriff auf <https://www.ncbi.nlm.nih.gov/pmc/articles/PMC4418150/>
- Bianco, P. (2014). "Mesenchymal stem cells. *Annual review of cell and developmental biology*, 30, 677–704. doi: 10.1146/annurev-cellbio-100913-013132
- BioStudies. (o.J.). *BioStudies < The European Bioinformatics Institute < EMBL-EBI*. Zugriff auf <https://www.ebi.ac.uk/biostudies/bioimages/studies/S-BIAD1092?key=69bafe9c-74ff>

- 492b-9e68-bd42655c4d1b
- Bladé, J., Beksac, M., Caers, J., Jurczyszyn, A., von Lilienfeld-Toal, M., Moreau, P., ... Richardson, P. (2022, März). Extramedullary disease in multiple myeloma: A systematic literature review. *Blood Cancer Journal*, 12 (3), 1–10. Zugriff auf <https://www.nature.com/articles/s41408-022-00643-3> doi: 10.1038/s41408-022-00643-3
- Blonska, M., Zhu, Y., Chuang, H. H., You, M. J., Kunkalla, K., Vega, F. & Lin, X. (2015, Februar). Jun-regulated genes promote interaction of diffuse large B-cell lymphoma with the microenvironment. *Blood*, 125 (6), 981–991. Zugriff auf <https://www.ncbi.nlm.nih.gov/pmc/articles/PMC4319238/> doi: 10.1182/blood-2014-04-568188
- Bokeh Development Team. (2018). *Bokeh: Python library for interactive visualization* [Manual]. Zugriff auf <https://bokeh.pydata.org/en/latest/>
- Bolado-Carrancio, A., Rukhlenko, O. S., Nikanova, E., Tsyganov, M. A., Wheeler, A., Garcia-Munoz, A., ... Kholodenko, B. N. (2020, Juli). Periodic propagating waves coordinate RhoGTPase network dynamics at the leading and trailing edges during cell migration. *eLife*, 9, e58165. Zugriff auf <https://elifesciences.org/articles/58165> doi: 10.7554/eLife.58165
- Bondi, A. B. (2000, September). Characteristics of scalability and their impact on performance. In *Proceedings of the 2nd international workshop on Software and performance* (S. 195–203). New York, NY, USA: Association for Computing Machinery. Zugriff auf <https://dl.acm.org/doi/10.1145/350391.350432> doi: 10.1145/350391.350432
- Bosch-Queralt, M., Tiwari, V., Damkou, A., Vaculčiaková, L., Alexopoulos, I. & Simons, M. (2022, März). A fluorescence microscopy-based protocol for volumetric measurement of lysolecithin lesion-associated de- and re-myelination in mouse brain. *STAR protocols*, 3 (1), 101141. doi: 10.1016/j.xpro.2022.101141
- Boswell, D. & Foucher, T. (2011). *The Art of Readable Code: Simple and Practical Techniques for Writing Better Code* (1st Aufl.). O'Reilly Media, Inc.
- Bou Zerdan, M., Nasr, L., Kassab, J., Saba, L., Ghossein, M., Yaghi, M., ... Chaulagain, C. P. (2022). Adhesion molecules in multiple myeloma oncogenesis and targeted therapy. *International Journal of Hematologic Oncology*, 11 (2), IJH39. Zugriff auf <https://www.ncbi.nlm.nih.gov/pmc/articles/PMC9136637/> doi: 10.2217/ijh-2021-0017
- Brandl, A., Solimando, A. G., Mokhtari, Z., Tabares, P., Medler, J., Manz, H., ... Beilhack, A. (2022, März). Junctional adhesion molecule C expression specifies a CD138low/neg multiple myeloma cell population in mice and humans. *Blood Advances*, 6 (7), 2195–2206. Zugriff auf <https://doi.org/10.1182/bloodadvances.2021004354> doi: 10.1182/bloodadvances.2021004354
- Brandl, G. (2021). *Sphinx*. Zugriff auf <http://sphinx-doc.org/sphinx.pdf>
- Brankatschk, R., Bodenhausen, N., Zeyer, J. & Bürgmann, H. (2012, Juni). Simple Absolute Quantification Method Correcting for Quantitative PCR Efficiency Variations for Microbial Community Samples. *Applied and Environmental Microbiology*, 78 (12), 4481–4489. Zugriff auf <https://journals.asm.org/doi/10.1128/AEM.07878-11> doi: 10.1128/AEM.07878-11
- Breiman, L. (2001, Oktober). Random Forests. *Machine Learning*, 45 (1), 5–32. Zugriff auf <https://doi.org/10.1023/A:1010933404324> doi: 10.1023/A:1010933404324
- Brooke, J. (1996, Juni). SUS: A 'Quick and Dirty' Usability Scale. In *Usability Evaluation In Industry* (1st Aufl., S. 207–212). CRC Press. Zugriff auf <https://www.taylorfrancis.com/books/9781498710411/chapters/10.1201/9781498710411-35> doi: 10.1201/9781498710411-35
- Bubendorf, L. (2001, August). High-throughput microarray technologies: From genomics to clinics. *European Urology*, 40 (2), 231–238. doi: 10.1159/000049777
- Budurlean, L., Tukaramrao, D. B., Zhang, L., Dovat, S. & Broach, J. (2024, März). Integrating Optical

- Genome Mapping and Whole Genome Sequencing in Somatic Structural Variant Detection. *Journal of Personalized Medicine*, 14 (3), 291. Zugriff auf <https://www.ncbi.nlm.nih.gov/pmc/articles/PMC10971281/> doi: 10.3390/jpm14030291
- Burger, R., Guenther, A., Bakker, F., Schmalzing, M., Bernand, S., Baum, W., ... Gramatzki, M. (2001). Gp130 and ras mediated signaling in human plasma cell line INA-6: A cytokine-regulated tumor model for plasmacytoma. *The Hematology Journal: The Official Journal of the European Haematology Association*, 2 (1), 42–53. doi: 10.1038/sj.thj.6200075
- Bustin, S. A. (2014, Dezember). The reproducibility of biomedical research: Sleepers awake! *Biomolecular Detection and Quantification*, 2, 35–42. Zugriff auf <https://www.sciencedirect.com/science/article/pii/S2214753515000030> doi: 10.1016/j.bdq.2015.01.002
- Bustin, S. A., Benes, V., Garson, J., Hellemans, J., Huggett, J., Kubista, M., ... Vandesompele, J. (2013, November). The need for transparency and good practices in the qPCR literature. *Nature Methods*, 10 (11), 1063–1067. Zugriff auf <https://www.nature.com/articles/nmeth.2697> doi: 10.1038/nmeth.2697
- Caplan, A. (1991). Mesenchymal stem cells. *Journal of orthopaedic research : official publication of the Orthopaedic Research Society*, 9 (5), 641–50. Zugriff auf <http://www.ncbi.nlm.nih.gov/pubmed/1870029> doi: 10.1002/jor.1100090504
- Caplan, A. I. (1994, Juli). The mesengenic process. *Clinics in plastic surgery*, 21 (3), 429–435.
- Carlson, M. (2016). *Org.Hs eg.db (Bioconductor)*. Zugriff auf <http://bioconductor.org/packages/org.Hs.eg.db/> doi: 10.18129/B9.bioc.org.Hs.eg.db
- Chacon, S. & Straub, B. (2014). *Pro Git* (2nd Aufl.). Apress. Zugriff auf <https://git-scm.com/book/en/v2>
- Charlier, F., Weber, M., Izak, D., Harkin, E., Magnus, M., Lalli, J., ... Repplinger, S. (2022, Oktober). *Trevismd/statannotations: V0.5*. Zenodo. Zugriff auf <https://zenodo.org/record/7213391> doi: 10.5281/ZENODO.7213391
- Chatterjee, M., Hönenmann, D., Lentzsch, S., Bommert, K., Sers, C., Herrmann, P., ... Bargou, R. C. (2002, November). In the presence of bone marrow stromal cells human multiple myeloma cells become independent of the IL-6/gp130/STAT3 pathway. *Blood*, 100 (9), 3311–3318. doi: 10.1182/blood-2002-01-0102
- Chauhan, D., Uchiyama, H., Akbarali, Y., Urashima, M., Yamamoto, K., Libermann, T. & Anderson, K. (1996, Februar). Multiple myeloma cell adhesion-induced interleukin-6 expression in bone marrow stromal cells involves activation of NF-kappaB. *Blood*, 87, 1104–12. doi: 10.1182/blood.V87.3.1104.bloodjournal8731104
- Chen, C., Yu, W., Tober, J., Gao, P., He, B., Lee, K., ... Tan, K. (2019, Dezember). Spatial Genome Reorganization between Fetal and Adult Hematopoietic Stem Cells. *Cell reports*, 29 (12), 4200–4211.e7. Zugriff auf <https://www.ncbi.nlm.nih.gov/pmc/articles/PMC7262670/> doi: 10.1016/j.celrep.2019.11.065
- Chen, H. & Zhou, L. (2022, Juni). Treatment of ischemic stroke with modified mesenchymal stem cells. *International Journal of Medical Sciences*, 19 (7), 1155–1162. Zugriff auf <https://www.ncbi.nlm.nih.gov/pmc/articles/PMC9339408/> doi: 10.7150/ijms.74161
- Chen, W.-C., Hu, G. & Hazlehurst, L. A. (2020, Oktober). Contribution of the bone marrow stromal cells in mediating drug resistance in hematopoietic tumors. *Current Opinion in Pharmacology*, 54, 36–43. Zugriff auf <https://www.sciencedirect.com/science/article/pii/S1471489220300576> doi: 10.1016/j.coph.2020.08.006
- Chen, Y., Wang, Q., Mills, C. E., Kann, J. G., Shull, K. R., Tullman-Ercek, D. & Wang, M. (2021, Juli).

- High-Throughput Screening Test for Adhesion in Soft Materials Using Centrifugation. *ACS Central Science*, 7 (7), 1135–1143. Zugriff auf <https://www.ncbi.nlm.nih.gov/pmc/articles/PMC8323114/> doi: 10.1021/acscentsci.1c00414
- Cheng, Y., Li, W., Jin, T., Wu, S. & Zhang, L. (2023, Februar). [Frontiers and development in live-cell super-resolution fluorescence microscopy]. *Sheng Wu Yi Xue Gong Cheng Xue Za Zhi = Journal of Biomedical Engineering = Shengwu Yixue Gongchengxue Zazhi*, 40 (1), 180–184. doi: 10.7507/1001-5515.202210060
- Ciabrelli, F. & Cavalli, G. (2015, Februar). Chromatin-Driven Behavior of Topologically Associating Domains. *Journal of Molecular Biology*, 427 (3), 608–625. Zugriff auf <https://www.sciencedirect.com/science/article/pii/S0022283614005129> doi: 10.1016/j.jmb.2014.09.013
- Cippitelli, M., Stabile, H., Kosta, A., Petillo, S., Lucantonio, L., Gismondi, A., ... Fionda, C. (2023, Januar). Role of NF- κ B Signaling in the Interplay between Multiple Myeloma and Mesenchymal Stromal Cells. *International Journal of Molecular Sciences*, 24 (3), 1823. Zugriff auf <https://www.mdpi.com/1422-0067/24/3/1823> doi: 10.3390/ijms24031823
- Codecov. (o. J.). Zugriff auf <https://docs.codecov.com/docs/quick-start>
- Cole, R. (2014). Live-cell imaging. *Cell Adhesion & Migration*, 8 (5), 452–459. doi: 10.4161/cam.28348
- Colucci, S., Brunetti, G., Oranger, A., Mori, G., Sardone, F., Specchia, G., ... Grano, M. (2011, Juni). Myeloma cells suppress osteoblasts through sclerostin secretion. *Blood Cancer Journal*, 1 (6), e27. Zugriff auf <https://www.ncbi.nlm.nih.gov/pmc/articles/PMC3255263/> doi: 10.1038/bcj.2011.22
- Committee on Strategies for Responsible Sharing of Clinical Trial Data, Board on Health Sciences Policy & Institute of Medicine. (2015). *Sharing Clinical Trial Data: Maximizing Benefits, Minimizing Risk*. Washington (DC): National Academies Press (US). Zugriff auf <http://www.ncbi.nlm.nih.gov/books/NBK269030/>
- Cooper, G. M. (2000). Cell Proliferation in Development and Differentiation. In *The Cell: A Molecular Approach*. 2nd edition (2. Aufl.). Sinauer Associates. Zugriff auf <https://www.ncbi.nlm.nih.gov/books/NBK9906/>
- da Silva Meirelles, L., Chagastelles, P. C. & Nardi, N. B. (2006, Juni). Mesenchymal stem cells reside in virtually all post-natal organs and tissues. *Journal of cell science*, 119 (Pt 11), 2204–2213. doi: 10.1242/jcs.02932
- Davidson-Pilon, C. (2019, August). Lifelines: Survival analysis in Python. *Journal of Open Source Software*, 4 (40), 1317. Zugriff auf <https://joss.theoj.org/papers/10.21105/joss.01317> doi: 10.21105/joss.01317
- Delgado Calle, J., Bellido, T. & David Roodman, G. D. (2013, November). Direct Cell-To-Cell Interactions Between Osteocytes and Multiple Myeloma (MM) Cells Upregulate Sost and Downregulate OPG Expression In Osteocytes: Evidence For Osteocytic Contributions To MM-Induced Bone Disease. *Blood*, 122 (21), 3140. Zugriff auf <https://www.sciencedirect.com/science/article/pii/S0006497119664128> doi: 10.1182/blood.V122.21.3140.3140
- Ding, W., Goldberg, D. & Zhou, W. (2023, August). PyComplexHeatmap: A Python package to visualize multimodal genomics data. *iMeta*, 2 (3), e115. doi: 10.1002/imt2.115
- Dixon, J. R., Jung, I., Selvaraj, S., Shen, Y., Antosiewicz-Bourget, J. E., Lee, A. Y., ... Ren, B. (2015, Februar). Chromatin architecture reorganization during stem cell differentiation. *Nature*, 518 (7539), 331–336. Zugriff auf <https://www.nature.com/articles/nature14222> doi: 10.1038/nature14222
- Dobin, A., Davis, C. A., Schlesinger, F., Drenkow, J., Zaleski, C., Jha, S., ... Gingeras, T. R. (2013, Januar). STAR: Ultrafast universal RNA-seq aligner. *Bioinformatics*, 29 (1), 15–21. Zugriff auf <https://www.ncbi.nlm.nih.gov/pmc/articles/PMC3530905/> doi: 10.1093/bioinformatics/bts635

- Doddi, S. & Rashid, M. H. (2024). Disparities in Multiple Myeloma Mortality Rate Trends by Demographic Status in the USA. *Cancer Diagnosis & Prognosis*, 4 (3), 288–294. doi: 10.21873/cdp.10322
- Dominici, M., Le Blanc, K., Mueller, I., Slaper-Cortenbach, I., Marini, F., Krause, D., ... Horwitz, E. (2006). Minimal criteria for defining multipotent mesenchymal stromal cells. The International Society for Cellular Therapy position statement. *Cytotherapy*, 8 (4), 315–317. doi: 10.1080/14653240600855905
- Dotterweich, J., Schlegelmilch, K., Keller, A., Geyer, B., Schneider, D., Zeck, S., ... Schütze, N. (2016, Dezember). Contact of myeloma cells induces a characteristic transcriptome signature in skeletal precursor cells -Implications for myeloma bone disease. *Bone*, 93, 155–166. doi: 10.1016/j.bone.2016.08.006
- D'souza, N., Rossignoli, F., Golinelli, G., Grisendi, G., Spano, C., Candini, O., ... Dominici, M. (2015, August). Mesenchymal stem/stromal cells as a delivery platform in cell and gene therapies. *BMC medicine*, 13, 186. doi: 10.1186/s12916-015-0426-0
- D'Souza, S., del Prete, D., Jin, S., Sun, Q., Huston, A. J., Kostov, F. E., ... Galson, D. L. (2011, Dezember). Gfi1 expressed in bone marrow stromal cells is a novel osteoblast suppressor in patients with multiple myeloma bone disease. *Blood*, 118 (26), 6871–6880. Zugriff auf <https://www.ncbi.nlm.nih.gov/pmc/articles/PMC3245209/> doi: 10.1182/blood-2011-04-346775
- Dunn, W., Burgun, A., Krebs, M.-O. & Rance, B. (2017, November). Exploring and visualizing multi-dimensional data in translational research platforms. *Briefings in Bioinformatics*, 18 (6), 1044–1056. Zugriff auf <https://www.ncbi.nlm.nih.gov/pmc/articles/PMC5862238/> doi: 10.1093/bib/bbw080
- Duvall, P. M., Matyas, S. & Glover, A. (2007). *Continuous Integration: Improving Software Quality and Reducing Risk* (1. Aufl.). Upper Saddle River, NJ: Addison-Wesley.
- Dziadowicz, S. A., Wang, L., Akhter, H., Aesoph, D., Sharma, T., Adjerooh, D. A., ... Hu, G. (2022, Januar). Bone Marrow Stroma-Induced Transcriptome and Regulome Signatures of Multiple Myeloma. *Cancers*, 14 (4), 927. Zugriff auf <https://www.mdpi.com/2072-6694/14/4/927> doi: 10.3390/cancers14040927
- Ekmekci, B., McAnany, C. E. & Mura, C. (2016, Juli). An Introduction to Programming for Bioscientists: A Python-Based Primer. *PLOS Computational Biology*, 12 (6), e1004867. Zugriff auf <https://journals.plos.org/ploscompbiol/article?id=10.1371/journal.pcbi.1004867> doi: 10.1371/journal.pcbi.1004867
- Engelhardt, M., Kortüm, K. M., Goldschmidt, H. & Merz, M. (2024, Februar). Functional cure and long-term survival in multiple myeloma: How to challenge the previously impossible. *Haematologica*. doi: 10.3324/haematol.2023.283058
- Evers, M., Schreder, M., Stühmer, T., Jundt, F., Ebert, R., Hartmann, T. N., ... Leich, E. (2023, März). Prognostic value of extracellular matrix gene mutations and expression in multiple myeloma. *Blood Cancer Journal*, 13 (1), 43. doi: 10.1038/s41408-023-00817-7
- Ewels, P., Magnusson, M., Lundin, S. & Käller, M. (2016, Oktober). MultiQC: Summarize analysis results for multiple tools and samples in a single report. *Bioinformatics*, 32 (19), 3047–3048. Zugriff auf <https://doi.org/10.1093/bioinformatics/btw354> doi: 10.1093/bioinformatics/btw354
- Excel, M. (2023, August). *Announcing Python in Excel: Combining the power of Python and the flexibility of Excel*. Zugriff auf <https://techcommunity.microsoft.com/t5/excel-blog/announcing-python-in-excel-combining-the-power-of-python-and-the-ba-p/3893439>
- Fairfield, H., Costa, S., Falank, C., Farrell, M., Murphy, C. S., D'Amico, A., ... Reagan, M. R. (2020). Multiple Myeloma Cells Alter Adipogenesis, Increase Senescence-Related and Inflammatory Gene Transcript Expression, and Alter Metabolism in Preadipocytes. *Frontiers in Oncology*, 10, 584683. doi: 10.3389/fonc.2020.584683
- Federer, L. M., Lu, Y.-L. & Joubert, D. J. (2016, Januar). Data literacy training needs of biomedical

- researchers. *Journal of the Medical Library Association : JMLA*, 104 (1), 52–57. Zugriff auf <https://www.ncbi.nlm.nih.gov/pmc/articles/PMC4722643/> doi: 10.3163/1536-5050.104.1.008
- Fermand, J.-P., Bridoux, F., Dispenzieri, A., Jaccard, A., Kyle, R. A., Leung, N. & Merlini, G. (2018, Oktober). Monoclonal gammopathy of clinical significance: A novel concept with therapeutic implications. *Blood*, 132 (14), 1478–1485. doi: 10.1182/blood-2018-04-839480
- Fernandez-Rebollo, E., Mentrup, B., Ebert, R., Franzen, J., Abagnale, G., Sieben, T., ... Wagner, W. (2017, Juli). Human Platelet Lysate versus Fetal Calf Serum: These Supplements Do Not Select for Different Mesenchymal Stromal Cells. *Scientific Reports*, 7, 5132. Zugriff auf <https://www.ncbi.nlm.nih.gov/pmc/articles/PMC5506010/> doi: 10.1038/s41598-017-05207-1
- Fernando, R. C., Mazzotti, D. R., Azevedo, H., Sandes, A. F., Rizzatti, E. G., de Oliveira, M. B., ... Colleoni, G. W. B. (2019, Januar). Transcriptome Analysis of Mesenchymal Stem Cells from Multiple Myeloma Patients Reveals Downregulation of Genes Involved in Cell Cycle Progression, Immune Response, and Bone Metabolism. *Scientific Reports*, 9. Zugriff auf <https://www.ncbi.nlm.nih.gov/pmc/articles/PMC6355867/> doi: 10.1038/s41598-018-38314-8
- Flier, J. S. (2022). The Problem of Irreproducible Bioscience Research. *Perspectives in Biology and Medicine*, 65 (3), 373–395. doi: 10.1353/pbm.2022.0032
- Forster, S. & Radpour, R. (2022, Juli). Molecular Impact of the Tumor Microenvironment on Multiple Myeloma Dissemination and Extramedullary Disease. *Frontiers in Oncology*, 12. Zugriff auf <https://www.frontiersin.org/journals/oncology/articles/10.3389/fonc.2022.941437/full> doi: 10.3389/fonc.2022.941437
- Frassanito, M. A., Cusmai, A., Iodice, G. & Dammacco, F. (2001, Januar). Autocrine interleukin-6 production and highly malignant multiple myeloma: Relation with resistance to drug-induced apoptosis. *Blood*, 97 (2), 483–489. doi: 10.1182/blood.v97.2.483
- Frede, J., Anand, P., Sotudeh, N., Pinto, R. A., Nair, M. S., Stuart, H., ... Lohr, J. G. (2021, November). Dynamic transcriptional reprogramming leads to immunotherapeutic vulnerabilities in myeloma. *Nature cell biology*, 23 (11), 1199–1211. Zugriff auf <https://www.ncbi.nlm.nih.gov/pmc/articles/PMC8764878/> doi: 10.1038/s41556-021-00766-y
- Friedenstein, A. & Kurolesova, A. I. (1971, August). Osteogenic precursor cells of bone marrow in radiation chimeras. *Transplantation*, 12 (2), 99–108.
- Friedenstein, A. J., Piatetzky-Shapiro, I. I. & Petrakova, K. V. (1966, Dezember). Osteogenesis in transplants of bone marrow cells. *Journal of embryology and experimental morphology*, 16 (3), 381–390.
- Gabr, M. M., Zakaria, M. M., Refaie, A. F., Ismail, A. M., Abou-El-Mahasen, M. A., Ashamallah, S. A., ... Ghoneim, M. A. (2013). Insulin-producing cells from adult human bone marrow mesenchymal stem cells control streptozotocin-induced diabetes in nude mice. *Cell transplantation*, 22 (1), 133–145. doi: 10.3727/096368912X647162
- Galbraith, C. G. (2023, Januar). Pumping up the volume. *Journal of Cell Biology*, 222 (2), e202212042. Zugriff auf <https://doi.org/10.1083/jcb.202212042> doi: 10.1083/jcb.202212042
- Gallego-Selles, A., Galvan-Alvarez, V., Martinez-Canton, M., Garcia-Gonzalez, E., Morales-Alamo, D., Santana, A., ... Martin-Rincon, M. (2022, Juli). Fast regulation of the NF-κB signalling pathway in human skeletal muscle revealed by high-intensity exercise and ischaemia at exhaustion: Role of oxygenation and metabolite accumulation. *Redox Biology*, 55, 102398. Zugriff auf <https://www.ncbi.nlm.nih.gov/pmc/articles/PMC9287614/> doi: 10.1016/j.redox.2022.102398
- Gao, D., Ji, L., Bai, Z., Ouyang, M., Li, P., Mao, D., ... Shou, M. Z. (2024, Januar). ASSISTGUI: Task-Oriented Desktop Graphical User Interface Automation (Nr. arXiv:2312.13108). arXiv. Zugriff

- auf <http://arxiv.org/abs/2312.13108> doi: 10.48550/arXiv.2312.13108
- Gao, S., Wang, Y.-T., Ma, G.-Y., Lu, M.-Q., Chu, B., Shi, L., ... Bao, L. (2024, April). Solitary bone plasmacytoma: Long-term clinical outcomes in a single center. *Current Problems in Cancer*, 50, 101095. doi: 10.1016/j.currproblcancer.2024.101095
- Garcés, J.-J., Simicek, M., Vicari, M., Brozova, L., Burgos, L., Bezdekova, R., ... Paiva, B. (2020, Februar). Transcriptional profiling of circulating tumor cells in multiple myeloma: A new model to understand disease dissemination. *Leukemia*, 34 (2), 589–603. doi: 10.1038/s41375-019-0588-4
- García-Ortiz, A., Rodríguez-García, Y., Encinas, J., Maroto-Martín, E., Castellano, E., Teixidó, J. & Martínez-López, J. (2021, Januar). The Role of Tumor Microenvironment in Multiple Myeloma Development and Progression. *Cancers*, 13 (2). Zugriff auf <https://www.ncbi.nlm.nih.gov/pmc/articles/PMC7827690/> doi: 10.3390/cancers13020217
- Gaur, T., Lengner, C. J., Hovhannisyan, H., Bhat, R. A., Bodine, P. V. N., Komm, B. S., ... Lian, J. B. (2005, September). Canonical WNT signaling promotes osteogenesis by directly stimulating Runx2 gene expression. *The Journal of Biological Chemistry*, 280 (39), 33132–33140. doi: 10.1074/jbc.M500608200
- Geng, Y., Chandrasekaran, S., Agastin, S., Li, J. & King, M. R. (2014, März). Dynamic Switch Between Two Adhesion Phenotypes in Colorectal Cancer Cells. *Cellular and Molecular Bioengineering*, 7 (1), 35–44. Zugriff auf <https://doi.org/10.1007/s12195-013-0313-8> doi: 10.1007/s12195-013-0313-8
- Ghobrial, I. M. (2012, Juli). Myeloma as a model for the process of metastasis: Implications for therapy. *Blood*, 120 (1), 20–30. Zugriff auf <https://www.ncbi.nlm.nih.gov/pmc/articles/PMC3390959/> doi: 10.1182/blood-2012-01-379024
- Giorgi, F. M., Ceraolo, C. & Mercatelli, D. (2022, April). The R Language: An Engine for Bioinformatics and Data Science. *Life*, 12 (5), 648. Zugriff auf <https://www.ncbi.nlm.nih.gov/pmc/articles/PMC9148156/> doi: 10.3390/life12050648
- Glavey, S. V., Naba, A., Manier, S., Claußer, K., Tahri, S., Park, J., ... Ghobrial, I. M. (2017, November). Proteomic characterization of human multiple myeloma bone marrow extracellular matrix. *Leukemia*, 31 (11), 2426–2434. Zugriff auf <https://www.nature.com/articles/leu2017102> doi: 10.1038/leu.2017.102
- Gomez-Cabrero, D., Abugessaisa, I., Maier, D., Teschendorff, A., Merkenschlager, M., Gisel, A., ... Tegnér, J. (2014, März). Data integration in the era of omics: Current and future challenges. *BMC Systems Biology*, 8 (2), I1. Zugriff auf <https://doi.org/10.1186/1752-0509-8-S2-I1> doi: 10.1186/1752-0509-8-S2-I1
- Gómez-López, G., Dopazo, J., Cigudosa, J. C., Valencia, A. & Al-Shahrour, F. (2019, Mai). Precision medicine needs pioneering clinical bioinformaticians. *Briefings in Bioinformatics*, 20 (3), 752–766. doi: 10.1093/bib/bbx144
- Goodman, S. N., Fanelli, D. & Ioannidis, J. P. A. (2016, Juni). What does research reproducibility mean? *Science Translational Medicine*, 8 (341), 341ps12-341ps12. Zugriff auf <https://www.science.org/doi/10.1126/scitranslmed.aaf5027> doi: 10.1126/scitranslmed.aaf5027
- Gorelick, M. & Ozsváld, I. (2020). *High Performance Python: Practical Performant Programming for Humans* (2. Aufl.). O'Reilly Media.
- Gosselin, R.-D. (2021, Februar). Insufficient transparency of statistical reporting in preclinical research: A scoping review. *Scientific Reports*, 11 (1), 3335. Zugriff auf <https://www.nature.com/articles/s41598-021-83006-5> doi: 10.1038/s41598-021-83006-5
- Gramatzki, M., Burger, R., Trautman, U., Marschalek, R., Lorenz, H., Hansen-Hagge, T., ... Kalden, J. (1994). Two new interleukin-6 dependent plasma cell lines carrying a chromosomal abnormality involving the IL-6 gene locus. *Blood*, 84 Suppl. 1 (1), 173a-173a. Zugriff auf <https://www.cellosaurus.org>

- .org/cellopub/CLPUB00060
- Granata, V., Crisafulli, L., Nastasi, C., Ficara, F. & Sobacchi, C. (2022, Mai). Bone Marrow Niches and Tumour Cells: Lights and Shadows of a Mutual Relationship. *Frontiers in Immunology*, 13. Zugriff auf <https://www.frontiersin.org/journals/immunology/articles/10.3389/fimmu.2022.884024/full> doi: 10.3389/fimmu.2022.884024
- GraphPad Prism 10 User Guide*. (2024). Zugriff auf <https://www.graphpad.com/guides/prism/latest/user-guide/multiple-variable-tables.htm>
- Greenstein, S., Krett, N. L., Kurosawa, Y., Ma, C., Chauhan, D., Hideshima, T., ... Rosen, S. T. (2003, April). Characterization of the MM.1 human multiple myeloma (MM) cell lines: A model system to elucidate the characteristics, behavior, and signaling of steroid-sensitive and -resistant MM cells. *Experimental Hematology*, 31 (4), 271–282. doi: 10.1016/s0301-472x(03)00023-7
- Gronthos, S., Graves, S. E., Ohta, S. & Simmons, P. J. (1994, Dezember). The STRO-1+ fraction of adult human bone marrow contains the osteogenic precursors. *Blood*, 84 (12), 4164–4173.
- Guan, X. L., Chang, D. P. S., Mok, Z. X. & Lee, B. (2023, November). Assessing variations in manual pipetting: An under-investigated requirement of good laboratory practice. *Journal of Mass Spectrometry and Advances in the Clinical Lab*, 30, 25–29. doi: 10.1016/j.jmsacl.2023.09.001
- Gupta, A., Harrison, P. J., Wieslander, H., Pielawski, N., Kartasalo, K., Partel, G., ... Wählby, C. (2019). Deep Learning in Image Cytometry: A Review. *Cytometry Part A*, 95 (4), 366–380. Zugriff auf <https://onlinelibrary.wiley.com/doi/abs/10.1002/cyto.a.23701> doi: 10.1002/cyto.a.23701
- Gupta, D., Attal, K. & Demner-Fushman, D. (2023, März). A dataset for medical instructional video classification and question answering. *Scientific Data*, 10 (1), 158. doi: 10.1038/s41597-023-02036-y
- Gupta, S., Master, S. & Graham, C. (2022, Oktober). Extramedullary Multiple Myeloma: A Patient-Focused Review of the Pathogenesis of Bone Marrow Escape. *World Journal of Oncology*, 13 (5), 311–319. Zugriff auf <https://www.ncbi.nlm.nih.gov/pmc/articles/PMC9635794/> doi: 10.14740/wjon1521
- Hallek, M., Bergsagel, P. L. & Anderson, K. C. (1998, Januar). Multiple Myeloma: Increasing Evidence for a Multistep Transformation Process. *Blood*, 91 (1), 3–21. Zugriff auf <https://www.ncbi.nlm.nih.gov/pmc/articles/PMC3901996/>
- Hannun, A., Digani, J., Katharopoulos, A. & Collobert, R. (2023). *MLX*. Apple. Zugriff auf <https://github.com/ml-explore/mlx>
- Harada, T., Hiasa, M., Teramachi, J. & Abe, M. (2021, September). Myeloma–Bone Interaction: A Vicious Cycle via TAK1–PIM2 Signaling. *Cancers*, 13 (17). Zugriff auf <https://www.ncbi.nlm.nih.gov/pmc/articles/PMC8431187/> doi: 10.3390/cancers13174441
- Harrington, D. P. & Fleming, T. R. (1982). A Class of Rank Test Procedures for Censored Survival Data. *Biometrika*, 69 (3), 553–566. Zugriff auf <https://www.jstor.org/stable/2335991> doi: 10.2307/2335991
- Harris, C. R., Millman, K. J., van der Walt, S. J., Gommers, R., Virtanen, P., Cournapeau, D., ... Oliphant, T. E. (2020, September). Array programming with NumPy. *Nature*, 585 (7825), 357–362. Zugriff auf <https://www.nature.com/articles/s41586-020-2649-2> doi: 10.1038/s41586-020-2649-2
- Hathi, D., Chanswangphuwana, C., Cho, N., Fontana, F., Maji, D., Ritchey, J., ... Shokeen, M. (2022, Januar). Ablation of VLA4 in multiple myeloma cells redirects tumor spread and prolongs survival. *Scientific Reports*, 12, 30. Zugriff auf <https://www.ncbi.nlm.nih.gov/pmc/articles/PMC8741970/> doi: 10.1038/s41598-021-03748-0
- Heinemann, L., Möllers, K. M., Ahmed, H. M. M., Wei, L., Sun, K., Nimmagadda, S. C., ... Khandanpour, C. (2022, Juni). Inhibiting PI3K–AKT–mTOR Signaling in Multiple Myeloma-Associated Mesenchymal Stem Cells Impedes the Proliferation of Multiple Myeloma Cells. *Frontiers in On-*

- cology, 12, 874325. Zugriff auf <https://www.ncbi.nlm.nih.gov/pmc/articles/PMC9251191/> doi: 10.3389/fonc.2022.874325
- Hiasa, M., Harada, T., Tanaka, E. & Abe, M. (2021, November). Pathogenesis and treatment of multiple myeloma bone disease. *Japanese Dental Science Review*, 57, 164–173. Zugriff auf <https://www.sciencedirect.com/science/article/pii/S1882761621000235> doi: 10.1016/j.jdsr.2021.08.006
- Hideshima, T., Mitsiades, C., Tonon, G., Richardson, P. G. & Anderson, K. C. (2007, August). Understanding multiple myeloma pathogenesis in the bone marrow to identify new therapeutic targets. *Nature Reviews Cancer*, 7 (8), 585–598. Zugriff auf <https://www.nature.com/articles/nrc2189> doi: 10.1038/nrc2189
- Hino, O. (2004, August). Studies of familial tumors using models: Genotype, phenotype, and dramatype in carcinogenesis. *International Journal of Clinical Oncology*, 9 (4), 257–261. Zugriff auf <https://doi.org/10.1007/s10147-004-0416-2> doi: 10.1007/s10147-004-0416-2
- Hoang, P. H., Cornish, A. J., Dobbins, S. E., Kaiser, M. & Houlston, R. S. (2019, August). Mutational processes contributing to the development of multiple myeloma. *Blood Cancer Journal*, 9 (8), 1–11. Zugriff auf <https://www.nature.com/articles/s41408-019-0221-9> doi: 10.1038/s41408-019-0221-9
- Hose, D., Rème, T., Hielscher, T., Moreaux, J., Messner, T., Seckinger, A., ... Goldschmidt, H. (2011, Januar). Proliferation is a central independent prognostic factor and target for personalized and risk-adapted treatment in multiple myeloma. *Haematologica*, 96 (1), 87–95. doi: 10.3324/haematol.2010.030296
- Hothorn, T. & Lausen, B. (2017). *Maximally Selected Rank Statistics in R*. Zugriff auf <https://rdrr.io/cran/maxstat/man/maxstat.test.html> doi: 10.32614/CRAN.package.maxstat
- Howe, A. & Chain, P. S. G. (2015). Challenges and opportunities in understanding microbial communities with metagenome assembly (accompanied by IPython Notebook tutorial). *Frontiers in Microbiology*, 6, 678. doi: 10.3389/fmicb.2015.00678
- Hu, Q., Wang, M., Wang, J., Tao, Y. & Niu, T. (2024). Development of a cell adhesion-based prognostic model for multiple myeloma: Insights into chemotherapy response and potential reversal of adhesion effects. *Oncology Research*, 32 (4), 753–768. Zugriff auf <https://www.techscience.com/or/v32n4/55760> doi: 10.32604/or.2023.043647
- Hu, X., Villodre, E. S., Larson, R., Rahal, O. M., Wang, X., Gong, Y., ... Debeb, B. G. (2021, Januar). Decorin-mediated suppression of tumorigenesis, invasion, and metastasis in inflammatory breast cancer. *Communications Biology*, 4 (1), 72. doi: 10.1038/s42003-020-01590-0
- Huang, S.-Y., Lin, H.-H., Yao, M., Tang, J.-L., Wu, S.-J., Hou, H.-A., ... Tien, H.-F. (2015). Higher Decorin Levels in Bone Marrow Plasma Are Associated with Superior Treatment Response to Novel Agent-Based Induction in Patients with Newly Diagnosed Myeloma - A Retrospective Study. *PloS One*, 10 (9), e0137552. doi: 10.1371/journal.pone.0137552
- Humphries, M. J. (2009). Cell adhesion assays. *Methods in Molecular Biology* (Clifton, N.J.), 522, 203–210. doi: 10.1007/978-1-59745-413-1_14
- Hunter, J. D. (2007, Mai). Matplotlib: A 2D Graphics Environment. *Computing in Science & Engineering*, 9 (3), 90–95. Zugriff auf <https://ieeexplore.ieee.org/document/4160265> doi: 10.1109/MCSE.2007.55
- Huth, J., Buchholz, M., Kraus, J. M., Schmucker, M., von Wichert, G., Krndija, D., ... Kestler, H. A. (2010, April). Significantly improved precision of cell migration analysis in time-lapse video microscopy through use of a fully automated tracking system. *BMC Cell Biology*, 11 (1), 24. Zugriff auf <https://doi.org/10.1186/1471-2121-11-24> doi: 10.1186/1471-2121-11-24
- Ibraheem, A., Attar-Schneider, O., Dabbah, M., Dolberg Jarchowsky, O., Tartakover Matalon, S., Lishner,

- M. & Drucker, L. (2019, Mai). BM-MSCs-derived ECM modifies multiple myeloma phenotype and drug response in a source-dependent manner. *Translational Research: The Journal of Laboratory and Clinical Medicine*, 207, 83–95. doi: 10.1016/j.trsl.2019.01.003
- Inaba, M. & Yamashita, Y. M. (2012, Oktober). Asymmetric Stem Cell Division: Precision for Robustness. *Cell Stem Cell*, 11 (4), 461–469. Zugriff auf <https://linkinghub.elsevier.com/retrieve/pii/S1934590912005401> doi: 10.1016/j.stem.2012.09.003
- Inc., P. T. (2015). *Collaborative data science*. Montreal, QC: Plotly Technologies Inc. Zugriff auf <https://plot.ly>
- Incerti, D., Thom, H., Baio, G. & Jansen, J. P. (2019, Mai). R You Still Using Excel? The Advantages of Modern Software Tools for Health Technology Assessment. *Value in Health*, 22 (5), 575–579. Zugriff auf <https://www.sciencedirect.com/science/article/pii/S1098301519300506> doi: 10.1016/j.jval.2019.01.003
- Ioannidis, J. P. A. (2005, August). Why Most Published Research Findings Are False. *PLOS Medicine*, 2 (8), e124. Zugriff auf <https://journals.plos.org/plosmedicine/article?id=10.1371/journal.pmed.0020124> doi: 10.1371/journal.pmed.0020124
- Iolascon, G., Liguori, S., Paoletta, M., Toro, G. & Moretti, A. (2023, Januar). Anti-sclerostin antibodies: A new frontier in fragility fractures treatment. *Therapeutic Advances in Musculoskeletal Disease*, 15, 1759720X231197094. Zugriff auf <https://doi.org/10.1177/1759720X231197094> doi: 10.1177/1759720X231197094
- Ito, S., Sato, T. & Maeta, T. (2021, April). Role and Therapeutic Targeting of SDF-1 α /CXCR4 Axis in Multiple Myeloma. *Cancers*, 13 (8), 1793. Zugriff auf <https://www.ncbi.nlm.nih.gov/pmc/articles/PMC8069569/> doi: 10.3390/cancers13081793
- Iyer, S. P., Beck, J. T., Stewart, A. K., Shah, J., Kelly, K. R., Isaacs, R., ... Munshi, N. C. (2014). A Phase IB multicentre dose-determination study of BHQ880 in combination with anti-myeloma therapy and zoledronic acid in patients with relapsed or refractory multiple myeloma and prior skeletal-related events. *British Journal of Haematology*, 167 (3), 366–375. Zugriff auf <https://onlinelibrary.wiley.com/doi/abs/10.1111/bjh.13056> doi: 10.1111/bjh.13056
- Jansen, B. J. H., Gilissen, C., Roelofs, H., Schaap-Oziemlak, A., Veltman, J. A., Raymakers, R. A. P., ... Adema, G. J. (2010, April). Functional differences between mesenchymal stem cell populations are reflected by their transcriptome. *Stem cells and development*, 19 (4), 481–490. doi: 10.1089/scd.2009.0288
- Johansen, M., Levring, M. B., Stokbro, K., Diaz-delCastillo, M., Khan, A. A., Wickstroem, L. A., ... Lund, T. (2023, Januar). Novel Developments in the Treatment of Multiple Myeloma-Associated Bone Disease. *Cancers*, 15 (23), 5585. Zugriff auf <https://www.mdpi.com/2072-6694/15/23/5585> doi: 10.3390/cancers15235585
- Johnsen, H. E., Bøgsted, M., Schmitz, A., Bødker, J. S., El-Galaly, T. C., Johansen, P., ... Dybkær, K. (2016, Dezember). The myeloma stem cell concept, revisited: From phenomenology to operational terms. *Haematologica*, 101 (12), 1451–1459. Zugriff auf <https://haematologica.org/article/view/7901> doi: 10.3324/haematol.2015.138826
- Jung, S.-H. & Lee, J.-J. (2022, April). Update on primary plasma cell leukemia. *Blood Research*, 57 (S1), 62–66. doi: 10.5045/br.2022.2022033
- Kaplan, E. L. & Meier, P. (1958, Juni). Nonparametric Estimation from Incomplete Observations. *Journal of the American Statistical Association*, 53 (282), 457–481. Zugriff auf <http://www.tandfonline.com/doi/abs/10.1080/01621459.1958.10501452> doi: 10.1080/01621459.1958.10501452
- Kashef, J. & Franz, C. M. (2015, Mai). Quantitative methods for analyzing cell-cell adhesion in de-

- velopment. *Developmental Biology*, 401 (1), 165–174. Zugriff auf <https://www.sciencedirect.com/science/article/pii/S001216061400579X> doi: 10.1016/j.ydbio.2014.11.002
- Kastritis, E., Moulopoulos, L. A., Terpos, E., Koutoulidis, V. & Dimopoulos, M. A. (2014, Dezember). The prognostic importance of the presence of more than one focal lesion in spine MRI of patients with asymptomatic (smoldering) multiple myeloma. *Leukemia*, 28 (12), 2402–2403. Zugriff auf <https://www.nature.com/articles/leu2014230> doi: 10.1038/leu.2014.230
- Katz, B.-Z. (2010, Juni). Adhesion molecules—The lifelines of multiple myeloma cells. *Seminars in Cancer Biology*, 20 (3), 186–195. Zugriff auf <https://linkinghub.elsevier.com/retrieve/pii/S1044579X10000246> doi: 10.1016/j.semcan.2010.04.003
- Kawano, M. M., Huang, N., Tanaka, H., Ishikawa, H., Sakai, A., Tanabe, O., ... Kuramoto, A. (1991). Homotypic cell aggregations of human myeloma cells with ICAM-1 and LFA-1 molecules. *British Journal of Haematology*, 79 (4), 583–588. Zugriff auf <https://onlinelibrary.wiley.com/doi/abs/10.1111/j.1365-2141.1991.tb08085.x> doi: 10.1111/j.1365-2141.1991.tb08085.x
- Kazman, R., Bianco, P., Ivers, J. & Klein, J. (2020, Dezember). *Maintainability* (Report). Carnegie Mellon University. Zugriff auf <https://kilthub.cmu.edu/articles/report/Maintainability/12954908/1> doi: 10.1184/R1/12954908.v1
- Keats, J. J., Chesi, M., Egan, J. B., Garbitt, V. M., Palmer, S. E., Braggio, E., ... Bergsagel, P. L. (2012, August). Clonal competition with alternating dominance in multiple myeloma. *Blood*, 120 (5), 1067–1076. doi: 10.1182/blood-2012-01-405985
- Kelleher, R. (2024, Januar). *NVIDIA CEO: ‘This Year, Every Industry Will Become a Technology Industry’*. Zugriff auf <https://blogs.nvidia.com/blog/nvidia-ceo-ai-drug-discovery-jp-morgan-healthcare-2024/>
- Kelly, B. S., Kirwan, A., Quinn, M. S., Kelly, A. M., Mathur, P., Lawlor, A. & Killeen, R. P. (2023, Mai). The ethical matrix as a method for involving people living with disease and the wider public (PPI) in near-term artificial intelligence research. *Radiography (London, England: 1995)*, 29 Suppl 1, S103-S111. doi: 10.1016/j.radi.2023.03.009
- Khalili, A. A. & Ahmad, M. R. (2015, August). A Review of Cell Adhesion Studies for Biomedical and Biological Applications. *International Journal of Molecular Sciences*, 16 (8), 18149. Zugriff auf <https://www.ncbi.nlm.nih.gov/pmc/articles/PMC4581240/> doi: 10.3390/ijms160818149
- Kibler, C., Schermutzki, F., Waller, H. D., Timpl, R., Müller, C. A. & Klein, G. (1998, Juni). Adhesive interactions of human multiple myeloma cell lines with different extracellular matrix molecules. *Cell Adhesion and Communication*, 5 (4), 307–323. doi: 10.3109/15419069809040300
- Kim, D., Langmead, B. & Salzberg, S. L. (2015, April). HISAT: A fast spliced aligner with low memory requirements. *Nature methods*, 12 (4), 357–360. Zugriff auf <https://www.ncbi.nlm.nih.gov/pmc/articles/PMC4655817/> doi: 10.1038/nmeth.3317
- Klausz, K., Cieker, M., Kellner, C., Oberg, H.-H., Kabelitz, D., Valerius, T., ... Peipp, M. (2017, September). A novel Fc-engineered human ICAM-1/CD54 antibody with potent anti-myeloma activity developed by cellular panning of phage display libraries. *Oncotarget*, 8 (44), 77552–77566. doi: 10.18632/oncotarget.20641
- Kluyver, T., Ragan-Kelley, B., Rez, F., Granger, B., Bussonnier, M., Frederic, J., ... Team, J. D. (2016). Jupyter Notebooks – a publishing format for reproducible computational workflows. In *Positioning and Power in Academic Publishing: Players, Agents and Agendas* (1. Aufl., S. 87–90). IOS Press. Zugriff auf <https://ebooks-iospress.nl/doi/10.3233/978-1-61499-649-1-87> doi: 10.3233/978-1-61499-649-1-87
- Krekel, H., Oliveira, B., Pfannschmidt, R., Bruynooghe, F., Laugher, B. & Bruhin, F. (2004). *Pytest*.

- Zugriff auf <https://github.com/pytest-dev/pytest>
- Krzywinski, M. & Savig, E. (2013, Juli). Multidimensional data. *Nature methods*, 10 (7), 595. Zugriff auf <https://www.ncbi.nlm.nih.gov/pmc/articles/PMC6092027/>
- Kumar, S. K. & Rajkumar, S. V. (2018, Juli). The multiple myelomas - current concepts in cytogenetic classification and therapy. *Nature Reviews. Clinical Oncology*, 15 (7), 409–421. doi: 10.1038/s41571-018-0018-y
- Kundu, S., Jha, S. B., Rivera, A. P., Flores Monar, G. V., Islam, H., Puttagunta, S. M., ... Sange, I. (2022, Februar). Multiple Myeloma and Renal Failure: Mechanisms, Diagnosis, and Management. *Cureus*, 14 (2), e22585. Zugriff auf <https://www.ncbi.nlm.nih.gov/pmc/articles/PMC8958144/> doi: 10.7759/cureus.22585
- Kuric, M. (2024, April). *Markur4/plotastic*. Zugriff auf <https://github.com/markur4/plotastic>
- Kuric, M., Beck, S., Schneider, D., Rindt, W., Evers, M., Meißner-Weigl, J., ... Ebert, R. (2024, April). Modeling Myeloma Dissemination In Vitro with hMSC-interacting Subpopulations of INA-6 Cells and Their Aggregation/Detachment Dynamics. *Cancer Research Communications*, 4 (4), 1150–1164. Zugriff auf <https://www.ncbi.nlm.nih.gov/pmc/articles/PMC11057410/> doi: 10.1158/2767-9764.CRC-23-0411
- Kuric, M. & Ebert, R. (2024, März). Plotastic: Bridging Plotting and Statistics in Python. *Journal of Open Source Software*, 9 (95), 6304. Zugriff auf <https://joss.theoj.org/papers/10.21105/joss.06304> doi: 10.21105/joss.06304
- Kyle, R. A. (1997, Februar). Monoclonal gammopathy of undetermined significance and solitary plasmacytoma. Implications for progression to overt multiple myeloma. *Hematology/Oncology Clinics of North America*, 11 (1), 71–87. doi: 10.1016/s0889-8588(05)70416-0
- Lai, T.-Y., Cao, J., Ou-Yang, P., Tsai, C.-Y., Lin, C.-W., Chen, C.-C., ... Lee, C.-Y. (2022, April). Different methods of detaching adherent cells and their effects on the cell surface expression of Fas receptor and Fas ligand. *Scientific Reports*, 12 (1), 5713. Zugriff auf <https://www.nature.com/articles/s41598-022-09605-y> doi: 10.1038/s41598-022-09605-y
- Lakhliifi, C., Lejeune, F.-X., Rouault, M., Khamassi, M. & Rohaut, B. (2023, April). Illusion of knowledge in statistics among clinicians: Evaluating the alignment between objective accuracy and subjective confidence, an online survey. *Cognitive Research: Principles and Implications*, 8, 23. Zugriff auf <https://www.ncbi.nlm.nih.gov/pmc/articles/PMC10118231/> doi: 10.1186/s41235-023-00474-1
- Landowski, T. H., Olashaw, N. E., Agrawal, D. & Dalton, W. S. (2003, April). Cell adhesion-mediated drug resistance (CAM-DR) is associated with activation of NF- κ B (RelB/p50) in myeloma cells. *Oncogene*, 22 (16), 2417–2421. Zugriff auf <https://www.nature.com/articles/1206315> doi: 10.1038/sj.onc.1206315
- Lee, J. Y. & Hong, S.-H. (2019, Dezember). Hematopoietic Stem Cells and Their Roles in Tissue Regeneration. *International Journal of Stem Cells*, 13 (1), 1–12. Zugriff auf <https://www.ncbi.nlm.nih.gov/pmc/articles/PMC7119209/> doi: 10.15283/ijsc19127
- Leek, J. T. & Peng, R. D. (2015, April). Statistics: P values are just the tip of the iceberg. *Nature*, 520 (7549), 612–612. Zugriff auf <https://www.nature.com/articles/520612a> doi: 10.1038/520612a
- Lentzsch, S., Gries, M., Janz, M., Bargou, R., Dörken, B. & Mapara, M. Y. (2003, Mai). Macrophage inflammatory protein 1-alpha (MIP-1 alpha) triggers migration and signaling cascades mediating survival and proliferation in multiple myeloma (MM) cells. *Blood*, 101 (9), 3568–3573. doi: 10.1182/blood-2002-08-2383
- Li, H., Handsaker, B., Wysoker, A., Fennell, T., Ruan, J., Homer, N., ... 1000 Genome Project Data Processing Subgroup (2009, August). The Sequence Alignment/Map format and SAMtools. *Bioin-*

- formatics*, 25 (16), 2078–2079. Zugriff auf <https://doi.org/10.1093/bioinformatics/btp352> doi: 10.1093/bioinformatics/btp352
- Li, Z., Zhang, Y. Y., Zhang, H., Yang, J., Chen, Y. & Lu, H. (2022, Juli). Asymmetric Cell Division and Tumor Heterogeneity. *Frontiers in Cell and Developmental Biology*, 10. Zugriff auf <https://www.frontiersin.org/journals/cell-and-developmental-biology/articles/10.3389/fcell.2022.938685/full> doi: 10.3389/fcell.2022.938685
- Liu, Z., Liu, H., He, J., Lin, P., Tong, Q. & Yang, J. (2020, Mai). Myeloma cells shift osteoblastogenesis to adipogenesis by inhibiting the ubiquitin ligase MURF1 in mesenchymal stem cells. *Science signaling*, 13 (633), eaay8203. Zugriff auf <https://www.ncbi.nlm.nih.gov/pmc/articles/PMC7376968/> doi: 10.1126/scisignal.aay8203
- Localio, A. R., Goodman, S. N., Meibohm, A., Cornell, J. E., Stack, C. B., Ross, E. A. & Mulrow, C. D. (2018, Juni). Statistical Code to Support the Scientific Story. *Annals of Internal Medicine*, 168 (11), 828–829. Zugriff auf <https://www.acpjournals.org/doi/10.7326/M17-3431> doi: 10.7326/M17-3431
- Long, H. S., Greenaway, S., Powell, G., Mallon, A.-M., Lindgren, C. M. & Simon, M. M. (2022, Januar). Making sense of the linear genome, gene function and TADs. *Epigenetics & Chromatin*, 15 (1), 4. Zugriff auf <https://doi.org/10.1186/s13072-022-00436-9> doi: 10.1186/s13072-022-00436-9
- Love, M. I., Huber, W. & Anders, S. (2014, Dezember). Moderated estimation of fold change and dispersion for RNA-seq data with DESeq2. *Genome Biology*, 15 (12), 550. Zugriff auf <https://doi.org/10.1186/s13059-014-0550-8> doi: 10.1186/s13059-014-0550-8
- Mai, E. K., Hielscher, T., Kloth, J. K., Merz, M., Shah, S., Raab, M. S., ... Hillengass, J. (2015, Juni). A magnetic resonance imaging-based prognostic scoring system to predict outcome in transplant-eligible patients with multiple myeloma. *Haematologica*, 100 (6), 818–825. Zugriff auf <https://www.ncbi.nlm.nih.gov/pmc/articles/PMC4450628/> doi: 10.3324/haematol.2015.124115
- Maichl, D. S., Kirner, J. A., Beck, S., Cheng, W.-H., Krug, M., Kuric, M., ... Jundt, F. (2023, September). Identification of NOTCH-driven matrisome-associated genes as prognostic indicators of multiple myeloma patient survival. *Blood Cancer Journal*, 13 (1), 1–6. Zugriff auf <https://www.nature.com/articles/s41408-023-00907-6> doi: 10.1038/s41408-023-00907-6
- Majithia, N., Rajkumar, SV., Lacy, MQ., Buadi, FK., Dispenzieri, A., Gertz, MA., ... Kumar, SK. (2016, November). Early relapse following initial therapy for multiple myeloma predicts poor outcomes in the era of novel agents. *Leukemia*, 30 (11), 2208–2213. Zugriff auf <https://www.ncbi.nlm.nih.gov/pmc/articles/PMC5541860/> doi: 10.1038/leu.2016.147
- Mangolini, M. & Ringshausen, I. (2020, Februar). Bone Marrow Stromal Cells Drive Key Hallmarks of B Cell Malignancies. *International Journal of Molecular Sciences*, 21 (4), 1466. Zugriff auf <https://www.ncbi.nlm.nih.gov/pmc/articles/PMC7073037/> doi: 10.3390/ijms21041466
- Martin, S. K., Diamond, P., Williams, S. A., To, L. B., Peet, D. J., Fujii, N., ... Zannettino, A. C. W. (2010, Mai). Hypoxia-inducible factor-2 is a novel regulator of aberrant CXCL12 expression in multiple myeloma plasma cells. *Haematologica*, 95 (5), 776–784. doi: 10.3324/haematol.2009.015628
- Mateos María-Victoria, Hernández Miguel-Teodoro, Giraldo Pilar, de la Rubia Javier, de Arriba Felipe, Corral Lucía López, ... San Miguel Jesús-F. (2013). Lenalidomide plus Dexamethasone for High-Risk Smoldering Multiple Myeloma. *New England Journal of Medicine*, 369 (5), 438–447. Zugriff auf <https://www.nejm.org/doi/full/10.1056/NEJMoa1300439> doi: 10.1056/NEJMoa1300439
- Mättig, P. (2022, November). Classifying exploratory experimentation – three case studies of exploratory experimentation at the LHC. *European Journal for Philosophy of Science*, 12 (4), 66. Zugriff auf <https://doi.org/10.1007/s13194-022-00496-4> doi: 10.1007/s13194-022-00496-4
- McCall, M. N., McMurray, H. R., Land, H. & Almudevar, A. (2014, August). On non-detects in qPCR

- data. *Bioinformatics*, 30 (16), 2310–2316. Zugriff auf <https://www.ncbi.nlm.nih.gov/pmc/articles/PMC4133581/> doi: 10.1093/bioinformatics/btu239
- McDonald, M. M., Reagan, M. R., Youlten, S. E., Mohanty, S. T., Seckinger, A., Terry, R. L., ... Croucher, P. I. (2017, Juni). Inhibiting the osteocyte-specific protein sclerostin increases bone mass and fracture resistance in multiple myeloma. *Blood*, 129 (26), 3452–3464. doi: 10.1182/blood-2017-03-773341
- McKay, B. S., Irving, P. E., Skumatz, C. M. & Burke, J. M. (1997, November). Cell-cell adhesion molecules and the development of an epithelial phenotype in cultured human retinal pigment epithelial cells. *Experimental Eye Research*, 65 (5), 661–671. doi: 10.1006/exer.1997.0374
- McKinney, W. (2010). Data Structures for Statistical Computing in Python. In S. van der Walt & J. Millman (Hrsg.), *Proceedings of the 9th Python in Science Conference* (S. 56–61). Austin, Texas. doi: 10.25080/Majora-92bf1922-00a
- Mckinney, W. (2011, Januar). Pandas: A Foundational Python Library for Data Analysis and Statistics. *Python High Performance Science Computer*. Zugriff auf https://www.researchgate.net/publication/265194455_pandas_a_Foundational_Python_Library_for_Data_Analysis_and_Statistics
- Mesirov, J. P. (2010, Januar). Accessible Reproducible Research. *Science*, 327 (5964), 415–416. Zugriff auf <https://www.science.org/doi/10.1126/science.1179653> doi: 10.1126/science.1179653
- Moleiro, A. F., Conceição, G., Leite-Moreira, A. F. & Rocha-Sousa, A. (2017). A Critical Analysis of the Available In Vitro and Ex Vivo Methods to Study Retinal Angiogenesis. *Journal of Ophthalmology*, 2017, 3034953. doi: 10.1155/2017/3034953
- Moñivas Gallego, E. & Zurita Castillo, M. (2024, April). Mesenchymal stem cell therapy in ischemic stroke trials. A systematic review. *Regenerative Therapy*, 27, 301–306. Zugriff auf <https://www.ncbi.nlm.nih.gov/pmc/articles/PMC11021793/> doi: 10.1016/j.reth.2024.03.026
- Monster, J. L., Kemp, L. J., Busslinger, G. A., Vliem, M. J., Derkx, L. L., Staes, A. A., ... Gloerich, M. (2024, Juni). Cell division-dependent dissemination following E-cadherin loss underlies initiation of diffuse-type gastric cancer. *The Journal of Pathology*, 263 (2), 226–241. doi: 10.1002/path.6277
- Moran, M. (2003). Arguments for rejecting the sequential Bonferroni in ecological studies. *Oikos*, 100 (2), 403–405. Zugriff auf <https://onlinelibrary.wiley.com/doi/abs/10.1034/j.1600-0706.2003.12010.x> doi: 10.1034/j.1600-0706.2003.12010.x
- Morrison, S. J. & Spradling, A. C. (2008, Februar). Stem Cells and Niches: Mechanisms That Promote Stem Cell Maintenance throughout Life. *Cell*, 132 (4), 598–611. Zugriff auf [https://www.cell.com/cell/abstract/S0092-8674\(08\)00139-6](https://www.cell.com/cell/abstract/S0092-8674(08)00139-6) doi: 10.1016/j.cell.2008.01.038
- Motulsky, H. (2017). *Intuitive Biostatistics: A Nonmathematical Guide to Statistical Thinking* (4. Aufl.). New York: Oxford University Press.
- Mrozik, K. M., Cheong, C. M., Hewett, D., Chow, A. W., Blaschuk, O. W., Zannettino, A. C. & Vandyke, K. (2015). Therapeutic targeting of N-cadherin is an effective treatment for multiple myeloma. *British Journal of Haematology*, 171 (3), 387–399. Zugriff auf <https://onlinelibrary.wiley.com/doi/abs/10.1111/bjh.13596> doi: 10.1111/bjh.13596
- Muruganandan, S., Roman, A. A. & Sinal, C. J. (2009, Januar). Adipocyte differentiation of bone marrow-derived mesenchymal stem cells: Cross talk with the osteoblastogenic program. *Cellular and molecular life sciences : CMLS*, 66 (2), 236–253. doi: 10.1007/s00018-008-8429-z
- Myers, G. J., Sandler, C. & Badgett, T. (2011). *The art of software testing* (3rd Aufl.). Wiley Publishing. Zugriff auf <https://malenezi.github.io/malenezi/SE401/Books/114-the-art-of-software-testing-3-edition.pdf>
- Nair, R. R., Gebhard, A. W., Emmons, M. F. & Hazlehurst, L. A. (2012, Januar). Chapter Six - Emerging

- Strategies for Targeting Cell Adhesion in Multiple Myeloma. In K. S. M. Smalley (Hrsg.), *Advances in Pharmacology* (Bd. 65, S. 143–189). Academic Press. Zugriff auf <https://www.sciencedirect.com/science/article/pii/B9780123979278000063> doi: 10.1016/B978-0-12-397927-8.00006-3
- Nakamura, S., Maruyama, A., Kondo, Y., Kano, A., De Sousa, O. M., Iwahashi, M., ... Ohnuma, K. (2018, März). Asymmetry Between Sister Cells of Pluripotent Stem Cells at the Onset of Differentiation. *Stem Cells and Development*, 27 (5), 347–354. Zugriff auf <https://www.ncbi.nlm.nih.gov/pmc/articles/PMC5833898/> doi: 10.1089/scd.2017.0113
- Nalbant, P. & Dehmelt, L. (2018, August). Exploratory cell dynamics: A sense of touch for cells? *Biological Chemistry*, 399 (8), 809–819. Zugriff auf [https://www.degruyter.com/document/doi/10.1515/hsz-2017-0341](https://www.degruyter.com/document/doi/10.1515/hsz-2017-0341/html) doi: 10.1515/hsz-2017-0341
- Nature Video Content.* (o.J.). Zugriff auf <https://support.nature.com/en/support/solutions/articles/6000210836-requirements-to-play-video-content-on-the-site>
- Neri, P. & Bahlis, N. J. (2012, August). Targeting of Adhesion Molecules as a Therapeutic Strategy in Multiple Myeloma. *Current Cancer Drug Targets*, 12 (7), 776–796. Zugriff auf <http://www.eurekaselect.com/openurl/content.php?genre=article&issn=1568-0096&volume=12&issue=7&spage=776> doi: 10.2174/156800912802429337
- Newville, M., Stensitzki, T., Allen, D. B. & Ingargiola, A. (2014, September). *LMFIT: Non-Linear Least-Square Minimization and Curve-Fitting for Python*. Zenodo. Zugriff auf <https://zenodo.org/record/11813> doi: 10.5281/zenodo.11813
- Ngomdir, L., Bharathwaj, V. V., Nimmy, P., Sindhu, R., Dhamodhar, D., Sathiyapriya, S., ... RajMohan, M. (2023, Juli). Therapeutic Use of Anti-Sclerostin Antibody in the Treatment of Multiple Myeloma: A Systematic Review. *Journal of Pharmacy & Bioallied Sciences*, 15 (Suppl 1), S738-S741. Zugriff auf <https://www.ncbi.nlm.nih.gov/pmc/articles/PMC10466553/> doi: 10.4103/jpbs.jpbs_560_22
- Niehorster, D. C. (2021, Dezember). Optic Flow: A History. *i-Perception*, 12 (6), 20416695211055766. Zugriff auf <https://www.ncbi.nlm.nih.gov/pmc/articles/PMC8652193/> doi: 10.1177/20416695211055766
- Nilsson, K., Bennich, H., Johansson, S. G. & Pontén, J. (1970, Oktober). Established immunoglobulin producing myeloma (IgE) and lymphoblastoid (IgG) cell lines from an IgE myeloma patient. *Clinical and Experimental Immunology*, 7 (4), 477–489.
- Nitta, C. F., Pierce, M., Elia, J., Ruiz, J., Hipol, A.-D., Fong, N., ... Chan, L. L.-Y. (2023, Oktober). A rapid and high-throughput T cell immunophenotyping assay for cellular therapy bioprocess using the Cellaca® PLX image cytometer. *Journal of Immunological Methods*, 521, 113538. doi: 10.1016/j.jim.2023.113538
- Nowotschin, S. & Hadjantonakis, A.-K. (2010, August). Cellular dynamics in the early mouse embryo: From axis formation to gastrulation. *Current opinion in genetics & development*, 20 (4), 420–427. doi: 10.1016/j.gde.2010.05.008
- Nunes, J. & Loeffler, D. (2024, März). Asymmetric Cell Division of Hematopoietic Stem Cells: Recent Advances, Emerging Concepts, and Future Perspectives. *Frontiers in Hematology*, 3. Zugriff auf <https://www.frontiersin.org/journals/hematology/articles/10.3389/frhem.2024.1373554/full> doi: 10.3389/frhem.2024.1373554
- Oba, Y., Lee, J. W., Ehrlich, L. A., Chung, H. Y., Jelinek, D. F., Callander, N. S., ... Roodman, G. D. (2005, März). MIP-1alpha utilizes both CCR1 and CCR5 to induce osteoclast formation and increase adhesion of myeloma cells to marrow stromal cells. *Experimental Hematology*, 33 (3), 272–278. doi: 10.1016/j.exphem.2004.11.015
- Ocias, L. F., Larsen, T. S., Vestergaard, H., Friis, L. S., Abildgaard, N., Frederiksen, H. & Academy of Geriatric Cancer Research (AgeCare). (2016). Trends in hematological cancer in the elderly in

- Denmark, 1980-2012. *Acta Oncologica (Stockholm, Sweden)*, 55 Suppl 1, 98–107. doi: 10.3109/0284186X .2015.1115124
- O'Connor, B. P., Raman, V. S., Erickson, L. D., Cook, W. J., Weaver, L. K., Ahonen, C., ... Noelle, R. J. (2004, Januar). BCMA Is Essential for the Survival of Long-lived Bone Marrow Plasma Cells. *The Journal of Experimental Medicine*, 199 (1), 91–98. Zugriff auf <https://www.ncbi.nlm.nih.gov/pmc/articles/PMC1887725/> doi: 10.1084/jem.20031330
- Okuno, Y., Takahashi, T., Suzuki, A., Ichiba, S., Nakamura, K., Okada, T., ... Imura, H. (1991, Februar). In vitro growth pattern of myeloma cells in liquid suspension or semi-solid culture containing interleukin-6. *International Journal of Hematology*, 54 (1), 41–47.
- Openai/gpt-2. (2024, Juli). OpenAI. Zugriff auf <https://github.com/openai/gpt-2>
- Ordak, M. (2023, September). ChatGPT's Skills in Statistical Analysis Using the Example of Allergology: Do We Have Reason for Concern? *Healthcare (Basel, Switzerland)*, 11 (18), 2554. doi: 10.3390/healthcare11182554
- Paiva, B., Paino, T., Sayagues, J.-M., Garayoa, M., San-Segundo, L., Martín, M., ... San Miguel, J. F. (2013, November). Detailed characterization of multiple myeloma circulating tumor cells shows unique phenotypic, cytogenetic, functional, and circadian distribution profile. *Blood*, 122 (22), 3591–3598. doi: 10.1182/blood-2013-06-510453
- Paiva, B., Pérez-Andrés, M., Vídriales, M.-B., Almeida, J., de las Heras, N., Mateos, M.-V., ... Myeloma Stem Cell Network (MSCNET) (2011, April). Competition between clonal plasma cells and normal cells for potentially overlapping bone marrow niches is associated with a progressively altered cellular distribution in MGUS vs myeloma. *Leukemia*, 25 (4), 697–706. doi: 10.1038/leu.2010.320
- Paszke, A., Gross, S., Massa, F., Lerer, A., Bradbury, J., Chanan, G., ... Chintala, S. (2019, Dezember). PyTorch: An Imperative Style, High-Performance Deep Learning Library (Nr. arXiv:1912.01703). arXiv. Zugriff auf <http://arxiv.org/abs/1912.01703> doi: 10.48550/arXiv.1912.01703
- Pattarone, G., Acion, L., Simian, M., Mertelsmann, R., Follo, M. & Iarussi, E. (2021, Mai). Learning deep features for dead and living breast cancer cell classification without staining. *Scientific Reports*, 11, 10304. Zugriff auf <https://www.ncbi.nlm.nih.gov/pmc/articles/PMC8119670/> doi: 10.1038/s41598-021-89895-w
- Peng, R. D. (2011, Dezember). Reproducible Research in Computational Science. *Science*, 334 (6060), 1226–1227. Zugriff auf <https://www.science.org/doi/10.1126/science.1213847> doi: 10.1126/science.1213847
- Peras, I., Klemenčič Mirazchiyski, E., Japelj Pavešić, B. & Mekiš Recek, Ž. (2023, September). Digital versus Paper Reading: A Systematic Literature Review on Contemporary Gaps According to Gender, Socioeconomic Status, and Rurality. *European Journal of Investigation in Health, Psychology and Education*, 13 (10), 1986–2005. Zugriff auf <https://www.ncbi.nlm.nih.gov/pmc/articles/PMC10606230/> doi: 10.3390/ejihpe13100142
- Perez, F. & Granger, B. E. (2007, Mai). IPython: A System for Interactive Scientific Computing. *Computing in Science & Engineering*, 9 (3), 21–29. Zugriff auf <https://ieeexplore.ieee.org/document/4160251> doi: 10.1109/MCSE.2007.53
- Pérez-Andrés, M., Almeida, J., Martín-Ayuso, M., Moro, M. J., Martín-Nuñez, G., Galende, J., ... Spanish Network of Cancer Research Centers (C03/10) (2005, März). Clonal plasma cells from monoclonal gammopathy of undetermined significance, multiple myeloma and plasma cell leukemia show different expression profiles of molecules involved in the interaction with the immunological bone marrow microenvironment. *Leukemia*, 19 (3), 449–455. doi: 10.1038/sj.leu.2403647
- Perneger, T. V. (1998, April). What's wrong with Bonferroni adjustments. *BMJ : British Medical Journal*,

- 316 (7139), 1236–1238. Zugriff auf <https://www.ncbi.nlm.nih.gov/pmc/articles/PMC1112991/>
- Pfaffl, M. W. (2001, Mai). A new mathematical model for relative quantification in real-time RT-PCR. *Nucleic Acids Research*, 29 (9), e45. Zugriff auf <https://www.ncbi.nlm.nih.gov/pmc/articles/PMC55695/>
- Pichler, J., Narzt, W., Pirklbauer, K. & Zwinz, M. (1998, August). A reusability concept for process automation software. In *11th International Conference on Software Engineering and its Applications (ICSEA)*. Paris, France. Zugriff auf https://www.researchgate.net/publication/2537098_A_Reusability_Concept_for_Process_Automation_Software
- Pittenger, M. F., Mackay, A. M., Beck, S. C., Jaiswal, R. K., Douglas, R., Mosca, J. D., ... Marshak, D. R. (1999, April). Multilineage Potential of Adult Human Mesenchymal Stem Cells. *Science*, 284 (5411), 143–147. Zugriff auf <https://www.science.org/doi/10.1126/science.284.5411.143> doi: 10.1126/science.284.5411.143
- Podar, K. & Leleu, X. (2021, Oktober). Relapsed/Refractory Multiple Myeloma in 2020/2021 and Beyond. *Cancers*, 13 (20), 5154. Zugriff auf <https://www.ncbi.nlm.nih.gov/pmc/articles/PMC8534171/> doi: 10.3390/cancers13205154
- Polager, S. & Ginsberg, D. (2009, Oktober). P53 and E2f: Partners in life and death. *Nature Reviews Cancer*, 9 (10), 738–748. Zugriff auf <https://www.nature.com/articles/nrc2718> doi: 10.1038/nrc2718
- Potere, N., Buono, M. G. D., Niccoli, G., Crea, F., Toldo, S. & Abbate, A. (2019, Februar). Developing LRP1 Agonists into a Therapeutic Strategy in Acute Myocardial Infarction. *International Journal of Molecular Sciences*, 20 (3). Zugriff auf <https://www.ncbi.nlm.nih.gov/pmc/articles/PMC6387161/> doi: 10.3390/ijms20030544
- Price, A., Schroter, S., Clarke, M. & McAneney, H. (2018, September). Role of supplementary material in biomedical journal articles: Surveys of authors, reviewers and readers. *BMJ Open*, 8 (9), e021753. Zugriff auf <https://www.ncbi.nlm.nih.gov/pmc/articles/PMC6157527/> doi: 10.1136/bmjopen-2018-021753
- Purschke, M., Rubio, N., Held, K. D. & Redmond, R. W. (2010, November). Phototoxicity of Hoechst 33342 in time-lapse fluorescence microscopy. *Photochemical & Photobiological Sciences*, 9 (12), 1634–1639. Zugriff auf <https://pubs.rsc.org/en/content/articlelanding/2010/pp/c0pp00234h> doi: 10.1039/C0PP00234H
- Pushparaj, P. N. (2020). Revisiting the Micropipetting Techniques in Biomedical Sciences: A Fundamental Prerequisite in Good Laboratory Practice. *Bioinformation*, 16 (1), 8. Zugriff auf <https://www.ncbi.nlm.nih.gov/pmc/articles/PMC6986936/> doi: 10.6026/97320630016008
- Pylvänäinen, J. W., Gómez-de-Mariscal, E., Henriques, R. & Jacquemet, G. (2023, Dezember). Live-cell imaging in the deep learning era. *Current Opinion in Cell Biology*, 85, 102271. Zugriff auf <https://www.sciencedirect.com/science/article/pii/S0955067423001205> doi: 10.1016/j.ceb.2023.102271
- The Python Language Reference. (2024). Zugriff auf <https://docs.python.org/3/reference/index.html>
- Qamar, S., Öberg, R., Malyshev, D. & Andersson, M. (2023, Oktober). A hybrid CNN-Random Forest algorithm for bacterial spore segmentation and classification in TEM images. *Scientific Reports*, 13 (1), 18758. Zugriff auf <https://www.nature.com/articles/s41598-023-44212-5> doi: 10.1038/s41598-023-44212-5
- Qian, X., Yang, Y., Deng, Y., Liu, Y., Zhou, Y., Han, F., ... Yuan, H. (2023, April). SETDB1 induces lenalidomide resistance in multiple myeloma cells via epithelial-mesenchymal transition and PI3K/AKT pathway activation. *Experimental and Therapeutic Medicine*, 25 (6), 274. Zugriff auf <https://www.ncbi.nlm.nih.gov/pmc/articles/PMC10189757/> doi: 10.3892/etm.2023.11973
- Qiang, Y.-W., Barlogie, B., Rudikoff, S. & Shaughnessy, J. D. (2008, April). Dkk1-induced inhibition of

- Wnt signaling in osteoblast differentiation is an underlying mechanism of bone loss in multiple myeloma. *Bone*, 42 (4), 669–680. doi: 10.1016/j.bone.2007.12.006
- Quanbeck, A., Hennessy, R. G. & Park, L. (2022, November). Applying concepts from "rapid and agile implementation to advance implementation research. *Implementation Science Communications*, 3 (1), 118. doi: 10.1186/s43058-022-00366-3
- Qureshi, R., Shaughnessy, D., Gill, K. A. R., Robinson, K. A., Li, T. & Agai, E. (2023, April). Are ChatGPT and large language models "the answer" to bringing us closer to systematic review automation? *Systematic Reviews*, 12, 72. Zugriff auf <https://www.ncbi.nlm.nih.gov/pmc/articles/PMC10148473/> doi: 10.1186/s13643-023-02243-z
- R Core Team. (2018). *R: A language and environment for statistical computing* [Manual]. Vienna, Austria. Zugriff auf <https://www.R-project.org/>
- Rafopoulos, H., Laadem, A., Hesketh, P. J., Goldschmidt, J., Gabrail, N., Osborne, C., ... Crawford, J. (2016, April). Sotatercept (ACE-011) for the treatment of chemotherapy-induced anemia in patients with metastatic breast cancer or advanced or metastatic solid tumors treated with platinum-based chemotherapeutic regimens: Results from two phase 2 studies. *Supportive Care in Cancer*, 24 (4), 1517–1525. Zugriff auf <https://doi.org/10.1007/s00520-015-2929-9> doi: 10.1007/s00520-015-2929-9
- Raje, N., Terpos, E., Willenbacher, W., Shimizu, K., García-Sanz, R., Durie, B., ... Roodman, G. D. (2018, März). Denosumab versus zoledronic acid in bone disease treatment of newly diagnosed multiple myeloma: An international, double-blind, double-dummy, randomised, controlled, phase 3 study. *The Lancet Oncology*, 19 (3), 370–381. Zugriff auf [https://www.thelancet.com/journals/lanonc/article/PIIS1470-2045\(18\)30072-X/abstract](https://www.thelancet.com/journals/lanonc/article/PIIS1470-2045(18)30072-X/abstract) doi: 10.1016/S1470-2045(18)30072-X
- Rajkumar, S. V., Dimopoulos, M. A., Palumbo, A., Blade, J., Merlini, G., Mateos, M.-V., ... Miguel, J. F. S. (2014, November). International Myeloma Working Group updated criteria for the diagnosis of multiple myeloma. *The Lancet. Oncology*, 15 (12), e538–548. doi: 10.1016/S1470-2045(14)70442-5
- Rajkumar, S. V. & Kumar, S. (2020, September). Multiple myeloma current treatment algorithms. *Blood Cancer Journal*, 10 (9), 94. Zugriff auf <https://www.ncbi.nlm.nih.gov/pmc/articles/PMC7523011/> doi: 10.1038/s41408-020-00359-2
- Ramakers, C., Ruijter, J. M., Deprez, R. H. & Moorman, A. F. (2003, März). Assumption-free analysis of quantitative real-time polymerase chain reaction (PCR) data. *Neuroscience Letters*, 339 (1), 62–66. Zugriff auf <https://linkinghub.elsevier.com/retrieve/pii/S0304394002014234> doi: 10.1016/S0304-3940(02)01423-4
- Rayhan, A. & Gross, D. (2023). *The Rise of Python: A Survey of Recent Research*. doi: 10.13140/RG.2.2.27388.92809
- Read the Docs.* (2024). Zugriff auf <https://docs.readthedocs.io/en/stable/index.html>
- Rebl, H., Finke, B., Schroeder, K. & Nebe, J. B. (2010, Oktober). Time-dependent metabolic activity and adhesion of human osteoblast-like cells on sensor chips with a plasma polymer nanolayer. *The International Journal of Artificial Organs*, 33 (10), 738–748.
- Reyes, C. D. & García, A. J. (2003, Oktober). A centrifugation cell adhesion assay for high-throughput screening of biomaterial surfaces. *Journal of Biomedical Materials Research Part A*, 67A (1), 328–333. Zugriff auf <https://onlinelibrary.wiley.com/doi/10.1002/jbm.a.10122> doi: 10.1002/jbm.a.10122
- Ribatti, D., Tamia, R. & Annese, T. (2020, Juni). Epithelial-Mesenchymal Transition in Cancer: A Historical Overview. *Translational Oncology*, 13 (6), 100773. doi: 10.1016/j.tranon.2020.100773
- Richardson, G., Knudby, A., Chen, W., Sawada, M., Lovitt, J., He, L. & Naeni, L. Y. (2023, November). Dense neural network outperforms other machine learning models for scaling-up lichen cover maps in Eastern Canada. *PLOS ONE*, 18 (11), e0292839. Zugriff auf <https://www.ncbi.nlm.nih.gov/pmc/>

- articles/PMC10659193/ doi: 10.1371/journal.pone.0292839
- Rigsby, R. E. & Parker, A. B. (2016, September). Using the PyMOL application to reinforce visual understanding of protein structure. *Biochemistry and Molecular Biology Education: A Bimonthly Publication of the International Union of Biochemistry and Molecular Biology*, 44 (5), 433–437. doi: 10.1002/bmb.20966
- Robey, P. (2017, April). “Mesenchymal stem cells”: Fact or fiction, and implications in their therapeutic use. *F1000Research*, 6, F1000 Faculty Rev-524. Zugriff auf <https://www.ncbi.nlm.nih.gov/pmc/articles/PMC5399967/> doi: 10.12688/f1000research.10955.1
- Robinson, M. D., McCarthy, D. J. & Smyth, G. K. (2010, Januar). edgeR: A Bioconductor package for differential expression analysis of digital gene expression data. *Bioinformatics (Oxford, England)*, 26 (1), 139–140. Zugriff auf <https://www.ncbi.nlm.nih.gov/pubmed/19910308> doi: 10.1093/bioinformatics/btp616
- Robitaille, M. C., Byers, J. M., Christodoulides, J. A. & Raphael, M. P. (2022, November). Self-supervised machine learning for live cell imagery segmentation. *Communications Biology*, 5 (1), 1–8. Zugriff auf <https://www.nature.com/articles/s42003-022-04117-x> doi: 10.1038/s42003-022-04117-x
- Roccaro, A. M., Mishima, Y., Sacco, A., Moschetta, M., Tai, Y.-T., Shi, J., ... Ghobrial, I. M. (2015, Juli). CXCR4 Regulates Extra-Medullary Myeloma through Epithelial-Mesenchymal-Transition-like Transcriptional Activation. *Cell Reports*, 12 (4), 622–635. doi: 10.1016/j.celrep.2015.06.059
- Roukos, V., Pegoraro, G., Voss, T. C. & Misteli, T. (2015, Februar). Cell cycle staging of individual cells by fluorescence microscopy. *Nature protocols*, 10 (2), 334–348. Zugriff auf <https://www.ncbi.nlm.nih.gov/pmc/articles/PMC6318798/> doi: 10.1038/nprot.2015.016
- Roy, P., Mukherjee, T., Chatterjee, B., Vijayaragavan, B., Banoth, B. & Basak, S. (2017, März). Non-canonical NF κ B mutations reinforce pro-survival TNF response in multiple myeloma through an autoregulatory RelB:p50 NF κ B pathway. *Oncogene*, 36 (10), 1417–1429. Zugriff auf <https://www.nature.com/articles/onc2016309> doi: 10.1038/onc.2016.309
- Roy, P., Sarkar, U. & Basak, S. (2018, Mai). The NF- κ B Activating Pathways in Multiple Myeloma. *Biomedicines*, 6 (2), 59. Zugriff auf <http://www.mdpi.com/2227-9059/6/2/59> doi: 10.3390/biomedicines6020059
- Ruan, Y., Kim, H. N., Ogana, H. A., Gang, E. J., Li, S., Liu, H.-C., ... Kim, Y.-M. (2022, Januar). In vitro and in vivo effects of AVA4746, a novel competitive antagonist of the ligand binding of VLA-4, in B-cell acute lymphoblastic leukemia. *Experimental and Therapeutic Medicine*, 23 (1), 47. doi: 10.3892/etm.2021.10969
- Rueden, C. T., Schindelin, J., Hiner, M. C., DeZonia, B. E., Walter, A. E., Arena, E. T. & Eliceiri, K. W. (2017, November). ImageJ2: ImageJ for the next generation of scientific image data. *BMC Bioinformatics*, 18 (1), 529. Zugriff auf <https://doi.org/10.1186/s12859-017-1934-z> doi: 10.1186/s12859-017-1934-z
- Ruijter, J. M., Barnewall, R. J., Marsh, I. B., Szentirmay, A. N., Quinn, J. C., van Houdt, R., ... van den Hoff, M. J. B. (2021, Juni). Efficiency Correction Is Required for Accurate Quantitative PCR Analysis and Reporting. *Clinical Chemistry*, 67 (6), 829–842. Zugriff auf <https://doi.org/10.1093/clinchem/hvab052> doi: 10.1093/clinchem/hvab052
- Ruiz-Villalba, A., Ruijter, J. M. & van den Hoff, M. J. B. (2021, Mai). Use and Misuse of Cq in qPCR Data Analysis and Reporting. *Life*, 11 (6), 496. Zugriff auf <https://www.ncbi.nlm.nih.gov/pmc/articles/PMC8229287/> doi: 10.3390/life11060496
- Ruksakulpiwat, S., Kumar, A. & Ajibade, A. (2023, Mai). Using ChatGPT in Medical Research: Current Status and Future Directions. *Journal of Multidisciplinary Healthcare*, 16, 1513–1520. Zugriff auf

- <https://www.ncbi.nlm.nih.gov/pmc/articles/PMC10239248/> doi: 10.2147/JMDH.S413470
- Rummler, M., Ziouti, F., Bouchard, A. L., Brandl, A., Duda, G. N., Bogen, B., ... Willie, B. M. (2021, Januar). Mechanical loading prevents bone destruction and exerts anti-tumor effects in the MOPC315.BM.Luc model of myeloma bone disease. *Acta Biomaterialia*, 119, 247–258. doi: 10.1016/j.actbio.2020.10.041
- Sacchetti, B., Funari, A., Remoli, C., Giannicola, G., Kogler, G., Liedtke, S., ... Bianco, P. (2016). No identical "mesenchymal stem cells" at different times and sites: Human committed progenitors of distinct origin and differentiation potential are incorporated as adventitial cells in microvessels. *Stem Cell Reports*, 6 (6), 897–913. Zugriff auf <http://dx.doi.org/10.1016/j.stemcr.2016.05.011> doi: 10.1016/j.stemcr.2016.05.011
- Sandve, G. K., Nekrutenko, A., Taylor, J. & Hovig, E. (2013, Oktober). Ten Simple Rules for Reproducible Computational Research. *PLoS Computational Biology*, 9 (10), e1003285. Zugriff auf <https://www.ncbi.nlm.nih.gov/pmc/articles/PMC3812051/> doi: 10.1371/journal.pcbi.1003285
- Santos, B. S., Silva, I., Ribeiro-Dantas, M. d. C., Alves, G., Endo, P. T. & Lima, L. (2020, Oktober). COVID-19: A scholarly production dataset report for research analysis. *Data in Brief*, 32, 106178. doi: 10.1016/j.dib.2020.106178
- Sanz-Rodríguez, F., Ruiz-Velasco, N., Pascual-Salcedo, D. & Teixidó, J. (1999, Dezember). Characterization of VLA-4-dependent myeloma cell adhesion to fibronectin and VCAM-1: VLA-4-dependent Myeloma Cell Adhesion. *British Journal of Haematology*, 107 (4), 825–834. Zugriff auf <http://doi.wiley.com/10.1046/j.1365-2141.1999.01762.x> doi: 10.1046/j.1365-2141.1999.01762.x
- Sarin, V., Yu, K., Ferguson, I. D., Gugliemini, O., Nix, M. A., Hann, B., ... Wiita, A. P. (2020, Oktober). Evaluating the efficacy of multiple myeloma cell lines as models for patient tumors via transcriptomic correlation analysis. *Leukemia*, 34 (10), 2754–2765. doi: 10.1038/s41375-020-0785-1
- Schrödinger, LLC. (2015, November). *The PyMOL molecular graphics system*. Zugriff auf <https://pymol.org/>
- Seabold, S. & Perktold, J. (2010). Statsmodels: Econometric and Statistical Modeling with Python. In *Python in Science Conference* (S. 92–96). Austin, Texas. Zugriff auf <https://conference.scipy.org/proceedings/scipy2010/seabold.html> doi: 10.25080/Majora-92bf1922-011
- Seckinger, A., Delgado, J. A., Moser, S., Moreno, L., Neuber, B., Grab, A., ... Vu, M. D. (2017, März). Target Expression, Generation, Preclinical Activity, and Pharmacokinetics of the BCMA-T Cell Bispecific Antibody EM801 for Multiple Myeloma Treatment. *Cancer Cell*, 31 (3), 396–410. Zugriff auf [https://www.cell.com/cancer-cell/abstract/S1535-6108\(17\)30016-8](https://www.cell.com/cancer-cell/abstract/S1535-6108(17)30016-8) doi: 10.1016/j.ccr.2017.02.002
- Seckinger, A., Hillengass, J., Emde, M., Beck, S., Kimmich, C., Dittrich, T., ... Hose, D. (2018). CD38 as Immunotherapeutic Target in Light Chain Amyloidosis and Multiple Myeloma-Association With Molecular Entities, Risk, Survival, and Mechanisms of Upfront Resistance. *Frontiers in Immunology*, 9, 1676. doi: 10.3389/fimmu.2018.01676
- Shahriyari, L. & Komarova, N. L. (2013, Oktober). Symmetric vs. Asymmetric Stem Cell Divisions: An Adaptation against Cancer? *PLoS ONE*, 8 (10), e76195. Zugriff auf <https://www.ncbi.nlm.nih.gov/pmc/articles/PMC3812169/> doi: 10.1371/journal.pone.0076195
- Sharma, N., Smadbeck, J. B., Abdallah, N., Zepeda-Mendoza, C., Binder, M., Pearce, K. E., ... Baughn, L. B. (2021, Oktober). The Prognostic Role of MYC Structural Variants Identified by NGS and FISH in Multiple Myeloma. *Clinical Cancer Research*, 27 (19), 5430. Zugriff auf <https://www.ncbi.nlm.nih.gov/pmc/articles/PMC8738776/> doi: 10.1158/1078-0432.CCR-21-0005
- Shen, Y. J., Mishima, Y., Shi, J., Sklavenitis-Pistofidis, R., Redd, R. A., Moschetta, M., ... Ghobrial, I. M. (2021, April). Progression signature underlies clonal evolution and dissemination of multiple myeloma.

- Blood*, 137 (17), 2360–2372. doi: 10.1182/blood.2020005885
- Shenghui, H., Nakada, D. & Morrison, S. J. (2009). Mechanisms of Stem Cell Self-Renewal. *Annual Review of Cell and Developmental Biology*, 25 (1), 377–406. Zugriff auf <https://doi.org/10.1146/annurev.cellbio.042308.113248> doi: 10.1146/annurev.cellbio.042308.113248
- Sherina, V., McMurray, H. R., Powers, W., Land, H., Love, T. M. T. & McCall, M. N. (2020, Dezember). Multiple imputation and direct estimation for qPCR data with non-detects. *BMC Bioinformatics*, 21 (1), 1–15. Zugriff auf <https://bmcbioinformatics.biomedcentral.com/articles/10.1186/s12859-020-03807-9> doi: 10.1186/s12859-020-03807-9
- Siclari, V., Guise, T. & Chirgwin, J. (2007, Januar). Molecular interactions between breast cancer cells and the bone microenvironment drive skeletal metastases. *Cancer metastasis reviews*, 25, 621–33. doi: 10.1007/s10555-006-9023-1
- Siegel, R. L., Giaquinto, A. N. & Jemal, A. (2024). Cancer statistics, 2024. *CA: A Cancer Journal for Clinicians*, 74 (1), 12–49. Zugriff auf <https://onlinelibrary.wiley.com/doi/abs/10.3322/caac.21820> doi: 10.3322/caac.21820
- Simonyan, K. & Zisserman, A. (2015, April). Very Deep Convolutional Networks for Large-Scale Image Recognition. *arXiv:1409.1556 [cs]*. Zugriff auf <http://arxiv.org/abs/1409.1556>
- Smith, A. M., Niemeyer, K. E., Katz, D. S., Barba, L. A., Githinji, G., Gymrek, M., ... Vanderplas, J. T. (2018). Journal of Open Source Software (JOSS): Design and first-year review. *PeerJ Preprints*, 4, e147. doi: 10.7717/peerj-cs.147
- Solimando, A. G., Brandl, A., Mattenheimer, K., Graf, C., Ritz, M., Ruckdeschel, A., ... Beilhack, A. (2018, März). JAM-A as a prognostic factor and new therapeutic target in multiple myeloma. *Leukemia*, 32 (3), 736–743. Zugriff auf <http://www.nature.com/articles/leu2017287> doi: 10.1038/leu.2017.287
- Solimando, A. G., Da Vià, M. C., Leone, P., Borrelli, P., Croci, G. A., Tabares, P., ... Beilhack, A. (2020, April). Halting the vicious cycle within the multiple myeloma ecosystem: Blocking JAM-A on bone marrow endothelial cells restores the angiogenic homeostasis and suppresses tumor progression. *Haematologica*. doi: 10.3324/haematol.2019.239913
- Solimando, A. G., Malerba, E., Leone, P., Prete, M., Terragna, C., Cavo, M. & Racanelli, V. (2022, September). Drug resistance in multiple myeloma: Soldiers and weapons in the bone marrow niche. *Frontiers in Oncology*, 12, 973836. Zugriff auf <https://www.ncbi.nlm.nih.gov/pmc/articles/PMC9533079/> doi: 10.3389/fonc.2022.973836
- Spaepen, P., De Boodt, S., Aerts, J.-M. & Sloten, J. V. (2011). Digital image processing of live/dead staining. *Methods in Molecular Biology (Clifton, N.J.)*, 740, 209–230. doi: 10.1007/978-1-61779-108-6_21
- Sprynski, A. C., Hose, D., Caillot, L., Rème, T., Shaughnessy, J. D., Barlogie, B., ... Klein, B. (2009, Mai). The role of IGF-1 as a major growth factor for myeloma cell lines and the prognostic relevance of the expression of its receptor. *Blood*, 113 (19), 4614–4626. Zugriff auf <https://www.ncbi.nlm.nih.gov/pmc/articles/PMC2691749/> doi: 10.1182/blood-2008-07-170464
- Stancheva, I. (2011, Juni). Revisiting Heterochromatin in Embryonic Stem Cells. *PLoS Genetics*, 7 (6), e1002093. Zugriff auf <https://www.ncbi.nlm.nih.gov/pmc/articles/PMC3107196/> doi: 10.1371/journal.pgen.1002093
- Standal, T., Seidel, C., Plesner, T., Sanderson, R., Waage, A., Børset, M. & Sundan, A. (2002, November). Osteoprotegerin is bound, internalized, and degraded by multiple myeloma cells. *Blood*, 100, 3002–7. doi: 10.1182/blood-2002-04-1190
- St Johnston, D. & Ahringer, J. (2010, Mai). Cell polarity in eggs and epithelia: Parallels and diversity. *Cell*, 141 (5), 757–774. doi: 10.1016/j.cell.2010.05.011

- Stock, P., Bruckner, S., Winkler, S., Dollinger, M. M. & Christ, B. (2014, April). Human bone marrow mesenchymal stem cell-derived hepatocytes improve the mouse liver after acute acetaminophen intoxication by preventing progress of injury. *International journal of molecular sciences*, 15 (4), 7004–7028. doi: 10.3390/ijms15047004
- Sullivan, G. M. & Feinn, R. S. (2021, August). Facts and Fictions About Handling Multiple Comparisons. *Journal of Graduate Medical Education*, 13 (4), 457–460. Zugriff auf <https://www.ncbi.nlm.nih.gov/pmc/articles/PMC8370375/> doi: 10.4300/JGME-D-21-00599.1
- Sun, B., Guo, J., Yang, D., Hu, Q., Ma, H., Tian, P., ... Zhao, X. (2024, März). Granzyme B-based CAR T cells block metastasis by eliminating circulating tumor cells. bioRxiv. Zugriff auf <https://www.biorxiv.org/content/10.1101/2024.03.18.585442v1> doi: 10.1101/2024.03.18.585442
- Szeliski, R. (2011). Feature detection and matching. In *Computer vision: Algorithms and applications* (S. 181–234). London: Springer London. Zugriff auf https://link.springer.com/chapter/10.1007/978-1-84882-935-0_4 doi: 10.1007/978-1-84882-935-0_4
- Tabolacci, C., De Martino, A., Mischiati, C., Feriotto, G. & Beninati, S. (2019, Januar). The Role of Tissue Transglutaminase in Cancer Cell Initiation, Survival and Progression. *Medical Sciences*, 7 (2), 19. Zugriff auf <https://www.ncbi.nlm.nih.gov/pmc/articles/PMC6409630/> doi: 10.3390/medsci7020019
- Tai, Y.-T., Li, X.-F., Breitkreutz, I., Song, W., Neri, P., Catley, L., ... Anderson, K. C. (2006, Juli). Role of B-cell-activating factor in adhesion and growth of human multiple myeloma cells in the bone marrow microenvironment. *Cancer Research*, 66 (13), 6675–6682. doi: 10.1158/0008-5472.CAN-06-0190
- Tam, P. P. & Beddington, R. S. (1987, Januar). The formation of mesodermal tissues in the mouse embryo during gastrulation and early organogenesis. *Development (Cambridge, England)*, 99 (1), 109–126.
- Taskiran, I. I., Spanier, K. I., Dickmänen, H., Kempynck, N., Pančíková, A., Ekşí, E. C., ... Aerts, S. (2024, Februar). Cell-type-directed design of synthetic enhancers. *Nature*, 626 (7997), 212–220. Zugriff auf <https://www.nature.com/articles/s41586-023-06936-2> doi: 10.1038/s41586-023-06936-2
- Team, T. P. D. (2020, Februar). *Pandas-dev/pandas: Pandas*. Zenodo. Zugriff auf <https://doi.org/10.5281/zenodo.3509134> doi: 10.5281/zenodo.3509134
- Teoh, G. & Anderson, K. C. (1997, Februar). INTERACTION OF TUMOR AND HOST CELLS WITH ADHESION AND EXTRACELLULAR MATRIX MOLECULES IN THE DEVELOPMENT OF MULTIPLE MYELOMA. *Hematology/Oncology Clinics of North America*, 11 (1), 27–42. Zugriff auf <http://www.sciencedirect.com/science/article/pii/S0889858805704135> doi: 10.1016/S0889-8588(05)70413-5
- Teramachi, J., Silbermann, R., Yang, P., Zhao, W., Mohammad, K. S., Guo, J., ... Kurihara, N. (2016, Februar). Blocking the ZZ Domain of Sequestosome1/p62 Suppresses Myeloma Growth and Osteoclast Formation In Vitro and Induces Dramatic Bone Formation in Myeloma-Bearing Bones In Vivo. *Leukemia*, 30 (2), 390–398. Zugriff auf <https://www.ncbi.nlm.nih.gov/pmc/articles/PMC4740189/> doi: 10.1038/leu.2015.229
- Terpos, E., Migkou, M., Christoulas, D., Gavriatopoulou, M., Eleutherakis-Papaiakovou, E., Kanellias, N., ... Dimopoulos, M. A. (2016, Mai). Increased circulating VCAM-1 correlates with advanced disease and poor survival in patients with multiple myeloma: Reduction by post-bortezomib and lenalidomide treatment. *Blood Cancer Journal*, 6 (5), e428. Zugriff auf <https://www.ncbi.nlm.nih.gov/pmc/articles/PMC4916305/> doi: 10.1038/bcj.2016.37
- Terpos, E., Ntanasis-Stathopoulos, I., Gavriatopoulou, M. & Dimopoulos, M. A. (2018, Januar). Pathogenesis of bone disease in multiple myeloma: From bench to bedside. *Blood Cancer Journal*, 8 (1), 7. doi: 10.1038/s41408-017-0037-4
- Thompson, S., Dowrick, T., Ahmad, M., Xiao, G., Koo, B., Bonmati, E., ... Clarkson, M. J. (2020, Juli).

- SciKit-Surgery: Compact libraries for surgical navigation. *International Journal of Computer Assisted Radiology and Surgery*, 15 (7), 1075–1084. doi: 10.1007/s11548-020-02180-5
- ThumallaPally, N., Meshref, A., Mousa, M. & Terjanian, T. (2017, Januar). Solitary plasmacytoma: Population-based analysis of survival trends and effect of various treatment modalities in the USA. *BMC Cancer*, 17, 13. Zugriff auf <https://www.ncbi.nlm.nih.gov/pmc/articles/PMC5216567/> doi: 10.1186/s12885-016-3015-5
- Tong, A., Kuchroo, M., Gupta, S., Venkat, A., San Juan, B. P., Rangel, L., ... Krishnaswamy, S. (2023, März). *Learning transcriptional and regulatory dynamics driving cancer cell plasticity using neural ODE-based optimal transport*. Zugriff auf <http://biorxiv.org/lookup/doi/10.1101/2023.03.28.534644> doi: 10.1101/2023.03.28.534644
- Trapnell, C., Roberts, A., Goff, L., Pertea, G., Kim, D., Kelley, D. R., ... Pachter, L. (2012, März). Differential gene and transcript expression analysis of RNA-seq experiments with TopHat and Cufflinks. *Nature Protocols*, 7 (3), 562–578. doi: 10.1038/nprot.2012.016
- Tsubaki, M., Seki, S., Takeda, T., Chihara, A., Arai, Y., Morii, Y., ... Nishida, S. (2020, Oktober). The HGF/Met/NF- κ B Pathway Regulates RANKL Expression in Osteoblasts and Bone Marrow Stromal Cells. *International Journal of Molecular Sciences*, 21 (21), 7905. Zugriff auf <https://www.ncbi.nlm.nih.gov/pmc/articles/PMC7663721/> doi: 10.3390/ijms21217905
- Turesson, I., Bjorkholm, M., Blimark, C. H., Kristinsson, S., Velez, R. & Landgren, O. (2018, April). Rapidly changing myeloma epidemiology in the general population: Increased incidence, older patients, and longer survival. *European journal of haematology*, 10.1111/ejh.13083. Zugriff auf <https://www.ncbi.nlm.nih.gov/pmc/articles/PMC6195866/> doi: 10.1111/ejh.13083
- Ullah, I., Subbarao, R. B. & Rho, G. J. (2015, April). Human mesenchymal stem cells - current trends and future prospective. *Bioscience Reports*, 35 (2), e00191. Zugriff auf <https://www.ncbi.nlm.nih.gov/pmc/articles/PMC4413017/> doi: 10.1042/BSR20150025
- Ullah, T. R. (2019, August). The role of CXCR4 in multiple myeloma: Cells' journey from bone marrow to beyond. *Journal of Bone Oncology*, 17, 100253. doi: 10.1016/j.jbo.2019.100253
- Urashima, M., Chauhan, D., Uchiyama, H., Freeman, G. & Anderson, K. (1995, April). CD40 ligand triggered interleukin-6 secretion in multiple myeloma. *Blood*, 85 (7), 1903–1912. Zugriff auf <https://ashpublications.org/blood/article/85/7/1903/123565/CD40-ligand-triggered-interleukin6-secretion-in> doi: 10.1182/blood.V85.7.1903.bloodjournal8571903
- Uthamacumaran, A. & Zenil, H. (2022, Juli). A Review of Mathematical and Computational Methods in Cancer Dynamics. *Frontiers in Oncology*, 12. Zugriff auf <https://www.frontiersin.org/journals/oncology/articles/10.3389/fonc.2022.850731/full> doi: 10.3389/fonc.2022.850731
- Väänänen, H. K. (1993, August). Mechanism of bone turnover. *Annals of Medicine*, 25 (4), 353–359. doi: 10.3109/07853899309147297
- Vallat, R. (2018, November). Pingouin: Statistics in Python. *Journal of Open Source Software*, 3 (31), 1026. Zugriff auf <https://joss.theoj.org/papers/10.21105/joss.01026> doi: 10.21105/joss.01026
- Vallet, S., Mukherjee, S., Vaghela, N., Hideshima, T., Fulciniti, M., Pozzi, S., ... Raje, N. (2010, März). Activin A promotes multiple myeloma-induced osteolysis and is a promising target for myeloma bone disease. *Proceedings of the National Academy of Sciences of the United States of America*, 107 (11), 5124–5129. Zugriff auf <https://www.ncbi.nlm.nih.gov/pmc/articles/PMC2841922/> doi: 10.1073/pnas.0911929107
- van Rossum, G., Lehtosalo, J. & Langa, L. (2014). *PEP 484 – Type Hints / peps.python.org*. Zugriff auf <https://peps.python.org/pep-0484/>
- Vande Broek, I., Vanderkerken, K., Van Camp, B. & Van Riet, I. (2008). Extravasation and homing

- mechanisms in multiple myeloma. *Clinical & Experimental Metastasis*, 25 (4), 325–334. doi: 10.1007/s10585-007-9108-4
- Van Valckenborgh, E., Croucher, P. I., De Raeve, H., Carron, C., De Leenheer, E., Blacher, S., ... Vanderkerken, K. (2004, September). Multifunctional role of matrix metalloproteinases in multiple myeloma: A study in the 5T2MM mouse model. *The American Journal of Pathology*, 165 (3), 869–878. doi: 10.1016/S0002-9440(10)63349-4
- van Zutphen, L. F. M., Baumans, V. & Beynen, A. C. (Hrsg.). (2001). *Principles of laboratory animal science: A contribution to the humane use and care of animals and to the quality of experimental results* (Rev. ed Aufl.). Amsterdam ; New York: Elsevier.
- Verzella, D., Cornice, J., Arboretti, P., Vecchiotti, D., Di Vito Nolfi, M., Capece, D., ... Franzoso, G. (2022, September). The NF- κ B Pharmacopeia: Novel Strategies to Subdue an Intractable Target. *Biomedicines*, 10 (9), 2233. Zugriff auf <https://www.ncbi.nlm.nih.gov/pmc/articles/PMC9496094/> doi: 10.3390/biomedicines10092233
- Wadgaonkar, R., Phelps, K. M., Haque, Z., Williams, A. J., Silverman, E. S. & Collins, T. (1999, Januar). CREB-binding protein is a nuclear integrator of nuclear factor-kappaB and p53 signaling. *The Journal of Biological Chemistry*, 274 (4), 1879–1882. doi: 10.1074/jbc.274.4.1879
- Walewska, A., Janucik, A., Tynecka, M., Moniuszko, M. & Eljaszewicz, A. (2023, November). Mesenchymal stem cells under epigenetic control – the role of epigenetic machinery in fate decision and functional properties. *Cell Death & Disease*, 14 (11), 1–12. Zugriff auf <https://www.nature.com/articles/s41419-023-06239-4> doi: 10.1038/s41419-023-06239-4
- Wang, W., Yang, X., Dai, J., Lu, Y., Zhang, J. & Keller, E. T. (2019, Juni). Prostate cancer promotes a vicious cycle of bone metastasis progression through inducing osteocytes to secrete GDF15 that stimulates prostate cancer growth and invasion. *Oncogene*, 38 (23), 4540–4559. doi: 10.1038/s41388-019-0736-3
- Waskom, M. L. (2021, April). Seaborn: Statistical data visualization. *Journal of Open Source Software*, 6 (60), 3021. Zugriff auf <https://joss.theoj.org/papers/10.21105/joss.03021> doi: 10.21105/joss.03021
- Webster, G. A. & Perkins, N. D. (1999, Mai). Transcriptional Cross Talk between NF- κ B and p53. *Molecular and Cellular Biology*, 19 (5), 3485–3495. Zugriff auf <https://www.ncbi.nlm.nih.gov/pmc/articles/PMC84141/>
- Weetall, M., Hugo, R., Maida, S., West, S., Wattanasin, S., Bouhel, R., ... Friedman, C. (2001, Juni). A Homogeneous Fluorometric Assay for Measuring Cell Adhesion to Immobilized Ligand Using V-Well Microtiter Plates. *Analytical Biochemistry*, 293 (2), 277–287. Zugriff auf <https://linkinghub.elsevier.com/retrieve/pii/S0003269701951401> doi: 10.1006/abio.2001.5140
- Weiss, C. J. (2022, September). Visualizing protein big data using Python and Jupyter notebooks. *Biochemistry and Molecular Biology Education: A Bimonthly Publication of the International Union of Biochemistry and Molecular Biology*, 50 (5), 431–436. doi: 10.1002/bmb.21621
- West, K. (2018, Juli). *Reinventing Research: Agile in the Academic Laboratory / Agile Alliance*. Zugriff auf <https://www.agilealliance.org/resources/experience-reports/reinventing-research-agile-in-the-academic-laboratory/>
- Weyburne, D. W. (2014, April). New thickness and shape parameters for the boundary layer velocity profile. *Experimental Thermal and Fluid Science*, 54, 22–28. Zugriff auf <https://www.sciencedirect.com/science/article/pii/S089417771400017X> doi: 10.1016/j.expthermflusci.2014.01.008
- Wickham, H. (2014, September). Tidy Data. *Journal of Statistical Software*, 59, 1–23. Zugriff auf <https://doi.org/10.18637/jss.v059.i10> doi: 10.18637/jss.v059.i10

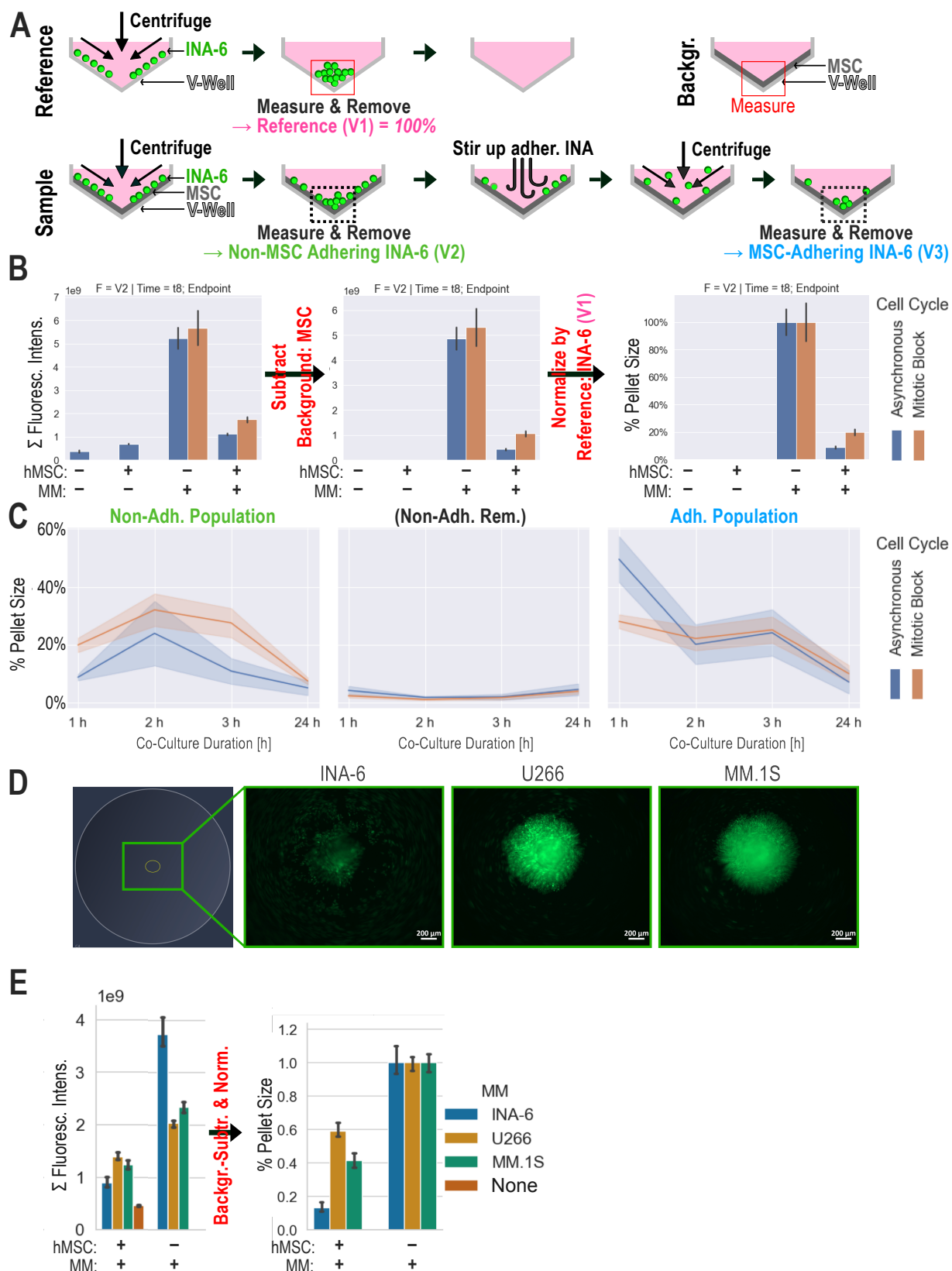
- Wilkins, A., Kemp, K., Ginty, M., Hares, K., Mallam, E. & Scolding, N. (2009, Juli). Human bone marrow-derived mesenchymal stem cells secrete brain-derived neurotrophic factor which promotes neuronal survival in vitro. *Stem cell research*, 3 (1), 63–70. doi: 10.1016/j.scr.2009.02.006
- Wilkinson, M. D., Dumontier, M., Aalbersberg, I. J., Appleton, G., Axton, M., Baak, A., ... Mons, B. (2016, März). The FAIR Guiding Principles for scientific data management and stewardship. *Scientific Data*, 3 (1), 160018. Zugriff auf <https://www.nature.com/articles/sdata201618> doi: 10.1038/sdata.2016.18
- Wilmore, J. R. & Allman, D. (2017, August). Here, there, and anywhere? Arguments for and against the physical plasma cell survival niche. *Journal of immunology (Baltimore, Md. : 1950)*, 199 (3), 839–845. Zugriff auf <https://www.ncbi.nlm.nih.gov/pmc/articles/PMC5651088/> doi: 10.4049/jimmunol.1700461
- Witwer, K. W. (2013, Februar). Data submission and quality in microarray-based microRNA profiling. *Clinical chemistry*, 59 (2), 392–400. Zugriff auf <https://www.ncbi.nlm.nih.gov/pmc/articles/PMC4037921/> doi: 10.1373/clinchem.2012.193813
- Wohlford, G. F., Buckley, L. F., Kadariya, D., Park, T., Chiabando, J. G., Carbone, S., ... Van Tassell, B. (2021, Mai). A phase 1 clinical trial of SP16, a first-in-class anti-inflammatory LRP1 agonist, in healthy volunteers. *PLoS ONE*, 16 (5), e0247357. Zugriff auf <https://www.ncbi.nlm.nih.gov/pmc/articles/PMC8101931/> doi: 10.1371/journal.pone.0247357
- Wong, A. D. & Searson, P. C. (2017, November). Mitosis-mediated intravasation in a tissue-engineered tumor-microvessel platform. *Cancer research*, 77 (22), 6453–6461. Zugriff auf <https://www.ncbi.nlm.nih.gov/pmc/articles/PMC5690825/> doi: 10.1158/0008-5472.CAN-16-3279
- Wouters, J., Kalender-Atak, Z., Minnoye, L., Spanier, K. I., De Waegeneer, M., Bravo González-Blas, C., ... Aerts, S. (2020, August). Robust gene expression programs underlie recurrent cell states and phenotype switching in melanoma. *Nature cell biology*, 22 (8), 986–998. Zugriff auf <https://doi.org/10.1038/s41556-020-0547-3> doi: 10.1038/s41556-020-0547-3
- Xie, W., Schultz, M. D., Lister, R., Hou, Z., Rajagopal, N., Ray, P., ... Ren, B. (2013, Mai). Epigenomic Analysis of Multi-lineage Differentiation of Human Embryonic Stem Cells. *Cell*, 153 (5), 1134–1148. Zugriff auf <https://www.ncbi.nlm.nih.gov/pmc/articles/PMC3786220/> doi: 10.1016/j.cell.2013.04.022
- Xu, W., Zhang, X., Qian, H., Zhu, W., Sun, X., Hu, J., ... Chen, Y. (2004, Juli). Mesenchymal stem cells from adult human bone marrow differentiate into a cardiomyocyte phenotype in vitro. *Experimental biology and medicine (Maywood, N.J.)*, 229 (7), 623–631.
- Yamada, K. M., Doyle, A. D. & Lu, J. (2022, Oktober). Cell–3D matrix interactions: Recent advances and opportunities. *Trends in Cell Biology*, 32 (10), 883–895. Zugriff auf <https://www.sciencedirect.com/science/article/pii/S0962892422000629> doi: 10.1016/j.tcb.2022.03.002
- Yamashita, Y. M., Yuan, H., Cheng, J. & Hunt, A. J. (2010, Januar). Polarity in Stem Cell Division: Asymmetric Stem Cell Division in Tissue Homeostasis. *Cold Spring Harbor Perspectives in Biology*, 2 (1), a001313. Zugriff auf <https://www.ncbi.nlm.nih.gov/pmc/articles/PMC2827902/> doi: 10.1101/cshperspect.a001313
- Yang, A., Troup, M. & Ho, J. W. (2017, Juli). Scalability and Validation of Big Data Bioinformatics Software. *Computational and Structural Biotechnology Journal*, 15, 379–386. Zugriff auf <https://www.ncbi.nlm.nih.gov/pmc/articles/PMC5537105/> doi: 10.1016/j.csbj.2017.07.002
- Yang, P., Qu, Y., Wang, M., Chu, B., Chen, W., Zheng, Y., ... Qian, Z. (2022, Juni). Pathogenesis and treatment of multiple myeloma. *MedComm*, 3 (2), e146. Zugriff auf <https://www.ncbi.nlm.nih.gov/pmc/articles/PMC9162151/> doi: 10.1002/mco2.146
- Yang, Y., Macleod, V., Bendre, M., Huang, Y., Theus, A. M., Miao, H.-Q., ... Sanderson, R. D. (2005,

- Februar). Heparanase promotes the spontaneous metastasis of myeloma cells to bone. *Blood*, 105 (3), 1303–1309. doi: 10.1182/blood-2004-06-2141
- Zarnegar, B. J., Wang, Y., Mahoney, D. J., Dempsey, P. W., Cheung, H. H., He, J., ... Cheng, G. (2008, Dezember). Noncanonical NF- κ B activation requires coordinated assembly of a regulatory complex of the adaptors cIAP1, cIAP2, TRAF2 and TRAF3 and the kinase NIK. *Nature Immunology*, 9 (12), 1371–1378. Zugriff auf <https://www.nature.com/articles/ni.1676> doi: 10.1038/ni.1676
- Zehentmeier, S., Roth, K., Cseresnyes, Z., Sercan, Ö., Horn, K., Niesner, R. A., ... Hauser, A. E. (2014, August). Static and dynamic components synergize to form a stable survival niche for bone marrow plasma cells. *European Journal of Immunology*, 44 (8), 2306–2317. doi: 10.1002/eji.201344313
- Zeissig, M. N., Zannettino, A. C. W. & Vandyke, K. (2020, Dezember). Tumour Dissemination in Multiple Myeloma Disease Progression and Relapse: A Potential Therapeutic Target in High-Risk Myeloma. *Cancers*, 12 (12). Zugriff auf <https://www.ncbi.nlm.nih.gov/pmc/articles/PMC7761917/> doi: 10.3390/cancers12123643
- Zeiss OAD Feature Extractors. (o. J.). Zugriff auf https://github.com/zeiss-microscopy/OAD/blob/master/Machine_Learning/Feature_Extractors/feature_extractors.md
- Zepeda-Moreno, A., Taubert, I., Hellwig, I., Hoang, V., Pietsch, L., Lakshmanan, V. K., ... Ho, A. D. (2011). Innovative method for quantification of cell-cell adhesion in 96-well plates. *Cell Adhesion & Migration*, 5 (3), 215–219. Zugriff auf <https://www.ncbi.nlm.nih.gov/pmc/articles/PMC3210204/> doi: 10.4161/cam.5.3.14648
- Zerbino, D. R., Achuthan, P., Akanni, W., Amode, M. R., Barrell, D., Bhai, J., ... Flicek, P. (2018, Januar). Ensembl 2018. *Nucleic Acids Research*, 46 (D1), D754-D761. Zugriff auf <https://doi.org/10.1093/nar/gkx1098> doi: 10.1093/nar/gkx1098
- Zhou, F., Meng, S., Song, H. & Claret, F. X. (2013, November). Dickkopf-1 is a key regulator of myeloma bone disease: Opportunities and challenges for therapeutic intervention. *Blood reviews*, 27 (6), 261–267. Zugriff auf <https://www.ncbi.nlm.nih.gov/pmc/articles/PMC4133945/> doi: 10.1016/j.blre.2013.08.002
- Zhou, Y., Zhou, B., Pache, L., Chang, M., Khodabakhshi, A. H., Tanaseichuk, O., ... Chanda, S. K. (2019, April). Metascape provides a biologist-oriented resource for the analysis of systems-level datasets. *Nature Communications*, 10 (1), 1523. Zugriff auf <https://www.nature.com/articles/s41467-019-09234-6> doi: 10.1038/s41467-019-09234-6
- Ziemann, M., Eren, Y. & El-Osta, A. (2016, August). Gene name errors are widespread in the scientific literature. *Genome Biology*, 17 (1), 177. Zugriff auf <https://doi.org/10.1186/s13059-016-1044-7> doi: 10.1186/s13059-016-1044-7
- Zou, Y. S., Klausner, M., Ghabrial, J., Stinnett, V., Long, P., Morsberger, L., ... Tang, G. (2024, Mai). A comprehensive approach to evaluate genetic abnormalities in multiple myeloma using optical genome mapping. *Blood Cancer Journal*, 14 (1), 1–5. Zugriff auf <https://www.nature.com/articles/s41408-024-01059-x> doi: 10.1038/s41408-024-01059-x

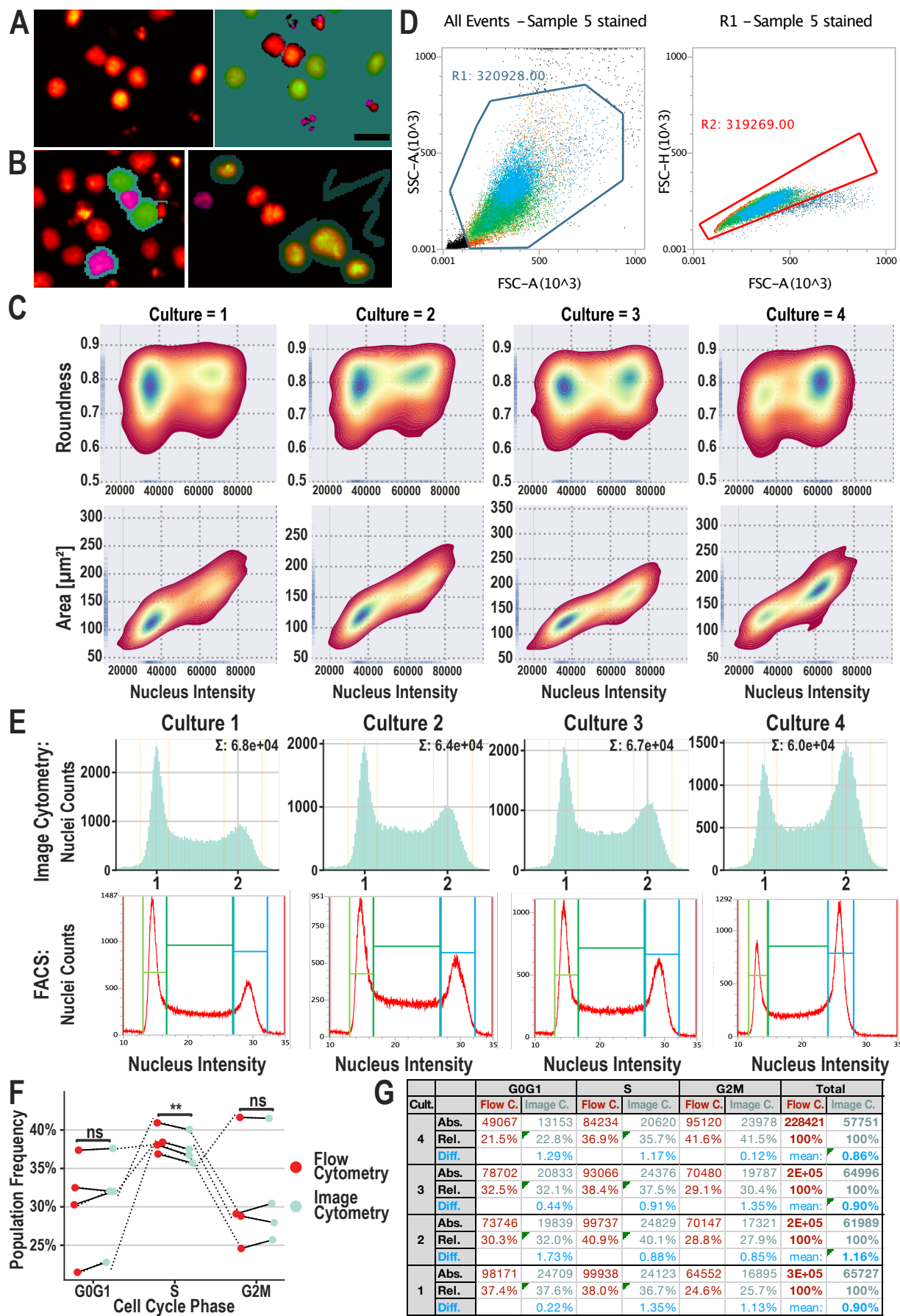
Appendices

A Supplementary Data & Methods

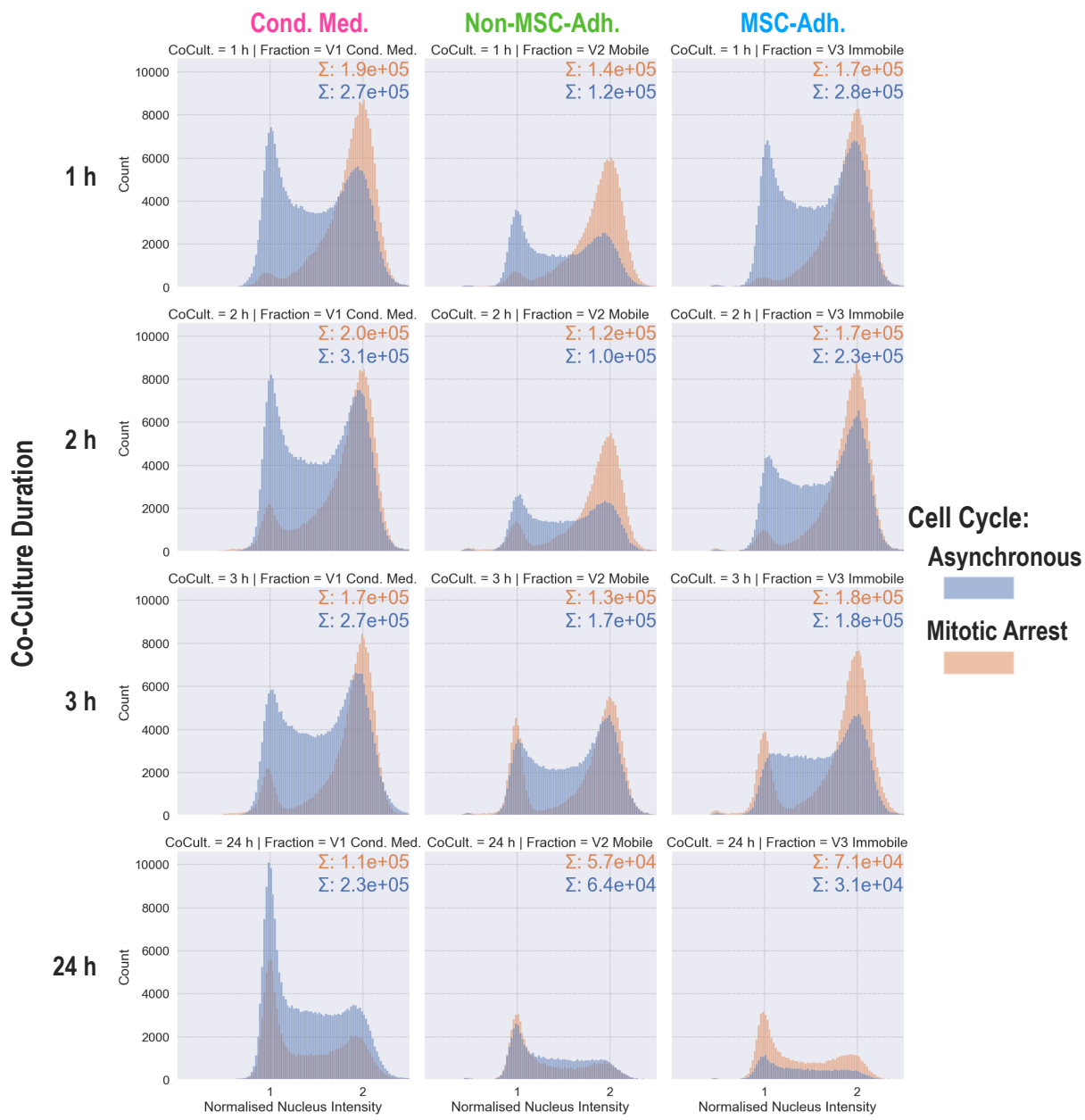
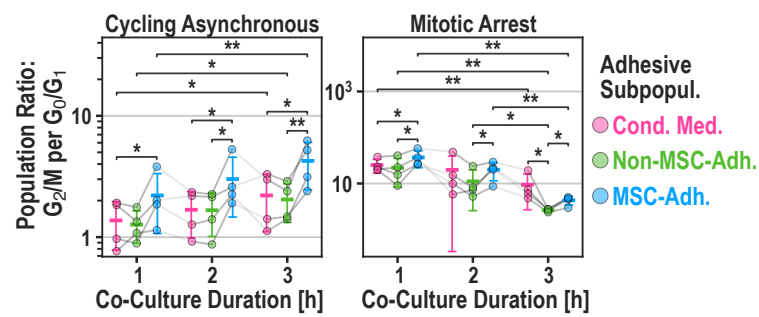
A.1 Figures



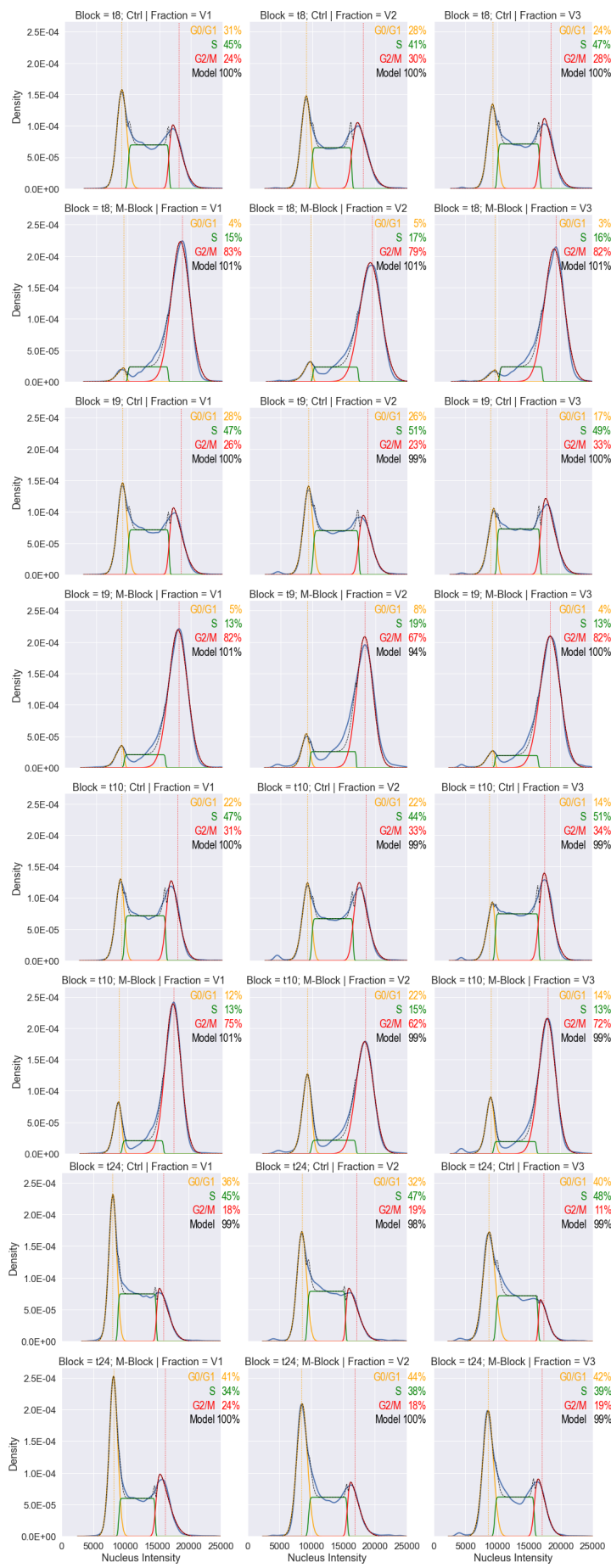
Appendix A.1 Figure 1: Principle and quantification of the V-well adhesion assay of fluorescently labeled myeloma cells adapted by Weetall et al. (2001). **A:** Sample: Subsequent rounds of centrifugation and removal of cell pellet yielded the size of adhesive subpopulations. Fluorescently stained INA-6 cells were added to an hMSC monolayer. Non-adherent INA-6 cells (V2) were pelleted in the well-tip. Pellets were quantified by fluorescence brightness and isolated by pipetting. Immobile INA-6 cells (V3) were manually detached by forceful pipetting. Reference: Omitting adhesive hMSC-layer yielded 100 % non-adherent cells (V1) after the first centrifugation step; Background: hMSC monolayer was used as background signal. **B:** Calculation of the population size relative to total cells starting with pellet intensity. The shown example is the pellet gained by centrifuging mobile subpopulation (V2) after 1 h of co-culture. (see Abbildung 3 for context): Intensity values from pellet images were summarized. After subtracting the unlabeled hMSC signal and normalization by a full-size pellet (reference), the resulting values represented the fraction of the adhesive subpopulation. **C:** One of three biological replicates summarized in Abbildung 3. Line range shows the standard deviation of four technical replicates. Non.Adh. Rem.: Fluorescence signal after removal of V2. **D:** Example images of myeloma cell lines (INA-6, U266, MM.1S) pelleted in the tip of V-wells. The leftmost image shows the recorded area in a complete V-well. Scale bar = 200 µm. **E:** Results from (D) comparing adhesion strength of three myeloma cell lines to hMSC. Error bars represent technical deviation. MM: Multiple Myeloma. This content has been taken as is from Kuric et al. (2024), published in *Cancer Research Communications* under the CC BY 4.0 license.



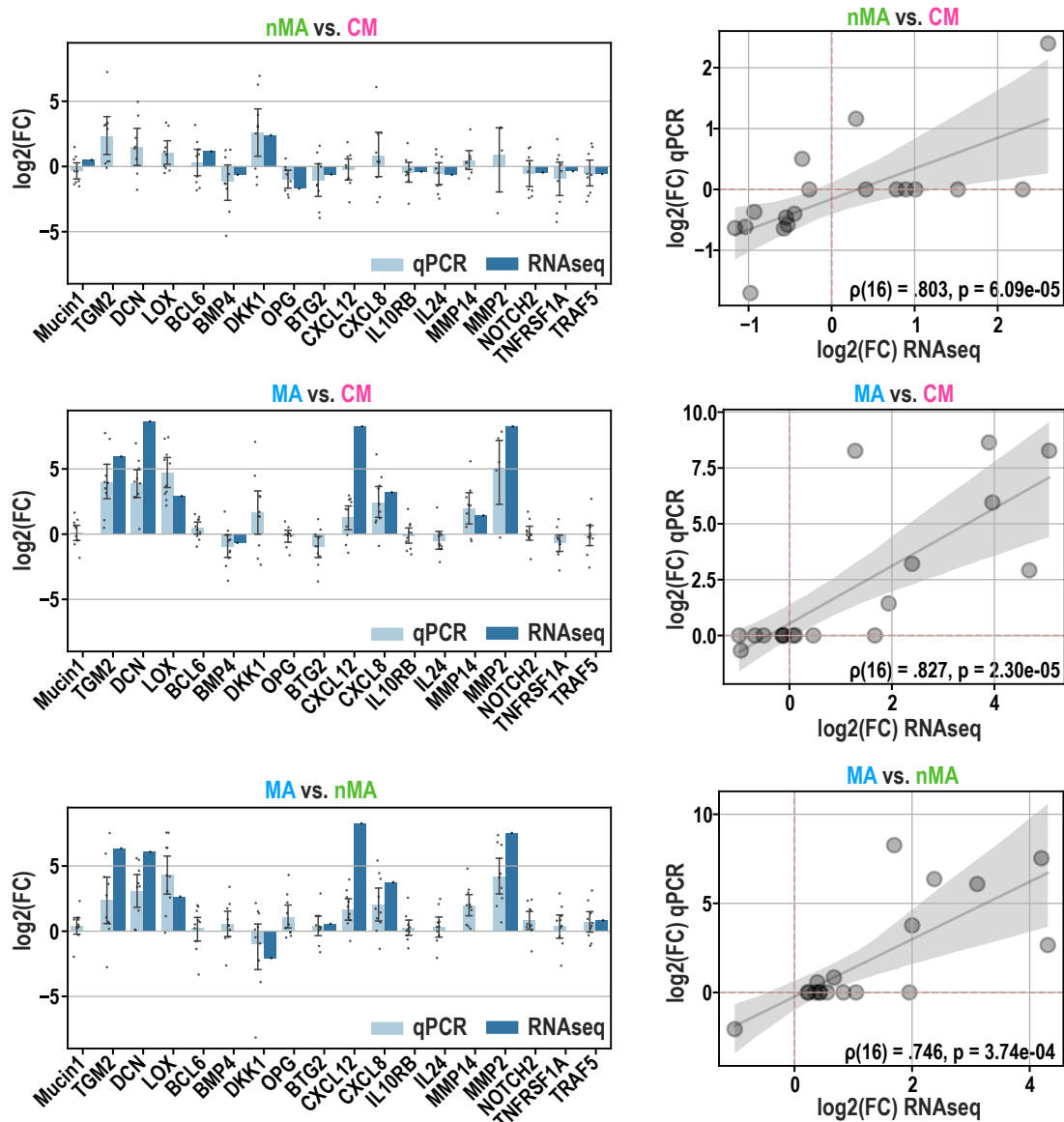
Appendix A.1 Figure 2: Validation of image cytometric analysis of cell cycle in four INA-6 cultures. **A:** Left: Example image cytometric scan: INA-6 cells were stained with Hoechst33342 and scanned by automated fluorescence microscopy. Right: The image was segmented using a convolutional neural network (ZEISS ZEN intellesis) trained to discern healthy nuclei (green) from fragmented ones (magenta). Doublets are excluded by setting an area- and roundness threshold. Scale bar: 20 μm . **B:** Two example images from the training set. **C:** Quality of image cytometric data was ensured by plotting the distribution of nuclei brightnesses vs. the distribution of both nuclei-roundnesses and nuclei-areas. Nuclei with double fluorescence intensity have the same roundness while their area increases, as expected from a cell in G2 phase. **D:** The same samples from (C) were also measured with flow cytometry. Representative example of gating strategy: Left: Dead cells were excluded by setting a minimum threshold for side-scattering (SSC-A). Right: Doublets were excluded by setting a maximum threshold for forward scatter area (FSC-A) (sample "5" represents culture "4" in this figure). **E:** Cell cycle profiles of four independent INA-6 cultures were measured by both image cytometry (top) and flow cytometry (bottom). For both methods, frequencies of G0/G1, S, and G2M were summed up by setting fluorescence intensity thresholds. **F:** Image cytometry yields the same frequencies for G0/G1, S, and G2M when compared to flow cytometry. RM-ANOVA showed that the method has no significant effect on the frequencies of cell cycle populations [$F(1, 3) = 1.421, p\text{-unc} = .32$]. **G:** Results from (F) in tabular form. On average, frequencies for G0/G1, S, and G2M measured by Image cytometry differ by 0.95 percent points compared to flow cytometry measurement. Cult.: Culture; C.: Image cytometry; Abs.: Absolute cell count; Rel.: Relative cell count; Diff.: Difference between relative cell counts determined by flow cytometry and image cytometry. This content has been taken as is from Kuric et al. (2024), published in *Cancer Research Communications* under the CC BY 4.0 license.

A**B**

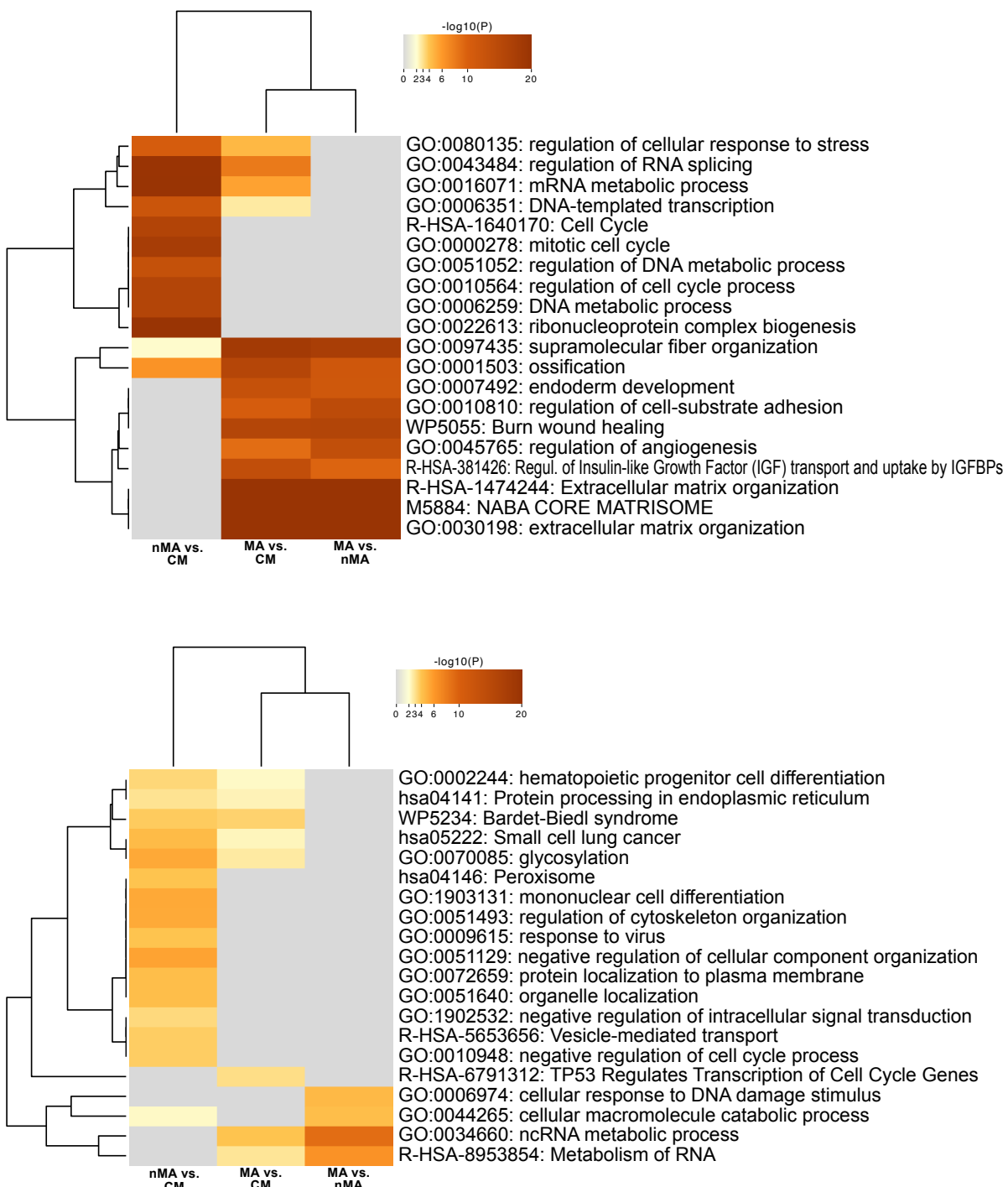
Appendix A.1 Figure 3: Cell cycle analysis of INA-6 pellets gained from V-Well Adhesion assay (Abbildung 3). **A:** Cell cycle profiles of MSC-adhering subpopulations. INA-6 cells were synchronized by double thymidine block followed by nocodazole. Cell cycle was released directly before addition to hMSCs. Histograms were normalized and summed up across all biological replicates ($n = 4$). Technical replicates (3) were pooled prior to cell cycle profiling. CoCult. = Co-culture duration. Fraction = Adhesion subpopulations. **B:** Similar figure to Fig. 3C displaying ratio of INA-6 populations (G2/M to G0/G1). **Statistics::** Paired t-test (B). This content has been taken as is from Kuric et al. (2024), published in *Cancer Research Communications* under the CC BY 4.0 license.



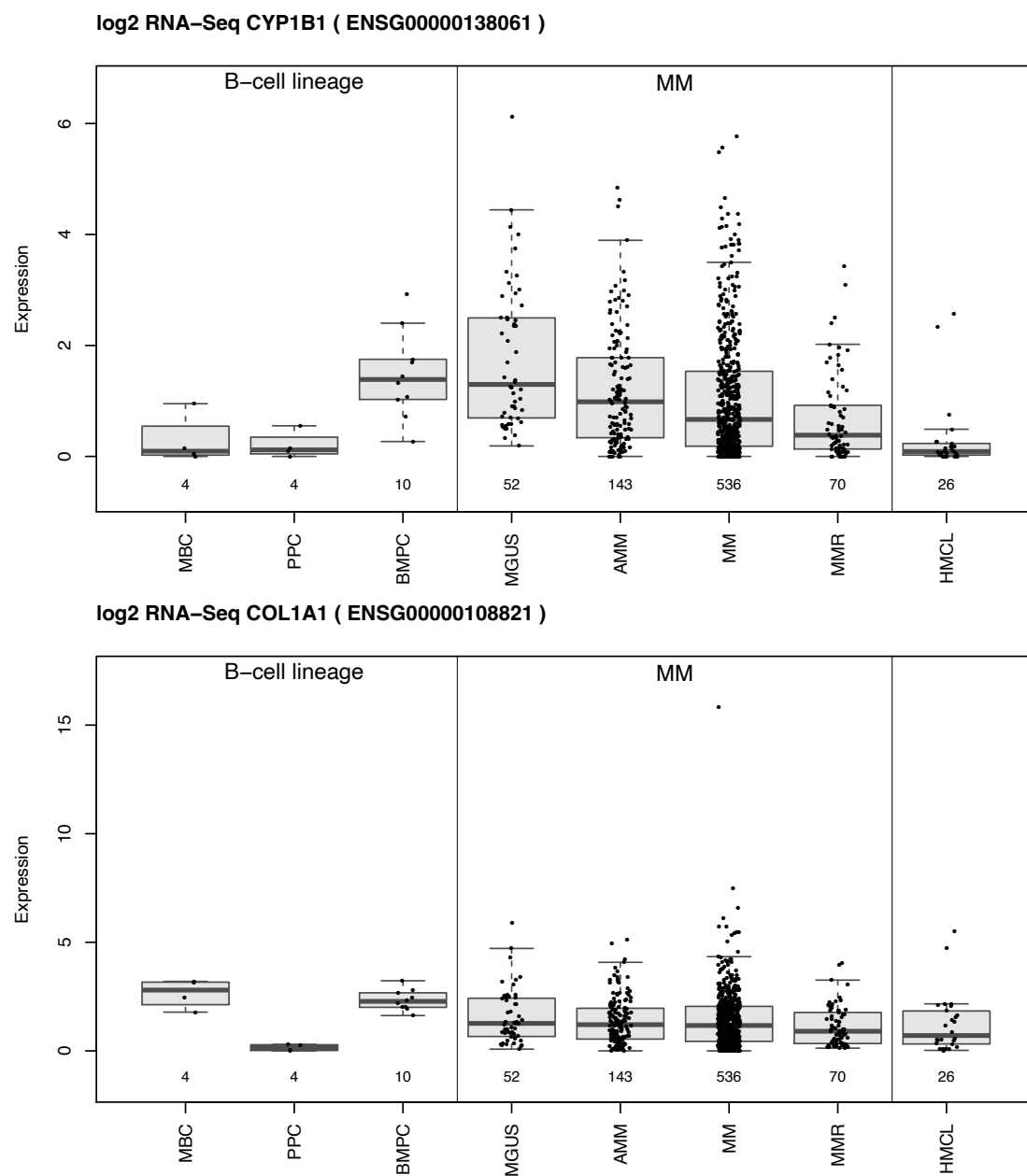
Appendix A.1 Figure 4: Representative (one of the four independent sample sets as seen in Appendix A: Abbildung 3) curve fitting analysis of cell cycle profiles generated by Image Cytometry. t8, t9, t10, and t24 refer to 1, 2, 3, and 24 hours after the addition of INA-6 cells to hMSCs. This content has been taken as is from Kuric et al. (2024), published in *Cancer Research Communications* under the CC BY 4.0 license.



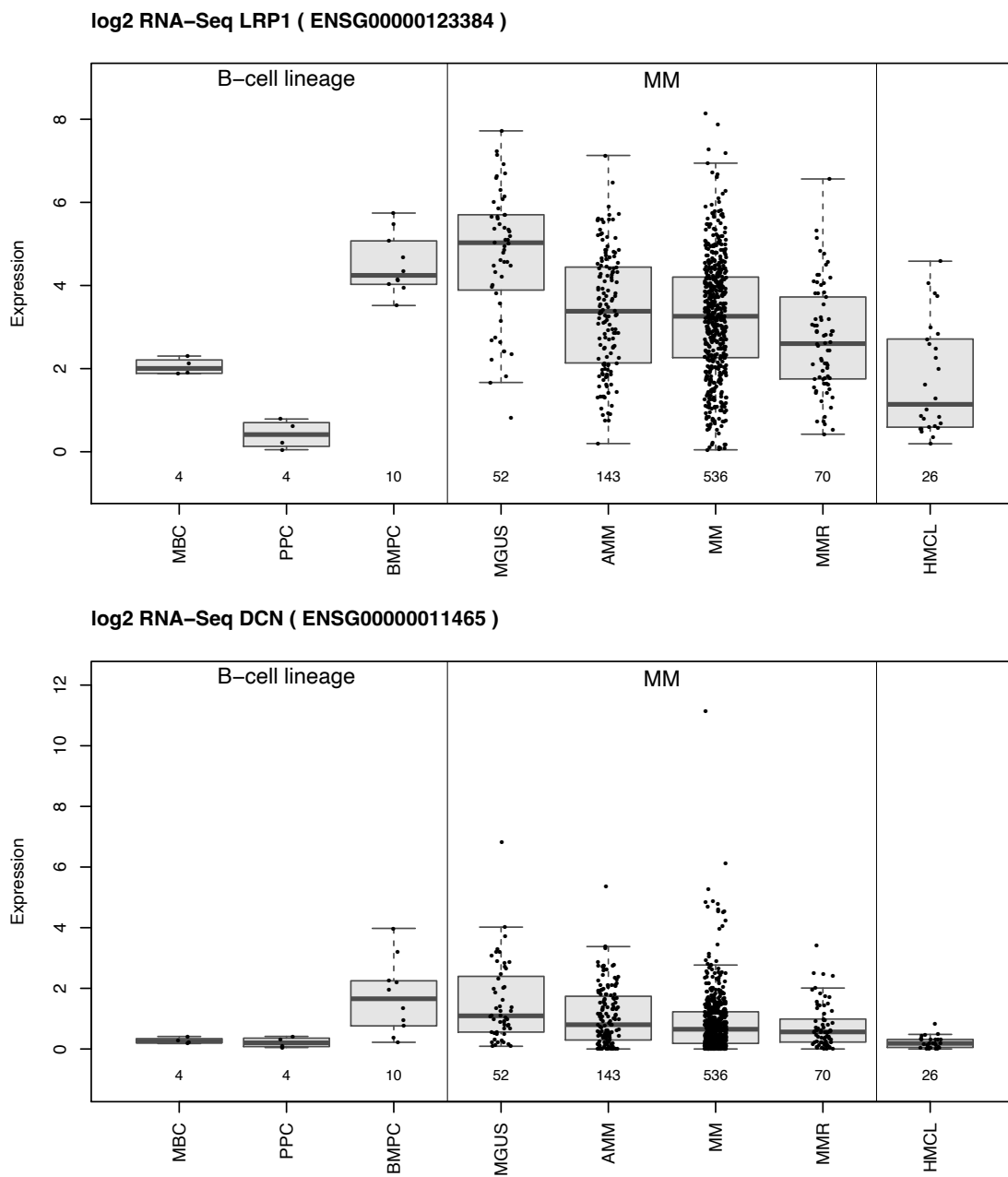
Appendix A.1 Figure 5: Correlation of RNAseq with qPCR Left: Validation of RNAseq results (Abbildung 4) with qPCR showing the \log_2 (foldchange expression) of 18 genes. For qPCR, Datapoints each represent one biological replicate ($n = 10$), which is the mean of technical replicates ($n = 3$). Bar height represents mean of biological replicates, error bars show standard deviation of biological replicates. Right: Correlation between qPCR and RNAseq in terms of \log_2 (mean foldchange expression per gene). Each dot represents one gene shown in the barplot to the left. Genes measured with qPCR that showed no differential expression in RNAseq were set to have a $-\log_2(FC) = 0$. Shaded area shows the confidence interval of linear regression. Correlation coefficient was calculated using Spearman's rank. $N = 18$ genes. FC: Fold change expression. This content has been taken as is from Kuric et al. (2024), published in *Cancer Research Communications* under the CC BY 4.0 license.



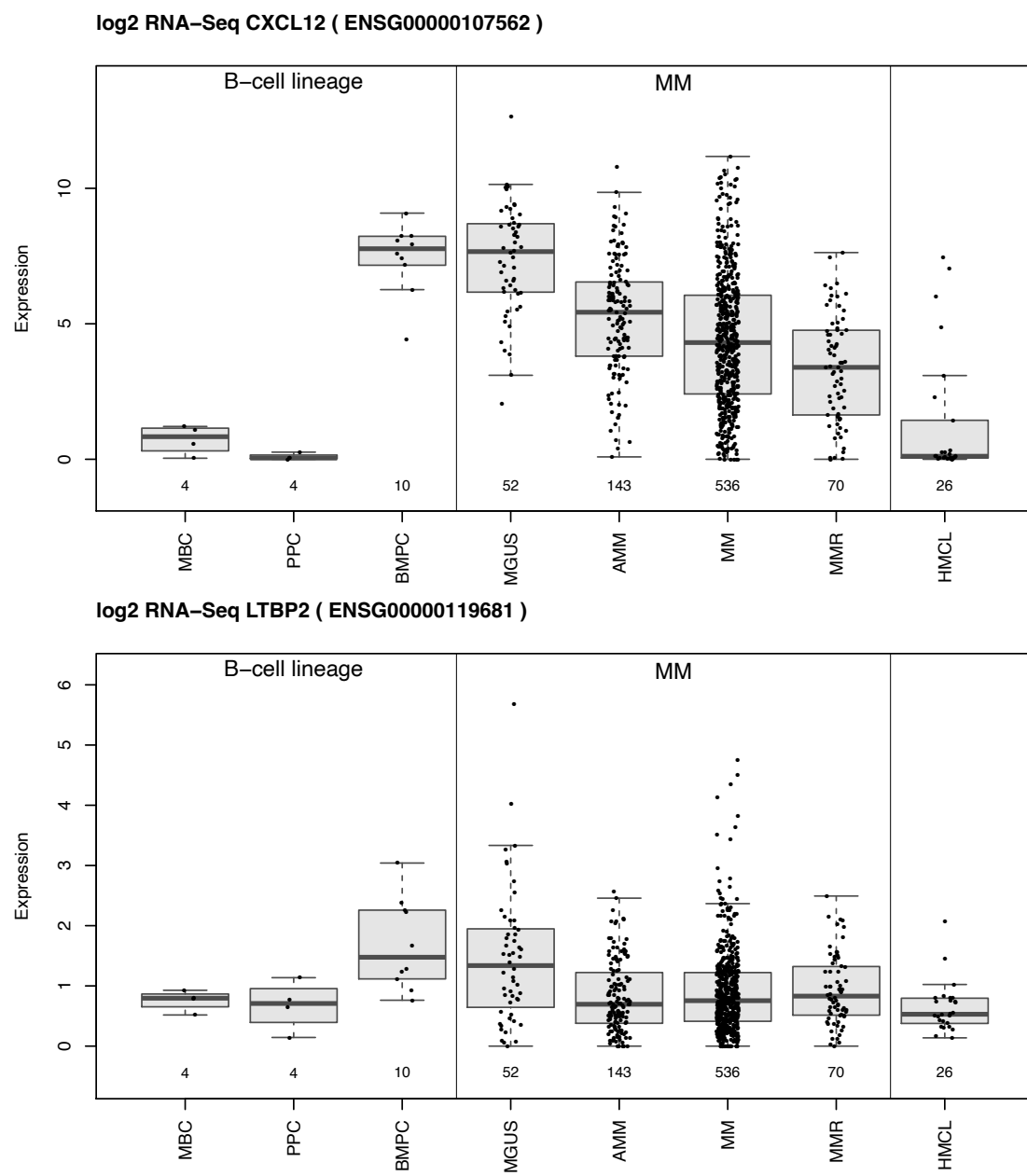
Appendix A.1 Figure 6: Functional enrichment analysis by Metascape using genes that are differentially expressed between MSC-interacting subpopulations. Top: Upregulated genes. Bottom: Downregulated genes. This content has been taken as is from Kuric et al. (2024), published in *Cancer Research Communications* under the CC BY 4.0 license.



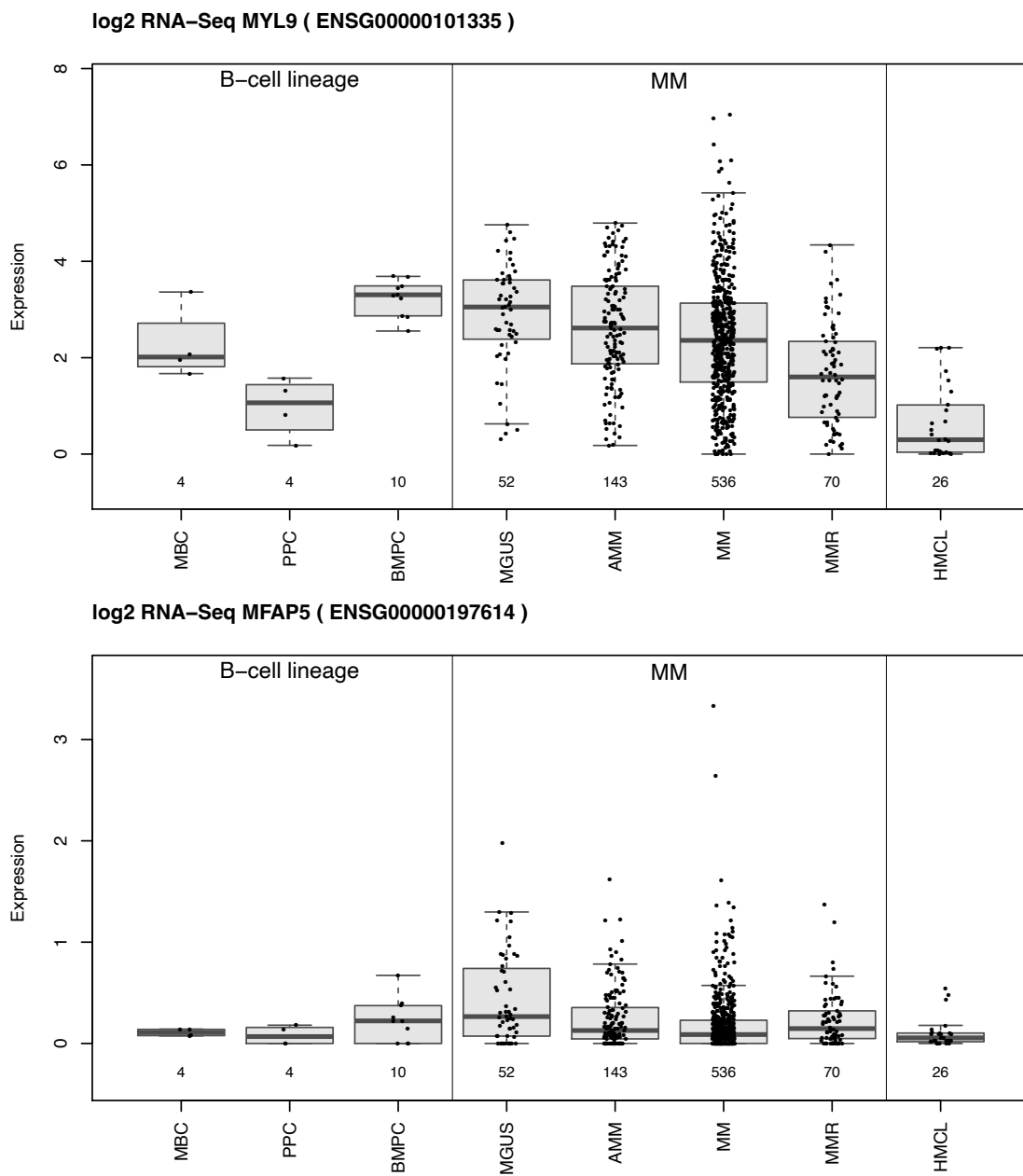
Appendix A.1 Figure 7: Expression levels of adhesion genes that are downregulated and associated with survival ($p < 0.01$). Bone Marrow Plasma Cell (BMPC), Monoclonal Gammopathy of Undetermined Significance (MGUS), Smoldering Multiple Myeloma (sMM), Multiple Myeloma (MM), Multiple Myeloma Relapse (MMR). This content has been taken as is from Kuric et al. (2024), published in *Cancer Research Communications* under the CC BY 4.0 license.



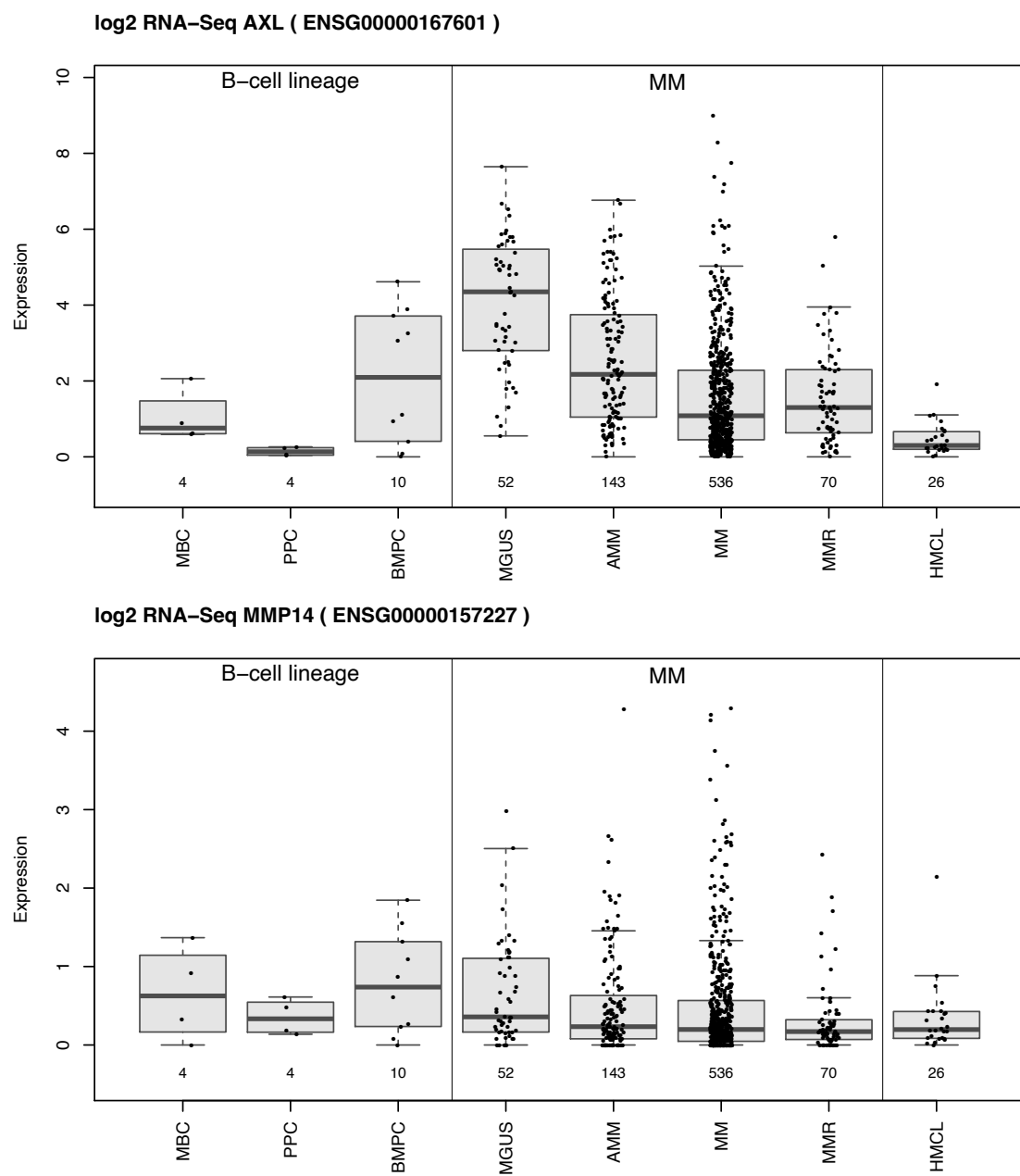
Appendix A.1 Figure 7: continued from previous page



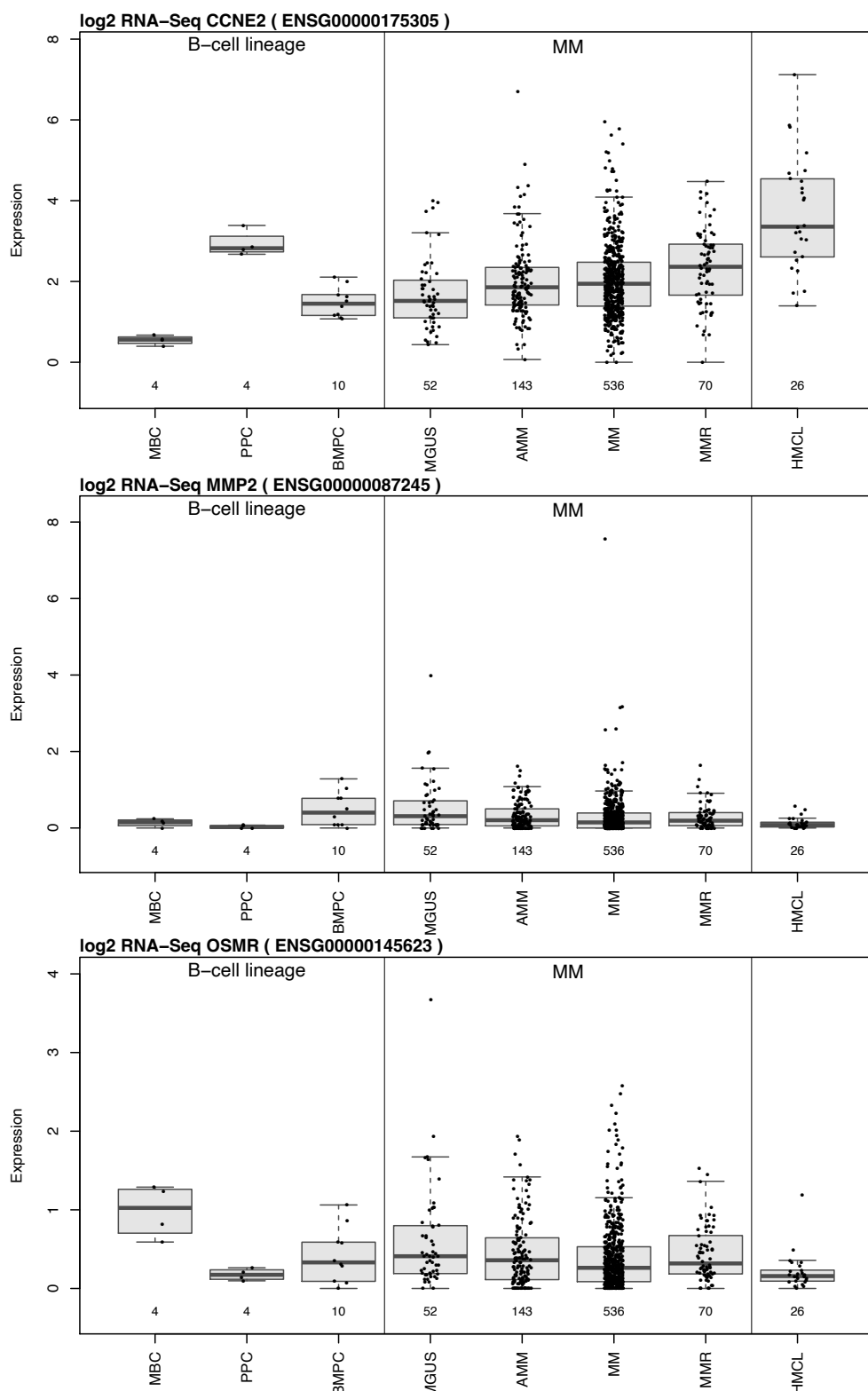
Appendix A.1 Figure 7: continued from previous page



Appendix A.1 Figure 7: continued from previous page



Appendix A.1 Figure 7: continued from previous page



Appendix A.1 Figure 8: Expression levels of adhesion genes that are not downregulated and associated with survival ($p < 0.01$). Bone Marrow Plasma Cell (BMPC), Monoclonal Gammopathy of Undetermined Significance (MGUS), Smoldering Multiple Myeloma (sMM), Multiple Myeloma (MM), Multiple Myeloma Relapse (MMR). This content has been taken as is from Kuric et al. (2024), published in *Cancer Research Communications* under the CC BY 4.0 license.

A.2 Tables

Appendix A.2 Table 1: List of hMSC donors, myeloma cell lines, and their mycoplasma test status. If no unique donors were available, hMSC donors were used twice for the same experiment at different passages. WPSC: Well plate sandwich centrifugation. This content has been taken as is from Kuric et al. (2024), published in *Cancer Research Communications* under the CC BY 4.0 license.

Cell Type	Donor / Line	Donor Ages	Donor Sex	Date of negative Mycoplasma test	Experiment(s)	Figures
Myeloma Cell Line	INA-6	80	m	09.02.22	All	All
	U266			10.10.22	- Validation of V-Well Adhesion Assay	S1E
	MM1.S			24.02.22		
hMSC	1639	49	m	not tested	- Validation of V-Well Adhesion Assay - Time-lapse: INA-6 on dispersed hMSC	S1E 1D; 2[A-E]
	1571	72	m	not tested	- Saturation of hMSCs	1[A-B]
	1573	47	m	not tested		
	1578	82	m	not tested		
	1842	63	m	not tested	- INA-6 Viability dependent on time and hMSC adhesion surface (INA not washed off)	1E right
	1843	60	m	not tested		
	1537	77	f	not tested		
	1794	82	m	not tested		
	1779	61	m	not tested	- INA-6 Viability dependent on time and hMSC adhesion surface (INA washed off)	1[C, E left]
	1849	69	m	not tested		
	1854	80	f	not tested		
	1605	71	f	not tested	- Time-lapse: INA-6 on dispersed hMSC	1D; 2[A-E]
	1650	57	m	not tested		
	1859	64	f	not tested	- Time-lapse: INA-6 on confluent hMSC	2[G-I]
	1863	79	f	not tested		
	1861	52	f	not tested		
	1818	81	f	not tested	- Cell Cycle Profiling after V-well assay	3C
	1824	82	f	not tested	(Donor measured twice, different passages) - V-well adhesion assay of mitotically blocked INA-6 followed by Cell Cycle Profiling after V-well assay	3[B,C]
	1827	56	m	not tested	- V-well adhesion assay of mitotically blocked INA-6 followed by Cell Cycle Profiling after V-well assay	3[B,C]
	1501	59	m	not tested	- INA-6 AI-assisted count during WPSC (INA-6 stained with celltracker green)	4B
	1643	75	f	not tested		

continued on next page

Appendix A Tabelle 1 – continued from previous page

hMSC	1718	67	m	not tested		
	1720	58	m	not tested		
	1653	65	m	not tested		
	1591	78	m	not tested	- WPSC (MACS) followed by RNA-seq, Metascape analysis, and qPCR validation	4[A,C,D,E]; 5[A-C]
					- WPSC (Wash) followed by qPCR-Validation and Luminescent Viability assays	4[C-E], 4F
	1654	74	m	not tested	- WPSC (MACS) followed by RNA-seq, Metascape analysis, and qPCR validation	4[A,C,D,E]; 5[A-C]
					- WPSC (Wash) followed by qPCR-Validation and Luminescent Viability assays	4[C-E], 4F
	1655	78	f	not tested	- WPSC (MACS) followed by RNAseq, Metascape analysis, and qPCR validation	4[A,C,D,E]; 5[A-C]
	1668	80	f	not tested		
	1670	66	f	not tested		
	1701	81	m	not tested		
	1702	79	f	not tested	- WPSC (Wash) followed by qPCR-Validation and Luminescent Viability assays	4[C-E], 4F
	1600	77	m	not tested		
	1681	56	m	not tested	- WPSC (Wash) followed by Luminescent Viability assays	4F
	1672	65	m	not tested	- WPSC (Wash) followed by qPCR-Validation	4[C-E]

Appendix A.2 Table 2: Adhesion genes (from Abbildung 6A) categorized by a continuous down-regulation across disease progression. Bone Marrow Plasma Cell (BMPC), Monoclonal Gammapathy of Undetermined Significance (MGUS), Smoldering Multiple Myeloma (sMM), Multiple Myeloma (MM), Multiple Myeloma Relapse (MMR). p-adj. = adjusted p-values (Benj.-Hoch.). This content has been taken as is from Kuric et al. (2024), published in *Cancer Research Communications* under the CC BY 4.0 license.

Regulation during disease progression	Gene	Ensemble ID	Progression Free / Overall Survival	Better Prognosis with high/low expression	Association of expression with survival	
					[p-unc]	[p-adj]
False	ADAMTS1	ENSG00000154734	Prog. Free	low	0.031875	0.084719
			Overall	low	0.048755	0.120104
	ADAMTS2	ENSG00000087116	Prog. Free	high	0.63795	0.767059
			Overall	high	0.811174	0.890528
	BGN	ENSG00000182492	Prog. Free	high	0.38065	0.533967
			Overall	high	0.279004	0.426961
	CAVIN1	ENSG00000177469	Prog. Free	high	0.407479	0.548739
			Overall	high	0.210903	0.3492
	CCDC80	ENSG00000091986	Prog. Free	high	0.002038	0.015833
			Overall	high	0.023743	0.077356
	CCN1	ENSG00000142871	Prog. Free	high	0.285568	0.443729
			Overall	low	0.931563	0.961309
	CCN2	ENSG00000118523	Prog. Free	high	0.030562	0.083425
			Overall	high	0.002889	0.024263
	CCNE2	ENSG00000175305	Prog. Free	low	0.012138	0.046195
			Overall	low	0.000534	0.008638
	CDH11	ENSG00000140937	Prog. Free	high	0.413948	0.550115
			Overall	high	0.044627	0.117163
	CEMIP	ENSG00000103888	Prog. Free	high	0.798984	0.877146
			Overall	low	0.287022	0.428378
	COL12A1	ENSG00000111799	Prog. Free	high	0.340978	0.491983
			Overall	low	0.829338	0.900679
	COL16A1	ENSG00000084636	Prog. Free	low	0.281112	0.443629
			Overall	low	0.162895	0.293792
	COL4A1	ENSG00000187498	Prog. Free	high	0.040286	0.098969
			Overall	high	0.009472	0.039863
	COL4A2	ENSG00000134871	Prog. Free	high	0.0124	0.046195
			Overall	high	0.175895	0.3063
	COL5A1	ENSG00000130635	Prog. Free	high	0.368403	0.524066
			Overall	low	0.860512	0.914414
	COL6A3	ENSG00000163359	Prog. Free	low	0.103315	0.208697
			Overall	low	0.197836	0.336625
	COL8A1	ENSG00000144810	Prog. Free	high	0.680745	0.807636
			Overall	high	0.289334	0.428378
	CREB3L1	ENSG00000157613	Prog. Free	low	0.165978	0.310441
			Overall	low	0.047989	0.120104
	EDIL3	ENSG00000164176	Prog. Free	high	0.863476	0.899083
			Overall	low	0.496663	0.611744
	F3	ENSG00000117525	Prog. Free	high	0.091858	0.197397
			Overall	high	0.009177	0.039863
	FBN1	ENSG00000166147	Prog. Free	high	0.472247	0.603376
			Overall	low	0.401546	0.533633
	FLNC	ENSG00000128591	Prog. Free	high	0.18539	0.329735
			Overall	low	0.474071	0.598515
	FN1	ENSG00000115414	Prog. Free	high	0.843432	0.896701
			Overall	low	0.421268	0.552573
	FBN1	ENSG00000166147	Prog. Free	high	0.472247	0.603376
			Overall	low	0.401546	0.533633
	FLNC	ENSG00000128591	Prog. Free	high	0.18539	0.329735

continued on next page

Appendix A Tabelle 2 – continued from previous page

		Overall	low	0.474071	0.598515
FN1	ENSG00000115414	Prog. Free	high	0.843432	0.896701
		Overall	low	0.421268	0.552573
FOSB	ENSG00000125740	Prog. Free	low	0.585138	0.712035
		Overall	high	0.942273	0.961309
GJA1	ENSG00000152661	Prog. Free	high	0.333512	0.491983
		Overall	low	0.34262	0.467631
GREM1	ENSG00000166923	Prog. Free	high	0.457976	0.59302
		Overall	low	0.591104	0.685623
HBEGF	ENSG00000113070	Prog. Free	low	0.145103	0.281656
		Overall	low	0.051592	0.124067
HTRA1	ENSG00000166033	Prog. Free	high	0.01203	0.046195
		Overall	high	0.040407	0.116603
IGFBP3	ENSG00000146674	Prog. Free	high	0.248011	0.410641
		Overall	low	0.841566	0.904236
IGFBP7	ENSG00000163453	Prog. Free	low	0.009533	0.043766
		Overall	low	0.024942	0.078722
ITGA11	ENSG00000137809	Prog. Free	high	0.97438	0.97438
		Overall	low	0.966513	0.976178
KLF11	ENSG00000172059	Prog. Free	low	0.229416	0.39273
		Overall	low	0.060892	0.133697
LAMB1	ENSG00000091136	Prog. Free	high	0.477921	0.603376
		Overall	high	0.604163	0.685623
LOX	ENSG00000113083	Prog. Free	low	0.748901	0.840433
		Overall	low	0.035028	0.104055
MMP2	ENSG00000087245	Prog. Free	high	2.29E-05	0.002316
		Overall	high	0.044615	0.117163
NFKBIZ	ENSG00000144802	Prog. Free	high	0.725256	0.832396
		Overall	high	0.310216	0.441293
NR4A1	ENSG00000123358	Prog. Free	high	0.0214	0.065497
		Overall	high	0.060042	0.133697
NR4A2	ENSG00000153234	Prog. Free	high	0.275313	0.441375
		Overall	high	0.11176	0.217072
OSMR	ENSG00000145623	Prog. Free	high	0.000567	0.007153
		Overall	high	0.01287	0.046422
PDGFRB	ENSG00000113721	Prog. Free	high	0.691005	0.807636
		Overall	high	0.599357	0.685623
POSTN	ENSG00000133110	Prog. Free	low	0.858041	0.899083
		Overall	low	0.496348	0.611744
PTX3	ENSG00000163661	Prog. Free	high	0.020943	0.065497
		Overall	high	0.045241	0.117163
PXDN	ENSG00000130508	Prog. Free	low	0.403966	0.548739
		Overall	low	0.172495	0.305648
SERPINE1	ENSG00000106366	Prog. Free	low	0.543711	0.669693
		Overall	high	0.869146	0.914414
SERPINH1	ENSG00000149257	Prog. Free	low	0.001825	0.015833
		Overall	low	0.004399	0.026138
SIX1	ENSG00000126778	Prog. Free	high	0.784446	0.870649
		Overall	high	0.592089	0.685623
SMAD3	ENSG00000166949	Prog. Free	low	0.027411	0.0791
		Overall	low	0.016437	0.055338
SPARC	ENSG00000113140	Prog. Free	high	0.073989	0.162455
		Overall	high	0.244069	0.391285
SPOCK1	ENSG00000152377	Prog. Free	low	0.531524	0.662765
		Overall	low	0.303273	0.437579
SULF1	ENSG00000137573	Prog. Free	high	0.190403	0.331564
		Overall	high	0.388706	0.523458
THBS2	ENSG00000186340	Prog. Free	low	0.318676	0.480392
		Overall	high	0.292654	0.428378

continued on next page

Appendix A Tabelle 2 – continued from previous page

	VPS37B	ENSG00000139722	Prog. Free	low	0.1478	0.281656
			Overall	low	0.199975	0.336625
True	ACTN1	ENSG00000072110	Prog. Free	high	0.170661	0.313396
			Overall	high	0.007728	0.035478
	ADAM12	ENSG00000148848	Prog. Free	high	0.019179	0.062487
			Overall	high	0.081847	0.168704
	AEBP1	ENSG00000106624	Prog. Free	high	0.010829	0.046195
			Overall	high	0.057228	0.133697
	AXL	ENSG00000167601	Prog. Free	high	0.001496	0.015105
			Overall	high	3.64E-05	0.00184
	CD99	ENSG00000002586	Prog. Free	low	0.916833	0.941333
			Overall	low	0.083964	0.169607
	COL1A1	ENSG00000108821	Prog. Free	high	0.000303	0.004367
			Overall	high	0.000593	0.008638
	COL1A2	ENSG00000164692	Prog. Free	high	0.298023	0.456066
			Overall	high	0.566636	0.673297
	COL3A1	ENSG00000168542	Prog. Free	high	0.025985	0.07719
			Overall	high	0.010794	0.042917
	COL5A2	ENSG00000204262	Prog. Free	low	0.74501	0.840433
			Overall	low	0.99967	0.99967
	COL6A1	ENSG00000142156	Prog. Free	high	0.011972	0.046195
			Overall	high	0.011048	0.042917
	COL6A2	ENSG00000142173	Prog. Free	high	0.261528	0.426037
			Overall	high	0.3235	0.447582
	CXCL12	ENSG00000107562	Prog. Free	high	0.000116	0.002927
			Overall	high	0.000648	0.008638
	CXCL8	ENSG00000169429	Prog. Free	low	0.839416	0.896701
			Overall	high	0.224913	0.366391
	CYP1B1	ENSG00000138061	Prog. Free	high	0.008641	0.041735
			Overall	high	0.000684	0.008638
	DCN	ENSG0000011465	Prog. Free	high	0.004827	0.030473
			Overall	high	0.000247	0.008327
	DUSP1	ENSG00000120129	Prog. Free	high	0.695686	0.807636
			Overall	high	0.454061	0.583718
	FBLN1	ENSG00000077942	Prog. Free	high	0.002676	0.019305
			Overall	high	0.003734	0.026138
	GNB3	ENSG00000111664	Prog. Free	high	0.003748	0.025234
			Overall	high	0.005734	0.03048
	GSTP1	ENSG00000084207	Prog. Free	high	0.972219	0.97438
			Overall	low	0.668091	0.749746
	IGFBP4	ENSG00000141753	Prog. Free	high	0.008677	0.041735
			Overall	high	0.007089	0.034093
	IL1R1	ENSG00000115594	Prog. Free	high	0.126318	0.250159
			Overall	high	0.256501	0.398563
	ITGA5	ENSG00000161638	Prog. Free	high	0.094893	0.19967
			Overall	high	0.159113	0.29219
	ITGAX	ENSG00000140678	Prog. Free	high	0.006717	0.036021
			Overall	high	0.003123	0.024263
	ITGB5	ENSG00000082781	Prog. Free	low	0.436018	0.57192
			Overall	high	0.539497	0.648681
	LAMA4	ENSG00000112769	Prog. Free	high	0.018518	0.062345
			Overall	high	0.104178	0.206314
	LAMB2	ENSG00000172037	Prog. Free	high	0.015472	0.053885
			Overall	high	0.001354	0.013865
	LOXL2	ENSG00000134013	Prog. Free	high	0.808671	0.878235
			Overall	low	0.933264	0.961309
	LRP1	ENSG00000123384	Prog. Free	high	0.006458	0.036021
			Overall	high	0.000434	0.008638
	LTBP2	ENSG00000119681	Prog. Free	high	9.03E-05	0.002927
			Overall	high	0.011656	0.043603

continued on next page

Appendix A Tabelle 2 – continued from previous page

True	LUM	ENSG00000139329	Prog. Free	high	0.05158	0.118399
		Overall	high	0.065084	0.139862	
	MAP3K8	ENSG00000107968	Prog. Free	high	0.000958	0.010755
			Overall	high	0.01617	0.055338
	MAP4K4	ENSG00000071054	Prog. Free	high	0.041155	0.098969
			Overall	high	0.31743	0.445284
	MFAP5	ENSG00000197614	Prog. Free	high	0.000243	0.004094
			Overall	high	0.004269	0.026138
	MMP14	ENSG00000157227	Prog. Free	high	6.93E-05	0.002927
			Overall	high	0.006691	0.033787
	MXRA5	ENSG00000101825	Prog. Free	high	0.034865	0.088035
			Overall	high	0.033819	0.103505
	MYL9	ENSG00000101335	Prog. Free	high	0.000146	0.00295
			Overall	high	1.56E-05	0.001572
	NRP1	ENSG00000099250	Prog. Free	high	0.001888	0.015833
			Overall	high	0.002212	0.020312
	PAPLN	ENSG00000100767	Prog. Free	high	0.034256	0.088035
			Overall	high	0.159113	0.29219
	TEX14	ENSG00000121101	Prog. Free	high	0.237488	0.399771
			Overall	low	0.518581	0.631044
	TGFB1	ENSG00000120708	Prog. Free	high	0.102621	0.208697
			Overall	high	0.004299	0.026138
	TGM2	ENSG00000198959	Prog. Free	high	0.058634	0.131601
			Overall	high	0.119621	0.227958
	THBS1	ENSG00000137801	Prog. Free	high	0.39286	0.543545
			Overall	high	0.456572	0.583718
	TNC	ENSG00000041982	Prog. Free	high	0.012806	0.046195
			Overall	high	0.004752	0.026663
	TNS1	ENSG00000079308	Prog. Free	high	0.338737	0.491983
			Overall	high	0.757617	0.840872
	TPM1	ENSG00000140416	Prog. Free	high	0.029263	0.0821
			Overall	high	0.001373	0.013865
	TUBA1A	ENSG00000167552	Prog. Free	low	0.006776	0.036021
			Overall	low	0.042929	0.117163
	TUBB6	ENSG00000176014	Prog. Free	low	0.186088	0.329735
			Overall	low	0.060071	0.133697
	VCAN	ENSG00000038427	Prog. Free	high	0.042782	0.100487
			Overall	high	0.080757	0.168704
	ZFP36L1	ENSG00000185650	Prog. Free	high	0.922693	0.941333
			Overall	high	0.24957	0.393852

Appendix A.2 Table 3: List of primers. Some primers required a melting step to be performed before fluorescent readout to remove byproducts. This content has been taken as is from Kuric et al. (2024), published in *Cancer Research Communications* under the CC BY 4.0 license.

Primer	Sequence 5' - 3'	base pairs [bp]	annealing temp. [°C]
36B4_s	tgcatacgatccccattctatcat	122	60
36B4_as	aggcagatggatcagccaaga		
BCL6_s	tagagcccataaaacggtccat	221	55 + Melting Step at 77 °C
BCL6_as	cgc当地attgagccgagatgtgt		
BMP4_s	tacatgcggatcttaccg	132	58
BMP4_as	atgttcttcgtggtaagc		
BTG2_s	gtattcttgttaggccgacactaa	264	60 + Melting Step at 78 °C
BTG2_as	tcttaagggtattcggtttggaa		
CXCL8_s	actgagagtattgagatggacc	251	55 + Melting Step at 77 °C
CXCL8_as	ccctacaacagacccacacaatac		
CXCL12_s	gattttcgaaagccatgttcca	119	56
CXCL12_as	caatgcacacttgtctgttgtt		
DCN_s	caacaacaagcttaccagatcac	160	57
DCN_as	tggaaaagactcacaccgaataaga		
DKK1_s	gcactgatgagtactgcgctag	129	56
DKK1_as	ttttgcagtaattcccgggc		
IL10RB_s	gagtgaggctgtctgtgagcaa	139	55
IL10RB_as	cttgtaaacgcaccacagcaag		
IL24_s	caaacagttggacgtagaaggc	149	55
IL24_as	tggaaatgacacagggaaacaaacca		
LOX_s	ctgctcagattccccaaag	125	57
LOX_as	tggcatcaagcaggcatag		
MMP2_s	ttgttattgtatggcatcgctcaga	155	56
MMP2_as	cgtataccgcatcaatctttccg		
MMP14_s	cgc当地agattgtatgcgtc	140	57
MMP14_as	tcccttcccagactttgatg		
MUC1_s	gcagcctctcgatataacctg	200	58
MUC1_as	gttagtggggactcgctca		
NOTCH2_s	gtgcttgtgaacacttgtgcc	185	55
NOTCH2_as	cactcgcatctgttatccaccaatg		
OPG_s	no sequence available (Proprietary primers from Qiagen: QT00014294 TNFRSF11B_1_SG)		60
OPG_as			
PRICKLE1_s	cagaggtatatcatgaaggacggc	102	56
PRICKLE1_as	gtcccaccaaatatgttccccac		
TGM2_s	caacccctctcatcgagacttccg	100	58
TGM2_as	tcatccacgactccacccag		
TNFRSF1A_s	ctccttcaccgcttcagaaaaacc	153	55
TNFRSF1A_as	ttcactccaataatgcccgtactg		
TRAF5_s	tgc当地ctgttagataaaagaggatcatca	177	56
TRAF5_as	aacactgcacagggtgaaataagc		

A.3 Materials & Methods

Isolation and Culturing of Primary Human Bone Marrow-Derived Mesenchymal Stromal Cells

Primary human Mesenchymal Stromal Cells (MSCs) were obtained from the femoral head of patients (Appendix A: Tabelle 1) undergoing elective hip arthroplasty. Material was collected with written informed consent of all patients and the procedure was approved by the local Ethics Committee of the University of Würzburg (186/18). In brief, bone marrow was washed with MSC-medium (Dulbecco's modified Eagle's medium (DMEM/F12, Thermo Fisher Scientific, Darmstadt, Germany) supplemented with 10 % Fetal Calf Serum (FCS, Bio&Sell GmbH, Feucht, Germany, Fernandez-Rebollo et al. (2017)), 100 U/ml penicillin, 0.1 mg/ml streptomycin (Thermo Fisher Scientific), 50 µg/ml ascorbate and 100 nmol/l sodium selenite (both Sigma-Aldrich GmbH, Munich, Germany)) and centrifuged at 250 g for 5 min. The pellet was washed four times with MSC-medium and resulting supernatants containing released cells were collected. Cells were pelleted and cultured at a density of 1×10^9 cells per 175 cm² culture flask. After two days non-attached cells were washed away and adherent ones were cultivated in MSC-medium until confluence. Then, they were either frozen in liquid nitrogen or directly utilized for experiments. hMSC cultures were sustained for a maximum of two passages. All cells were cultured at 37 °C and at 5 % CO₂.

Culturing of Myeloma Cell Lines

The plasmacytoma cell line INA-6 [[RRID:CVCL_5209](#); DSMZ, Braunschweig, Germany, authenticated by DSMZ in 2014 (Burger et al., 2001; Gramatzki et al., 1994)] was cultivated in RPMI1640 medium (Thermo Fisher Scientific) supplemented with 20 % (v/v) FCS, 100 µg/ml gentamicin, 2 mmol/l L-glutamine (both Thermo Fisher Scientific), 1 mmol/l sodium pyruvate, 100 nmol/l sodium selenite (both Sigma Aldrich GmbH) and 2 ng/ml recombinant human interleukin-6 (IL-6; Miltenyi Biotec, Bergisch Gladbach, Germany). INA-6 were passaged three times per week by diluting them to 1×10^5 cells/ml, 2×10^5 cells/ml, or 4×10^5 cells/ml for 3, 2, and 1 days of culturing, respectively. MM.1S [[RRID:CVCL_8792](#)] (Greenstein et al., 2003), and U266 cells [[CVCL_0566](#)] (Nilsson et al., 1970) were propagated and cultivated in RPMI1640 medium comprising 10 % (v/v) FCS, 100 U/ml penicillin, 100 µg/ml streptomycin, 2 mmol/l L-glutamine, and 1 mmol/l sodium pyruvate. All cells were cultured at 37 °C and at 5 % CO₂.

Co-Culturing of Primary hMSCs and INA-6 and MSC-Conditioning of Medium

For each co-culture, hMSCs were seeded out 24 h prior to INA-6 addition to generate MSC-conditioned medium (CM). CM from different donors was collected separately and used immediately when adding INA-6. To ensure that CM was free of hMSCs, it was strained (40 µm) and centrifuged for 15 min at 250 g. INA-6 cells were washed with PBS (5 min, 1200 rpm), resuspended in MSC-medium and added to hMSCs such that co-culture comprised 33 % (v/v) of CM gathered directly from the respective hMSC-donor. Co-cultures did not contain IL-6 (Chatterjee et al., 2002).

Collagen I Coating

Collagen I solution (isolated from rat tail, Corning, NY, USA) was diluted 1:2 (75 ng/mL) in acetic acid (0.02 N), applied to 96-well plates (30 µL in each well) and incubated for 2 h at room temperature. Acetic acid was removed and wells were washed once with 100 µL of PBS. Coated plates were stored dry at 4 °C.

Fluorescent Staining of Cells

For each live staining, cells were strained (70 µm) to remove clumps and washed (5 min, 250 g) once with the respective media (without FCS) and then resuspended in staining reagents. For *CellTrackerTMGreen CMFDA Dye* and *CellTrackerTMDeep Red Dye* (Thermo Fisher Scientific) staining, 1 mL staining solution for a maximum of 1×10^6 cells was prepared. Staining was done at room temperature (RT) for 15 min using 5 µM CMFDA (5-Chlormethyl-fluoresceindiacetat) and 5 min of 1–2 µM DeepRed. To reduce background, stained cells were pelleted, resuspended in cell medium (containing FCS), incubated for 30 min (37 °C, 5% CO₂), washed in cell medium, resuspended in 100–1000 µL and counted.

For PKH26 staining (Sigma Aldrich GmbH), a maximum of 1×10^4 cells was resuspended in 500 µL diluent C before swiftly adding 500 µL of staining solution (1 µL diluted in 500 µL diluent C) and incubating cells for 5 min at RT. The staining reaction was stopped by adding 1 mL of FCS-containing medium and adding 3 mL of FCS-free medium. Cells were washed with 10 mL of FCS-containing medium, resuspended in 100–1000 µL cell medium, and counted.

For Calcein-AM (Calcein-O,O'-diacetat-tetrakis-(acetoxyethyl)-ester) (Thermo Fisher Scientific) staining, end concentrations of 0.5 µM were used. 12.5 µL of diluted stock solution (2.5 µM) was carefully added to 50 µL of the co-culture and incubated for 10 min at 37 °C.

For Hoechst 33342 staining, cells were washed once with PBS, resuspended in a maximum of 500 µL of PBS, and fixed with 5 mL of ice-cold ethanol (70 % v/v) by vigorously pipetting up and down to dissociate aggregates. Cells were washed once with PBS and stained with 2.5 µg/mL Hoechst 33342 (Thermo Fisher Scientific) diluted in PBS for 1 hour at 37 °C.

Automated Fluorescence Microscopy

To remove clumps for microscopic applications, we cultured cells in 40 µm strained medium containing FCS. To reduce background fluorescence and phototoxicity, we used phenol-red free versions of the respective medium, if available.

All microscopy equipment was acquired from ZEISS. The microscope was an *Axio Observer 7* with confocal *ApoTome.2* equipped with a motorized reflector revolver and motorized scanning table (130 × 100 mm). The microscope was mounted on an Antivibrations-Set (Axio Observer (D)) with two antivibration carrier plates, each equipped with two vibration dampening feet. The light source was a *microLED 2* for transmission light and (for fluorescence) *Colibri 7* (R[G/Y]B-UV) for five channels of incident light (385 nm, 475 nm, 555 nm, 590 nm und 630 nm). For excitation (EX) and emission (EM) light filtering and beam splitting (BS) we used the following reflectors: *96 HE BFP shift free* (E) (EX: 390 / 40 nm, BS: 420 nm, EM: 450 / 40 nm), *43 HE Cy 3 shift free* (E) (EX: 550 / 25 nm, BS: 570 nm, EM: 605 / 70 nm), *38 HE eGFP shift free* (E) (EX: 470 / 40 nm, BS: 495 nm, EM: 525 / 50 nm) and *90 HE LED* (E) (EX: 385 + 475 + 555

+ 630 nm, BS: 405 + 493 + 575 + 653 nm, EM: 425/30 + 514/30 + 592/30 + 709/100 nm). We used the black and white camera *Axiocam 506 mono* (D) and if not stated otherwise, 2 × 2 binning was used for fluorescence imaging. For mosaic acquisitions (“tiles”) we used a tiling overlap of 8–10 % and image tiles were not stitched. Images were magnified 5x and 10x (*Fluar 5x/0.25 M27* and *EC Plan-Neofluar 10x/0.3 Ph1 M27*).

Cell Viability and Apoptosis Assay

To examine cell viability and apoptosis, cells were seeded in a 96-well plate (1×10^4 cells per well) to be measured inside culture wells after respective incubation time immediately. ATP-amount and Caspase 3/7 activity were used as a proxy for viability and apoptosis rates, respectively. They were assessed using the *CellTiter-Glo Luminescent Cell Viability Assay* and the *Caspase-Glo 3/7 Assay*, respectively (Promega GmbH, Mannheim, Germany), according to the manufacturer’s instructions. Luminescence was measured with an Orion II Luminometer (Berthold Detection Systems, Pforzheim, Germany).

Microscopic Characterization of hMSC Saturation

For saturating hMSC with INA-6, hMSCs were stained with *CellTracker Green*, plated out on 384-well plates (Greiner Bio-One GmbH, Frickenhausen, Germany) at 5×10^3 hMSC/cm² and cultured for 24 h. INA-6 cells were stained with *CellTracker DeepRed*, resuspended in MSC-medium, added to adhering hMSCs in different amounts (5×10^3 INA6/cm², 1×10^3 INA6/cm², 2×10^3 INA6/cm²) and co-cultured for 24 h and 48 h. The complete co-culture was scanned and the number of INA-6 cells adhering to one hMSC was counted manually for 100 MSCs for each technical replicate. Fluorescent images were digitally re-stained (INA-6 green, hMSC inverse black).

Analysis of INA-6 Survival and Aggregation Depending on hMSC Confluence

To describe aggregate growth and survival of INA-6 depending on hMSC density, unstained hMSCs were seeded out into 96-well plates (white, clear bottom, Greiner) at different densities (see Seeding Table). To ensure nutrient supply, we used lower cell densities for longer co-culturing durations while maintaining constant ratios of INA-6 to adhesion surface provided by hMSCs. Those plates that were to be assessed after 72 h of co-culturing received an additional 100 µL of fresh MSC-medium after 24 h of co-culturing (total volume of 300 µL), and after 48 h of co-culturing, 100 µL was gently removed from the co-culture and carefully replaced with fresh MSC-medium without disturbing the co-culture on the bottom.

To describe aggregate growth, complete wells were scanned using 10x magnification, phase contrast, 2 × 2 binning, and autofocus focusing on each tile both before and after harvesting. Afterwards, INA-6 cells were harvested for measuring viability and apoptosis.

For luminescent assessment of cell survival, INA-6 cells were harvested by removing co-culture medium, adding 150 µL of MSC-medium, and then stirred by strongly pipetting up and down twice while aiming the pipette tip at the upper corner, lower left, and lower right of the well bottom (‘Mercedes star’). Washing and stirring was repeated once before washing wells again with 150 µL MSC-medium. Harvested INA-6 cells were strained (40 µm filter), pelleted, and resuspended in 200 µL MSC-medium.

Seeding Table: Seeding densities for describing growth and survival of INA-6 depending on hMSC density. Co-cult. dur.: Co culturing duration; MSC-adh. surface: adhesion surface provided by hMSCs; vol.: volume. This content has been taken as is from Kuric et al. (2024), published in *Cancer Research Communications* under the CC BY 4.0 license.

Co-cult. dur. [h]	hMSC density [1000 hMSC/cm ²]	INA-6 density [1000 INA6/cm ²]	Ratios INA : MSC (adh. surface)	Seeding vol. [μ L]	End vol. [μ L]
24	2, 10, 40	10	1:0.2, 1:1, 1:confluent	200	200
48	1, 5, 40	5	1:0.2, 1:1, 1:confluent	200	200
72	1, 5, 40	5	1:0.2, 1:1, 1:confluent	200	300 [after 24 h: +100], [after 48 h: exchange 100]

Cells were counted using Neubauer chambers, re-distributed into 96-well plates (white, clear bottom) with 1×10^5 INA-6 cells per well, and then subjected to viability and apoptosis assays.

To minimize the loss of sensitive apoptotic cells, another approach was used to measure viability and apoptosis without harvesting INA-6 cells. hMSCs and INA-6 were seeded out individually in parallel to the co-cultures. Prior to measuring viability and apoptosis, culture volume was adjusted to 150 μ L by removing 50 μ L or 150 μ L for the timepoints 48 h or 72 h, respectively (carefully not to stir up culture on bottom). 100 μ L of luminescent reagents were then added directly to 150 μ L of co-culture. The fold change of viability or apoptosis that is due to MSC interaction ($FC_{\text{MSC Interaction}}$) was then calculated using the following formula, with L being the mean of four technical replicates measured in relative luminescent units per seconds [RLU/s], and $L_{\text{Co Culture}}$, L_{MSC} , $L_{\text{INA-6}}$ the luminescence measured in the co-culture, hMSCs alone, and INA-6 alone, respectively.

$$FC_{\text{MSC Interaction}} = \frac{L_{\text{Co Culture}}}{L_{\text{MSC}} + L_{\text{INA-6}}}$$

Time-Lapse Characterization of INA-6 Aggregation, Detachment and Division

In order to record the aggregation and detachment of INA-6 in contact with hMSCs, hMSCs (5×10^3 cells/cm²) were fluorescently stained with PKH26 and plated onto 8-well μ -Slides (ibidi, Gräfelfing, Germany). hMSCs were incubated for 24 h before being placed into an ibidi Stage Top Incubation System and were equilibrated to the incubation system for a minimum of 3 h (80 % humidity and 5 % CO₂). INA-6 cells (2×10^4 cells/cm²) were washed and resuspended in 33 % (v/v) MSC-conditioned medium before adding them directly before acquisition start in a small volume (10 μ L). Brightfield and fluorescence images of 13 mm² of co-culture were acquired every 15 minutes for 63 h. Movement speed of the motorized table was adjusted to the lowest setting that allows acquisition of the complete region within 15 minutes.

Respective events of interest were analyzed manually and categorized into defined event parameters. Events were binned across the time axis using these boundaries: [0.0, 12.85, 25.7, 38.55, 51.4, 64.25]. We collected a minimum of events per recording and analysis so that each time bin contained at least 5 values, except when analyzing detachment events, since these did not appear before 20 h of incubation for some replicates. For each recording and event parameter, the event count was normalized by dividing by the total number of events per time bin.

We determined the frequency and the cause of aggregation by looking for two interacting INA-6 cells and went backward in time to see if they were two daughter cells or if two independent INA-6 cells had

collided. We determined the frequency of aggregates with detaching cells by tracing their growth across the complete time-lapse and looking for detachment events. We picked random 100 aggregates by including aggregates from both the border and center of the well.

We characterized detachment events by noting multiple parameters manually: Time point of detachment, aggregate size (at the time of detachment), the last interaction partner, and the number of detaching INA-6 cells.

For characterizing cell division events, we recorded a new set of time-lapse videos using unstained hMSCs that were grown to confluence for 24 h (4×10^4 hMSCs/cm²) to provide for unlimited adhesion surface. We categorized daughter cells in terms of their mobility (mobility being the speed of putative movements or “rolling”). The mobility criteria were met if one INA-6 daughter cell moved farther than half a cell radius within one frame (15 min) relative to the MSC-adherent INA-6 cell which was required to stand still in-between respective frames. We measured the “rolling” duration by subtracting the time point of the last perceived movement from the time point of division. We excluded those division events from the measurement of rolling duration if INA-6 cells underwent apoptosis shortly after division.

Cell Cycle Synchronization at M-Phase

INA-6 cells were arrested at mitosis by double thymidine (2 mM) treatments followed by 5 h of nocodazole (500 ng/mL) incubation. In detail: 3×10^5 cells/mL INA-6 in 4 mL were treated with 2 mM thymidine (Sigma Aldrich GmbH) for 16.5 h. Cells were released by washing them in INA-6 medium once and allowed to cycle for 9 h before treating them with 2 mM thymidine for 18 h a second time. Afterwards, cells were released and allowed to cycle for 2 h before treating them with 100 ng/mL nocodazole (Sigma Aldrich GmbH) for 5 h. Arrested INA-6 were released by washing them once and resuspending them in MSC-medium with 33 % MSC-conditioned medium. Cell cycle profile was checked using image cytometry (Appendix A: Abbildung 2).

V-Well Adhesion Assay

This assay was modified from (Weetall et al., 2001). 96 v-well plates were coated with collagen I (rat tail, Corning). Collagen coating ensures that confluent hMSCs withstand centrifugation even after hMSCs in the well tip were removed. hMSCs (4×10^4 cells/cm²) were seeded out and grown to confluence for 24 h in collagen-coated v-well plates. To ensure that only INA-6 are pelleted in the v-well tip, hMSCs were removed from the well-tip by touching the well-ground with a 10 µL pipette and roughly pipetting hMSCs away.

Arrested INA-6 (1×10^4 cells/cm²) were released by washing them once in PBS and resuspending them in 33 % (v/v) MSC-conditioned medium before adding them on top of confluent hMSCs. INA-6 adhered for 1, 2, 3, and 24 h before the complete co-culture was stained with 0.5 µM Calcein-AM (10 min at 37 °C). Non-adherent INA-6 were pelleted by centrifugation using a Hettich 1460 rotor ($r = 124$ mm) at 2000 rpm (555 g) for 10 min.

The well tip was imaged by fluorescence microscopy with 5x magnification, 96 HE emission filter, auto-focus configured for maximum signal intensity, 2 × 2 binning and 14 bit grayscale depth. Pellet brightness was analyzed in ZEN 2.6 (Zeiss) by summing up pixel brightnesses across the complete pellet image.

Background brightness was acquired from a cell culture with only hMSCs. Reference brightness was acquired from a cell culture with only INA-6, defining 100 % pellet brightness without adhesion. Background intensity was subtracted before normalizing by reference. Outliers were removed from technical replicates ($n = 4$) if their z-score was larger than 1.5σ technical variation.

After measuring pellet brightnesses, the cell pellet was removed by pipetting 10 μL from the well tip. Pellets of the same technical replicates were pooled, washed in PBS, resuspended in 200 μL PBS, added to 1.8 mL ice-cold 70 % ethanol, and stored at -20°C . Remaining non-MSC-adhering INA-6 cells were removed by replacing culture medium with 100 μL of medium. MSC-adherent INA-6 were manually detached by rapid pipetting and equally pelleted, analyzed, and isolated.

Cell Cycle Profiling

INA-6 cells were fixed in 70 % ice-cold ethanol, washed, resuspended in PBS, distributed in 96-well plates, and stained with Hoechst 33342 (2.5 $\mu\text{g}/\text{mL}$ in PBS) for 1 h at 37°C . For image cytometric cell cycle profiling, plates were scanned completely using automated fluorescence microscopy with 5x magnification, 96 HE emission filter, 1 \times 1 binning, 14 bit depth, and an illumination time that fills 70 % of the grayscale range. The autofocus was configured to re-adjust every second tile. A pre-trained convolutional neural network (“DeepFeatures 2 reduced”, *Intellessis*, Zeiss) was fine-tuned to segment scans into background, single nuclei, and fragmented nuclei. Nuclei were filtered to exclude fragmented nuclei and those nuclei with extreme size (within the range of 50–500 μm^2) and roundness (within the range of 0.4–1.0). Cell cycle profiles were normalized by the mode of the nucleus intensities within the G0/G1 peak. To retrieve frequencies of cells cycling in G0/G1, S, and G2 phase, the brightness distribution of all single nuclei was fitted to the sum of three Gaussian curves (“Skewed Gaussian Model” for G0/G1 and G2 phase, and “Rectangle Model” for S phase) using the python package LMFIT (Newville et al., 2014) (Appendix A: Abbildung 4). The Gaussian curves were used to calculate the cell frequencies for each cell cycle phase by integration using the composite trapezoidal rule implemented by numpy.trapz (Harris et al., 2020).

For validation of image cytometry, 5 mL of INA-6 stock culture was removed and ethanol fixed as described above. Flow cytometry analyses were performed using an *Attune Nxt Flow Cytometer* (Thermo Fisher Scientific). Data analyses were performed using FlowJo V10 software (TreeStar, USA).

Protocol: Well Plate Sandwich Centrifugation (WPSC)

96-well plates (flat bottom, clear) were coated with collagen I (rat tail, Corning) to ensure that confluent hMSCs withstand centrifugation and repeated washing. hMSCs (2×10^4 cells/cm 2) were seeded out and grown to confluence for 72 hours in collagen-coated 96-well plates. To remove aggregates from the medium and prevent clogging of magnetic columns, any FCS-containing fluid was strained with a 40 μm cell strainer.

- **Collect MSC-Conditioned Medium and Add INA-6:**

1. Collect hMSC-conditioned medium (CM) from the well plates and replace it with 100 μL of fresh hMSC medium. Collect CM from different donors separately.
2. Strain CM (40 μm) and centrifuge for 15 minutes at 250 g to ensure that CM does not contain

hMSCs.

3. Dilute CM by mixing 2 parts of CM with 1 part of MSC-medium (dilute 1.5 fold).
4. Count INA-6 cells and retrieve enough cells to fill all 96 wells with 2×10^4 INA6/cm² (6.8×10^4 cells per well, covering approximately 65 % of the well bottom).
5. Centrifuge INA-6 (5 minutes, 250 g) and resuspend them in a volume of diluted CM to reach a concentration of 6.8×10^5 INA6/mL.
6. Add 100 µL INA-6 suspension to hMSCs (end volume: 200 µL; end concentration: 33 % (v/v) hMSC-conditioned medium).
7. Incubate for 24 hours at 37 °C and 5 % CO₂.
- **Prepare CM-INA6 Reference:**
 8. Add 100 µL of fresh MSC-medium into each well of an empty 96-well plate (not coated).
 9. Add 100 µL of INA-6 suspension (6.8×10^5 INA-6/mL in diluted CM).
 10. Incubate for 24 hours at 37 °C and 5 % CO₂.
- **Collect CM-INA6 and nMA-INA6:**
 11. Pre-warm well plate centrifuge to 37 °C.
 12. Prepare a counter-weight by filling 200 µL of water into all wells of an empty 96-well plate.
 13. Prepare well-plate sandwiches:
 - a. Turn an empty 96-well plate (“catching plate”) upside down and place one on top of the co-culture-plate, the CM-INA6 reference plate, and the counter-weight so that all well openings align.
 - b. Fix well plates using tape with reusable adhesive (e.g., *Leukofix*).
 14. Turn both plates around. Medium will spill from the co-culture plate into the catching plate.
 15. Centrifuge plate for 40 seconds at 1000 rpm with the catching plate facing the ground.
 16. Remove the adhesive tape and the co-culture plate.
 17. Turn the co-culture plate around and add 30 µL of washing medium (MSC-medium 0% FCS, 3 mM EDTA) gently by touching the wall of each well and pressing the pipette slowly.
 - a. Work quickly to ensure that co-culture does not dry. We recommend using a multipette (Eppendorf).
 - b. Many nMA-INA6 are removed by physical force applied by adding 30 µL of medium and not just by centrifugation. Hence, it is critical to apply the same dispensing technique across all replicates. We recommend using a multipette (Eppendorf) that can apply 30 µL with controllable pressure, since its push-button retains a long pushing path even for dispensing small volumes, unlike push-buttons from the usual 100 µL pipettes that reduce the pushing-path for smaller volumes.
 - c. Centrifugation minimizes technical variability by replacing one step of manual pipetting. Also, it ensures that confluent MSCs remain unharmed. Manual pipetting on the other hand would require touching the well-bottom to remove all fluids which damages the adhesive hMSC layer.
 18. Turn the co-culture plate upside down, place it onto the catching plate and re-apply adhesive tape to fix the well plate sandwich.
 19. Repeat steps 14-18 two more times until the catching plate contains 290 µL of medium in each well.

20. Pool CM-INA6 from the catching plate that was fixed to the reference plate.
21. Pool nMA-INA6 from the catching plate that was fixed to the co-culture plate.
22. Collect remaining INA-6 by adding 100 µL of PBS into each well of the catching plates, collect and pool with CM-INA6 or nMA-INA6.
23. Strain CM-INA6 and nMA-INA6 using 40 µm cell strainer.
24. Isolate MA-INA6 by continuing with either accutase dissociation or rough pipetting.
- **Collect MA-INA6 by Accutase Dissociation Followed by MAC Sorting:**
25. Block 2 mL tubes with sorting buffer (PBS, 2 mM EDTA, 1% BSA) for 1 hour at 4 °C.
26. Dilute accutase (Sigma Aldrich GmbH) (400 to 600 units/mL) 4-fold in cold PBS. Always keep accutase on ice, since accutase loses activity at room temperature.
27. Add 50 µL of cold accutase (directly after the last centrifugation step) and incubate co-culture plate for 5 minutes at 37 °C.
28. Place a co-culture plate onto a shaker and shake for 1 minute at 300 rpm.
29. Collect cell suspension from wells and stop the reaction by adding 500 µL of FCS to pooled cell suspension.
30. Evaluate presence of adherent INA-6 cells and the integrity of confluent hMSCs under the microscope.
31. Repeat steps 27-30 until all INA-6 cells have dissociated or until confluent hMSCs start to tear.
32. Strain cell suspension (30 µm). This yields MA-INA6.
33. Pellet MA-INA6, nMA-INA6, and CM-INA6 (1200 rpm, 10 minutes).
34. Resuspend MA-INA6 in 86 µL sorting buffer (PBS, 2 mM EDTA, 1 percent BSA).
35. Resuspend CM-INA6 and nMA-INA6 in 300 µL cold diluted accutase and incubate for 3 minutes at 37 °C to ensure equal treatment for all samples.
36. Stop accutase by adding 200 µL of FCS (100 percent).
37. Pellet CM-INA6 and nMA-INA6 (1200 rpm, 10 minutes) and resuspend in 86 µL sorting buffer (PBS, 2 mM EDTA, 1 percent BSA).
38. Transfer samples into 2 mL tubes that were blocked with sorting buffer.
39. Add 10 µL of CD45 coated magnetic beads (Miltenyi Biotec B.V. & Co. KG, Bergisch Gladbach).
40. Place tubes into rotator and incubate for 15 minutes at 4 °C.
41. Continue with MAC sorting according to the manual. Use an MS column and wash 3 times.
42. Improve purity of eluted MA-INA6 by straining eluate (30 µm) (wash strainer using 1 mL of sorting buffer) and applying it onto an MS column a second time. Wash three times.
43. Collect 20 µL per eluate and apply it onto a 96 well plate to evaluate purity.
 - a. Incubate plate for 24 hours.
 - b. Count the number of adherent cells (hMSCs) per INA-6 using phase contrast microscopy.
 - c. We reached a mean purity of 3.2×10^{-4} ($\pm 2.2 \times 10^{-4}$) hMSCs per MA-INA6.
 - d. hMSC contamination did not have an impact on RNAseq, since those genes that are highly expressed in hMSCs (*DKK1*, *OPG*, *BCL6*, *BMP4*, *BTG2*, *IL10RB*, *IL24*, *NOTCH2*, *TNFRSF1A*, *TRAF5*, *TGM2*, *DCN*, *LOX*, *MMP14*, *MMP2*, *CXCL12*, *CXCL8*, *VCAM1*, *ALPL*,

FGF5, *FGFR2*), did not appear as differentially expressed in MA-INA6 (data not shown). RNAseq detected 0.44 ± 0.16 CPM-normalized counts of *VCAM1* transcripts in MA-INA6, however, it was excluded like all genes with less than 1 count in at least 2 of 5 replicates.

44. Count cells using a Neubauer chamber.
45. Pellet samples (250 g for 5 minutes).
46. Resuspend in respective medium or lysis buffer (e.g., RA1 for RNA extraction).
- **Collect MA-INA6 by Rough Pipetting (No MAC Sorting):**
47. After the last centrifugation step, add hMSC-medium to each well of the co-culture plate to reach a volume of 150 μL .
- a. Since the yield of MA-INA6 was large, we dissociated MA-INA6 cells from hMSCs by vigorous pipetting (for further samples after RNAseq, see Appendix A.2: Tabelle 1). Since no enzymatic digestion is used, we reckoned that there would be no need for MAC sorting. Confluent hMSCs withstand this procedure and don't dissociate as single cells, which can be removed by straining cells (30 μm). We reached similar purities as for MAC-sorting (data not shown).
48. Using a multi-channel pipette (100 μL), gently raise 90 μL into the tips.
49. Lean pipette tip on the upper well-border and roughly pipette up and down once.
50. Repeat step 48 at the lower right and lower left well border (Total of 3 pipetting steps “Mercedes Star”).
51. Attach a catching plate onto the co-culture and centrifuge for 40 seconds at 500 rpm (28 g).
52. Repeat steps 46-50 until a sufficient amount of MA-INA6 is removed.
53. Control purity of MA-INA6 by placing out aliquot onto an empty 96 well plate.
54. Collect MA-INA6 from catching plate.
55. Remove hMSCs by straining cell suspension (30 μm).
56. Count cells using a Neubauer chamber.
57. Pellet MA-INA6 (250 g for 5 minutes).
58. Resuspend in respective medium or lysis buffer.

Centrifugal Force: We used a Hettich 1460 rotor ($r = 124$ mm) (Hettich GmbH & Co. KG, Tuttlingen, Germany). For calculating the centrifugal force that acts onto the co-culture within well plate sandwiches, we subtracted the height of the catching plate (14.4 mm, Greiner 96-well plate) and the depth of each well (10.9 mm). This yields a radius of 98.7 mm, which translates to the following centrifugal forces: 500 rpm: 28 g; 1000 rpm: 110 g; 2000 rpm: 441 g.

Washing medium containing EDTA: Washing medium containing EDTA: EDTA removes calcium from integrins, which are required for adhesion. It is not strong enough to dissociate INA-6 from hMSCs, but could help with removing INA-6 from other INA-6. For generating samples for RNAseq, we added 3 mM of EDTA to the washing medium. For further samples, we did not add EDTA to the washing medium, since we found that it does not increase yield for all biological replicates consistently (data not shown). We suspect that integrin-mediated adhesion depends on hMSC donor or internal variance of INA-6. We recommend using 3 mM of EDTA, however, this requires further optimizations like including an incubation time at 37 °C after the addition of washing medium to account for biological variance. However, this could take long incubation times of up to 60 minutes (Lai et al., 2022).

Track Cell Number During WPSC

To track the cell count during WPSC, INA-6 cells were stained with *CellTracker green*, and both co-culturing and catching plates were scanned after each centrifugation step. For each round of centrifugation, an empty catching plate was used. A pre-trained convolutional neural network (*Intellesis*, Zeiss) was fine-tuned to segment the scans into background, cells, and cell borders. Single cells were counted, and the cumulative sum for each catching plate was calculated.

Sub-Culturing After WPSC of MSC-Interacting INA-6 Subpopulations

After CM-INA6, nMA-INA6, and MA-INA6 were isolated, they were counted with a Neubauer chamber using all nine quadrants and diluted to 1×10^5 cells/mL in MSC-medium (10% FCS, no IL-6 except for control). 100 µL of cell suspension was applied to 96-well plates, incubated for 48 hours at 37 °C and 5% CO₂, and then subjected to viability and apoptosis assays.

RNA Isolation

Total RNA was isolated from INA-6 cells using the *NucleoSpin RNA II Purification Kit* (Macherey-Nagel, Düren, Germany) according to the manufacturer's instructions.

RNaseq, Differential Expression and Functional Enrichment Analysis of INA-6 cells

FASTQ files were merged to the respective sample. The quality of FASTQ files was assessed with FastQC (Andrews, 2010) and a joint report was created with MultiQC (Ewels et al., 2016). FASTQ files were aligned with STAR (Dobin et al., 2013) to the GRCh38 reference genome build (Zerbino et al., 2018). Quality and alignment statistics of final BAM files were assessed with samtools stats (H. Li et al., 2009), and a joint report with FastQC reports by MultiQC was generated.

Raw read counts were generated with HTSeq (Anders et al., 2015) using the union method. HTSeq runs internally in STAR. Differential gene expression analysis was performed with edgeR (Robinson et al., 2010) in R 3.6.3 (R Core Team, 2018), according to the edgeR manual. Counts were merged and genes with zero counts in all samples were removed (number of genes: 36380). The whole count table was annotated with R Bioconductor human annotation data package org.Hs.eg.db (Carlson, 2016). A DGEList Element was created with the raw counts, gene information, i.e., Ensembl GeneIDs, HUGO Symbol, Genename, and ENTREZ GeneIDs and a sample grouping metadata table.

```
1 y <- DGEList(counts=ct2[,-1:4], group=meta.data$group, genes=ct2[,1:4])
```

Counts were filtered to keep only those genes which have at least 1 read per million in at least 2 samples (number of genes: 14136). Afterwards, normalization factors were recalculated.

```
1 keep <- rowSums(cpm(y)>1) >=2
2 y <- y[keep, , keep.lib.size=FALSE]
3 y1 <- calcNormFactors(y)
```

A design matrix was created with the grouping factor by treatment condition (group=F1, F2, F3, which are abbreviations for CM-INA6, nMA-INA6, MA-INA6, respectively)

```
1 design = model.matrix(~0+group)
```

Dispersion was estimated, the resulting coefficient of biological variation (BCV) is 0.135, i.e., BCV expression values vary up and down by 13.5% between samples.

```
1 y1.1 <- estimateDisp(y1, design)
2 BCV <- sqrt(model.F$y1.1$common.dispersion)
```

A generalized linear model (glmQLFit function) was fitted.

```
1 fit <- glmQLFit(y1.1, design)
```

and pairwise comparisons were made, e.g.

```
1 F1vsF2 <- glmQLFTest(fit, contrast=makeContrasts(groupF1 - groupF2, levels=design))
2 DE.F1vsF2 <- topTags(F1vsF2, n=nrow(F1vsF2), p.value=0.05)
```

Afterwards, gene list of differentially expressed genes were used for functional enrichment analysis with Metascape (Y. Zhou et al., 2019).

RT-qPCR

For cDNA synthesis, 1 µg of total RNA was reverse transcribed with Oligo(dT)15 primers and Random Primers (both Promega GmbH) and *Superscript IV* reverse transcriptase (Thermo Fisher Scientific) according to the manufacturer's instructions. For quantitative PCR, the cDNA was diluted 1:10, and qPCR was performed in 20 µL using 2 µL of cDNA, 10 µL of *GoTaq qPCR Master Mix* (Promega GmbH), and 5 pmol of sequence-specific primers obtained from biomers.net GmbH (Ulm, Germany) or Qiagen GmbH (Hilden, Germany) (see Appendix A.2: Tabelle 3 for primer sequences and PCR conditions). qPCR conditions were as follows: 95 °C for 3 minutes; 40 cycles: 95 °C for 10 seconds; respective annealing temperature for 10 seconds; 72 °C for 10 seconds; followed by melting curve analysis for the specificity of qPCR products using an *TOptical Gradient 96 PCR Thermal Cycler* (Analytik Jena AG, Jena, Germany). Samples that showed unspecific byproducts were discarded. Ct values were measured in three technical replicates (triplicates). Non-detects were discarded. One of three technical replicates was treated as an outlier and excluded if its z-score crossed 1.5 σ technical variation. We normalized expression by the housekeeping gene *36B4*. Efficiencies were determined in each reaction by linear regression of log-transformed amplification curves (Ramakers et al., 2003). Differential expression was calculated based on a modified ΔΔC_t formula that separated exponents to apply individual efficiencies to each C_t value:

$$\begin{aligned} \text{Fold Change} &= \frac{E_{\text{tar}}^{\Delta C_t_{\text{tar}(co - treated)}}}{E_{\text{ref}}^{\Delta C_t_{\text{ref}(co - treated)}}} \\ &= \frac{E_{\text{tar},\text{co}}^{Ct_{\text{tar},\text{co}}} \div E_{\text{tar},\text{treated}}^{Ct_{\text{tar},\text{treated}}}}{E_{\text{ref},\text{co}}^{Ct_{\text{ref},\text{co}}} \div E_{\text{ref},\text{treated}}^{Ct_{\text{ref},\text{treated}}}} \end{aligned}$$

- $E_{\text{tar},\text{co}}$ = Efficiency of the target gene measured in the control sample
- $Ct_{\text{tar},\text{co}}$ = Ct value of the target gene measured in the control sample
- tar = Target Gene
- ref = Reference Gene
- treated = Treated sample
- co = Control Sample

Fold change expression was normalized by the median of CM-INA6 (and not sample-wise, as commonly used in $\Delta\Delta C_t$) since some genes were not expressed without direct hMSC contact (e.g., *MMP2*), and also in order to display variation of CM-INA6 next to nMA-INA6 and MA-INA6.

Statistics

For molecular analyses, each data point represents one biological replicate, defined as the mean of all technical replicates of co-cultures seeded from the same batch of hMSCs and/or INA-6 cells on the same day. For analyses of time-lapse recordings, each data point represents the normalized event count from one co-culture recording. Unique hMSCs were prioritized for each biological replicate or recording (see Appendix A: Tabelle 1). Bars and lines represent the mean, and error bars represent the standard deviation of all hMSC donors or recordings (= all biological replicates).

Metric, normally distributed, dependent data were analyzed using factorial RM-ANOVA and paired Student's t-tests. Results of RM-ANOVA are reported as follows

$$[F(df_1, df_2) = F; p = p\text{-value}],$$

where df_1 is the degrees of freedom of the observed effect, df_2 is the degrees of freedom of the error, and F is the F-statistic (Vallat, 2018). If sphericity was met, p -values were not corrected using the Greenhouse-Geisser method ($p\text{-unc}$).

$$\begin{aligned} df_1 &= k - 1 && (k = \text{number of groups}) \\ df_2 &= (k - 1)(n - 1) && (n = \text{number of samples in each group}) \\ F &= \frac{SS_{\text{Effect}}/df_1}{SS_{\text{Error}}/df_2} && (\text{SS} = \text{Sums of squares for effect or error}) \end{aligned}$$

If data points within dependent sample pairs were missing, such pairs were excluded from paired t-tests while others from the same subject remained.

Metric non-normal distributed, independent data was analyzed using the Kruskal-Wallis H-test and Mann-Whitney U tests. Results of the Kruskal-Wallis H-test are reported as

$$H(df) = H$$

, with df being the degrees of freedom and H being the Kruskal-Wallis H statistic, corrected for ties (Vallat, 2018).

Metric bivariate non-normal distributed data was correlated using Spearman's rank correlation and reported as:

$$\rho(df) = \rho, p = p\text{-value}$$

, where ρ is Spearman's rank correlation coefficient. df is calculated as

$$df = n - 2 \quad (n = \text{number of observations})$$

These tests were applied using Python (3.10) packages pingouin (0.5.1) and statsmodels (0.14.0) (Seabold & Perktold, 2010; Vallat, 2018). Data was plotted using seaborn (Waskom, 2021) and plotastic

(Kuric & Ebert, 2024). Sphericity was ensured by Mauchly's test. Normality was checked with the Shapiro-Wilk test for $n > 3$.

Data points were log10 transformed to convert the scale from multiplicative ("fold change") to additive, or to fulfill sphericity requirements. p -values derived from patient survival data were corrected using the Benjamini-Hochberg procedure. For other post-hoc analyses, p -values were not adjusted for family-wise error rate in order to minimize type I errors. To prevent type II errors, the same conclusions were validated by different experimental setups and through varying hMSCs donors across experiments (see Appendix A: Tabelle 1).

Significant p -values from pairwise tests were annotated as stars between data groups

$$p\text{-value} = 0.05 > * > 0.01 > ** > 10^{-3} > *** > 10^{-4} > ****.$$

If too many significant pairs were detected, only those pairs of interest were annotated.

No power calculation was performed to determine sample size, since samples were limited by availability of primary hMSC donors. Experiments were repeated until a minimum of three biological replicates were gathered.

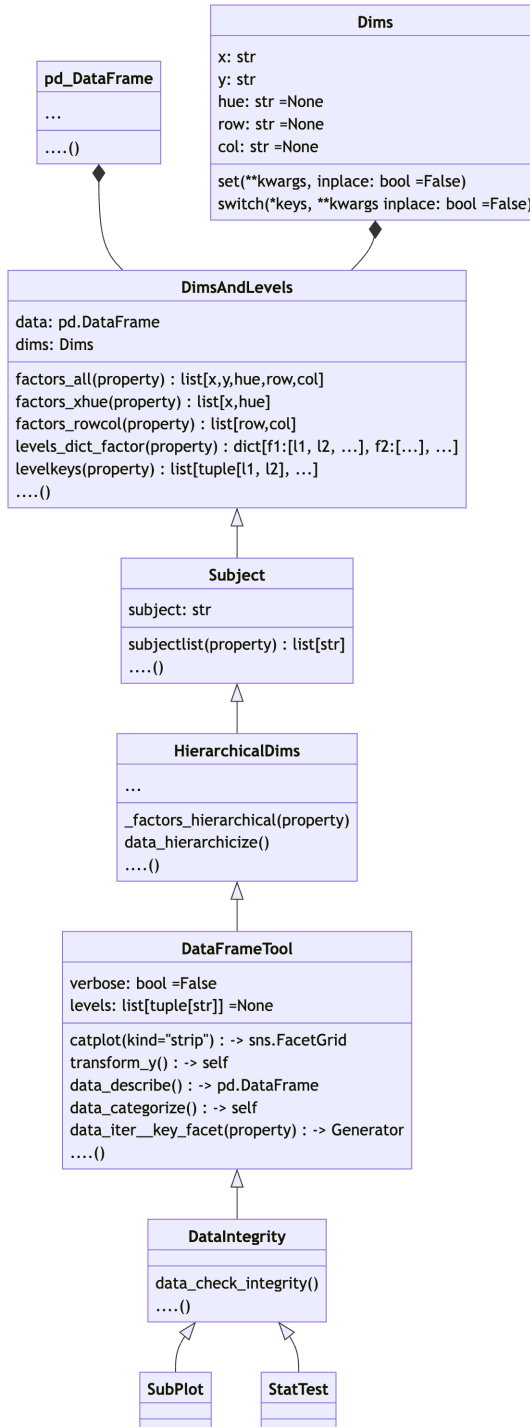
Patient Cohort, Analysis of Survival and Expression

Patient samples ($n = 873$) were collected at the University Hospital Heidelberg and processed as described (Seckinger et al., 2017, 2018), and are available at the European Nucleotide Archive (ENA) via accession numbers PRJEB36223 and PRJEB37100. Consecutive patients with monoclonal gammopathy of unknown significance (MGUS) ($n = 62$), asymptomatic ($n = 259$), symptomatic, therapy-requiring ($n = 764$), and relapsed/refractory myeloma ($n = 90$), as well as healthy donors ($n = 19$) as comparators were included in the study approved by the ethics committee (#229/2003, #S-152/2010) after written informed consent.

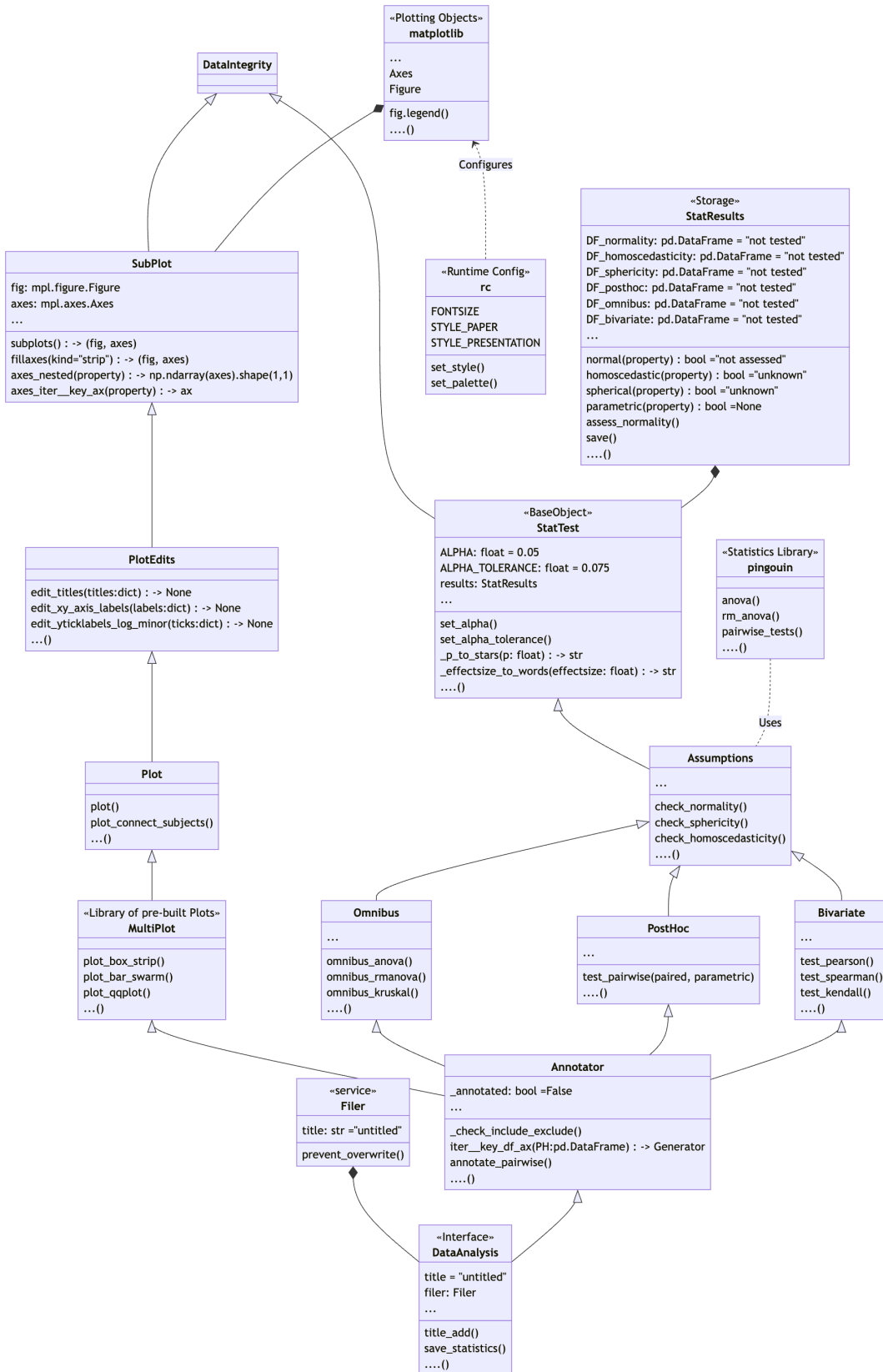
Gene expression was measured by RNA sequencing as previously described (Seckinger et al., 2018). Gene expression is defined as the \log_2 transformed value of normalized counts + 1 (as pseudocount). Progression-free (PFS) and overall survival (OS) were analyzed for the subset of previously untreated symptomatic myeloma patients. For delineating "high" and "low" expression of target adhesion ($n = 101$) and cell cycle ($n = 173$) genes, thresholds per gene were calculated with maximally selected rank statistics by the maxstat package in R (Hothorn & Lausen, 2017). PFS and OS were analyzed for high vs. low expression with the Kaplan-Meier method (Kaplan & Meier, 1958). Significant differences between the curves were analyzed with log-rank tests (Harrington & Fleming, 1982). p -values were corrected for multiple testing by the Benjamini-Hochberg method. Analyses were performed with R version 3.6.3 (R Core Team, 2018).

B Documentation of `plotastic`

B.1 Class Diagram



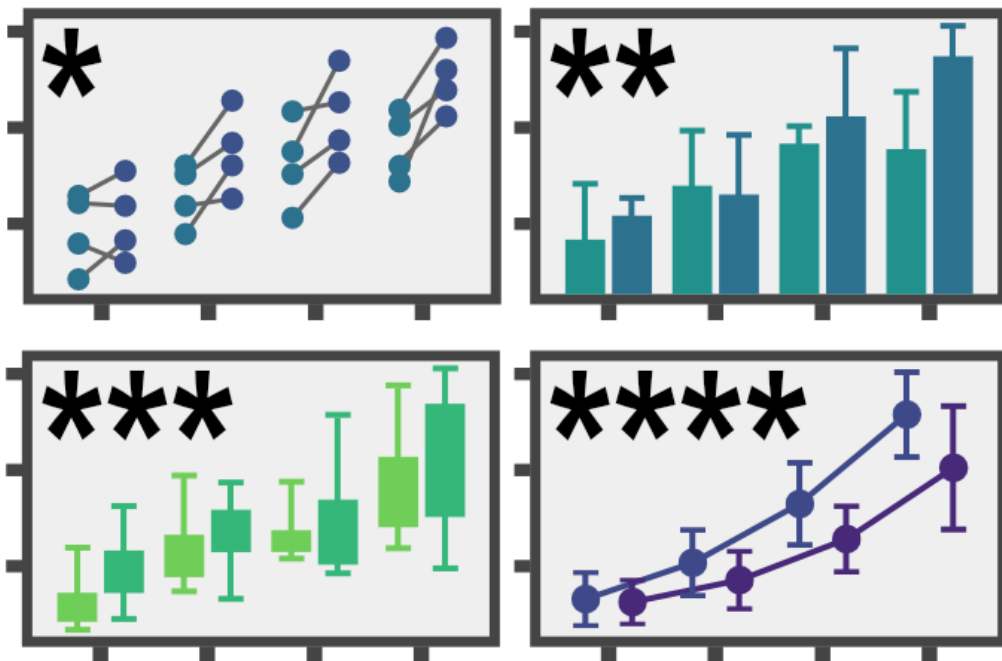
Appendix B.1 Figure 1: Class diagram of plotastic (upper part): The architecture of plotastic begins with classes that are related to handling a pandas.DataFrame object which stores the data, and defining dimensions to group the data (y, x, hue, col, row). This diagram ends with the classes SubPlot and StatTest and is continued on the next page. Arrow shapes follow the UML (unified modeling language): A hollow triangle indicates inheritance (“*is a*”) and a filled diamond indicates composition (“*has a*”).



Appendix B.1 Figure 1: continued from previous page The architecture of plotastic continues after the class DataIntegrity with classes for plotting (SubPlot) and statistical testing (StatTest) and ends with the class DataAnalysis, which serves as the main user interface. Arrow shapes follow the UML (unified modeling language): A hollow triangle indicates inheritance ("is a") and a filled diamond indicates composition ("has a").

B.2 Readme

The following pages are the README.md of `plotastic` found in the Python Package Index (PyPi) (pypi.org/project/plotastic), and on GitHub (github.com/markur4/plotastic).



code style black codecov 79% JOSS 10.21105/joss.06304

plotastic: Bridging Plotting and Statistics

Installation

Install from PyPi:

```
pip install plotastic
```

Install from GitHub: (experimental, check CHANGELOG.md)

```
pip install git+https://github.com/markur4/plotastic.git
```

Requirements

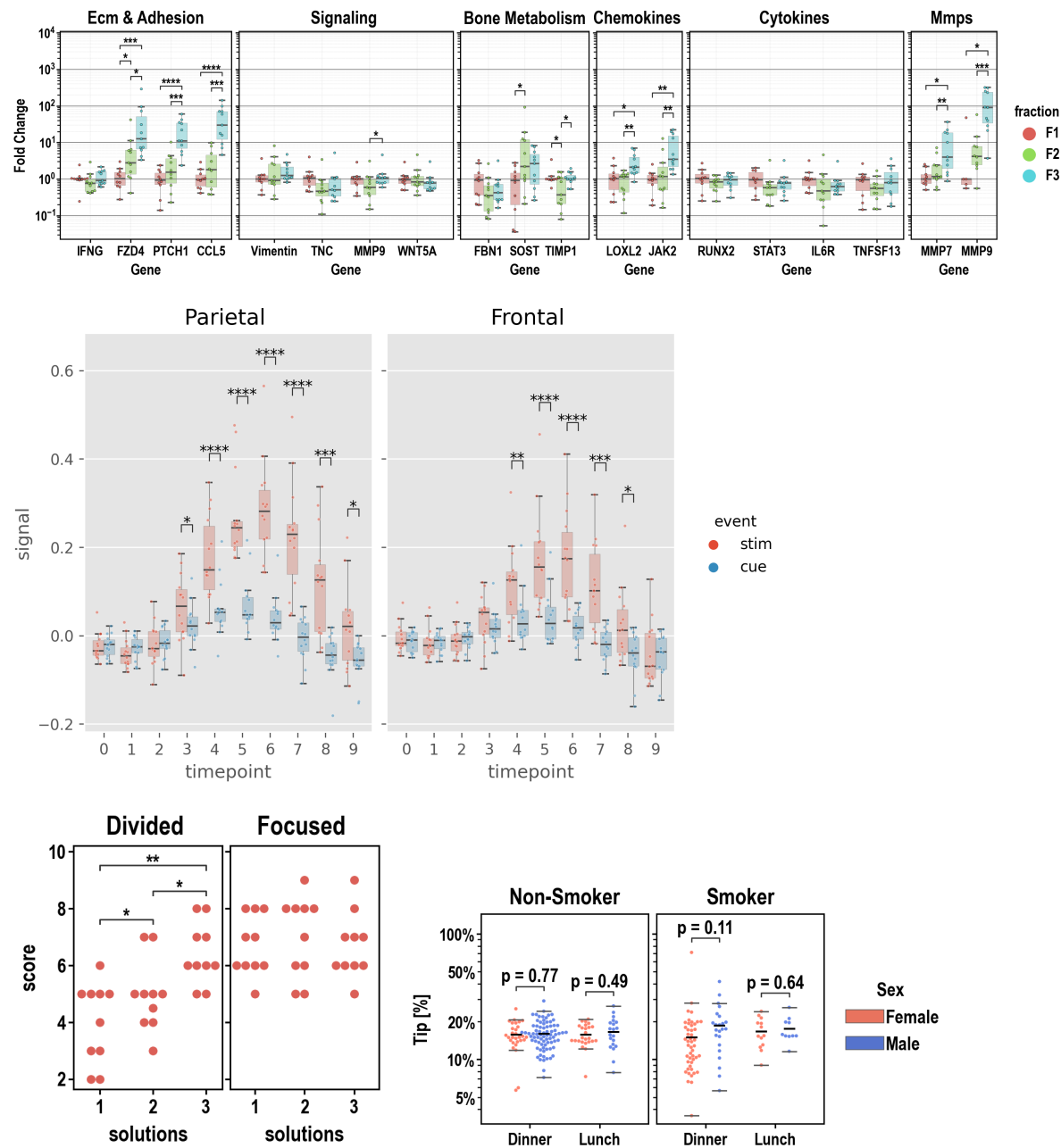
- Python >= 3.11 (*not tested with earlier versions*)

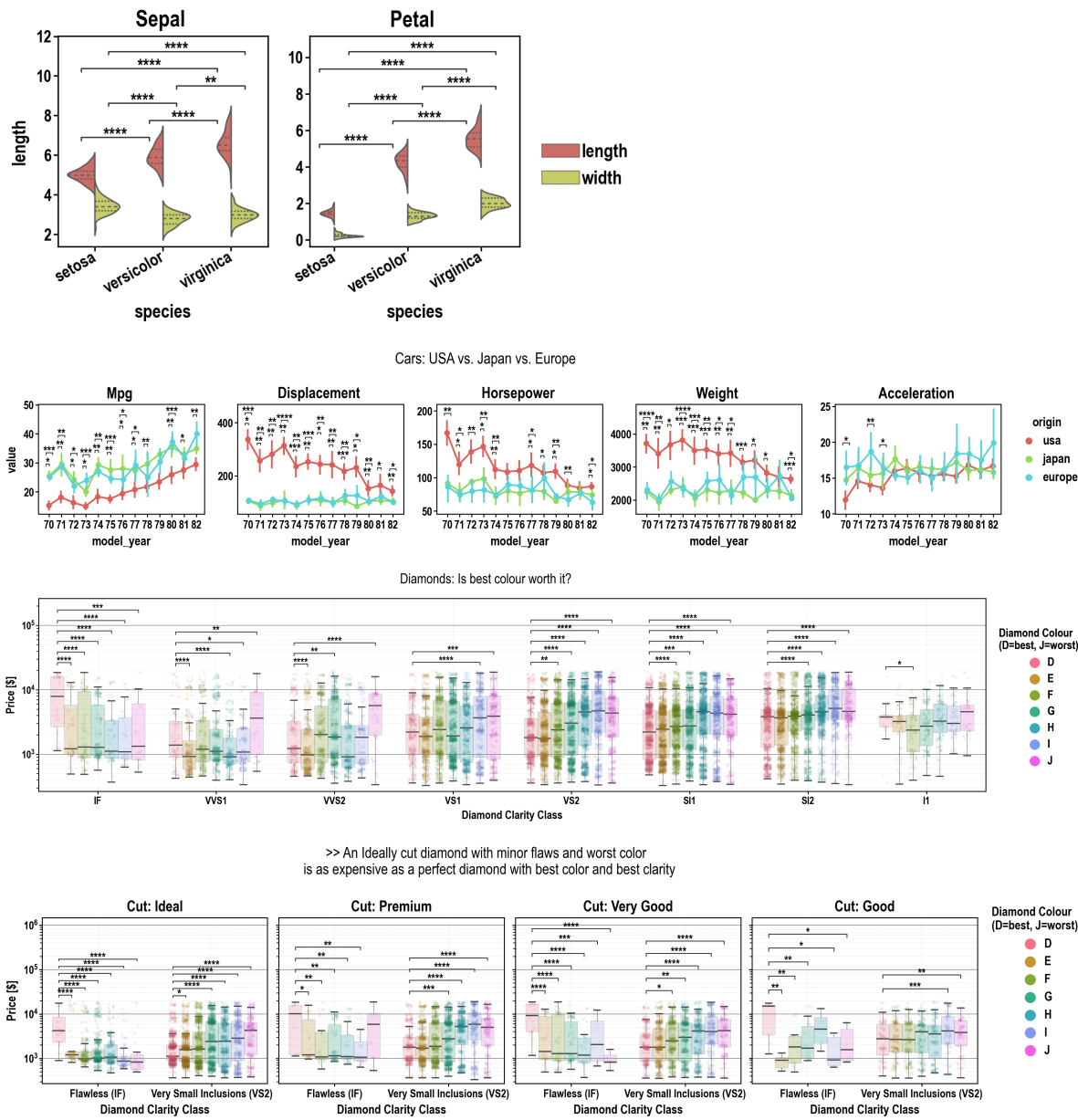
- pandas == 1.5.3 (*pingouin needs this*)
- seaborn <= 0.12.2 (*later versions reworked hue*)

Example Gallery

► (click to unfold)

(Mouse) Click on Images for Code! (Mouse)





>About plotastic

▶ 🧑 Summary

plotastic addresses the challenges of transitioning from exploratory data analysis to hypothesis testing in Python's data science ecosystem. Bridging the gap between **seaborn** and **pingouin**, this library offers a unified environment for plotting and statistical analysis. It simplifies the workflow with a user-friendly syntax and seamless integration with familiar **seaborn** parameters (`y`, `x`, `hue`, `row`, `col`). Inspired by **seaborn**'s consistency, **plotastic** utilizes a **DataAnalysis** object to intelligently pass parameters to **pingouin** statistical functions. The library systematically groups the data according to the needs of statistical tests and plots, conducts visualisation, analyses and supports extensive customization options. In essence, **plotastic** establishes a protocol for configuring statical analyses through plotting parameters.

This approach streamlines the process, translating `seaborn` parameters into statistical terms, providing researchers and data scientists with a cohesive and user-friendly solution in python.!

Workflow:

1. Import & Prepare your pandas DataFrame

- We require a long-format pandas dataframe with categorical columns
- If it works with seaborn, it works with plotastic!

2. Make a DataAnalysis Object

- `DataAnalysis(DataFrame, dims={x, y, hue, row, col})`
- Check for empty data groups, differing samplesizes, NaN-count, etc. automatically

3. Explore Data

- Check Data integrity, unequal samplesizes, empty groups, etc.
- Quick preliminary plotting with e.g. `DataAnalysis.catplot()`

4. Adapt Data

- Categorize multiple columns at once
- Transform dependent variable
- Each step warns you, if you introduced NaNs without knowledge!
- etc.

5. Perform Statistical Tests

- Check Normality, Homoscedasticity, Sphericity
- Perform Omnibus tests (ANOVA, RMANOVA, Kruskal-Wallis, Friedman)
- Perform PostHoc tests (Tukey, Dunn, Wilcoxon, etc.) based on `pg.pairwise_tests()`

6. Plot figure

- Use pre-defined and optimized multi-layered plots with one line (e.g. strip over box)!
- Annotate statistical results (p-values as *, **, ***, etc.) with full control over which data to include or exclude!

7. Save all results at once!

- One DataAnalysis object holds:
 - One DataFrame in `self.data`
 - One Figure in `self.fig, self.axes`
 - Multiple statistical results: `self.results`
- Use `DataAnalysis.save_statistics()` to save all results to different sheets collected in one .xlsx filesheet per test

► Translating Plots into Statistics!

In Principle:

- Categorical data is separable into `seaborn`'s categorization parameters: `x, y, hue, row, col`. We call those "*dimensions*".
- These dimensions are assigned to statistical terms:
 - `y` is the **dependent variable (DV)**
 - `x` and `hue` are **independent variables (IV)** and are treated as **within/between factors** (categorical variables)
 - `row` and `col` are **grouping variables** (categorical variables)
 - A `subject` may be specified for within/paired study designs (categorical variable)

- For each level of **row** or **col** (or for each combination of **row-** and **col** levels), statistical tests will be performed with regards to the two-factors **x** and **hue**

Example with ANOVA:

- Imagine this example data:
 - Each day you measure the tip of a group of people.
 - For each tip, you note down the **day**, **gender**, **age-group** and whether they **smoke** or not.
 - Hence, this data has 4 categorical dimensions, each with 2 or more *levels*:
 - **day**: 4 levels (*monday, tuesday, wednesday, Thursday*)
 - **gender**: 2 levels (*male, female*)
 - **smoker**: 2 levels (*yes, no*)
 - **age-group**: 2 levels (*young, old*)
- Each category is assigned to a place of a plot, and when calling statistical tests, we assign them to statistical terms (in comments):

```

◦ # dims is short for dimensions
dims = dict(           # STATISTICAL TERM:
    y = "tip",         # y-axis, dependent variable
    x = "day",          # x-axis, independent variable (within-
    subject factor)
    hue = "gender",    # color, independent variable (within-
    subject factor)
    col = "smoker",    # axes, grouping variable
    row = "age-group" # axes, grouping variable
)

```

- We perform statistical testing groupwise:
 - For each level-combinations of **smoker** and **age-group**, a two-way ANOVA will be performed (with **day** and **gender** as **between** factors for each datagroup):
 - 1st ANOVA assesses datapoints where **smoker=yes** AND **age-group=young**
 - 2nd ANOVA assesses datapoints where **smoker=yes** AND **age-group=old**
 - 3rd ANOVA assesses datapoints where **smoker=no** AND **age-group=young**
 - 4th ANOVA assesses datapoints where **smoker=no** AND **age-group=old**
 - Three-way ANOVAs are not possible (yet), since that would require setting e.g. **col** as the third factor, or implementing another dimension (e.g. **hue2**).

► ! Disclaimer about Statistics

This software was inspired by ...

- ... ***Intuitive Biostatistics*** - Fourth Edition (2017); Harvey Motulsky
- ... ***Introduction to Statistical Learning with applications in Python*** - First Edition (2023); Gareth James, Daniela Witten, Trevor Hastie, Robert Tibshirani, Jonathan Taylor
- ... talking to other scientists struggling with statistics

 **plotastic** can help you with...

- ... gaining some practical experience when learning statistics
- ... quickly gain statistical implications about your data without switching to another software
- ... making first steps towards a full statistical analysis
- ... plotting publication grade figures (check statistics results with other software)
- ... publication grade statistical analysis **IF** you really know what you're doing OR you have back-checked your results by a professional statistician
- ... quickly test data transformations (log)

🚫 **plotastic** can NOT ...

- ... replace a professional statistician
- ... teach you statistics, you need some basic knowledge (but is awesome for practicing!)
- ... test for multicollinearity (Absence of multicollinearity is required by ANOVA!)
- ... perform stringent correction for multiple testing (e.g. bonferroni), as statistical tests are applied to sub-facets of the whole dataframe for each axes, which depends on the definition of x, hue, col, etc. Hence, corrected p-values might over-estimate the significance of your results.

🟡 Be critical and responsible with your statistical analysis!

- **Expect Errors:** Don't trust automated systems like this one!
- **Document your work in *ridiculous detail*:**
 - Include the applied tests, the number of technical replicates and the number of biological/independent in each figure legend
 - State explicitly what each datapoint represents:
 - 1 datapoint = 1 Technical replicate?
 - 1 datapoint = The mean of all technical replicate per independent replicate/subject?
 - State explicitly what the error-bars mean: Standard deviation? Confidence interval?
 - (Don't mix technical with biological/independent variance)
 - Report if/how you removed outliers
 - Report if you did or did not apply correction methods (multiple comparisons, Greenhouse Geyser, etc.) and what your rationale is (exploratory vs. confirmatory study? Validation through other methods to reduce Type I error?)
- **Check results with professionals:**
 - "Here is my data, here is my question, here is my analysis, here is my interpretation. What do you think?"

▶ ✅ Feature List

- ✅ : Complete and tested
- 👍 : Complete
- 📅 : Planned or unfinished (no date)
- 🧑 : Maybe..? (Rather not...)
- 🚫 : Not planned, don't want
- 😢 : Help Please..?

▼ Plotting

- 👍 Make and Edit Plots: Implemented ✅

- All (non-facetgrid) seaborn plots should work, not tested
- QQ-Plot
- Kaplan-Meyer-Plot
- Interactive Plots (where you click stuff and adjust scale etc.)
 - That's gonna be a lot of work!
- Support for `seaborn.FacetGrid`
 - Why not? - `plotastic` uses `matplotlib` figures and fills its axes with `seaborn` plot functions. In my opinion, that's the best solution that offers the best adaptability of every plot detail while being easy to maintain
- Support for `seaborn.objects` (same as Facetgrid)
 - Why not? - I don't see the need to refactor the code
- NEED HELP WITH: The hidden state of `matplotlib` figures/plots/stuff that gets drawn:
 - I want to save the figure in `DataAnalysis.fig` attribute. As simple as that sounds, `matplotlib` does weird stuff, not applying changes after editing the plot.
 - It'd be cool if I could control the changes to a `DataAnalysis` object better (e.g. using `inplace=True` like with `pd.DataFrame`). But I never figured out how to control `matplotlib` figure generation, even with re-drawing the figure with `canvas`. It's a mess and I wasted so much time already.

▼ Multi-Layered Plotting

- Box-plot + swarm
- Box-plot + strip
- Violin + swarm/strip

▼ Statistics

- Assumption testing
 - Normality (e.g. Shapiro-Wilk)
 - Homoscedasticity (e.g. Levene)
 - Sphericity (e.g. Mauchly)
- Omnibus tests
 - ANOVA, RMANOVA, Kruskal-Wallis, Friedman
 - Mixed ANOVA
 - Annotate Results into Plot
- PostHoc
 - `pg.pairwise_tests()`
 - Works with all primary options. That includes all parametric, non-parametric, paired, unpaired, etc. tests (*t-test*, paired *t-test*, *MWU*, *Wilcoxon*, etc.)
 - Annotate Stars into plots (*, **, etc.)
 - Specific pairs can be included/excluded from annotation
 - Make correction for multiple testing go over complete DataFrame and not Facet-wise:
- Bivariate
 - Find and Implement system to switch between numerical and categorical x-axis
 - Function to convert numerical data into categorical data by binning?
 - Pearson, Spearman, Kendall

▼ Analysis Pipelines

Idea: Put all those statistical tests into one line. I might work on this only after everything's implemented and working confidently and well!

- 🐦 `between_samples(parametric=True)`: ANOVA + Tukey (if Normality & Homoscedasticity are given)
- 🐦 `between_samples(parametric=False)`: Kruskal-Wallis + Dunn
- 🐦 `within_samples(parametric=True)`: RM-ANOVA + multiple paired t-tests (if Normality & Sphericity are given)
- 🐦 `within_samples(parametric=False)`: Friedman + multiple Wilcoxon



How To Use

Documentations

1. Example Gallery

1. Quick Example: FMRI
2. qPCR (paired, parametric)
3. Cars (unpaired, non-parametric)
4. Diamonds (unpaired, non-parametric)
5. Attention (paired/mixed, parametric)
6. Iris (unpaired, parametric)
7. Tips (unpaired, parametric)

2. Data

1. Set/Switch Dimensions

3. Plotting

1. Quick & Simple: MultiPlots
2. Constructing Plots
3. Legends
4. Styles

Quick Example

Import plotastic and example Data

```
import matplotlib.pyplot as plt
import plotastic as plst

# Import Example Data (Long-Format)
DF, _dims = plst.load_dataset("fmri", verbose = False)
DF.head()
```

Assign each column to a dimension (**y**, **x**, **hue**, **col**, **row**):

```
dims = dict(
    y = "signal",      # y-axis, dependent variable
    x = "timepoint",   # x-axis, independent variable & within-subject
    factor
    hue = "event",     # color, grouping variable & within-subject factor
    col = "region"     # axes, grouping variable
)
```

Initialize DataAnalysis Object

```
DA = plst.DataAnalysis(
    data=DF,           # Dataframe, long format
    dims=dims,         # Dictionary with y, x, hue, col, row
    subject="subject", # Datapoints are paired by subject (optional)
    verbose=False,     # Print out info about the Data (optional)
)
```

Perform Statistics

No arguments need to be passed, although `**kwargs`, are passed to respective `pingouin` functions.

```
DA.check_normality() # Normal Distribution?
DA.check_sphericity() # Sphericity?
DA.omnibus_rm_anova() # Repeated Measures ANOVA
DA.test_pairwise() # Post-hoc tests
```

Save Results:

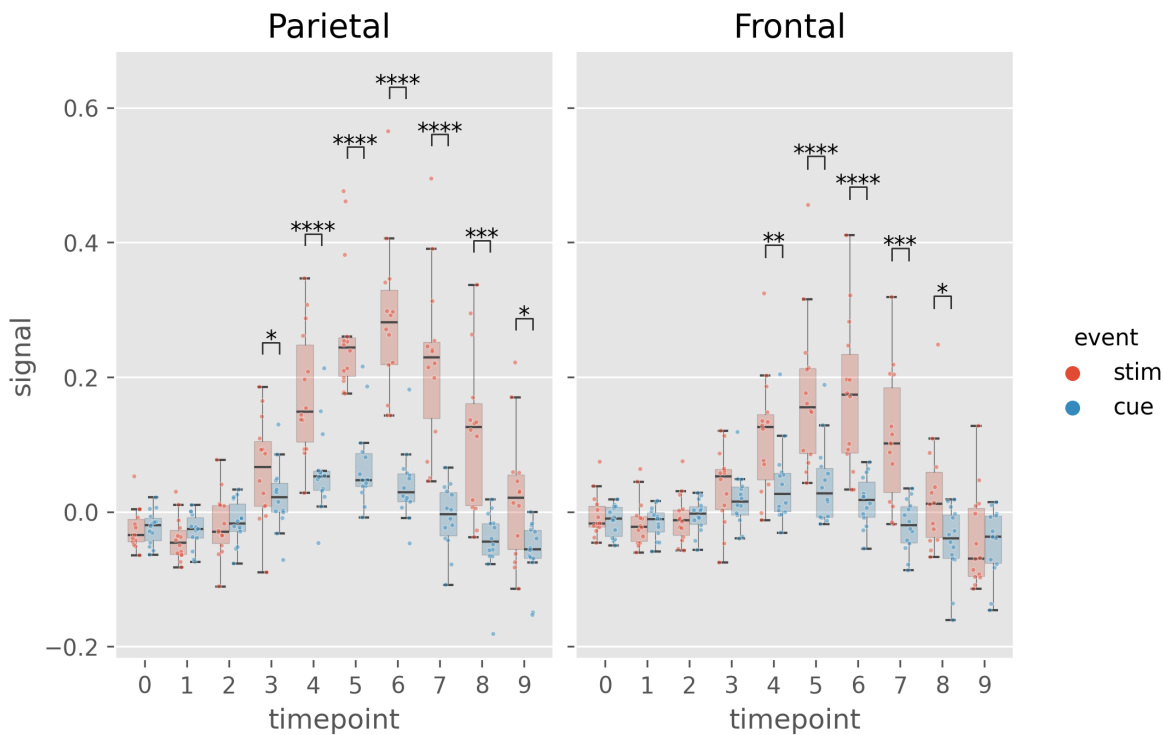
Output is one excel file containing results of all performed tests (normality, anova, t-tests, etc.) in different sheets

```
DA.save_statistics("example.xlsx")
```

Annotate post-hoc results into plot:

```
(DA
    .plot_box_strip() # Pre-built plotting function initializes plot
    .annotate_pairwise( # Annotate results from DA.test_pairwise()
        include="__HUE" # Use only significant pairs across each hue
    )
)
```

```
# Saving the plot like matplotlib!
plt.savefig("example.png", dpi=200, bbox_inches="tight")
```



🧪 Testing

▶ (click to unfold)

- Download/Clone repository
- Install development tools `pip install .[dev]`
- Run tests
 - Run `pytest ./tests`
 - To include a coverage report run `pytest ./tests -cov--cov-report=html` and open `./htmlcov/index.html` with your browser.

🤝 Community Guidelines

▶ (click to unfold)

When interacting with the community, you must adhere to the [Code of Conduct](#)

Contribute

I am grateful for [pull requests!](#)

- Make sure to understand the code (e.g. see Class diagram in this Readme)
- Run tests before submitting a pull request

Reporting Issues & Problems

If you need help, please open an [issue](#) on this repository.

- Please provide a minimal example to reproduce the problem.

Support

If you need help, please open an [issue](#) on this repository.

👉 Cite These!

▶ **(click to unfold)**

Kuric et al., (2024). plotastic: Bridging Plotting and Statistics in Python. *Journal of Open Source Software*, 9(95), 6304, <https://doi.org/10.21105/joss.06304>

Vallat, R. (2018). Pingouin: statistics in Python. *Journal of Open Source Software*, 3(31), 1026, <https://doi.org/10.21105/joss.01026>

Waskom, M. L., (2021). seaborn: statistical data visualization. *Journal of Open Source Software*, 6(60), 3021, <https://doi.org/10.21105/joss.03021>.

```
@article{Kuric2024,
  doi = {10.21105/joss.06304},
  url = {https://doi.org/10.21105/joss.06304},
  year = {2024}, publisher = {The Open Journal},
  volume = {9},
  number = {95},
  pages = {6304},
  author = {Martin Kuric and Regina Ebert},
  title = {plotastic: Bridging Plotting and Statistics in Python},
  journal = {Journal of Open Source Software}
}

@article{Waskom2021,
  doi = {10.21105/joss.03021},
  url = {https://doi.org/10.21105/joss.03021},
  year = {2021},
  publisher = {The Open Journal},
  volume = {6},
  number = {60},
  pages = {3021},
  author = {Michael L. Waskom},
  title = {seaborn: statistical data visualization},
  journal = {Journal of Open Source Software}
}

@article{Vallat2018,
  title = "Pingouin: statistics in Python",
  author = "Vallat, Raphael",
  journal = "The Journal of Open Source Software",
  volume = 3,
```

```
number    = 31,  
pages     = "1026",  
month     = nov,  
year      = 2018  
}
```

B.3 Example Analysis “qpcr”

The following pages are a jupyter notebook from an example analysis using plotastic. This notebook and further analyses examples are found on GitHub (github.com/markur4/plotastic). The qPCR dataset was derived from the experiments described in Chapter 1 Abbildung 4 and was changed into a public test dataset by exchanging the original gene names with random ones while preserving gene classes and quantitative fold changes.

qPCR

April 9, 2024

```
[ ]: import plotastic as plst
import matplotlib.pyplot as plt
import seaborn as sns
import pandas as pd

[ ]: # Set Plot Style
plst.set_style("paper")
# plst.set_palette("hls", verbose=True)
plst.set_palette(["#db5f57", "#91db57", "#57d3db"])

#! You chose this color palette: ['#db5f57', '#91db57', '#57d3db', '#db5f57',
'#91db57', '#57d3db', '#db5f57', '#91db57']

['#db5f57',
 '#91db57',
 '#57d3db',
 '#db5f57',
 '#91db57',
 '#57d3db',
 '#db5f57',
 '#91db57']
```

1 Example Analysis: qPCR

Raw Data: https://github.com/markur4/plotastic/tree/main/src/plotastic/example_data/data

Original Source: (unpublished)

```
[ ]: # Import Example Data
DF, _dims = plst.load_dataset("qpcr", verbose=False)
dims = dict(
    y="fc",
    x="gene",
    hue="fraction",
    # col= 'method',
    row="class",
)
DA = plst.DataAnalysis(DF, dims, subject="subject", verbose=False)
```

```
[ ]: DA.transform_y("log10", inplace=True) # Log transform
DA.check_normality() # -> Only few groups are not normal -> parametric
```

				W	pval	normal	n
	class	gene	fraction				
Bone Metabolism	F1	FBN1	0.936873	0.518768	True	10	
		SOST	0.880395	0.131862	True	10	
		TIMP1	0.745494	0.004807	False	9	
	F2	FBN1	0.954764	0.705148	True	11	
		SOST	0.967810	0.863610	True	11	
		TIMP1	0.914325	0.274168	True	11	
	F3	FBN1	0.915247	0.281020	True	11	
		SOST	0.923112	0.345415	True	11	
		TIMP1	0.937230	0.488505	True	11	
Chemokines	F1	LOXL2	0.930358	0.451421	True	10	
		JAK2	0.897331	0.204749	True	10	
	F2	LOXL2	0.874630	0.088876	True	11	
		JAK2	0.960025	0.772006	True	11	
	F3	LOXL2	0.943678	0.564652	True	11	
		JAK2	0.878406	0.099301	True	11	
Cytokines	F1	RUNX2	0.947142	0.634825	True	10	
		STAT3	0.933422	0.482382	True	10	
		IL6R	0.927258	0.421472	True	10	
		TNFSF13	0.907481	0.264130	True	10	
	F2	RUNX2	0.915611	0.283765	True	11	
		STAT3	0.907354	0.226836	True	11	
		IL6R	0.985709	0.989621	True	11	
		TNFSF13	0.958855	0.757330	True	11	
	F3	RUNX2	0.924060	0.353917	True	11	
		STAT3	0.932663	0.438418	True	11	
		IL6R	0.826181	0.020798	False	11	
		TNFSF13	0.970421	0.890746	True	11	
ECM & Adhesion	F1	IFNG	0.715267	0.001349	False	10	
		FZD4	0.981633	0.973303	True	10	
		PTCH1	0.911578	0.292008	True	10	
		CCL5	0.969121	0.882582	True	10	
	F2	IFNG	0.899109	0.180269	True	11	
		FZD4	0.979590	0.963841	True	11	
		PTCH1	0.986610	0.990734	True	10	
		CCL5	0.925780	0.407685	True	10	
	F3	IFNG	0.905665	0.216509	True	11	
		FZD4	0.923819	0.351743	True	11	
		PTCH1	0.957827	0.744318	True	11	
		CCL5	0.940093	0.521596	True	11	
MMPs	F1	MMP7	0.955749	0.752957	True	9	
		MMP9	0.675286	0.005186	False	5	
	F2	MMP7	0.926078	0.372552	True	11	

		MMP9	0.971128	0.901100	True	10
	F3	MMP7	0.924886	0.361455	True	11
		MMP9	0.913554	0.268549	True	11
Signaling	F1	Vimentin	0.919696	0.354424	True	10
		TNC	0.928589	0.434161	True	10
		NOTCH1	0.922084	0.374662	True	10
		WNT5A	0.903581	0.239742	True	10
	F2	Vimentin	0.957763	0.743507	True	11
		TNC	0.959813	0.769352	True	11
		NOTCH1	0.977556	0.951045	True	11
		WNT5A	0.937156	0.487661	True	11
	F3	Vimentin	0.910924	0.250109	True	11
		TNC	0.884194	0.117578	True	11
		NOTCH1	0.779982	0.005132	False	11
		WNT5A	0.812114	0.013581	False	11

[]: DA.check_sphericity()

		spher	W	chi2	dof	pval	\
class	fraction						
Bone Metabolism	F1	0	True	0.592922	3.658847	2	0.160506
	F2	0	True	0.703252	3.168356	2	0.205116
	F3	0	True	0.832864	1.645964	2	0.439120
Chemokines	F1	0	True	NaN	NaN	1	1.000000
	F2	0	True	NaN	NaN	1	1.000000
	F3	0	True	NaN	NaN	1	1.000000
Cytokines	F1	0	True	0.629185	3.577934	5	0.614197
	F2	0	False	0.262747	11.657816	5	0.040987
	F3	0	False	0.210032	13.610980	5	0.019012
ECM & Adhesion	F1	0	True	0.486690	5.560987	5	0.354712
	F2	0	True	0.295164	8.202615	5	0.149255
	F3	0	True	0.297080	10.586623	5	0.061736
MMPs	F1	0	True	NaN	NaN	1	1.000000
	F2	0	True	NaN	NaN	1	1.000000
	F3	0	True	NaN	NaN	1	1.000000
Signaling	F1	0	True	0.536227	4.812474	5	0.442437
	F2	0	True	0.554009	5.151113	5	0.400336
	F3	0	False	0.117602	18.669462	5	0.002375
		group	count	n per group			
class	fraction						
Bone Metabolism	F1	0	3	[10, 10, 9]			
	F2	0	3	[11, 11, 11]			
	F3	0	3	[11, 11, 11]			
Chemokines	F1	0	2	[10, 10]			
	F2	0	2	[11, 11]			
	F3	0	2	[11, 11]			

Cytokines	F1	0	4	[10, 10, 10, 10]
	F2	0	4	[11, 11, 11, 11]
	F3	0	4	[11, 11, 11, 11]
ECM & Adhesion	F1	0	4	[10, 10, 10, 10]
	F2	0	4	[10, 11, 11, 10]
	F3	0	4	[11, 11, 11, 11]
MMPs	F1	0	2	[9, 5]
	F2	0	2	[11, 10]
	F3	0	2	[11, 11]
Signaling	F1	0	4	[10, 10, 10, 10]
	F2	0	4	[11, 11, 11, 11]
	F3	0	4	[11, 11, 11, 11]

```
[ ]: # Default is (paired) t-test, and since DA has subject: paired=True
DA.test_pairwise()
```

```
[ ]:
          gene      A      B  mean(A) \
class      fraction Contrast
ECM & Adhesion -       gene      -  CCL5   FZD4  0.591713
                  gene      -  CCL5   IFNG  0.591713
                  gene      -  CCL5  PTCH1  0.591713
                  gene      -  FZD4   IFNG  0.622994
                  gene      -  FZD4  PTCH1  0.622994
...
MMPs        NaN      gene * fraction  MMP9    F1     F3  0.256111
                  gene * fraction  MMP9    F2     F3  0.677357
                  F1      fraction * gene  NaN  MMP7   MMP9  0.032549
                  F2      fraction * gene  NaN  MMP7   MMP9  0.185211
                  F3      fraction * gene  NaN  MMP7   MMP9  0.742060

          std(A)  mean(B)  std(B) Paired \
class      fraction Contrast
ECM & Adhesion -       gene      0.253752  0.622994  0.266747  True
                  gene      0.253752 -0.026656  0.149430  True
                  gene      0.253752  0.469495  0.330886  True
                  gene      0.266747 -0.026656  0.149430  True
                  gene      0.266747  0.469495  0.330886  True
...
MMPs        NaN      gene * fraction  0.802159  1.845550  0.600687  True
                  gene * fraction  0.546148  1.845550  0.600687  True
                  F1      fraction * gene  0.228544  0.256111  0.802159  True
                  F2      fraction * gene  0.361750  0.677357  0.546148  True
                  F3      fraction * gene  0.567249  1.845550  0.600687  True

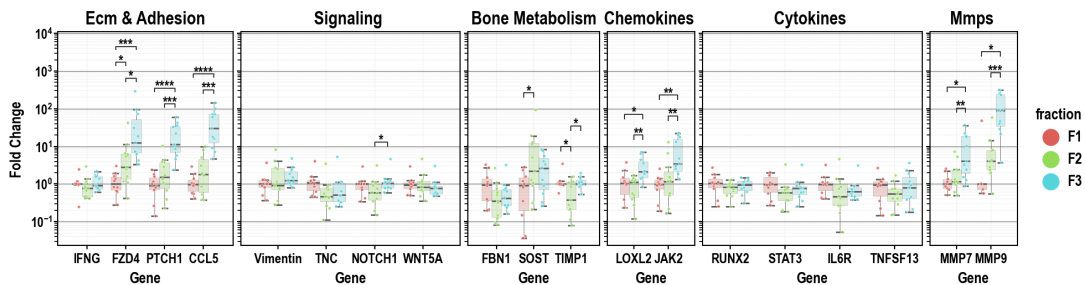
          Parametric      T      dof \
class      fraction Contrast
ECM & Adhesion -       gene      True -0.327586  10.0
```

		gene	True	7.882620	10.0	
		gene	True	1.320783	10.0	
		gene	True	7.532512	10.0	
		gene	True	2.105924	10.0	
..			
MMPs	NaN	gene * fraction	True	-3.513968	4.0	
		gene * fraction	True	-5.680475	9.0	
	F1	fraction * gene	True	-0.543884	4.0	
	F2	fraction * gene	True	-3.811156	9.0	
	F3	fraction * gene	True	-15.767066	10.0	
			alternative		p-unc	BF10 \
class		fraction Contrast				
ECM & Adhesion -		gene	two-sided	7.499799e-01		0.312
		gene	two-sided	1.339935e-05		1643.947
		gene	two-sided	2.160003e-01		0.598
		gene	two-sided	1.987311e-05		1165.781
		gene	two-sided	6.146203e-02		1.461
..			
MMPs	NaN	gene * fraction	two-sided	2.458360e-02		3.686
		gene * fraction	two-sided	3.016844e-04		111.751
	F1	fraction * gene	two-sided	6.154168e-01		0.448
	F2	fraction * gene	two-sided	4.145762e-03		12.636
	F3	fraction * gene	two-sided	2.163081e-08		4.845e+05
			hedges	**p-unc	Sign.	\
class		fraction Contrast				
ECM & Adhesion -		gene	-0.115597	ns	False	
		gene	2.856874	****	signif.	
		gene	0.398765	ns	False	
		gene	2.890772	****	signif.	
		gene	0.491362	0.061	toler.	
..			
MMPs	NaN	gene * fraction	-2.179426	*	signif.	
		gene * fraction	-2.024511	***	signif.	
	F1	fraction * gene	-0.255634	ns	False	
	F2	fraction * gene	-0.939861	**	signif.	
	F3	fraction * gene	-1.817138	****	signif.	
				pairs	cross	
class		fraction Contrast				
ECM & Adhesion -		gene		(CCL5, FZD4)	x	
		gene		(CCL5, IFNG)	x	
		gene		(CCL5, PTCH1)	x	
		gene		(FZD4, IFNG)	x	
		gene		(FZD4, PTCH1)	x	
..				

MMPs	NaN	gene * fraction	((MMP9, F3), (MMP9, F1))	hue
		gene * fraction	((MMP9, F3), (MMP9, F2))	hue
	F1	fraction * gene	((MMP9, F1), (MMP7, F1))	x
	F2	fraction * gene	((MMP9, F2), (MMP7, F2))	x
	F3	fraction * gene	((MMP9, F3), (MMP7, F3))	x

[167 rows x 19 columns]

```
[ ]: # Plot
(
  DA.switch("row", "col", verbose=False)
  .set(y="fc", inplace=False) # set y back to fc to display non-log values
  .plot_box_strip(
    subplot_kws=dict(
      figsize=(10, 2.5),
      width_ratios=[4, 5, 3, 2, 5, 2],
    ),
    strip_kws=dict(alpha=0.8),
  )
  .edit_grid()
  .edit_y_scale_log(10)
  .edit_xy_axis_labels(y_leftmost_col="Fold Change", x="Gene")
  .annotate_pairwise(include="__HUE")
)
plt.savefig("qpcr1.png", dpi=300, bbox_inches="tight")
```



C Submission Forms & Documents

C.1 Author Contributions



Statement of individual author contributions and of legal second publication rights to manuscripts included in the dissertation

Manuscript 1: Research Article (published)

Martin Kuric (MK), Susanne Beck (SB), Doris Schneider (DS), Wyonna Darleen Rindt (WDR), Marietheres Evers (MS), Jutta Meißner-Weigl, Sabine Zeck (SE), Melanie Krug, Marietta Herrmann, Tanja Nicole Hartmann, Ellen Leich, Maximilian Rudert, Denitsa Docheva, Anja Seckinger, Dirk Hose, Franziska Jundt (FJ), Regina Ebert (RE) (2024): Describing Myeloma Dissemination *in vitro* with hMSC-Interacting Subpopulations and their Aggregation/Detachment Dynamics, **Cancer Research Communications**

Participated in	Author Initials, Responsibility decreasing from left to right				
Study Design	<u>MK</u>	RE	FJ	Dirk Hose	Anja Seckinger
Methods Development	<u>MK</u>	DS	WDR		
Data Collection	<u>MK</u>	DS	SZ	Melanie Krug	Jutta Meißner-Weigl
Data Analysis and Interpretation	<u>MK</u>	SB	RE	FJ	Dirk Hose
Manuscript Writing Writing of Introduction Writing of Materials & Methods Writing of Discussion Writing of First Draft	<u>MK</u>	RE	FJ		All

Explanations: The content of this publication exceeds the usual scope (~29 pages Supplemental). It includes not only research findings but also survival data and protocols of new, established methods and their validations. The contribution of Martin Kuric was pivotal and predominant in all aspects of this work. DS assisted in the experimental procedures. Susanne Beck analyzed the raw data from RNAseq and survival data, which were interpreted, depicted, and summarized by Martin Kuric. "All" includes all authors unmentioned in the same row in no particular order.

Manuscript 2: Data Analysis Software (published)

Martin Kuric (MK), Regina Ebert (RE) (2024): plotastic: Bridging Plotting and Statistics in Python, **Journal of Open Source Software** 9(95), 6304, <https://doi.org/10.21105/joss.06304>

Participated in	Author Initials, Responsibility decreasing from left to right				
Study Design	<u>MK</u>				
Methods Development	<u>MK</u>				
Data Analysis and Interpretation	<u>MK</u>				
Manuscript Writing Writing of Statement of Need Writing of Example Writing of Overview	<u>MK</u>	RE			

Explanations: This chapter is the manuscript of a software paper. This paper, its structure (Statement of Need, Example and Overview), and its use as a chapter in this manuscript/chapter-based thesis has been approved by the GSLS Common Graduation Commission. The software and its initial idea were entirely designed, developed, tested, documented, and released by MK. The software comprises more than 8000 total lines of code (including ~2000 testable lines) and is comparable in size to a typical web

application. Study design includes the initial idea and designing the architecture of the software modules. Methods development includes the independent acquisition of python development skills, developing prototypes, and the implementation of features into the design architecture. Data collection includes collecting test datasets for the software testing suite. Data analysis and interpretation includes developing the software testing suite (using pytest and continuous integration tools) and writing the online documentation (manuals and examples). Manuscript writing included the release of this software, which involved version control using GitHub, packaging and deployment on PyPi. RE gave feedback on the manuscript draft and has raised the funds for financing.

Manuscript 3: Research Letter (published)

Daniela Simone Maichl (DSM), Julius Arthur Kirner (JAK), Susanne Beck (SB), Wen-Hui Cheng, Melanie Krug (MeK), Martin Kuric (MK), Carsten Patrick Ade, Thorsten Bischler, Franz Jakob, Dirk Hose, Anja Seckinger, Regina Ebert (RE) & Franziska Jundt (FJ) (2023): Identification of NOTCH-driven matrisome-associated genes as prognostic indicators of multiple myeloma patient survival, **Blood Cancer Journal**, 13:134, <https://doi.org/10.1038/s41408-023-00907-6>

Participated in	Author Initials, Responsibility decreasing from left to right				
Study Design Methods Development	DSM	JAK	FJ		
Data Collection	DSM	JAK	MeK	FJ	
Data Analysis and Interpretation	DSM	SB	FJ	<u>MK</u>	
Manuscript Writing Writing of Introduction Writing of Materials & Methods Writing of Discussion Writing of First Draft	DSM	FJ	RE	<u>MK</u>	

Explanations: This co-authorship is not a chapter in this dissertation. Martin Kuric produced figures of processed but complex-to-visualize data and gave feedback on the manuscript before submission.

Manuscript 4: Research Paper (Accepted, in press)

Wyonna Darleen Rindt (WDR), Melanie Krug (MeK), Shuntaro Yamada, Franziska Sennefelder, Louisa Belz, Wen-Hui Cheng, Azeem Muhammad, Martin Kuric (MK), Marietheres Evers, Ellen Leich, Tanja Nicole Hartmann, Ana Rita Pereira, Marietta Hermann, Jan Hansmann, Mohammed Ahmed Yassin, Kamal Mustafa, Regina Ebert (RE), and Franziska Jundt (FJ) (2024): A 3D bioreactor model to study osteocyte differentiation and mechanobiology under perfusion and compressive mechanical loading, **Acta Biomaterialia**, S1742-7061, <https://doi.org/10.1016/j.actbio.2024.06.041>

Participated in	Author Initials, Responsibility decreasing from left to right				
Study Design Methods Development	FJ	WDR	RE	<u>MK</u>	
Data Collection	WDR	MeK	FJ	<u>MK</u>	
Data Analysis and Interpretation	WDR	FJ	RE	<u>MK</u>	
Manuscript Writing Writing of Introduction Writing of Materials & Methods Writing of Discussion Writing of First Draft	WDR	FJ	RE	<u>MK</u>	

Explanations: This co-authorship is not a chapter in this dissertation. Martin Kuric contributed by counseling during weekly meetings in tight collaboration with Franziska Jundt's group, assisting WDR during laboratory experiments, image analysis and giving feedback on submitted manuscript.

Manuscript 5: Research Letter (published)

Marietheres Evers (ME), Martin Schreder (MS), Thorsten Stühmer (TStü), Franziska Jundt (FJ), Regina Ebert (RE), Tanja Nicole Hartmann (TNH), Michael Altenbuchinger (MA), Martina Rudelius (MR), Martin Kuric (MK), Wyonna Darleen Rindt (WDR), Torsten Steinbrunn (TSte), Christian Langer, Sofia Catalina Heredia-Guerrero, Hermann Einsele (HE), Ralf Christian Bargou (RCB), Andreas Rosenwald (AR), Ellen Leich (EL) (2023): Prognostic value of extracellular matrix gene mutations and expression in multiple myeloma, **Blood Cancer J.**, 13(1):43, <https://doi.org/10.1038/s41408-023-00817-7>

Participated in	Author Initials , Responsibility decreasing from left to right									
Study Design Methods Development	EL	ME	FJ	RCB	AR					
Data Collection	EL	MS	MR	TSte	HE					
Data Analysis and Interpretation	ME	MA	EL	TStü	FJ	RE	TNH	<u>MK</u>	WDR	TSte
Manuscript Writing Writing of Introduction Writing of Materials & Methods Writing of Discussion Writing of First Draft	ME	EL	MS	All						

Explanations: This co-authorship is not a chapter in this dissertation. Martin Kuric contributed by counseling during regular meetings with Ellen Leich's group and giving feedback on submitted manuscript. "All" includes all authors unmentioned in the same row in no particular order.

If applicable, the doctoral researcher confirms that she/he has obtained permission from both the publishers (copyright) and the co-authors for legal second publication.

The doctoral researcher and the primary supervisor confirm the correctness of the above mentioned assessment.

Martin Kuric 01.08.2024 Würzburg

Doctoral Researcher's Name	Date	Place	Signature
----------------------------	------	-------	-----------

Regina Ebert 01.08.2024 Würzburg

Primary Supervisor's Name	Date	Place	Signature
---------------------------	------	-------	-----------



Statement of individual author contributions to figures/tables of manuscripts included in the dissertation

Manuscript 1: Research Article (published)

Martin Kuric (MK), Susanne Beck (SB), Doris Schneider (DS), Wyonna Darleen Rindt (WDR), Marietheres Evers, Jutta Meißner-Weigl, Sabine Zeck (SZ), Melanie Krug, Marietta Herrmann (MH), Tanja Nicole Hartmann, Ellen Leich, Maximilian Rudert, Denitsa Docheva, Anja Seckinger, Dirk Hose, Franziska Jundt, Regina Ebert (RE) (2024): Describing Myeloma Dissemination *in vitro* with hMSC-Interacting Subpopulations and their Aggregation/Detachment Dynamics, **Cancer Research Communications**, <https://doi.org/10.1158/2767-9764.CRC-23-0411>

Figure	Author Initials , Responsibility decreasing from left to right				
1	<u>MK</u>	DS	RE		
2	<u>MK</u>	DS	RE		
3	<u>MK</u>	DS	WDR	SZ	RE
4	<u>MK</u>	DS	SB	RE	
5	<u>MK</u>	SB	RE		
6	<u>MK</u>	SB			
7	<u>MK</u>	RE			
S1	<u>MK</u>	DS	WDR	SZ	RE
S2	<u>MK</u>	MH	DS	RE	
S3	<u>MK</u>	DS	SZ	RE	
S4	<u>MK</u>	RE			
S5	<u>MK</u>	RE			
S6	<u>MK</u>	SB	RE		
Table	Author Initials , Responsibility decreasing from left to right				
1	<u>MK</u>	SB	RE		
2	<u>MK</u>	SB	RE		
S1	<u>MK</u>	DS	RE		
S2	<u>MK</u>	SB	RE		
S3	<u>MK</u>	RE			
S4	<u>MK</u>	DS	RE		

Manuscript 2: Data Analysis Software (published)

Martin Kuric, Regina Ebert (2024): plotastic: Bridging Plotting and Statistics in Python, **Journal of Open Source Software**, 9(95), 6304, <https://doi.org/10.21105/joss.06304>

Figure	Author Initials , Responsibility decreasing from left to right				
1	<u>MK</u>	RE			
Table	Author Initials , Responsibility decreasing from left to right				
1	<u>MK</u>				
2	<u>MK</u>				
Documentation	Author Initials , Responsibility decreasing from left to right				

README	<u>MK</u>				
Example Gallery	<u>MK</u>				
Features	<u>MK</u>				
Testing	Author Initials , Responsibility decreasing from left to right				
Test-Code (Pytest)	<u>MK</u>				
Continuous Integration	<u>MK</u>				

Explanations: All files are available on GitHub (<https://github.com/markur4/plotastic>) and installable via pypi.com. Documentations are found in the Readme, including example gallery and feature explanation. Software tests was written using pytest. Coverage of code by tests is reviewable with codecov (<https://app.codecov.io/gh/markur4/plotastic>). Continuous Integration is implemented using GitHub actions.

Manuscript 3: Research Letter (published)

Daniela Simone Maichl (DSM), Julius Arthur Kirner, Susanne Beck (SB), Wen-Hui Cheng, Melanie Krug, Martin Kuric, Carsten Patrick Ade, Thorsten Bischler, Franz Jakob, Dirk Hose, Anja Seckinger, Regina Ebert & Franziska Jundt (2023): Identification of NOTCH-driven matrisome-associated genes as prognostic indicators of multiple myeloma patient survival, **Blood Cancer Journal**, 13:134, <https://doi.org/10.1038/s41408-023-00907-6>

Figure	Author Initials , Responsibility decreasing from left to right				
1 a	DSM			SB	
1 b	DSM			SB	
1 c	DSM			SB	<u>MK</u>
1 d	DSM			SB	<u>MK</u>
Table	Author Initials , Responsibility decreasing from left to right				
1	DSM				

Explanations: This co-authorship is not a chapter in this dissertation. Martin Kuric plotted multidimensional diagrams using python and fine-adjusted them using professional design software (Affinity Publisher, Serif Ltd).

Manuscript 4: Research Paper (Accepted, in press)

Wyonna Darleen Rindt (WDR), Susanne Beck, Melanie Krug, Shuntaro Yamada (SY), Franziska Sennefelder (FS), Louisa Belz (LB), Wen-Hui Cheng, Azeem Muhammad, Martin Kuric (MK), Marietheres Evers, Ellen Leich, Tanja Nicole Hartmann, Ana Rita Pereira, Marietta Hermann, Jan Hansmann, Mohammed Ahmed Yassin (MAY), Kamal Mustafa, Regina Ebert, and Franziska Jundt (FJ) (2024): A 3D bioreactor model to study osteocyte differentiation and mechanobiology under perfusion and compressive mechanical loading, **Acta Biomaterialia**

Figure	Author Initials , Responsibility decreasing from left to right				
1	WDR	FJ	SY	RE	<u>MK</u>
2	WDR	FJ	MAY		
3	WDR	FJ	FS	LB	RE
4	WDR	FJ	FS	LB	RE
5	WDR	FJ	FS	LB	RE
6	WDR	FJ	SY	RE	<u>MK</u>
7	WDR	FJ	RE	<u>MK</u>	

Explanations: This co-authorship is not a chapter in this dissertation. Martin Kuric contributed by counseling on experimental procedures and data analysis, such as quantifying normalized fluorescence intensity of immunohistochemistry and qPCR.

Manuscript 5: Research Letter (published)

Marietheres Evers (ME), Martin Schreder, Thorsten Stühmer, Franziska Jundt, Regina Ebert, Tanja Nicole Hartmann, Michael Altenbuchinger, Martina Rudelius, Martin Kuric (MK), Wyonna Darleen Rindt, Torsten Steinbrunn, Christian Langer, Sofia Catalina Heredia-Guerrero, Hermann Einsele, Ralf Christian Bargou, Andreas Rosenwald, Ellen Leich (EL) (2023): Prognostic value of extracellular matrix gene mutations and expression in multiple myeloma, **Blood Cancer J.**, 13(1):43, <https://doi.org/10.1038/s41408-023-00817-7>

Figure	Author Initials, Responsibility decreasing from left to right				
1	ME	EL			
2	ME	EL			

Explanations: This co-authorship is not a chapter in this dissertation. Martin Kuric contributed indirectly through counseling and feedback on drafted manuscript.

I also confirm my primary supervisor's acceptance.

Martin Kuric

01.08.2024 Würzburg

Doctoral Researcher's Name

Date

Place

Signature

C.2 Affidavit

Affidavit

I hereby confirm that my thesis entitled "Development and Semi-Automated Analysis of an in vitro Model for Myeloma Cells Interacting with Mesenchymal Stromal Cells" is the result of my own work. I did not receive any help or support from commercial consultants. All sources and / or materials applied are listed and specified in the thesis.

Furthermore, I confirm that this thesis has not yet been submitted as part of another examination process neither in identical nor in similar form.

Würzburg
Place, Date

Signature

Eidesstattliche Erklärung

Hiermit erkläre ich an Eides statt, die Dissertation "Entwicklung und semi-automatisierte Analyse eines in vitro-Modells für Myelomzellen in Interaktion mit mesenchymalen Stromazellen" eigenständig, d.h. insbesondere selbstständig und ohne Hilfe eines kommerziellen Promotionsberaters, angefertigt und keine anderen als die von mir angegebenen Quellen und Hilfsmittel verwendet zu haben.

Ich erkläre außerdem, dass die Dissertation weder in gleicher noch in ähnlicher Form bereits in einem anderen Prüfungsverfahren vorgelegen hat.

Würzburg
Ort, Datum

Unterschrift

C.3 Curriculum Vitae

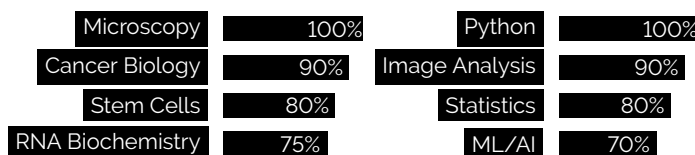
MARTIN KURIC

Cell Biologist | Data Scientist



WHO AM I?

As a cancer cell biologist with a strong passion for data analysis and machine learning, I am seeking a position where I can utilize my creativity to automate tasks, solve complex problems or handle big data.



SELECTED PROJECTS

2024	Python Software “ImageP” Accelerates batch processing of images of different sizes and types by >100%. <code>numpy</code> / <code>skimage</code> / <code>scipy</code>	GitHub Repository
2020-2024	Python Software “plotastic” Published a statistical library that self-configures based on intuitive plotting parameters. <code>pandas</code> / <code>matplotlib</code> / <code>pingouin</code> / <code>seaborn</code>	Journal of Open Source Software GitHub-Repository
2018-2024	Cancer Research Project Worked in a team with up to three technical assistants and published a list of genes with relevance for survival of myeloma patients. <code>Time-Lapse Microscopy</code> / <code>RNAseq</code> / <code>Analysis of Patient Survival</code>	Journal: Cancer Research Communications
26.05.2022	Deep-Learning Assisted Image Cytometry Measurement of per-cell parameters from large automated microscopy scans. <code>Convolutional Neural Networks</code> / <code>Image Segmentation</code>	Poster at "Achilles Conference"

EDUCATION

28.01.2019 – 2024	Dr. rer. nat. in Biomedicine Research focus: Dissemination of multiple myeloma & mesenchymal stromal cell interactions	Prof. Dr. Regina Ebert University of Würzburg
01.04.17 – 26.05.24 parallel to M.Sc. & PhD	Elite Biological Physics Interdisciplinary & international study program for exceptional students of physics or biology.	University of Bayreuth
01.10.15 – 15.08.18	M.Sc. in Biochemistry & Molecular Biology Research focus: RNA biochemistry, small RNAseq, stem cells & piRNAs in <i>S. mediterranea</i>	Prof. Dr. Claus-D. Kuhn University of Bayreuth
01.10.12 – 14.12.15	B.Sc. in Biochemistry Research focus: Cell biology, mitochondrial inheritance in <i>S. cerevisiae</i>	Prof. Dr. Benedikt Westermann University of Bayreuth

LANGUAGES

German, English - C2
Slovakian - passive
French, Spanish - A2

SOFT SKILLS

Quality Management
Project Management
Violent Free Communication

HOBBIES

Coding - Python
Music - Piano & Guitar
Gym - Lift. Grow. Repeat

Würzburg

08.07.2024

Location

Date

Signature